CHALMERS

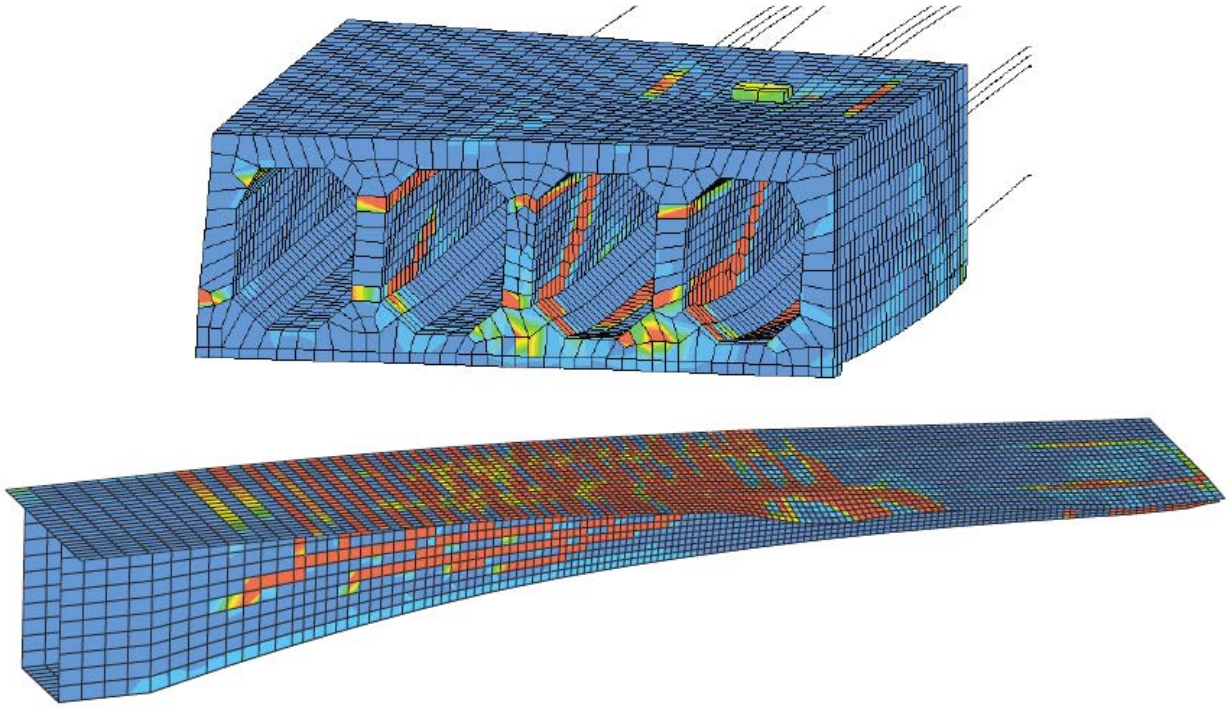

Shear and Torsion in Concrete Structures

Non-Linear Finite Element Analysis in Design and Assessment

HELÉN BROO

Department of Civil and Environmental Engineering
Structural Engineering, Concrete Structures
CHALMERS UNIVERSITY OF TECHNOLOGY
Göteborg, Sweden, 2008

THESIS FOR THE DEGREE OF DOCTOR OF PHILOSOPHY

Shear and Torsion in Concrete Structures

Non-Linear Finite Element Analysis in Design and Assessment

HELÉN BROO

Department of Civil and Environmental Engineering
Structural Engineering, Concrete Structures
CHALMERS UNIVERSITY OF TECHNOLOGY
Göteborg, Sweden, 2008

Shear and Torsion in Concrete Structures
Non-Linear Finite Element Analysis in Design and Assessment
HELÉN BROO
ISBN 978-91-7385-105-3

© HELÉN BROO, 2008

Doktorsavhandlingar vid Chalmers tekniska högskola
Ny serie 2786
ISSN 0346-718x

Department of Civil and Environmental Engineering
Structural Engineering, Concrete Structures
Chalmers University of Technology
SE-412 96 Göteborg
Sweden
Telephone: + 46 (0)31-772 1000

Cover:
Crack patterns as results from non-linear finite element analysis of a hollow core unit and a prestressed concrete box-girder bridge.

Chalmers Reproservice
Göteborg, Sweden, 2008

Shear and Torsion in Concrete Structures
Non-Linear Finite Element Analysis in Design and Assessment

HELÉN BROO
Department of Civil and Environmental Engineering
Structural Engineering, Concrete Structures
Chalmers University of Technology

ABSTRACT

For structural design and assessment of reinforced concrete members, non-linear finite element analysis has become an important tool. However, design and assessment of shear and torsion are still done with simplified analytical or empirical design methods. Modelling methods used to simulate response due to bending and normal forces are well established and verified. The reliability of modelling methods used to simulate response due to shear and torsion, on the other hand, are more often questioned.

This study shows how recognized material models implemented in a commercial finite element code can be used to simulate the non-linear shear response in concrete members, both with and without shear reinforcement. Apart from improving the knowledge and understanding of shear and torsion, the aim is to improve the traditional design and assessment methods and to give guidance for the evaluation of response and load-carrying capacity by using advanced non-linear finite element analysis.

Modelling methods for non-linear finite element analysis of the shear response and load-carrying capacity of concrete structures subjected to shear and torsion were worked out and verified by comparison with tests. Furthermore, these modelling methods were applied to hollow core units, hollow core floors and a prestressed concrete box-girder bridge. The modelling methods include relevant simplifications to avoid analyses that are too time-consuming. Combining solid or shell elements, in the parts of the structure where failure is expected, with beam elements elsewhere, was shown to be a reasonable modelling level with regard to the desired level of accuracy. The modelling methods proposed can be used separately or in combination with conventional methods to improve the design or assessment of complex structures with arbitrary geometries and loads, when failure due to shear and torsion is the main problem. The modelling methods have shown great potential to reveal higher load-carrying capacity than conventional approaches. Further, the methods have been helpful not only in understanding the behaviour of concrete members subjected to shear and torsion but also to see how analytical methods can be used more correctly. Much can be gained by using these methods instead of or together with traditional design methods.

Key words: Reinforced concrete, prestressed concrete, shear, torsion, hollow core unit, hollow core floor, box-girder bridge, non-linear finite element analysis.

Skjuvning och vridning i betongkonstruktioner
Olinjär finit elementanalys för dimensionering och utvärdering
HELÉN BROO
Institutionen för bygg- och miljöteknik
Konstruktionsteknik, Betongbyggnad
Chalmers tekniska högskola

SAMMANFATTNING

Olinjär finit elementanalys har blivit ett allt viktigare beräkningsverktyg för såväl dimensionering som utvärdering av armerade betongkonstruktioner. Dimensionering och utvärdering med hänsyn till tvärkraft och vridning görs dock fortfarande med analytiska eller empiriska metoder. Analyser av respons och bärförmåga till följd av böjandemoment och normal kraft utförs med tillförlitliga och verifierade metoder. Tillförlitligheten hos modelleringsmetoderna som används för att simulera responsen till följd av skjuvning och vridning har däremot ifrågasatts.

Denna studie visar hur välkända materialmodeller implementerade i ett kommersiellt finit elementprogram kan användas för att modellera den olinjära responsen vid skjuvning och vridning i betongkonstruktioner med och utan tvärkraftsarmering. Förutom att öka kunskapen om, och förståelsen för, skjuvning och vridning var målet att utveckla och förbättra dagens beräkningsmetoder och ge vägledning för utvärdering av respons och bärförmåga med hjälp av olinjära finit elementanalyser.

Modelleringsmetoder för olinjära finitelementanalyser av respons och bärförmåga hos betongkonstruktioner utsatta för skjuvning i kombination med vridning har utvecklats och verifierats mot försök. Modelleringsmetoderna har tillämpats på förspända hålelement, håldäck och en förspänd lådbalkbro. För att undvika orimligt långa beräkningstider har vissa förenklingar gjorts. Att använda solidelement eller skalelement enbart i de delar av strukturen där brott förväntas, i kombination med balkelement i övriga delar, har visat sig vara en lämplig modelleringsnivå med tanke på önskad noggrannhet. Genom att använda de framtagna modellringsmetoderna separat eller i kombination med dagens beräkningsmetoder kan dimensionering och utvärdering av komplexa konstruktioner med varierande geometri och last, och där brott på grund av tvärkraft och vridning är det huvudsakliga problemet, förbättras. Modelleringsmetoderna har visat stor potential för att påvisa högre bärförmåga jämfört med dagens utvärderingsmetoder. Metoderna har också varit till stor hjälp för att förstå verkningssättet hos betongkonstruktioner utsatta för skjuvning i kombination med vridning och för att se hur de analytiska beräkningsmetoderna kan användas på ett mer korrekt sätt än tidigare. Genom analyser med de framtagna metoderna kan betongkonstruktioners kapacitet utnyttjas bättre.

Nyckelord: armerad betong, förspänd betong, skjuvning, vridning, hålelement, håldäck, hålbjälklag, lådbalkbro, olinjär finitelementanalys.

LIST OF PUBLICATIONS

This thesis is based on the work contained in the following papers, referred to by Roman numerals in the text.

I. **Shear and torsion in prestressed hollow core units: Finite element analyses of full-scale tests.** Broo H., Lundgren K. and Engström B. *Structural Concrete,* Vol. 8, No. 2, pp. 87—100, 2007.

II. **Analyses of hollow core floors subjected to shear and torsion.** Lundgren K., Broo H. and Engström B. *Structural Concrete*, Vol. 5, No. 4, pp. 161—172, 2004.

III. **Shear and torsion interaction in presstressed hollow core units.** Broo H., Lundgren K. and Engström B. *Magazine of Concrete Research,* Vol. 57, No. 9, pp. 521—533, 2005.

IV. **Simulation of shear-type cracking and failure with non-linear finite element method.** Broo H., Plos M., Lundgren K. and Engström B. *Magazine of Concrete Research,* Vol. 59, No. 9, pp. 673—687, 2007.

V. **Non-linear finite element analysis of the shear response in prestressed concrete bridges.** Broo H., Plos M., Lundgren K. and Engström B. Submitted to *Magazine of Concrete Research,* February, 2008.

VI. **A parametric study of the shear response in prestressed concrete bridges by non-linear finite element analysis.** Broo H., Plos M., Lundgren K. and Engström B. Submitted to *Magazine of Concrete Research,* April, 2008.

The papers were written in collaboration with co-authors. The responsibility taken by the author of this thesis is specified here.

I. Did the main part of the planning and the writing of the paper. Participated in the planning of the tests and finite element analyses. Attended almost all tests. Made the finite element models and carried out all of the analyses.

II. Participated in the planning of the tests and finite element analyses. Attended the tests. Made the finite element model of one hollow core unit. Contributed comments on the results and article.

III. Did the main part of the planning and the writing of the paper. Participated in the planning of the tests and the finite element analyses. Attended the tests. Carried out all of the analyses.

IV.–VI. Carried out the main part of the planning and the writing of the papers. Made the finite element models and carried out all of the analyses.

Other publications within the Holcotors project, "Shear and torsion interaction in prestressed hollow core floors"

Shear and Torsion Interaction in Prestressed Hollow Core Slabs. Broo H., Lic 2005:2, Department of Civil and Environmental Engineering, Chalmers University of Technology, Göteborg, 2005.

Shear and torsion in hollow core slabs. Lundgren K., Broo H., Engström B. and Pajari M., *fib Symposium "Keep Concrete Attractive"*, Budapest, Hungary, 2005.

Shear and torsion in hollow core slabs: How advanced modelling can be used in design. Lundgren K., Broo H., Engström B. and Pajari M. *BIBM*, Amsterdam, the Netherlands, 2005.

Shear and torsion in hollow core slabs. Broo H., Lundgren K., Engström B. and Pajari M. *XIX Symposium on Nordic Concrete Research & Development*, Sandefjord, Norway, 2005.

Analyses of hollow core floors. Lundgren K. and Plos M., Report 04:7, Concrete Structures, Department of Structural Engineering and Mechanics, Chalmers University of Technology , Göteborg, Sweden, , 2004.

Analyses of two connected hollow core units. Lundgren K. and Plos M., Report 04:4 Concrete Structures, Department of Structural Engineering and Mechanics, Chalmers University of Technology, Göteborg, Sweden, 2004.

Finite Element Analyses of Hollow Core Units Subjected to Shear and Torsion. Broo H. and Lundgren K., Report 02:17 Concrete Structures, Department of Structural Engineering, Chalmers University of Technology, Göteborg, Sweden, 2002.

Pure torsion test on single slab units. Pajari M., VTT Research Notes 2273, VTT Building and Transport, Technical Research Centre of Finland, Espoo, Finland, 2004.

Shear torsion test on 400 mm hollow core floor. Pajari M., VTT Research Notes 2274, VTT Building and Transport, Technical Research Centre of Finland, Espoo, Finland, 2004.

Shear-torsion interaction tests on single hollow core slabs. Pajari M., VTT Research Notes 2275, VTT Building and Transport, Technical Research Centre of Finland, Espoo, Finland, 2004.

Test on 200 mm hollow core floor. Pajari M., VTT Research Notes 2276, VTT Building and Transport, Technical Research Centre of Finland, Espoo, Finland, 2004.

Other publications within the project "Shear and torsion in prestressed concrete bridges"

Design and assessment for shear and torsion in prestressed concrete bridges - A state-of-the-art investigation. Broo H., Report 2006:2, Concrete Structures, Division of Structural Engineering and Mechanics, Department of Civil and Environmental Engineering, Chalmers University of Technology, Göteborg, Sweden, 2006.

Reinforced and prestressed concrete beams subjected to shear and torsion., Broo, H., Plos M., Lundgren, K. and Engström, B. *Fracture mechanics of Concrete and Concrete structures*, 17-22 June, Catania, Italy, Vol. 2 pp. 881-888, 2007.

Non-linear FE analyses of prestressed concrete bridges subjected to shear and torsion., Broo, H., Plos M., Engström, B. and Lundgren, K. *XX Symposium on Nordic Concrete Research & Development*, June 8-11, Bålsta, Sweden, Submitted February, 2008.

Nonlinear FE analysis of shear behaviour in reinforced concrete – Modelling of shear panel tests. Martin, M., Master's Thesis 2007:46, Concrete Structures, Division of Structural Engineering, Department of Civil and Environmental Engineering, Chalmers University of Technology, Göteborg, Sweden, 2007.

Non-linear finite element analyses of prestressed concrete box-girder bridges subjected to shear and torsion - A parameter study. Engel, J. and Kong, S. Y., Master's Thesis 2008:3, Concrete Structures, Division of Structural Engineering, Department of Civil and Environmental Engineering, Chalmers University of Technology, Göteborg, Sweden, 2008.

Contents

ABSTRACT I

SAMMANFATTNING II

LIST OF PUBLICATIONS III

CONTENTS VI

PREFACE VIII

NOTATIONS IX

1 INTRODUCTION 1

1.1 Background 1

1.2 Aim, scope and limitations 1

1.3 Outline of the thesis 2

1.4 Original features 3

2 SHEAR AND TORSION IN CONCRETE MEMBERS 4

2.1 Shear and torsion induced cracking and failure 4

2.2 Conventional methods to predict the shear and torsion capacity 6

2.2.1 Members without shear reinforcement 6

2.2.2 Members with shear reinforcement 7

2.3 Conventional methods to predict the shear response 10

3 FINITE ELEMENT ANALYSES OF CONCRETE STRUCTURES SUBJECTED TO SHEAR AND TORSION 12

3.1 Modelling of reinforced concrete subjected to shear and torsion 12

3.2 Modelling of concrete response 14

3.2.1 Material models for concrete 14

3.2.2 Stress-strain relationships in smeared crack modelling 15

3.3 Safety formats for non-linear finite element analysis 19

4 ANALYSIS OF HOLLOW CORE SLABS 20

4.1 Precast prestressed hollow core slabs 20

4.1.1 Structural behaviour of hollow core floors 21

4.1.2 Structural behaviour of hollow core units 23

4.2 Modelling of hollow core units 24

4.2.1 A modelling method for hollow core units 24

4.2.2 Interaction diagrams for hollow core units 26

4.3 A modelling method for hollow core floors 29

4.4 An improved design approach for hollow core slabs 31

4.4.1 Design of hollow core floors using interaction diagrams 32

4.4.2 Design of hollow core floors with a model of a hollow core unit 33

5 ANALYSIS OF PRESTRESSED CONCRETE BRIDGES 35
5.1 Prestressed concrete bridges 35
5.2 A modelling method for large members with shear reinforcement 38
5.3 A modelling method for small members with shear reinforcement 43
5.4 The modelling method applied to a prestressed concrete bridge 45
5.5 A parametric study on a box-girder bridge 48

6 CONCLUSIONS 50
6.1 General conclusions 50
6.2 Conclusions about hollow core slabs 50
6.3 Conclusions about prestressed concrete bridges 52
6.4 Suggestions for future research 53

7 REFERENCES 55

Preface

This thesis investigates the extending use of non-linear finite element analysis for the design and assessment of concrete structures subjected to shear and torsion. It was carried out at Concrete Structures, Division of Structural Engineering, Department of Civil and Environmental Engineering, Chalmers University of Technology, Sweden. The work in this study was carried out in two research projects. The first, concerning shear and torsion interaction in hollow core slabs, part of a European project called "Holcotors", was conducted from March 2002 to December 2004. This research was financed by the 5th Framework of the European Commission, the International Prestressed Hollow Core Association, the "Bundesverband Spannbeton-Hohlplatten" in Germany, and by the partners involved, which were Chalmers University of Technology, the Technical Research Centre of Finland (VTT), Consolis Technology, Strängbetong, Castelo, and Echo. The second research project, Shear and torsion in prestressed concrete bridges, was conducted from August 2005 to June 2008, and financed by the Swedish Road Administration (Vägverket) and the Swedish Rail Administration (Banverket).

I am most grateful to my supervisor, Professor Björn Engström, and assistant supervisors, associated professor Karin Lundgren and assistant professor Mario Plos for guidance, support, encouragement and valuable discussions. In particular, I will remember the experience and joy of working closely with Karin in the "Holcotors" project. My thanks go to Professor Kent Gylltoft, who made it possible for me to join the Concrete Structures Research Group at Chalmers for which he provided a supportive and inspiring research environment.

I also want to thank all members of the "Holcotors" steering group for their interest in my work: Matti Pajari, VTT; Gösta Lindström, Strängbetong; Arnold Van Acker; Willem J. Bekker, Echo; Jan de Wit, Dycore; David Fernández-Ordónez, Castelo; Ronald Klein-Holte, VBI; Olli Korander, Consolis Technology; Nordy Robbens, Echo; Bart Thijs, Echo; and Javier Zubia, Castelo. Special thanks go to Matti Pajari for allowing me to attend the tests at VTT, and to use the data collected directly after the tests were carried out; he also provided the photographs and drawings, and gave permission to use them. For guidance and valuable discussion, I thank the members of the reference group of the second project: Ebbe Rosell, Vägverket; Elisabeth Hellsing, Banverket; Stefan Pup, Vägverket Konsult; Bo Westerberg, Tyréns; Richard Malm, KTH; Per Kettil, Skanska, and Kent Gylltoft, Chalmers.

Furthermore, I would like to thank my present and former colleagues, especially Rasmus Rempling, for their support and interest in my problems. I also thank everyone involved in our concrete group days, for stimulating discussions and good ideas. Last, but not least, my daughters, Hilma and Elsa, my fiancé, Tomas, and both of our families gave encouragement and help with child care, while my sister, Marie, read the whole text and offered helpful comments. Their wonderful support made it possible to complete this work.

Göteborg, April 2008

Helén Broo

Notations

Roman upper case letters

A	total cross-sectional area (including the inner hollow areas) of the transformed cross-section [m^2]
A_c	concrete cross-sectional area [m^2]
A_{ef}	effective area [m^2]
A_{sl}	cross-sectional area of longitudinal reinforcement [m^2
A_{st}	cross-sectional area of transverse reinforcement [m^2]
A_{sw}	Cross-sectional area of shear reinforcement [m^2]
B	Bogie load of type-vehicle [N]
E_c	modulus of elasticity of concrete [Pa]
E_p	modulus of elasticity of prestressing steel [Pa]
E_s	modulus of elasticity of reinforcing steel [Pa]
G_f	concrete fracture energy [N/m]
I_c	second moment of area of concrete section [m^4]
M	imposed moment [Nm]
P	prestressing force [Pa] or applied load [N]
Q	applied load [N]
R_d	design resistance [N]
R_k	characteristic resistance [N]
R_m	mean resistance [N]
S	first moment of area above and around the centroidal axis [m^3]
T	applied torsional moment [Nm]
T_{Ed}	applied torsional moment [Nm]
$T_{R,top}$	torsional capacity for the top flange [Nm]
$T_{R,web}$	torsional capacity for the outermost web [Nm]
V	applied shear force [N]
V_{Edi}	shear force in each wall due to torsion [N]
V_{ETd}	design value of acting shear force in the web due to torsion [N], as given in EN 1168
$V_{R,c}$	shear capacity [N]
$V_{Rd,c}$	design value of shear capacity [N], as given in EN 1168
$V_{Rd,max}$	design value of shear capacity determined by crushing of compression struts [Pa]
V_{Rdn}	design value of the shear capacity for simultaneous torsion [N], as given in EN 1168
$V_{Rd,s}$	design value of shear capacity determined by yielding of the shear reinforcement [Pa]
V_{Rn}	shear capacity for simultaneous torsion [N]
V_T	shear force in the web due to torsion [N]
W_t	sectional modulus for torsion [m^3]
$W_{t,top}$	sectional modulus for torsion for top flange [m^3]
$W_{t,web}$	sectional modulus for torsion for outermost web [m^3]

Roman lower case letters

b	width at the centroidal axis [m]
b_w	narrowest part of the cross-section in the tensile area [m]
$b_{w,out}$	thickness of the outermost web [m]
Σb_w	the sum of the widths at the centroidal axis of all webs [m]
d	effective depth [m]
e	eccentricity of the strands [m]
f_{cc}	concrete compressive strength [Pa]
f_{ct}	concrete tensile strength [Pa]
f_d	design strength [Pa]
f_k	characteristic strength [Pa]
f_m	mean strength [Pa]
f_p	tensile strength of prestressing steel [Pa]
f_{sl}	yield strength of longitudinal reinforcement [Pa]
f_{sv}	yield strength of transverse reinforcement [Pa]
f_u	ultimate strength of reinforcing or prestressing steel [Pa]
f_v	nominal concrete shear strength [Pa]
f_y	yield strength of reinforcing steel [Pa]
h	height [m] or crack band width [m]
l	length [m]
l_{pt}	transmission length of the prestressing strand [m]
l_x	distance between the section studied and the starting point of the transmission length [m]
q	load [N/m]
s_{rm}	mean crack spacing [m]
t	thickness [m]
t_{bottom}	thickness of the bottom flange [m]
t_{top}	thickness of the top flange [m]
u	outer circumference of the transformed cross-section [m]
z	z-coordinate of the point considered (origin at centroidal axis) [m] or internal lever arm [m]
w	crack width [m]

Greek lower case letters

α	angle between the shear reinforcement and the main tensile chord [degree]
β	reliability index
γ	shear strain [–]
γ_0	global safety factor
γ_c	partial safety factor for concrete
γ_m	partial safety factor for materials
γ_n	partial safety factor for action
γ_s	partial safety factor for reinforcing or prestressing steel
δ	displacement [m]
ε_1	principal tensile strain [–]
ε_2	principal compressive strain [–]
$\varepsilon^{cr}_{enn,ult}$	ultimate crack strain [–]
ε_x	strain in x-direction [–]
ε_y	strain in y-direction [–]

θ	angle for strut inclination [degree]
ρ	reinforcement amount [–]
σ_1	principal tensile stress [Pa]
σ_2	principal compressive stress [Pa]
σ_c	normal stress [Pa]
σ_{cp}	normal stress due to prestress [Pa]
τ	shear stress [Pa]
τ_V	shear stress from shear force [Pa]
τ_T	shear stress from torsional moment [Pa]
ϕ	diameter [m]

1 Introduction

1.1 Background

Concrete as a material has a non-linear response, and in reinforced concrete members the occurrence of cracks and yielding of reinforcement will cause stress redistribution within the member. However, in traditional engineering for the design and assessment of concrete structures, structural analyses are made by assuming linear response. Global or regional models, commonly linear beam or frame models, are used to determine sectional forces. The most heavily stressed sections, which are then designed or assessed with local sectional or regional models for capacity in the ultimate limit state, are affected by only one sectional force at a time, or the stresses from a variety of actions are assumed to interact linearly. For shear and torsion empirical or simplified analytical models are adopted.

The finite element method is an advanced and well-known method which has become an important tool and is increasingly used by practising engineers. It makes it possible to take into account non-linear response. The method can be used to study the behaviour of reinforced concrete members including stress redistribution. Various modelling methods can be used depending on the response or failure to be simulated. However, it is always important to validate the modelling method by test results and to be aware of the limitations of the model. The combination of element type, level of detailing and material models used is important when defining a modelling method. A verified modelling method could be used to study the behaviour of concrete members with geometries, material properties, reinforcement amounts, and load combination other than those tested. With a better understanding of the behaviour, the analytical models or the use of the analytical models could be improved.

Modelling methods used to simulate response due to bending and normal forces are well established and verified. Furthermore, they are commonly used by researchers and engineers, and the results are considered to be reliable. The reliability of modelling methods used to simulate response due to shear and torsion, on the other hand, are more often questioned. Although non-linear finite element analyses of reinforced concrete members subjected to shear have been reported by several researchers, recognized material models, not specially designed for shear, which are implemented in commercial finite element programs have not yet been used. With more reliable and verified modelling methods, the design and the assessment of reinforced concrete structures subjected to shear and torsion can be improved.

1.2 Aim, scope and limitations

The work was done to improve the knowledge and understanding of the shear and torsion responses in concrete members, both with and without shear reinforcement. The primary aim is to improve the application of non-linear finite element analysis in the design and assessment of reinforced concrete structures subjected to shear and torsion. Another aim is to introduce modelling methods and give guidance for the evaluation of response and load carrying capacity of (1) hollow core floors and (2) prestressed concrete bridges by using non-linear finite element analysis. Both the load

carrying capacity in the ultimate limit state and the response in the service state are treated. To accomplish this, modelling methods suitable for the applications were worked out and verified against tests carried out interactively with this work or found in the literature.

The modelling method worked out for prestressed concrete members without shear reinforcement was verified and applied to hollow core units and hollow core floors. Full-scale tests and the refinement of finite element models were carried out simultaneously in an interactive way. The tests, conducted at the Technical Research Centre of Finland (VTT), were planned cooperatively by VTT, Strängbetong and Chalmers University of Technology. The author took part in planning all the tests and attended almost all of them. Chalmers carried out the modelling. The author worked mainly with the modelling and analyses of hollow core units, but also participated in planning the analyses of hollow core floors. Two geometries of extruded hollow core units, 200 mm and 400 mm thick, provided with prestressing strands only in the bottom flange, were tested and analysed. The floors and units tested and analysed had no topping.

For large concrete members with shear reinforcement, a modelling method was worked out and verified with tests of shear panels and beams found in the literature. The modelling method was thereafter applied to a prestressed concrete box-girder bridge to evaluate the shear response and the load-carrying capacity for one critical load combination.

1.3 Outline of the thesis

The thesis consists of an introductory part and six papers, in which most of the work is presented. The shear response and shear failure of concrete members with and without shear reinforcement are covered in Chapter 2. Non-linear finite element analysis of concrete structures subjected to shear and torsion is dealt with in Chapter 3. The improved design approaches and the proposed modelling methods for hollow core units and floors are presented in Chapter 4, which also gives general information about hollow core slabs. Chapter 5 covers the modelling method worked out for analysis of prestressed concrete bridges, verifications and applications. In the last part, Chapter 6, the major conclusions are drawn and further research is suggested.

The analyses of the hollow core units and the floors are given in more detail in the first three papers. Paper I establishes the finite element models of prestressed hollow core units and compares results from analyses and full-scale tests. In Paper II a simple modelling method for complete floors is introduced. To analyse failure due to combined shear and torsion, the more detailed model of one hollow core unit is integrated with the floor model. Results from analyses are compared with those from full-scale tests of floors, some found in the literature and others conducted within the project carried out. The finite element models of hollow core units are used for analyses with selected combinations of shear and torsion, as given in Paper III. The resulting capacities, in the form of interaction diagrams, are compared with those obtained by the analytical method used in traditional design. In addition, the effects of

the shear span and the influence of the prestressing transfer zone on the capacity, due to combined shear and torsion, are investigated.

In the last three papers, the analyses of prestressed concrete bridges subjected to shear and torsion are presented. Paper IV presents the modelling method worked out; for verification several shear panel tests and two beam tests are simulated, and the results are compared. In Paper V, the modelling method is applied to a prestressed concrete bridge. The shear response and load carrying capacity of the Källösund Bridge are evaluated, compared and presented in this paper. In Paper VI, the finite element model of the Källösund Bridge is used to investigate the effects of: shear reinforcement inclination, web reinforcement amount, web thickness, and prestressing level, on the shear response and load carrying capacity.

1.4 Original features

The shear and torsion interaction in hollow core units, both individually and as part of a floor structure, is the subject of the first part of this study. Non-linear finite element analyses were alternated with full-scale tests; to the author's knowledge, this has not been previously done for hollow core units subjected to combined shear and torsion.

For hollow core units a method, using advanced non-linear finite element analyses to obtain the shear-torsion capacities shown in interaction diagrams, was proposed. For complete floors of hollow core units, a simplified global model was developed. With the modelling methods proposed, the design approach for hollow core floors can be improved and applied at simple or more advanced levels. The global floor model can be combined with the interaction diagrams or conventional design methods. Furthermore, the model of one hollow core unit can be integrated with the global floor model. Thus, the contribution in this thesis meets the needs of improved practical application and theoretical understanding for shear and torsion interaction in hollow core slabs.

In the last part of the study, the subject is the response and load carrying capacity of prestressed concrete bridges subjected to shear and torsion. Recognized material models implemented in a commercial finite element code were used to work out a modelling method which was verified by simulations of shear panel tests and beam tests. Thereafter, the modelling method was applied to a bridge structure and the shear response and load-carrying capacity were evaluated. To the author's knowledge, a modelling methodology like this has not been previously used for non-linear analysis of prestressed concrete bridges subjected to combined shear and torsion.

In the analyses of both hollow core slabs and a concrete bridge, several point loads were increased with displacement control. This was made possible by a separately modelled statically determinate system of beams; a prescribed displacement was applied at one point and the reaction force was transferred, in a controlled way, by the beam system to several points in the model. Similar arrangements may have been used by other researchers but it has not, to the author's knowledge, been reported.

2 Shear and torsion in concrete members

2.1 Shear and torsion induced cracking and failure

Both shear forces and torsional moments cause shear stresses, Figure 2.1. The shear stresses due to a transverse shear force are zero at the top and bottom of the cross-section, and their maximum is at the shear centre. The shear stresses caused by a torsional moment are distributed around the cross-section and their maximum is close to the surface and then decreasing towards the centre of the cross-section.

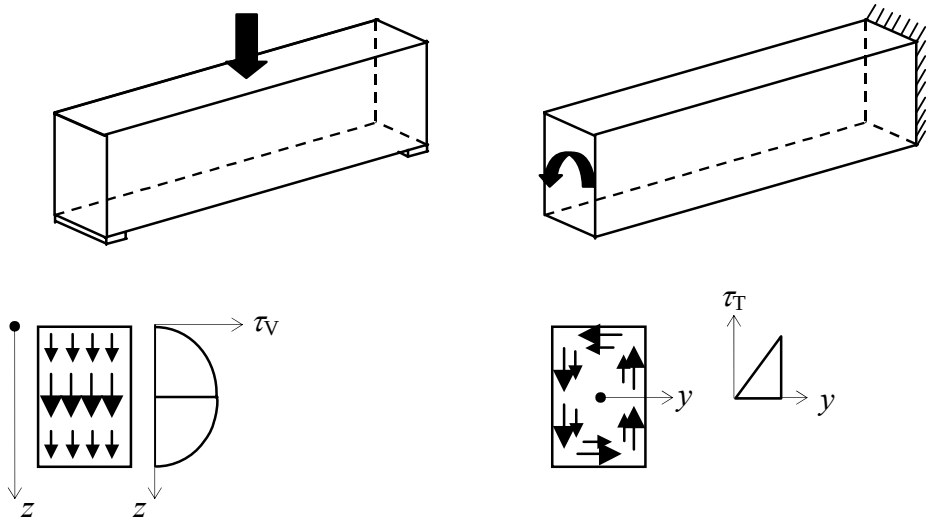

(a) *(b)*

Figure 2.1 Shear stresses in a rectangular cross-section of a concrete beam before cracking, due to (a) a transversal shear force, (b) a torsional moment.

When vertical shear and torsion act simultaneously on a member, the stresses from these influences interact. In a non-solid cross-section, for example a box-section, this means that one of the webs in the cross-section accumulates much higher stresses than the other, Figure 2.2.

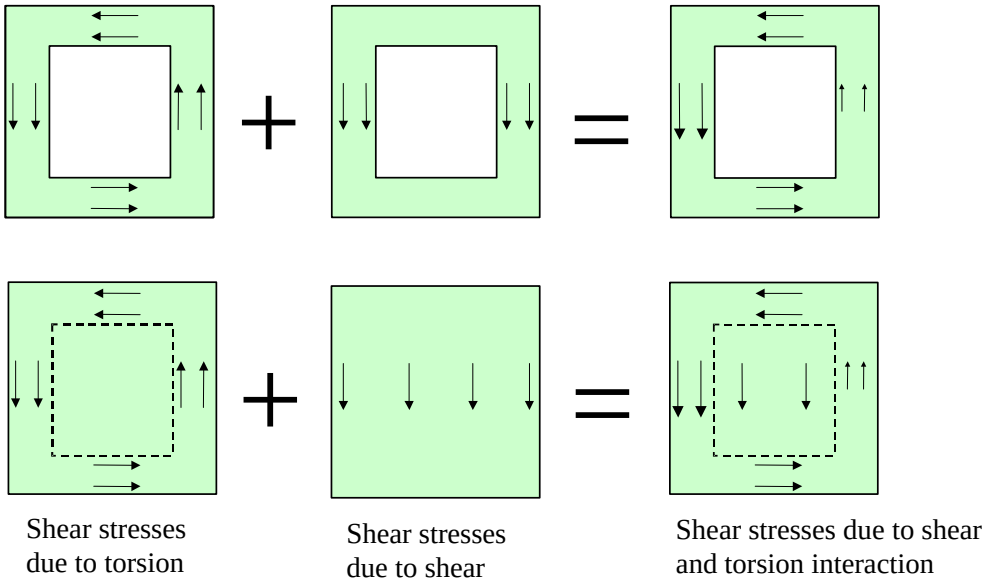

Figure 2.2 Shear and torsion interaction in a box cross-section and a solid cross-section.

High shear stresses can cause cracks in a concrete member. A crack is formed when the principal tensile stress, σ_1, in the concrete reaches a critical value, i.e. the concrete tensile strength, f_{ct}. The crack will form normal to the direction of the principal tensile stress. The inclination and the magnitude of the principal tensile stress depend on the total stress state. Longitudinal stresses due to bending moment or prestressing will influence the direction of the principal tensile stress. In regions subjected to significant shear stresses in relation to normal stresses, the principal tensile stress direction is inclined to the longitudinal axis of the member. Hence, the cracks due to shear are inclined to the member axis, and those caused by torsion spiral around the member. Different terms are used for these cracks, such as: diagonal cracks, inclined cracks, shear cracks or torsion cracks.

Whether the shear cracking results in a failure or not depends on weather the stresses can be redistributed. To reach a new equilibrium after shear cracking, longitudinal reinforcement and transverse reinforcement or friction in the crack, are required. The visible shear cracks are preceded by the formation of micro-cracks. The micro-cracking and the following crack formation change the stiffness relations in the concrete member, and a redistribution of stresses occurs, Hegger *et al.* (2004). The reduction of torsional stiffness due to cracking is much more severe than the loss of flexural stiffness. Shear cracks can start as either web-shear cracks or flexural shear cracks, Figure 2.3. Web-shear cracks are usually formed in regions not cracked by bending. The cracking starts in the more central parts of a web with an inclined crack which propagates both upwards and downwards until failure, a shear tension failure, or a new equilibrium is reached. Flexural cracks caused by bending could turn into flexural-shear cracks and result in failure, either by crushing or splitting of the compressive zone, shear-compressive failure in the struts, or by sliding along the inclined crack. When there is transverse reinforcement, shear sliding cannot take place before the transverse reinforcement yields.

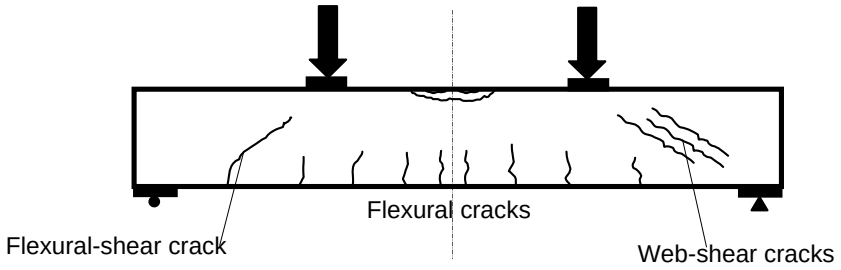

Figure 2.3 Flexural-shear crack and web-shear cracks caused by high shear stresses. Possible failure modes due to shear are either sliding in a shear crack or crushing of the concrete between two shear cracks.

The complex behaviour of reinforced concrete after shear crack initiation has been explained in several papers, for example ASCE-ACI Committe 445 on Shear and Torsion (1998), Vecchio and Collins (1986), Pang and Hsu (1995), Prisco and Gambarova (1995), Walraven and Stroband (1999), Zararis (1996), Soltani *et al.* (2003). The equilibrium conditions can be expressed in average stresses for a region containing several cracks, or in local stresses at a crack. The local stresses normal to the crack plane are carried by the reinforcement and by the bridging stresses of plain concrete (tension softening). Along the crack plane, the shear stresses are carried by aggregate interlocking and dowel action. The stresses will depend on the shear slip, the crack width, the concrete composition (strength, grading curve and maximum aggregate size) and, of course, the reinforcement (type, diameter and spacing); see fib (1999).

2.2 Conventional methods to predict the shear and torsion capacity

The methods presented here are all used for comparison with sectional forces, transverse shear force, torsional moment, or both, determined from independent overall structural analysis. Furthermore, they are valid only in the ultimate limit state, i.e. they can be used to predict only the ultimate capacity for shear, torsion or shear and torsion interaction.

2.2.1 Members without shear reinforcement

Shear capacity

For concrete members without shear reinforcement, the shear capacity is predicted with a nominal concrete shear strength, f_v. The estimation of the nominal shear strength differs from code to code. However, it is empirically determined from tests and influenced by: the height of the cross-section, the amount of longitudinal reinforcement, the compressive stresses due to prestressing or axial forces, and the concrete tensile strength. The shear capacity for a concrete member without shear reinforcement can generally be expressed as:

$$V_{\mathrm{Rd,c}} = b_w \cdot d \cdot f_v \tag{2.1}$$

where d is the effective depth of the cross-section and b_{w} is the narrowest part of the cross-section in the tensile area.

For prestressed single span concrete members without shear reinforcement, which are not cracked in bending, the shear capacity is limited by the tensile strength of the concrete, f_{ct}; it is assumed that a web-shear tension crack immediately results in failure. Hence, in the ultimate limit state the principal tensile stress is equal to the concrete tensile strength. The critical stress combination is assumed to be in a section at mid-depth, thus independent of the flexural moment. Furthermore, a web shear crack usually forms close to the support where the prestressing force is not fully developed and the concrete member is not yet cracked in bending. Accordingly, the shear capacity for web-shear tension failure can be calculated as, EN1992-1-1 (2004):

$$V_{\mathrm{R,c}} = \frac{I \cdot \sum b_{\mathrm{w}}}{S} \sqrt{f_{\mathrm{ct}}^2 + \alpha \cdot \sigma_{\mathrm{cp}} \cdot f_{\mathrm{ct}}} \tag{2.2}$$

where I is the second moment of area, S is the first moment of area above and around the centroidal axis, and b_{w} is the width of the cross-section at the centroidal axis. Furthermore, σ_{cp} is the concrete compressive stress at the centroidal axis, caused by axial loading or prestressing, $\alpha = l_x/l_{pt} \leq 1$, where l_x is the distance between the section considered and the starting point of the transmission length, and l_{pt} is the transmission length of the prestressing strand.

Shear-torsion capacity

The calculation model for shear capacity, when a section is simultaneously subjected to shear and torsion, is based on the assumption that shear stresses from both the transversal shear force and the torsional moment are added together. For a box-section, each wall is calculated separately according to Equation 2.1 or 2.2.

In Paper III analytical models for estimating shear capacity and torsional capacity are presented, as well as a model for estimating a reduced shear capacity due to torsion. In that paper the models are applied to a rather special type of cross-section, that of a hollow core unit. Nevertheless, the models are applicable to other thin walled prestressed cross-sections that do not have vertical or transverse reinforcement.

2.2.2 Members with shear reinforcement

Shear capacity

For concrete members with shear reinforcement, the capacity is estimated using simplified analytical or empirical design methods based on the truss model, Figure 2.4. In the original truss model, presented by Ritter and Mörsch in the early 20$^{\mathrm{th}}$ century, the total shear force is transferred by diagonal compressive stresses in struts inclined at an angle of $\theta = 45°$. The force transferred by the compressive struts

is lifted up by the shear reinforcement. The horizontal component of the compressive force is balanced by horizontal forces in the compressive and tensile chords. Later, a truss model with variable strut inclinations was introduced. The angle is determined by minimum energy principles or by choice. According to both EN1992-1-1 (2004) and Boverket (2004) the angle can be chosen between 21.8° and 45°, which corresponds to $\cot\theta = 2.5$ and $\cot\theta = 1.0$, respectively. The shear capacity determined by yielding of the shear reinforcement is calculated as:

$$V_{\mathrm{Rd,s}} = \frac{A_{\mathrm{sw}}}{s} \cdot z \cdot f_{\mathrm{ywd}} (\cot\theta + \cot\alpha) \sin\alpha \tag{2.3}$$

where A_{sw} is the cross-sectional area of a unit of the shear reinforcement, s is the spacing of the shear reinforcement, z is the lever arm of the compressive and tensile chord, f_{ywd} is the yield strength of the shear reinforcement, and α is the angle between the shear reinforcement and the main tensile chord.

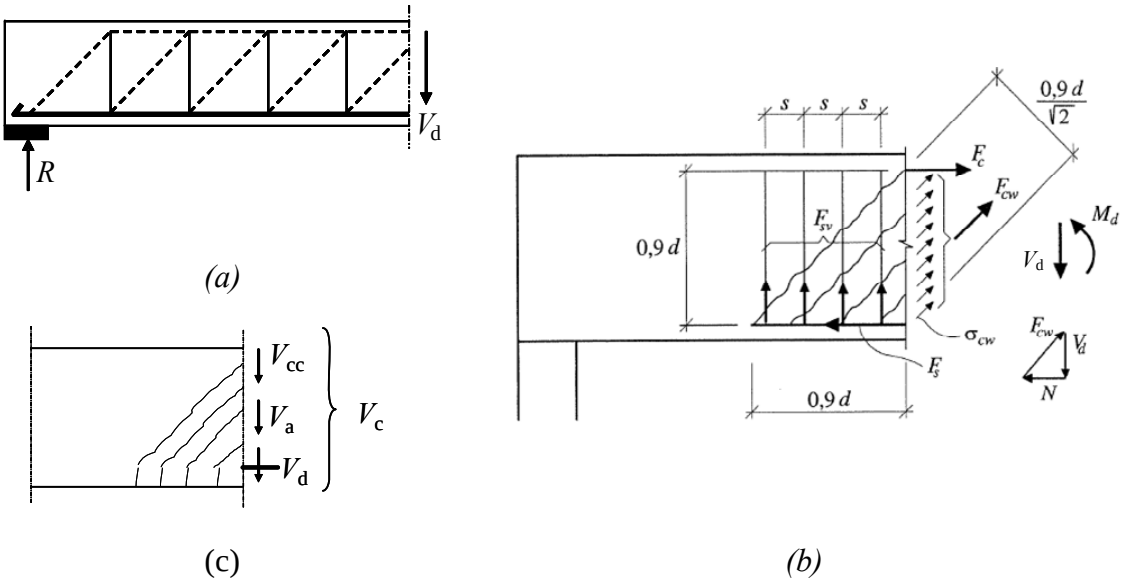

Figure 2.4 Models describing the transition of shear force after cracking. (a) Principle of the truss model; (b) Force compatibility for a truss model with strut inclinations of 45 °; (c) Although concrete contribution term, V_c, is empirical, it accounts for the shear transferred in the compression zone and in the crack: the softening of cracking concrete, the tension stiffening, the aggregate interlocking and dowel action.

In members with inclined chords, i.e. members with variable depth, the vertical components of the compressive and tensile forces in the chords influence the equilibrium, Figure 2.5. Furthermore, the length of the shear crack is affected; hence, the amount of shear reinforcement activated in the shear crack is also influenced. With notation according to Figure 2.5, the shear capacity for a member with inclined compressive chord and vertical shear reinforcement can be estimated as

$$V_{\mathrm{Ed}} - F_{\mathrm{cc}} \sin\gamma \le \frac{A_{\mathrm{sw}}}{\mathrm{s}} \cdot \frac{z}{\tan\theta - \tan\gamma} \cdot f_{\mathrm{ywd}} \tag{2.4}$$

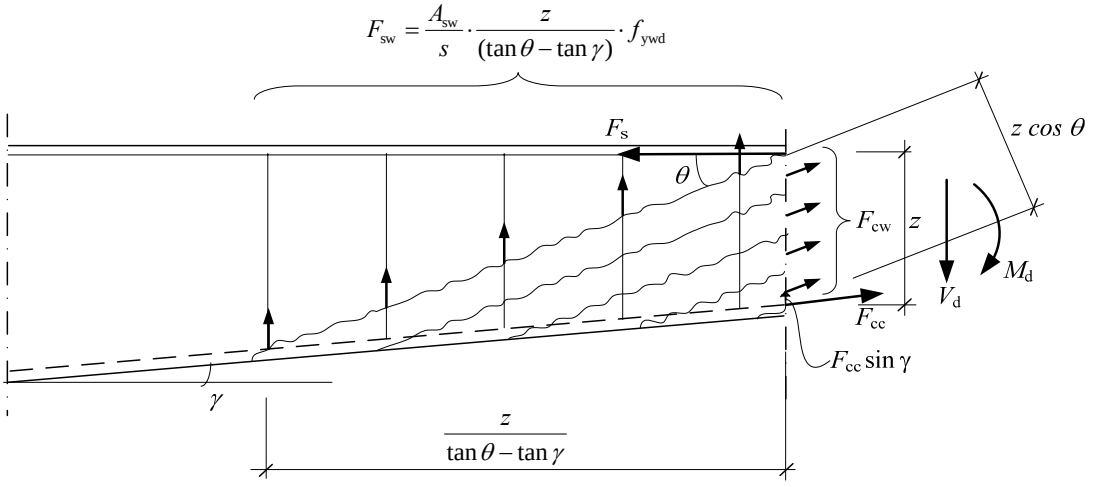

Figure 2.5 Truss model with inclined compressive chord, vertical shear reinforcement and variable angle of strut inclination.

It is also well known that for concrete members with shear reinforcement the shear capacity is larger than can be explained by the reinforcement contribution determined from a truss model. Therefore, the truss model can be combined with a *concrete contribution*, compensating for the difference in shear capacity found in tests and theoretically calculated capacities. Although the concrete term is empirical, it accounts for the shear transferred in the compression zone and in the crack, Figure 2.4 (c). The parameters influencing the *concrete contribution* are: the softening of cracking concrete, the bond between reinforcement and concrete, the aggregate interlocking in the crack, and the dowel action provided by the reinforcement. According to Boverket (2004), the shear capacity determined by the yielding of the shear reinforcement in a truss model with strut inclination of 45°, $V_{Rd,s}$ as in Equation 2.3, can be combined with a *concrete contribution* term, $V_{Rd,c}$, estimated according to Equation 2.1:

$$V_{Rd} = V_{Rd,s} + V_{Rd,c} \quad . \tag{2.5}$$

The maximum shear force which can be sustained by the member is limited by crushing of the compression struts and can be determined as

$$V_{Rd,max} = \alpha_{cw} \cdot b_w \cdot z \cdot \nu_1 \cdot f_{cd} \left(\frac{\cot\theta + \cot\alpha}{1 + \cot^2\theta} \right) \tag{2.6}$$

Here, f_{cd} is the concrete compressive strength, and ν_1 is a strength reduction factor for concrete cracked in shear. The interaction of stresses in the compression strut and any axial compressive stress is accounted for by the coefficient α_{cw}.

Torsion capacity and shear-torsion capacity

Analytical methods for prediction of the torsion capacity of reinforced concrete members provided with stirrups are based on the approximation that shear stresses are transferred along the circumference of the cross-section, within a thin-walled tube, which after cracking, is idealized as a space-truss. The space-truss consists of closed

stirrups, longitudinal bars at least in the corners and concrete compressive diagonals. According to Boverket (2004), the required transverse and longitudinal reinforcement are determined as

$$\frac{A_{st}}{s} \geq \frac{T_{Ed}}{2A_{ef} \cdot f_{sv}} \tan\theta \tag{2.7}$$

and

$$\frac{A_{sl}}{u_{ef}} \geq \frac{T_{Ed}}{2A_{ef} \cdot f_{sl} \cdot \tan\theta} \quad , \tag{2.8}$$

respectively, and added to the reinforcement needed for other actions. Here, A_{st} and A_{sl} are the cross-sectional area of the transverse and longitudinal reinforcement respectively; T_{Ed} is applied torsional moment, A_{ef} is the effective area enclosed by the centre-lines of the connecting walls (including inner hollow areas), u_{ef} is the outer circumference of the effective area, and f_{sv} and f_{sl} are the yield strength of the vertical and longitudinal reinforcement, respectively.

Alternatively, for each side of the tube, the methods available to predict the shear capacity can be used by transforming the shear stresses due to torsion into a transverse shear force, V_{Edi}, EN1992-1-1 (2004):

$$V_{Edi} = \frac{T_{Ed} \cdot z_i}{2A_{ef}} \tag{2.9}$$

where z_i is the side length of each wall. When there is combined transverse shear and torsion, the transformed shear force is added to the vertical shear force for each wall separately.

2.3 Conventional methods to predict the shear response

To predict the shear response of reinforced concrete members, from shear cracking to shear failure, more advanced methods are needed. Several numerical models have been proposed, for example the modified compression field theory (MCFT) of Vecchio and Collins (1986), the distributed stress field model (DSFM) of Vecchio (2000), the cracked membrane model (CMM) of Kaufmann and Marti (1998), the rotating-angle softened truss model (RA-STM) of Pang and Hsu (1995), the fixed-angle softened truss model (FA-STM) of Pang and Hsu (1996), and the softened membrane model (SMM) of Hsu and Zhu (2002).

All of these models are based on the smeared crack approach; i.e. the influences of cracks are smeared over a region and the calculations are made with average stresses and average strains. Stress equilibrium, strain compatibility and constitutive laws are used to predict the shear force for the strains chosen. Some models use a rotating crack concept, thus no relationship between shear stress and shear strain is needed for the concrete. Others are based on a fixed crack concept including a relationship for average shear stresses and average shear strains.

Such necessary constitutive laws, i.e. relationships between tensile stress and tensile strain, compressive stress and compressive strain, and shear stress and shear strain, have been established through full-scale tests of orthogonally reinforced shear panels, for instance by Vecchio and Collins (1986) and Pang (1991). Results from such tests showed that concrete in a diagonally cracked web is softer and weaker in compression than the concrete in a standard cylinder test, Vecchio and Collins (1993) and Belarbi and Hsu (1995). Figure 2.6 shows the relationships for the average principal tensile stress and average principal tensile strain used in the MCFT and in the softened truss models. In Paper IV the constitutive relationships for concrete in tension are presented and compared in analyses of shear panel tests. The constitutive relationships for concrete in tension can be seen as a way of including the *concrete contribution* to the shear capacity, i.e. the shear transferred across the shear cracks, which is influenced by the softening of cracking concrete, the bond between reinforcement and concrete, the aggregate interlocking, and the dowel action; see Section 2.2.

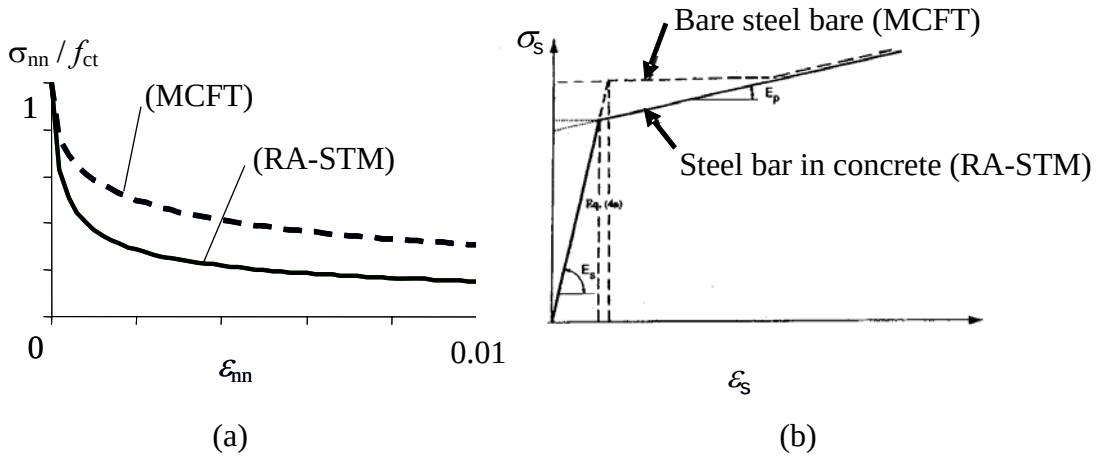

Figure 2.6 The relationships for average principal tensile stress and average principal tensile strain used in the MCFT and in the softened truss models, (a) concrete and (b) reinforcement.

In the same way as for the conventional methods to predict the shear capacity, these more enhanced methods are used for comparison with sectional forces determined from independent overall structural analysis.

3 Finite element analyses of concrete structures subjected to shear and torsion

The finite element method is an advanced and well-known method which has become an important tool and is increasingly used by practising engineers. Today, several commercial codes, which include recognized implemented material models suitable for concrete, are available on the market. Non-linear finite element analysis offers the option to represent the redistribution of sectional forces in statically indetermined structures. The redistribution of internal stresses can also be simulated by including the fracture energy associated with cracking concrete. Besides revealing higher load-carrying capacities, non-linear finite element analysis can be helpful in understanding the behaviour of a structure; the stress redistribution, and failure mode can be studied. However, it is always important to validate the modelling method with test results and to be aware of the limitations of the model. Reinforced concrete can be modelled with various levels of detailing and different material models can be adopted. A verified modelling method can be used to study the behaviour of concrete members with geometries, material properties, reinforcement amounts, and load combination other than those tested. Compared to making many tests, it is cheaper and easier to vary the models and run several analyses. With a better understanding of the behaviour, the analytical models themselves or the use of the analytical models can be improved.

Modelling methods used to simulate the response of bending and normal forces are well established and verified; they are commonly used by researchers and engineers, and the results are regarded as reliable. The reliability of modelling methods used to simulate response due to shear and torsion, on the other hand, are more questionable. Although non-linear finite element analyses of concrete members subjected to shear have been reported by several researchers, for example Ayoub and Filippou (1998), Yamamoto and Vecchio (2001), Vecchio and Shim (2004) and Kettil *et al.* (2005), recognized material models, not specially designed for shear, which are implemented in commercial finite element programs have not been adopted.

3.1 Modelling of reinforced concrete subjected to shear and torsion

Finite element modelling of reinforced concrete can be done with various levels of detailing, e.g. the interaction between the reinforcement and the concrete can be described in more or less detail. The response or failure to be simulated determines the level of detailing which must be chosen. To study a critical part or a critical detail in a larger reinforced concrete structure, the structural parts can be modelled with different levels of detailing and then combined. A general continuum model is formulated in a three-dimensional setting. By introducing additional assumptions or additional kinematic variables, the general setting can be reduced to models for plain strain, plain stress, plates, shells or beams. The element type to use depends on what type of response and failure the model should describe. For example, beam elements cannot describe shear cracking and shear failure or reduced torsional stiffness due to cracking. Plane stress elements, sometimes also called membrane elements, can be used to describe the shear response for walls or beams where the loading acts in the

plane of the element. If bending out of the plane needs to be taken into account, shell elements are needed instead of plain stress elements.

Detailed models suitable for the modelling of reinforced concrete members include not only separate constitutive models for plain concrete and steel, but also models for their interaction; i.e. the bond mechanism between the reinforcement and the concrete. If both the concrete and the reinforcement are modelled with continuum three-dimensional elements, three-dimensional interface elements describing the interaction between the concrete and the reinforcement can be used, see Figure 3.1. For the interface elements a special bond model, for example that of Lundgren (1999), can be used, which includes not only the bond stresses but also the splitting stresses activated when the reinforcement slips in the concrete. This means that the model can describe different bond stress-slip curves depending on the confinement of the surrounding concrete and whether or not the reinforcement yields. In addition to the constitutive relationships needed to describe the concrete and the reinforcing steel, a plasticity model is employed to describe the special bond mechanism. This is a very detailed modelling method which is not suitable for complete concrete members, but rather for analyses of reinforced concrete details.

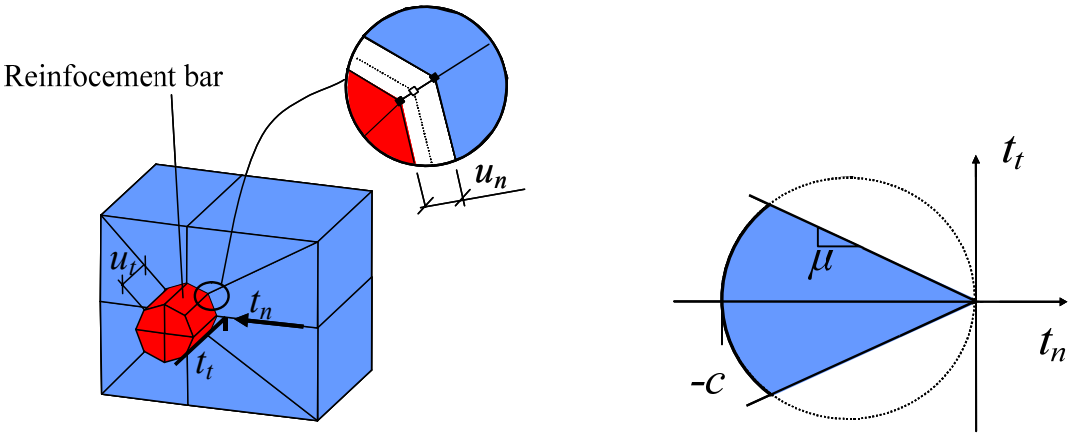

Figure 3.1 *Both the concrete and the reinforcing steel are modelled with continuum elements, and a three-dimensional interface element describes the interaction between them. A plasticity model is employed to describe the special bond mechanism. Lundgren (1999)*

A less detailed way of modelling reinforced concrete is to model the reinforcement with two-dimensional truss or beam elements, see Figure 3.2. The interaction between the concrete and the reinforcement can then be modelled with a two-dimensional interface element or spring elements describing the bond stress-slip relationship. The bond stress-slip relationship used is predefined and the interaction is not influenced by yielding of the reinforcement or high support pressure. This modelling method is suitable for smaller concrete members or for parts of concrete members. This level of detailing is needed if the slip of prestressing strands or reinforcement is important for the global response or the final failure, for example the modelling of a hollow core unit subjected to shear and torsion presented in Section 4 and Paper I.

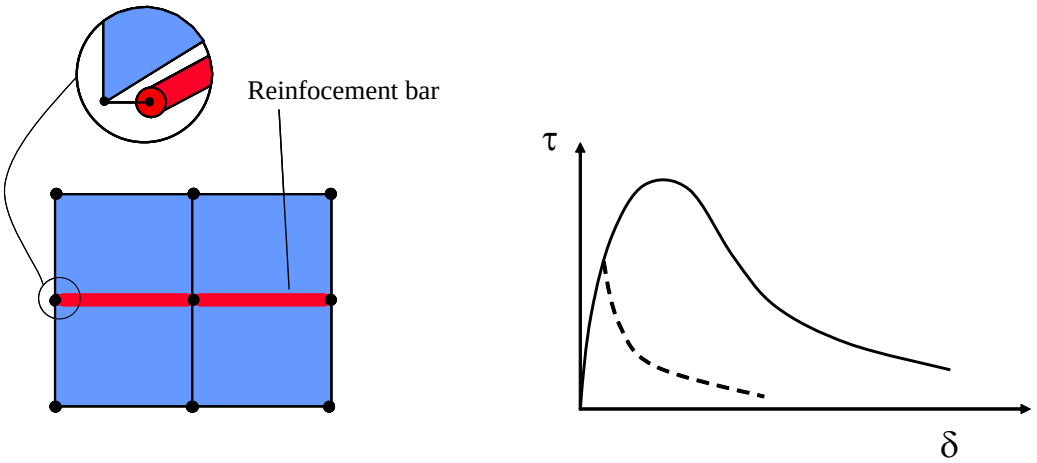

Figure 3.2 *The reinforcing steel is modelled with truss elements and a two-dimensional interface element; a predefined bond stress-slip relationship describes the interaction between the concrete and the steel.*

A modelling method more suitable for large reinforced concrete members is to assume full interaction between the reinforcement and the surrounding concrete, 'embedded reinforcement', i.e. the reinforcement has no degree of freedom of its own; it just adds stiffness to the concrete element, Figure 3.3. This can be used in combination with all types of elements, continuum or structural, suitable for describing the concrete.

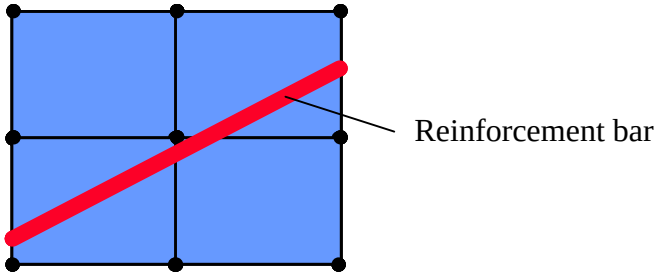

Figure 3.3 *The reinforcing steel is modelled with 'embedded reinforcement', i.e. full interaction is assumed between the steel and the concrete.*

3.2 Modelling of concrete response

3.2.1 Material models for concrete

Concrete as a material has a non-linear behaviour both in compression and in tension, Figure 3.4. To predict the behaviour of concrete structures, it is important to take this non-linear material response into account. Using non-linear material models in finite element analysis is one way of doing this.

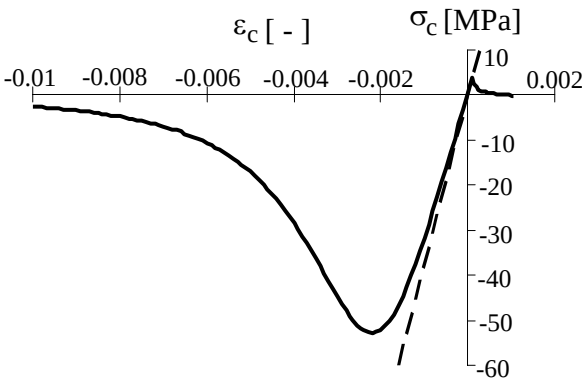

Figure 3.4 Typical non-linear uniaxial stress-strain relation for concrete, compared with elastic response.

The purpose of the material model is to describe the link between the deformations of the finite elements and the forces transmitted by them. Most of the commercial finite element programs are based on continuum models in which the material behaviour is described with a three-dimensional stress-strain relationship. This relationship can be based on elasticity, plasticity, damage or the smeared crack concept. The material models used for concrete are often based on several theories describing different phases of the material response. A plasticity model often describes the non-linear behaviour in compression, while the tensile response is described with another plasticity model, a damage model or a smeared crack model.

3.2.2 Stress-strain relationships in smeared crack modelling

Tension-softening

The smeared crack model was developed specially for cracking concrete under tensile load. The model is based on fracture mechanics to describe the relation between tensile stresses and the crack opening. The two basic ideas of non-linear fracture mechanics are that some tensile stress can be transferred after micro-cracking has started, and that this tensile stress depends on the crack opening rather then on the strain; see Figure 3.5. The area under the stress-crack opening curve represents the energy that is consumed, or dissipated, during the fracture process. This energy is denoted the fracture energy, G_f, and is assumed to be a material parameter. The material parameters needed, in addition to the fracture energy, to describe the formation of cracks are the concrete tensile strength, f_{ct}, and the shape of the stress-crack opening relation (traction-separation law). The deformation of a crack is smeared over a crack band width, h, which is the width of the band of the finite elements in which cracking localizes. The corresponding cracking strain is then equal to the crack opening, w, divided by the width of the crack band, h. In the smeared crack approach the deformation of one crack is smeared out over the crack band width. For unreinforced concrete this is typically chosen as one element length. For reinforced concrete, when the reinforcement is modelled as embedded and complete interaction with surrounding concrete is assumed, the deformation of one crack is

smeared over the mean crack distance instead. On the other hand, when slip is allowed between the reinforcement and the concrete, the crack band width is approximately the size of one element. Hence, the tensile stress versus strain used will depend on the size of the element.

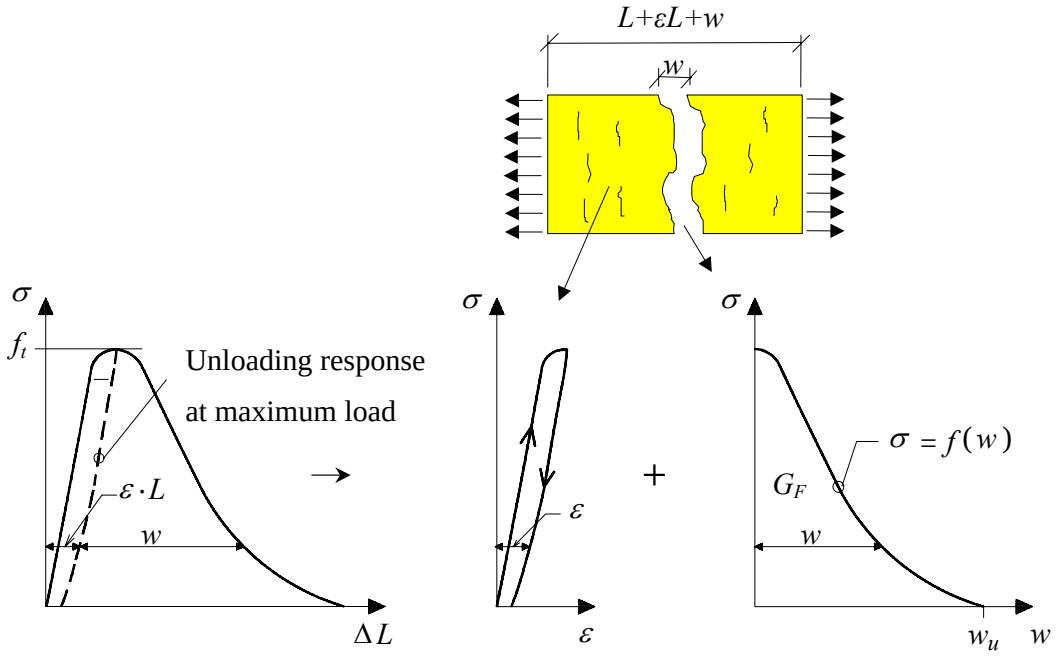

Figure 3.5 Mean stress-displacement relation for a uniaxial tensile test specimen, subdivided into a general stress-strain relation and a stress-displacement relation for the additional localised deformations.

Tension-stiffening

In a reinforced concrete member subjected to tensile forces, the concrete between the cracks carries tensile stresses which are transferred by the bond, thus contributing to the stiffness of the member. This is known as tension-stiffening. The tension-stiffening effect increases the overall stiffness of a reinforced concrete member in tension in comparison with that of a bare reinforcing bar. If a modelling level that describes the interaction between the reinforcement and the concrete is used, tension-stiffening does not need to be considered separately; it will be taken into account by the model. On the other hand, if full interaction between the reinforcement and the concrete is assumed, tension-stiffening can be taken into account in an approximate way through the constitutive relationship describing the materials, e.g. for the concrete in tension. Ways of doing this have been proposed by Lackner and Mang (2003).

Compression-softening

Owing to both the tension-softening response of cracking concrete and tension-stiffening effect, there are still significant transverse tensile stresses in the

compressive struts between the inclined shear cracks. Cracked concrete subjected to tensile strains in the direction perpendicular to that of the compression is softer and weaker than concrete in a standard compression cylinder test, Vecchio and Collins (1993) and Belarbi and Hsu (1995). Consequently, the compressive strength in the constitutive relationship used to describe the concrete in compression needs to be reduced, for example according to Vecchio and Collins as described in TNO (2004).

If a concrete compressive failure is localised within a small region, the size of which does not correspond to the size of the specimens used to calibrate the compression relationship used, the model cannot predict the response correctly. A compressive curve with the softening branch influenced by the size of the compression zone may solve this problem. However, in the program used for the analyses in this study, it is not possible to combine such a compressive-softening curve with the reduction of compressive strength due to lateral tensile strains. If the effect of reduced compressive strength, in order to simulate the response, is more important than the need to capture a concrete compression failure, the localization can be avoided by modelling the concrete in compression with an elastic-ideal plastic relationship instead. This was exemplified in the analyses of a bending beam and a box-beam given in Paper IV.

Concrete contribution to shear capacity

The smeared crack models can be classified by either the fixed crack approach or the rotating crack approach. In the first smeared crack models, the direction of the crack was assumed to be fixed and the shear tractions across the crack were treated with a 'shear-retention factor' to decrease the shear stiffness. The original fixed crack model was extended to the multiple non-orthogonal cracks model, in which several cracks in different directions can develop if the principal stress direction rotates. A threshold angle determines the smallest angle allowed between cracks, and thus limits the number of cracks that can form. Later, the rotating crack model, in which the crack direction is always perpendicular to the principal stress direction, was developed. No shear stress along the crack occurs; hence, no shear transfer model is needed. Although the rotating crack approach does not explicitly treat shear slip and shear stress transfer along a crack, it does simplify the calculations and is reasonably accurate under monotonic load where principal stress rotates a little, Maekawa *et al.* (2003). The rotating crack approach was adopted for almost all analyses made in this work.

In the same way as for the tension-stiffening effect, if a reinforced concrete member subjected to shear is modelled by assuming full interaction between the reinforcement and the concrete, the *concrete contribution* (Section 2.1) can be taken into account in an approximate way with the constitutive relationship describing the materials, e.g. for the concrete in tension. In Paper IV two approaches for the tension softening were compared:

- the curve by Hordijk (see TNO (2004)), where only the fracture energy of plain concrete is taken into account; and
- a curve modified according to the expression from the modified compression field theory (MCFT) of Collins and Mitchell (1991), which also attempts to take into account the *concrete contribution*;

see Figure 3.6. For the curve by Hordijk, the fracture energy is smeared over a length, *h*, the crack band width, which corresponds to the mean crack spacing obtained in the test or calculated according to Collins and Mitchell (1991).

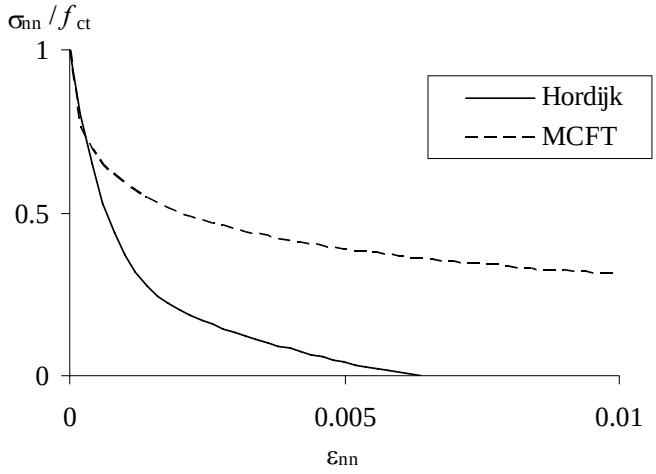

Figure 3.6 *Two tension-softening relations compared for a shear panel test. For the curve by Hordijk the fracture energy is smeared over a length of 150 mm (the crack band width, h), which corresponds to the calculated average crack spacing.*

Results from the analyses of several shear panel tests, see Section 5.3 and Paper IV, showed that with the Hordijk curve, the capacity was underestimated and the average strains, i.e. the crack widths, were overestimated. On the other hand, if the *concrete contribution* to the shear capacity was taken into account with the expression from MCFT, the capacity was often overestimated and the average strains underestimated.

The relationship from MCFT should be limited so that no stress is transferred after the reinforcement has started to yield. This is a problem when modifying the relationship for concrete in tension in a finite element program, since there is no obvious link between the steel strain in the reinforcement direction and the concrete strain in the principal strain direction. Hence, in a finite element analysis, the cracked concrete can still transfer tensile stresses in the principal stress direction even when the reinforcement in any direction yields, see Figure 3.7(a). Furthermore, the increase in mean concrete stress, is greater when modifying the tension softening relation to account for the *concrete contribution* in shear, than when modifying it for the tension-stiffening effect. Accordingly, a tension-softening relationship modified to account for the *concrete contribution* should not be used if shear is not a problem, which is why this modelling method is not general. This problem was highlighted by the analysis of a beam tested in four-point bending, Paper IV. The relations between the applied load and the vertical displacement, from both the analyses and the test, show that when the tension-softening was modelled according to MCFT, the response was too stiff and the capacity was overestimated; see Figure 3.7(b). Hence, even if the tension-softening curve is modified with respect to reinforcement yielding, it will give a response that is too stiff after cracking and before yielding for the parts of a member which are subjected to tension or bending but not to shear.

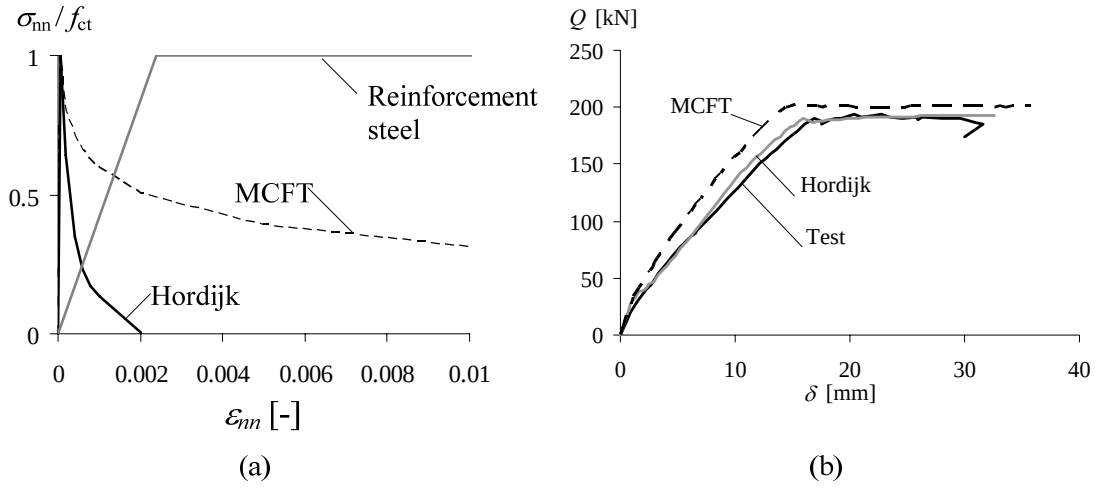

Figure 3.7 *(a) Relative stress versus strain; tension-softening curves for plain concrete and according the expression from MCFT compared with the tension curve for reinforcement. (b) Comparison of results from test and analyses of a reinforced concrete beam subjected to bending; applied load versus mid-deflection.*

3.3 Safety formats for non-linear finite element analysis

A general problem when using non-linear FE analysis for design or assessment is how to determine the reliability of the load-carrying capacity. A commonly used method to estimate the design resistance is to use the safety formats given in codes, such as the partial safety factor method. These formats are usually developed for section analysis. However, reducing the material strength properties with partial safety factors, in a non-linear analysis, influences not only the resistance of the structure but also the distribution of sectional forces and internal stresses. In Sustainable Bridges (2007) some formats which are suitable for non-linear analyses are presented. In Paper V the semi-probabilistic methods, the ECOV method (estimation of the variation coefficient of resistance) by Cervenka *et al.* (2007) and the one given in EN1992-2 (2005), are introduced and compared with the deterministic method using partial safety factors for the assessment of one load case and one critical section of a prestressed concrete box-girder bridge. It was shown that the format using partial safety factors gave an unrealistically conservative load-carrying capacity and that the semi-probabilistic methods used seemed more suitable for non-linear analysis.

4 Analysis of hollow core slabs

4.1 Precast prestressed hollow core slabs

Prestressed hollow core units are among the most advanced and widespread products in the precast industry. Prestressed hollow core units are prefabricated concrete elements that are normally 1200 mm wide, 200 – 400 mm thick and up to 20 m long. In the longitudinal direction they have cores which reduce the weight of the slab, see Figure 4.1. On average the voids represent about 50% of the total slab volume, ASSAP (2002). Due to differences in the shape of the cores and the edge profile, the cross-sections vary. The units are prestressed longitudinally by strands in the bottom flange, or in both the top and bottom flanges. Prestressed hollow core units are manufactured in well-equipped plants, using advanced technologies requiring little labour. The production of hollow core units and the concrete mix are quality controlled. The units are produced on casting-tensioning beds, by means of either a long line extrusion or a slip-forming process, and they are geometrically and structurally well formed. After hardening, the units are cut to the specified lengths and the prestressing strands are anchored by bond. Due to the production techniques they are not normally provided with transverse or vertical reinforcement. The main design parameters are: thickness of the unit, strand pattern and prestressing force.

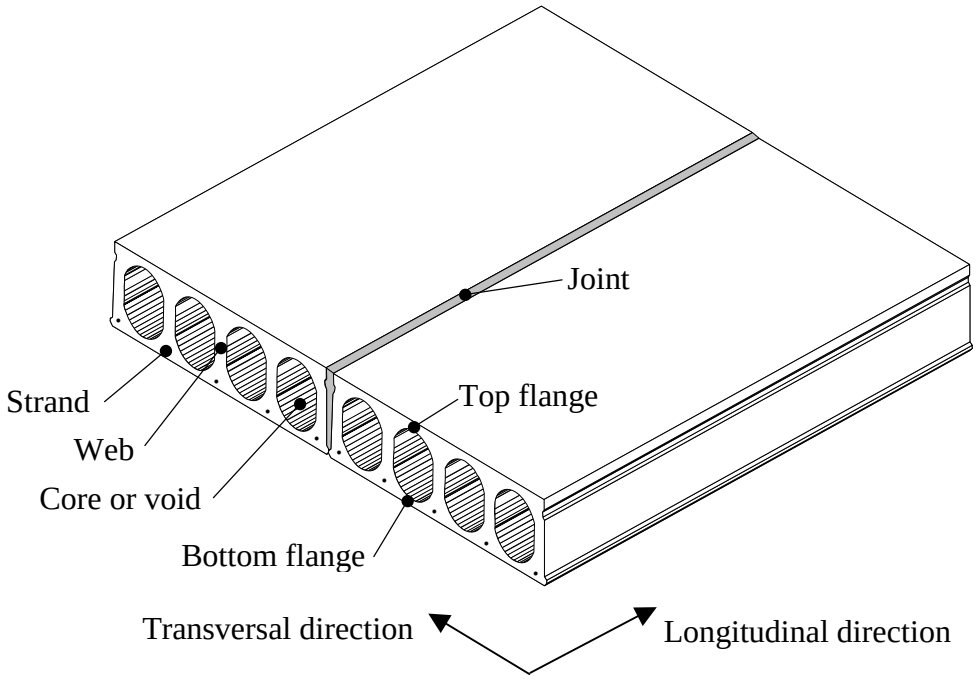

Figure 4.1 Frequently used terms for hollow core units.

Prestressed hollow core slabs are usually used for floors or roofs, but sometimes also for wall panels. In floors the hollow core units are placed next to each other, both ends are supported on a wall or a beam, and the joints between the units are grouted *in-situ*. The floor can be provided with a topping of plain or reinforced concrete. Hollow core floors also act as diaphragms transferring horizontal forces to shear walls.

4.1.1 Structural behaviour of hollow core floors

The main structural requirements for floors are vertical load bearing and the transverse distribution of load effects caused by concentrated loads. Hollow core units are usually designed to be simply supported and to resist bending moment and vertical shear; the longitudinal joints together with transverse ties are designed to transfer vertical shear to surrounding units. There are, however, many applications in which hollow core units are also subjected to combined shear and torsion. Some examples are slabs supported on three edges, slabs carrying a trimmer beam to support interrupted units, floors with columns in alternating positions at the ends of units, slabs supported on beams with divergent inclinations, and slabs with pronounced skew ends, see Figure 4.2.

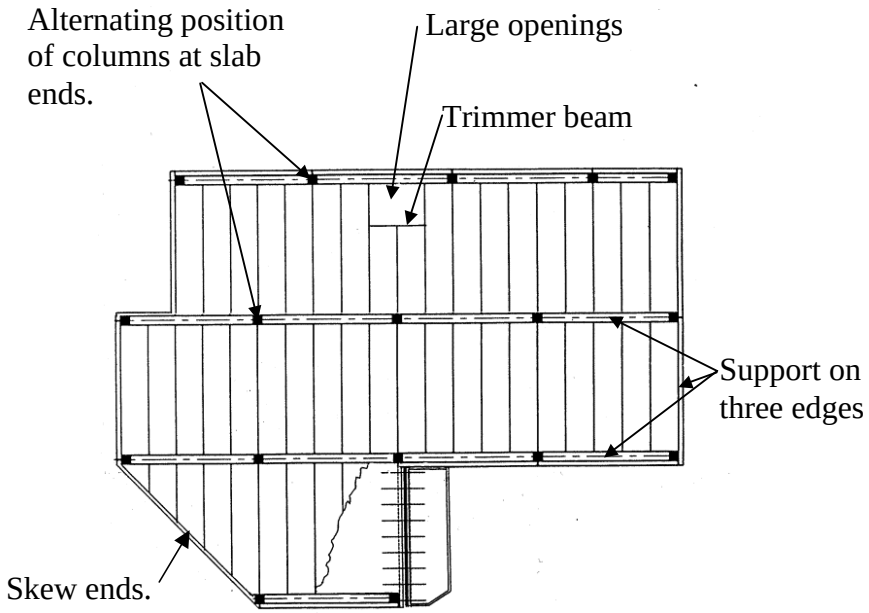

Figure 4.2 Practical examples in which shear forces, bending moments and torsional moment are simultaneously present in hollow core slabs. (Modified from a sketch by A. Van Acker, 2003)

When a uniform hollow core floor, simply supported on two opposite rigid supports, is uniformly loaded, all of the units deflect equally. Thus, one hollow core unit can be designed as a simply supported unit carrying its own load only. If only one hollow core unit in a floor is loaded, on the other hand, the adjacent units are forced to deflect, since the vertical shear forces are transversely distributed by the shear keys in the longitudinal joints. Hence, concentrated loading causes action effects, such as bending moment, vertical shear, and torsional moment, in the surrounding units as well. The distribution of these effects is not equal. The distribution of such load effects has been investigated by Stanton (1992) (see also Stanton (1987)), Van Acker (1984), and Pfeifer and Nelson (1983).

For practical design the distribution of load effects can be estimated by using diagrams given in the current European standard for hollow core slabs, EN 1168, CEN/TC229 (2005). There are diagrams provided for four load cases, see Figure 4.3: line load in the centre or at the edge, and point load in the centre or at the edge. All diagrams are for floors with five hollow core units. For floors with three or four supported edges, there are diagrams for estimating the reaction force along the longitudinal support exerted by a line load or by a point load in the mid-span. The units can then be designed for the bending moment, the shear force and the torsional moment supposed to be given by the diagrams and accompanying calculation methods. However, in EN 1168, it is not clear whether the distributions given are valid for the bending moments at mid-span or the shear forces at the supports. Unpublished work by Lindström (2004) indicates that some diagrams are valid for the bending moment at mid-span and others for the shear forces at the support.

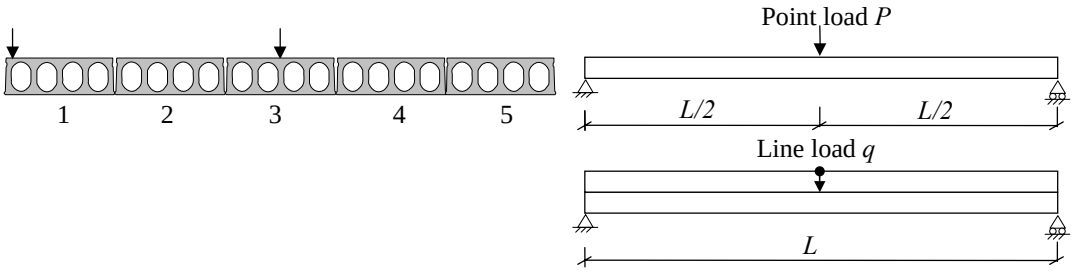

Figure 4.3 Load cases for which EN 1168 provides load distribution diagrams.

Normally, the joints are cracked and it is traditionally assumed that they act more or less as hinges. Consequently, the distribution of load effects to neighbouring units always introduces a torsional moment and corresponding deformations. However, these deformations introduce horizontal contact forces along the longitudinal joint between the hollow core units. The contact forces generate a torsional moment, which acts in the opposite direction to the torsional moment caused by the applied load, see Figure 4.4. In Paper II, a global finite element model proposed for whole floors takes this effect into account and also makes it possible to calculate the sectional forces, taking the distribution of load effects into account for hollow core floors with arbitrary geometries and loadings.

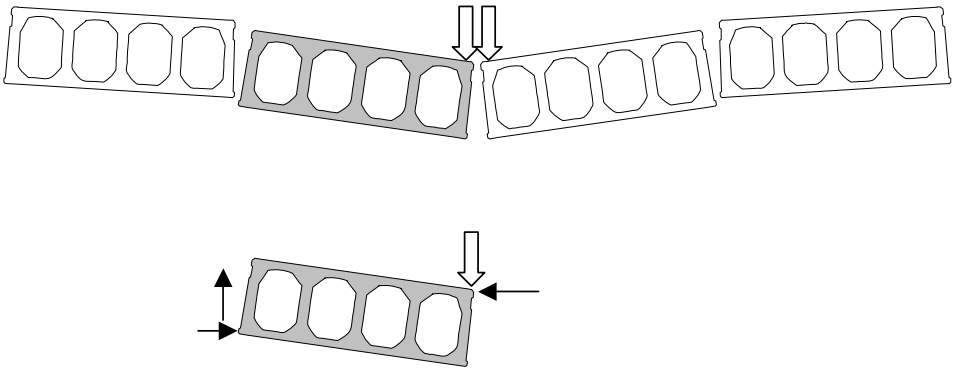

Figure 4.4 Forces acting on one of the loaded hollow core units.

4.1.2 Structural behaviour of hollow core units

Torsional loading on a hollow core unit produces shear stresses mainly in the perimetric zone of the unit. In the two outermost webs, these shear stresses act upwards in one and downwards in the other. A vertical shear force, on the other hand, produces shear stresses that are uniformly distributed between all of the webs. When vertical shear and torsion act simultaneously on one hollow core unit, the stresses from these influences interact. This means that one of the outermost webs in the cross-section accumulates much higher stresses than the others; however, close to failure, there may be some redistribution of stresses between the webs, see Figure 4.5.

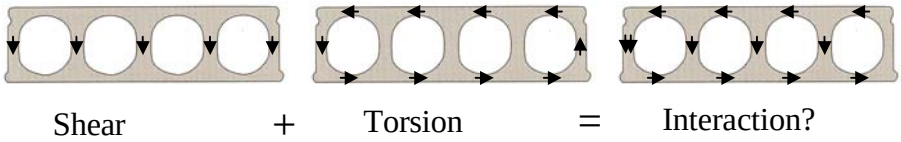

Figure 4.5 Shear stresses from vertical shear and from torsion interact in the cross-section of a hollow core unit.

Quite a lot of research has been done on vertical shear in hollow core units. The shear capacity was investigated experimentally, analytically, or both, by Walraven and Mercx (1983), Becker and Buettner (1985), Jonsson (1988), Pisanty (1992), Yang (1994), and Hoang (1997); and, in combination with flexible supports, also by Pajari (1995) and Pajari (1998). Procedures for predicting the shear capacity were published by Walraven and Mercx (1983), Pisanty (1992), Yang (1994) and Hoang (1997). The combination of shear and torsion in hollow core units is, however, not so well investigated. To the author's knowledge, the publication by Gabrielsson (1999), who focused on experiments and analytical modelling of eccentrically loaded hollow core units, and the work done within the Holcotors project, are the only ones dealing with this subject. However, in practical applications, which involve both shear and torsion, the hollow core units are grouted together to form a complete floor. There is some research on complete floors. For example, Walraven and van der Marel (1992) carried out tests on three-sided supported floors.

In EN 1168 the calculation method for shear capacity, if a section is simultaneously subjected to shear and torsion, is based on the assumption that shear stresses from both the vertical shear force and the torsional moment are added together in the outermost web. This gives a linear interaction between the capacities of shear force and torsional moment, however the redistribution of stresses within the hollow core unit is not accounted for. The failure mode for which the calculation method for the shear capacity is intended is the web shear tension failure (Section 2.2.1), which normally occurs close to the support where the prestressing force is not fully developed and the hollow core unit is not yet cracked in bending. In the standard it is assumed that the critical section for the reduced shear capacity is the same as the one for pure shear capacity. According to Walraven and Mercx (1983), the most critical point for a hollow core unit is where a plane inclined at 45° from the edge of the support intersects with the mid-depth plane, which is the weakest section of the web when the voids are circular, see Figure 4.6. However, for geometries with almost

rectangular voids, the webs are of even thickness, thus the critical point could be elsewhere, Yang *et al.* (2003). In Paper III analytical models for estimating shear capacity and torsional capacity are introduced, as well as a model for estimating a reduced shear capacity due to torsion.

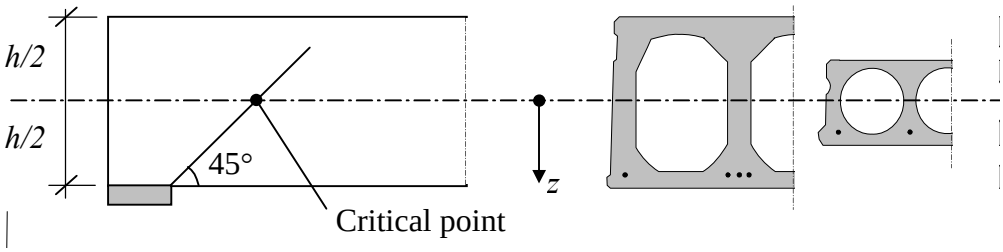

Figure 4.6 Most probable point for a shear tension crack to start, according to Walraven and Mercx (1983).

A hollow core unit subjected to torsion could start cracking in either of the flanges or in the outermost webs. By transforming the cross-section of the hollow core unit into an equivalent tubular cross-section, the torsional cracking resistance can be estimated on the basis of a closed thin-walled section. Whether this cracking results in failure or not depends on the possibilities for redistribution of the stresses.

There are of course other possible failure modes for simply supported hollow core units; for the behaviour of loading close to the support, Walraven and Mercx (1983) and Pajari (1989) have summarised some. One is anchorage failure, starting with the cracking of the bottom flange close to the support, due to bending moment or torsional moment, which could lead to a large slip of the strands resulting in failure. Furthermore, a flexural crack in the bottom flange could become an inclined crack due to shear and result in shear failure, either by crushing of the inclined compression strut or by shear sliding along the inclined crack.

When calculating the resistance of a hollow core unit for combined shear and torsion, (here denoted the shear-torsion capacity) by analytical methods, several failure modes have to be considered and the most critical point estimated. In Paper III (and Paper I), non-linear finite element analyses are used to evaluate the resistance of a hollow core unit for combined shear and torsion. The models proposed are capable of describing the possible failure modes, while also taking the softening of cracking concrete and stress redistribution into account.

4.2 Modelling of hollow core units

4.2.1 A modelling method for hollow core units

The modelling method, presented in Paper I, was worked out to enable the simulation of full-scale tests of hollow-core units subjected to combined shear and torsion, Pajari (2004a). The development of the finite element models as well as the planning of the tests was carried out simultaneously, in an interactive way. The models of a hollow core unit should be applicable in two ways: to analyse the effects of parameters that

influence the shear and torsion response and to be included in global models of whole floors to describe the behaviour at failure. Tests and finite element analyses were made using two geometries, one 200 mm thick and one 400 mm thick, for both hollow core units and whole floors.

In the model of one hollow core unit, eight-node solid elements were used only for the part of the unit where the failure was expected, close to the span load. The rest of the unit was modelled with three-node beam elements, see Figure 4.7. The solid elements were connected to the beam elements by assuming a stiff rotation of the cross-section and that the plane cross-section remained plane. The beam elements were assigned the properties of a hollow core unit by defining the cross-section with zones. In the part with solid elements, the strands were modelled with two-node bar elements, combined with interface elements and a pre-defined bond stress-slip relation, to simulate the interaction between the prestressing strand and the concrete. This level of detailing was needed to predict the maximum load, since this could be influenced by the slip of the strands. In the part of the model with beam elements, the strands were modelled as embedded reinforcement. This choice means that, in the beam elements, full interaction between the prestressing steel and the concrete was assumed. The concrete was modelled using non-linear fracture mechanics to describe the softening of cracking concrete; a rotating crack model based on total strain was used, see TNO (2002).

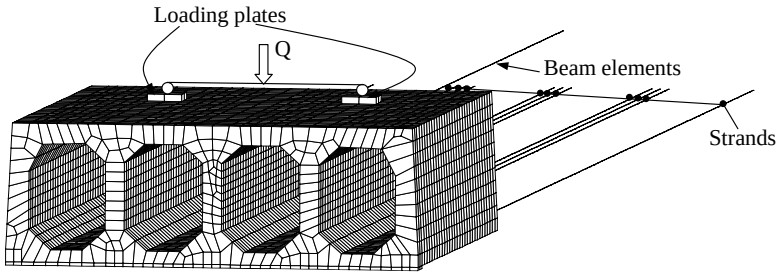

Figure 4.7 Mesh used in the analyses of the tests on 400 mm thick hollow core units.

This modelling method was verified by analysing several full-scale tests of hollow core units subjected to combined shear and torsion, see Paper I. These units were loaded with one point load or two point loads. The shear span was 2.5 times the height of the hollow core unit. Both centrically and eccentrically loaded units were tested and analysed with the finite element method. The principle of the test arrangement for a hollow core unit and the corresponding model used for the finite element analyses are shown in Figure 4.8. Material data for the concrete and the strands were evaluated from tests carried out by VTT, see Pajari (2004a).

In general, the finite element analyses of the experiments on hollow core units could describe quite well the overall behaviour including the: failure mode, crack pattern, maximum load, and load-displacement relations, see Figure 4.9 and Paper I. However, some of the analyses of the 200 mm thick hollow core unit underestimated the maximum load.

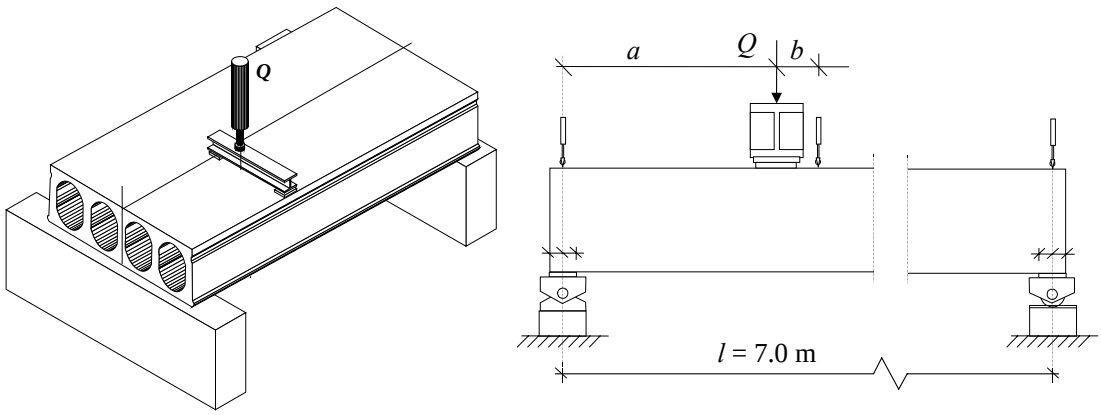

Figure 4.8 Principle of the testing arrangement for the tests of hollow core units, modified from Pajari (2004a).

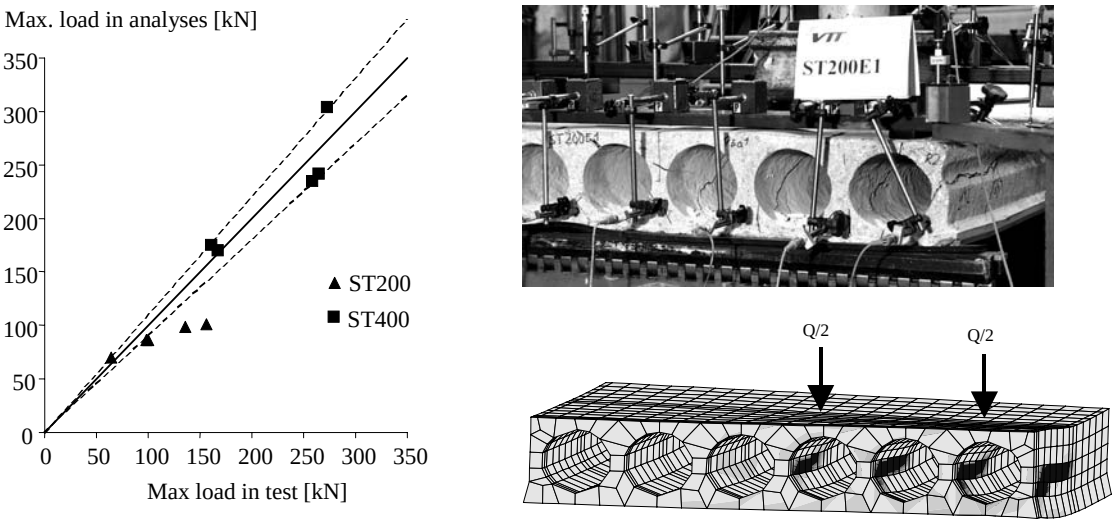

(a) (b)

Figure 4.9 (a) Maximum loads evaluated in analyses compared with the measured ones in the tests. The dashed lines show 10% deviation. (b) Crack pattern form the test ST200E1 and corresponding analysis.

4.2.2 Interaction diagrams for hollow core units

A methodology to establish shear and torsion interaction diagrams showing the capacity of a hollow core unit is presented in Paper III. By varying the loading from pure torsion to pure shear, and keeping the ratio between shear and torsion constant throughout each analysis, it was possible to establish shear and torsion interaction diagrams for various geometries of hollow core units. One of these combinations, for the 400 mm thick hollow core unit, was validated by full-scale tests, see Figure 4.10(a) and Pajari (2004a). In the model of one hollow core unit, described above, torsion was applied by twisting the ends with eccentric loads, B and C in Figure 4.10(b). The span was loaded with a point-load, A, distributed over the whole width of the unit. With a separately modelled loading arrangement, see

Figure 4.10(b), it was easy to vary the ratio between shear and torsion; it was also possible to run the finite element analyses with deformation-controlled loading.

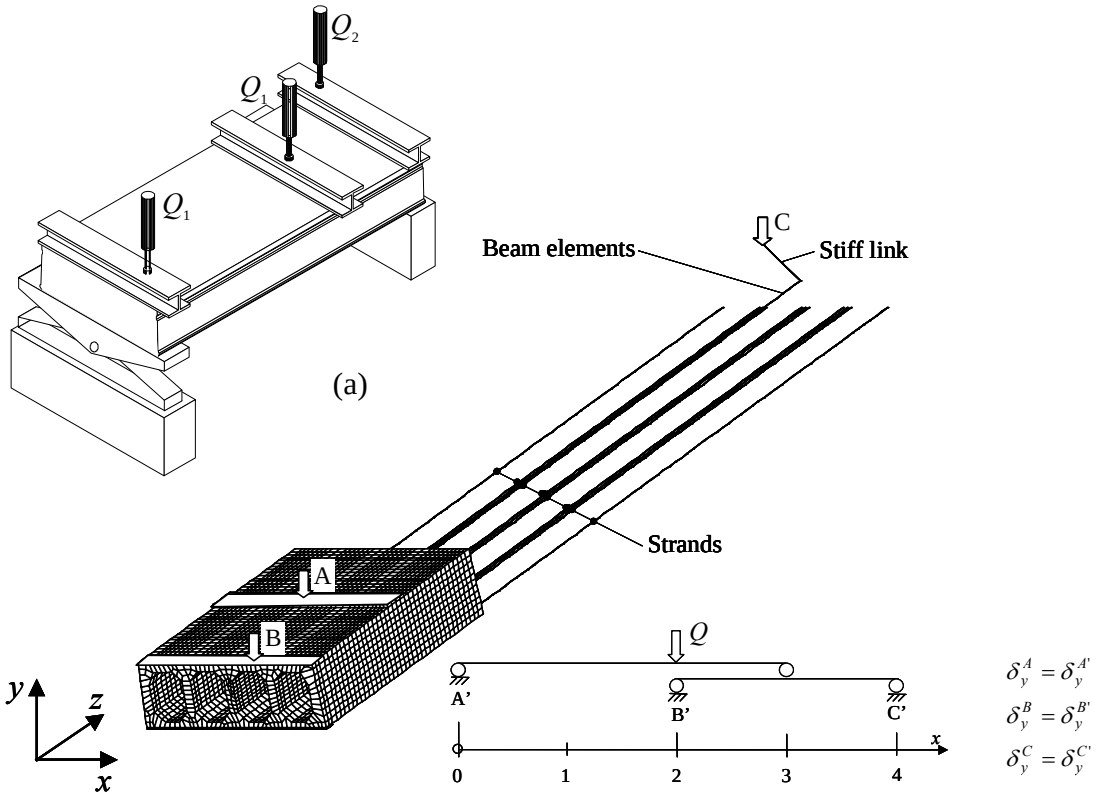

Figure 4.10 (a) Overview of test arrangement, modified from Pajari (2004a). (b) One of the models used in the analyses of individual hollow core units to obtain a shear and torsion interaction diagram. Selected load combinations, but with a constant ratio of shear and torsion, were obtained by loading in different positions along the x-axis of the loading arrangement.

As described earlier, solid elements were used close to the load in the span, where the failure is likely, and beam elements elsewhere to avoid too time-consuming analyses. Although beam elements are not capable of describing a failure due to combined shear and torsion, the solid elements can do this. A positive effect of these choices is that the shear and torsion failure always takes place in the part modelled in detail. It should be noted that this might not be true if the whole hollow core unit is modelled with solid elements (or in tests with similar arrangements); for some of the load combinations close to pure torsion, the failure might not take place in the shear span, but instead at the other support. Instead of adding an equal shear force at the opposite support, the use of beam elements in this part of the hollow core unit not only decreases the analysis time, but also solves this problem.

The finite element analyses of hollow core units revealed a non-linear interaction between shear-torsion capacities, rather than the linear relation given in EN 1168, see Figure 4.11. For most combinations of shear and torsion, the analyses gave higher capacities than the method in EN 1168. The increase was up to 55% for the 200 mm

thick unit, Figure 4.11(a), and up to 30% for the 400 mm thick unit, Figure 4.12. The failure mode changed gradually with the ratio of shear to torsion. The final crack pattern varied from a diagonal crack in the upper flange, for combinations close to pure torsion, to shear tension cracks in the webs and also bending cracks in the bottom flange, for combinations close to pure shear, see Figure 4.12. For several combinations, cracks were observed in the analyses before the maximum load was reached; this indicates a redistribution of stresses.

The effects of shear span and the influence of the prestressing transfer zone on the shear-torsion capacities were also assessed. As could be expected, the capacities were higher when the shear span was outside the prestressing transfer zone, except for loading close to pure torsion, see Figure 4.11(b). The shear spans influenced the capacities; shorter shear span gave higher capacities. This indicates that it is hard to predict a shear-torsion capacity that is not influenced by the boundaries.

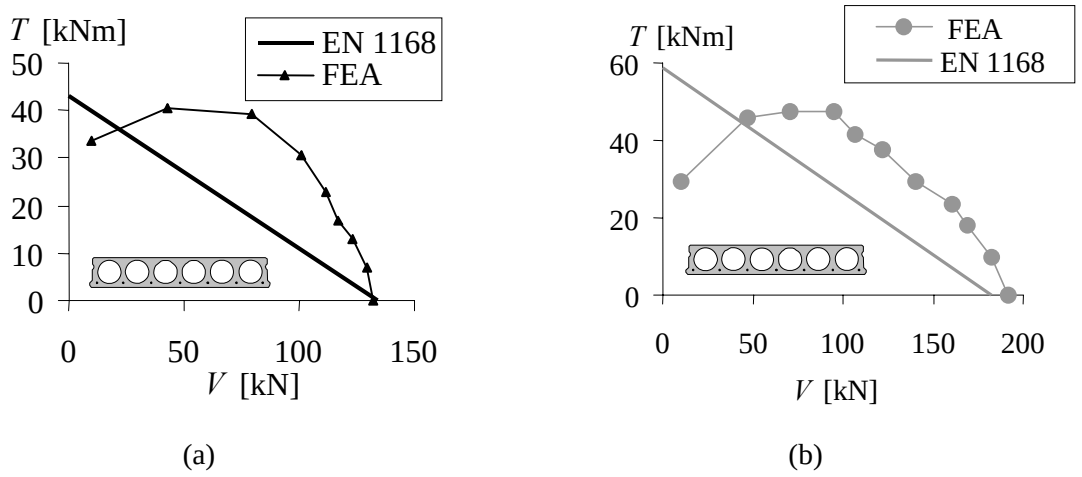

(a) (b)

Figure 4.11 Shear-torsion capacities presented in shear and torsion interaction diagrams: (a) for 200 mm units with the prestressing transfer region inside the shear span; (b) for 200 mm units with the prestressing transfer region outside the shear span. Each point is the result from one analysis, shear-torsion capacity: the shear force and torsional moment are calculated for the maximum load.

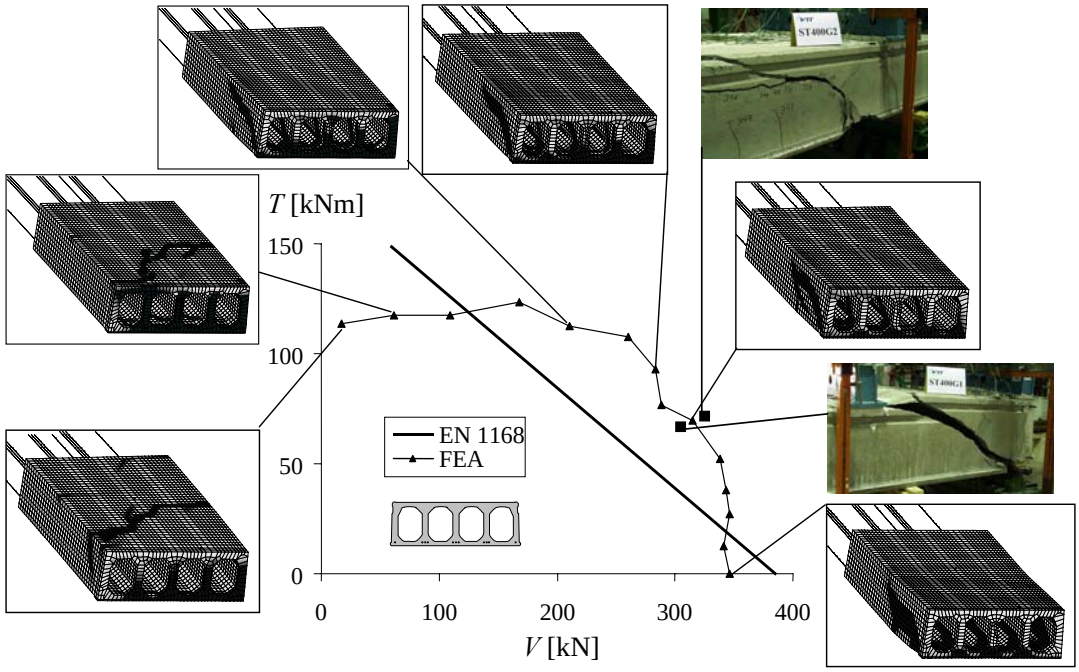

Figure 4.12 Shear and torsion interaction diagram for 400 mm units with the prestress transfer region inside the shear span. Each point is the result from one analysis, shear-torsion capacity: the shear force and torsional moment are calculated for the maximum load. Crack patterns just after maximum load for some load combinations.

4.3 A modelling method for hollow core floors

A modelling method for complete hollow core floors can be found in Paper II. The intention was to combine this global model with the model of one hollow core unit (Section 4.2) in the part of the floor were the failure was expected. The global floor model is thus not intended to be able to describe a shear and torsion failure of a floor, only its response until shear and torsion cracking occurs.

The cross-section of each hollow core unit is represented by one beam element, see Figure 4.13. Nodes known as slave nodes are positioned in the corners of the hollow core units; see Figure 4.13(b). These slave nodes are tied to the beam nodes in all directions, i.e. they are forced to follow the deflection and rotation of the cross-section, assuming plane sections remaining plane and a stiff rotation. Between the slave nodes in adjacent hollow core units, connecting elements are positioned. These describe the mechanical behaviour of the longitudinal joints between the units. In the normal direction, both compressive and tensile forces are allowed, but a very small stiffness is used for the tensile side, to represent cracked concrete in the joint. In the shear directions, (both vertically and in the direction along the hollow core units) a shear stiffness is used.

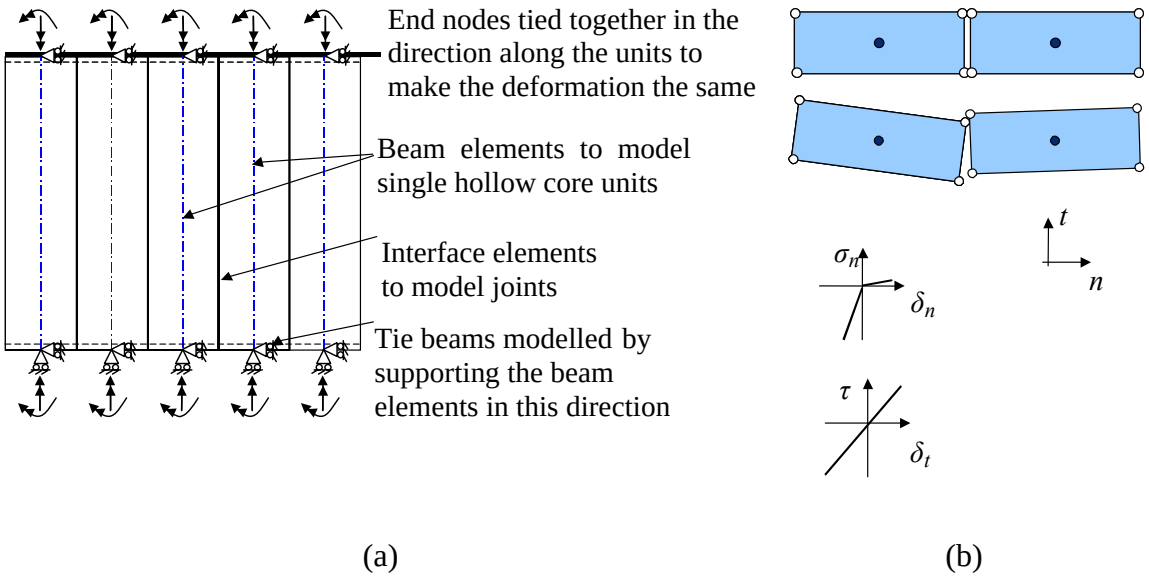

Figure 4.13 (a) Global model proposed for modelling whole hollow core floors. (b) Modelling of joints.

Comparisons with test results showed that this global model could, with reasonable accuracy, describe the real behaviour of hollow core floors. An example is shown in Figure 4.14, where the deformations measured in a test of a floor supported on three edges (Walraven and van der Marel (1992)) are compared with results from a finite element analysis. As can be seen, the general agreement is very good. For loads close to failure, the displacements were underestimated. However, the floor model is not intended to show the behaviour after cracks due to combined shear and torsion appear. Thus, the results are not unexpected.

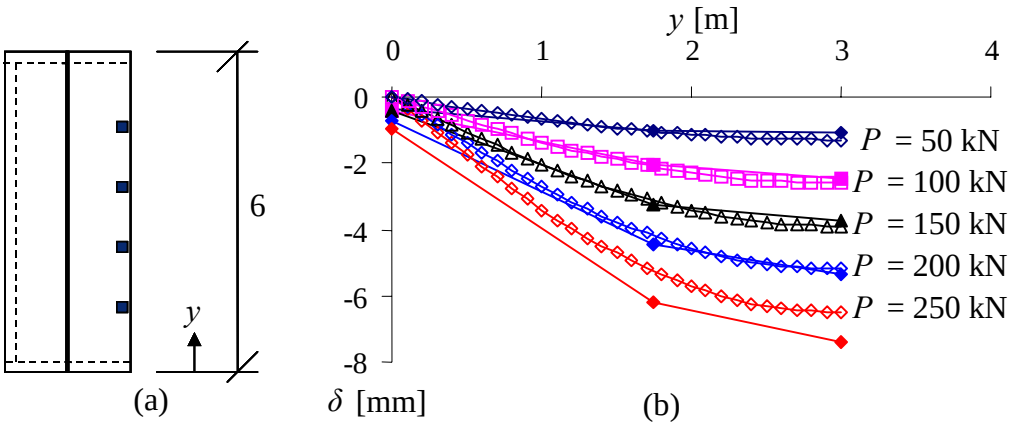

Figure 4.14 (a) Test set-up for a floor supported on three edges, test No. 1 (Walraven and van der Marel (1992)); point loads were applied in the marked positions; (b) The displacements measured in this test (filled markers) are compared with results from analysis.

4.4 An improved design approach for hollow core slabs

With the modelling methods proposed, the design approach for hollow core floors subjected to combined shear and torsion can be improved and applied at simple or more advanced levels. Including the traditional approach, the design can be applied at four levels, see Figure 4.15. Level IV represents the traditional approach by which designers work today: the sectional forces are estimated with diagrams provided in EN 1168, CEN/TC229 (2005), after which the sectional resistances are calculated with analytical models, see Section 2.2. An improvement of the design approach, Level III, is to use the proposed global floor model to evaluate the sectional forces, see Section 4.3. One is no longer limited to standard examples; instead floors with arbitrary geometries and load cases can be analysed. This can be combined with the traditional approach to calculate the sectional resistance. A further improvement, Level II, is to use the floor model to calculate the bending moment, shear force and torsional moment, while the finite element modelling of a hollow core unit offers shear and torsion interaction diagrams which give the resistance of the hollow core unit for the region selected; see Section 4.2.1. At design Level I, the model of one hollow core unit is integrated with the global floor model to enable modelling of failure due to combined shear and torsion in one hollow core unit within a floor, see Section 4.4.2.

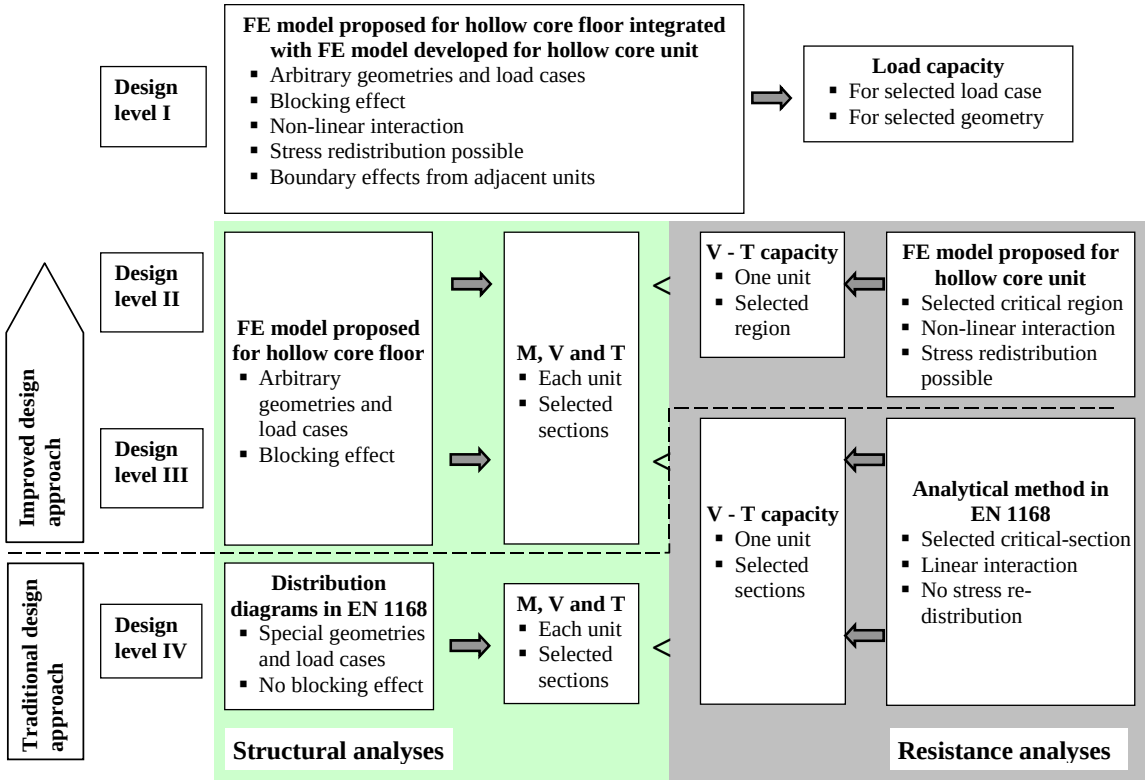

Figure 4.15 With the modelling methods proposed, the design approach for hollow core floors subjected to combined shear and torsion can be improved in steps. Including the traditional approach, the design can be applied at four levels.

4.4.1 Design of hollow core floors using interaction diagrams

An example of how a floor can be designed with interaction diagrams on the basis of the modelling methods developed (Level II and III in the improved design approach) is introduced here and capacities are compared with a test result. The floor consists of four 400 mm thick hollow core units; it is similar to one tested at VTT in 2002.

In the floor tested, the hollow core units were grouted together on supports made of concrete beams. The floor was first loaded with a one-point load of about 100 kN at 12 positions across the floor. Afterwards, the floor was loaded with a one-point load (No. 13) until failure; since punching failure in the loaded unit occurred, two more failure loadings were possible, each with two point loads at different positions. For more information about this test, see Pajari (2004b). Here one of the failure loadings with two point loads (No. 14) is considered, see Figure 4.16(a).

The floor model proposed was used for the whole floor, resulting in combined shear and torsion in each hollow core unit. The most critical unit was the one loaded; the maximum shear force and torsional moment occurred in the cross-section at the point loads. Figure 4.16(b), shows how the shear force and torsional moment in the critical cross-section increased with increasing load, together with the predicted resistance of the hollow core unit. Due to the dead weight, the shear force has a starting value, while the torsion is zero for dead weight only. As the prestressing transfer region is within the failure zone, the resistance of the unit is calculated according to this. The estimated maximum load according to the method in EN 1168 (Design Level III) was P = 357 kN; however when the shear and torsion interaction diagram from the finite element analyses described previously (Design Level II) was used, the estimated maximum load was P = 449 kN. These can be compared with the maximum load measured in the test, P = 521 kN. It should be noted that no safety parameters were included in any of the estimated failure loads.

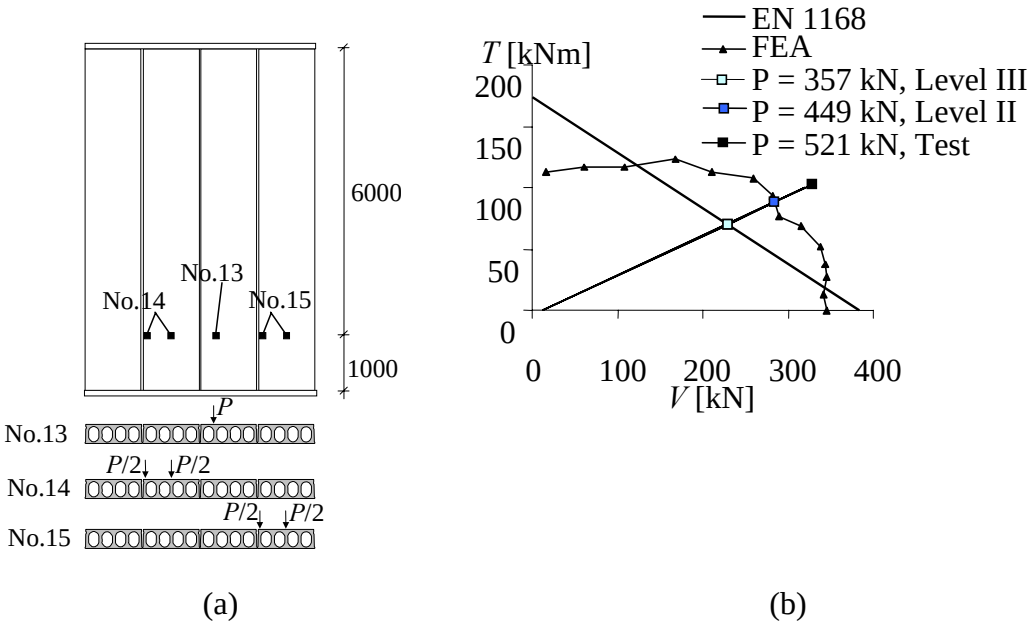

(a) (b)

Figure 4.16 (a) Floor tested and analysed; (b) The maximum load is determined in the shear and torsion interaction diagram for loading No. 14.

4.4.2 Design of hollow core floors with a model of a hollow core unit

To enable the prediction of the behaviour at failure due to combined shear and torsion in a hollow core floor, the more detailed model of one hollow core unit was integrated with the global floor model, see Figure 4.17. The floor tests described in the section before, see Figure 4.17(a), were analysed; three loadings were compared with test results. The agreement was quite good concerning failure mode, crack pattern, maximum load and displacements, see Figure 4.18 and Paper II.

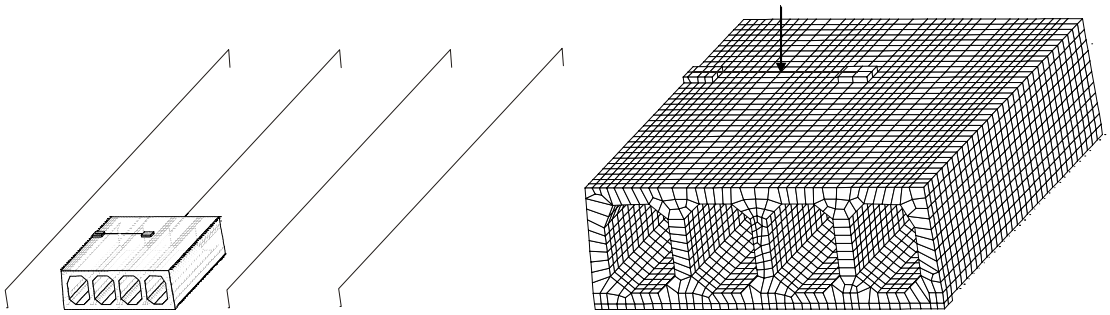

(a) *(b)*

Figure 4.17 (a) Finite element mesh with solid elements integrated with simplified global model, used in analysis of the floor tested by Pajari (2004a), load in position No. 14. (b) Part with solid elements enlarged.

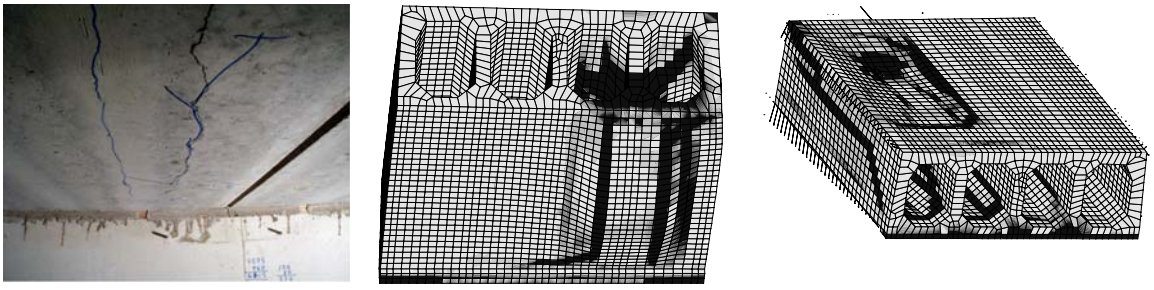

(a)

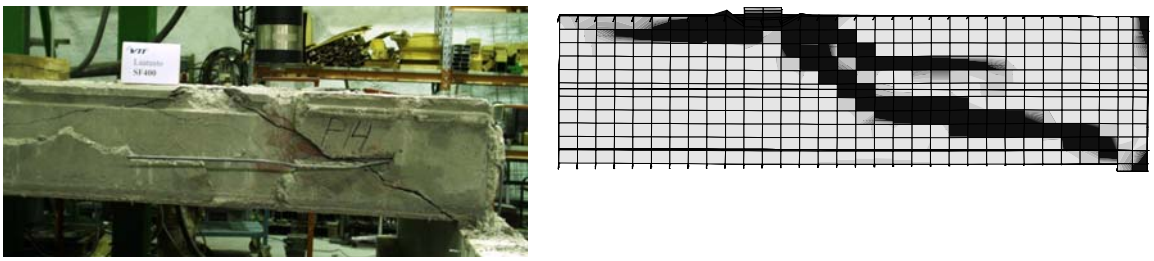

(b)

Figure 4.18 Crack patterns from floor tests and corresponding analyses: (a) loading position No.13; (b) loading position No.14.

Some of the tests and analyses indicated that a hollow core unit can carry greater amounts of shear and torsion, when placed in a floor system, than can be attributed only to the distribution of load effects to the neighbouring elements. An example is given in Figure 4.19. The explanation could be that the stress state in a unit placed in a floor differs from that in a single unit, even if the sectional forces, i.e. the shear force and the torsional moment, are the same. Consequently, the restraints at the boundaries of adjacent units seem to yield a more favourable stress state, or greater potential for redistribution within the unit. Future research may reveal whether this conclusion also holds for other floors and, if so, whether it can be taken into account in design.

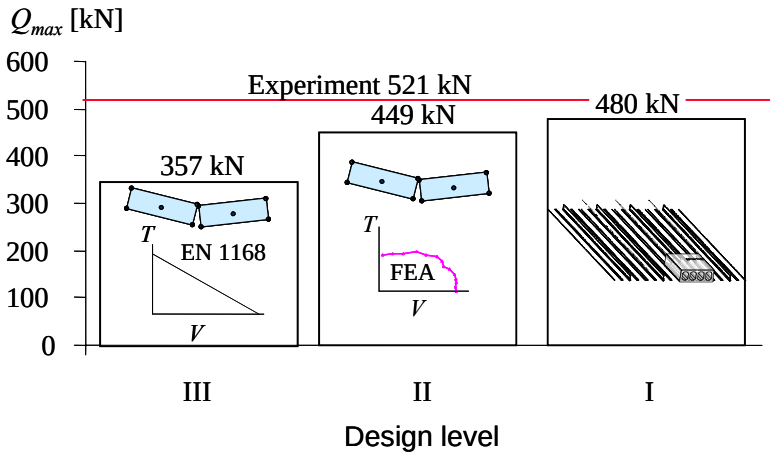

Figure 4.19 Maximum loads evaluated with levels I-III in the improved design approach compared with maximum load measured in the test, loading position No.14.

5 Analysis of prestressed concrete bridges

Since most of the existing bridges were designed and constructed, the traffic loads have increased and the structures have deteriorated. Hence, many bridges are now subjected to higher loads than they were designed for. It is therefore important to ensure that they behave properly under increased loads and actual conditions; when necessary, the existing bridges must be upgraded. The principal aim of design and assessment of concrete structures is the same: to demonstrate that the structure has the required load carrying capacity in the ultimate limit state and satisfactory performance under service conditions. However, in design there are large uncertainties in regard to the overall behaviour, the material properties, and the loads. A conservative design can be made without great cost. In assessment some of these uncertainties can be reduced by measurements, testing and monitoring. An overly conservative assessment may lead to a misapprehension that the requirements are not fulfilled, with unnecessary strengthening or demolition as a consequence. Therefore, it is important to predict the actual load carrying capacity as closely as possible.

For structural assessment of concrete bridges, the non-linear finite element method has become an important and increasingly used tool. In Sustainable Bridges (2007) it is stated that non-linear analysis is the analysis method with the highest potential for discovering any additional sources of the load-carrying capacity of concrete bridges. The number of references on this subject is rather limited: e.g. Huria *et al.* (1993), Chowdhury and Ray (1995), Shahrooz *et al.* (1994), Ho and Shahrooz (1998), Plos (2002), Plos and Gylltoft (2002) and Song *et al.* (2002). An overview of the structural assessment of bridges with the finite element method is presented in Sustainable Bridges (2007). The method has shown a greater potential in revealing higher load carrying capacity than conventional assessment methods. The structural effects utilized to achieve a higher capacity have mainly been associated with bending moment and normal forces. In these cases, the higher capacity can be explained by a more favourable force and stress distribution, when the structure has been analysed in three dimensions and by taking the fracture energy associated with cracking concrete into account, Plos (2002), Plos and Gylltoft (2002). Also the design of prestressed concrete bridges could benefit from improved verifications with non-linear finite element analyses.

5.1 Prestressed concrete bridges

The idea of prestressed concrete was developed in the early 1900s, and in the mid 1930s the first successful prestressed concrete bridges were built. After the Second World War, prestressed concrete bridges were widely used in the reconstruction of the infrastructure in Europe.

Box-girder bridges are suitable for spans from 40 m up to 270 m, Hewson (2003). The box girder is efficient for both longitudinal and transversal design, and the appearance is widely considered to be aesthetic. The high torsional stiffness of the box-girder makes it suitable for curved alignment. Either full-height scaffolding or a balanced cantilever method is used for construction. The first bridge built with the balanced cantilever method was a reinforced concrete bridge in Brazil in 1930, Hewson (2003).

In 1950 the method was used also for prestressed concrete bridges. With this method the box-girder is built in short segments out from each side of a pier in load balanced sequences. Bridge structures with one long span and two or four smaller spans normally have box-girders of varying depth. After casting, each segment is post-tensioned with prestressing tendons usually placed in the top flange, before the next section is constructed. While being erected, the structure is statically determinate and self balanced; the dead weight is balanced by the prestressing in the top flange. When the cantilevers from adjacent piers meet at mid-span, they are connected. This can be done with a hinge connection which disables transfer of bending moment while enabling shear transfer and relative longitudinal deformations, or with a connection that makes the bridge continuous in the span, Figure 5.1. Complementary prestressing in the bottom flange is needed in such a connection to prevent cracking due to long term effects and additional load.

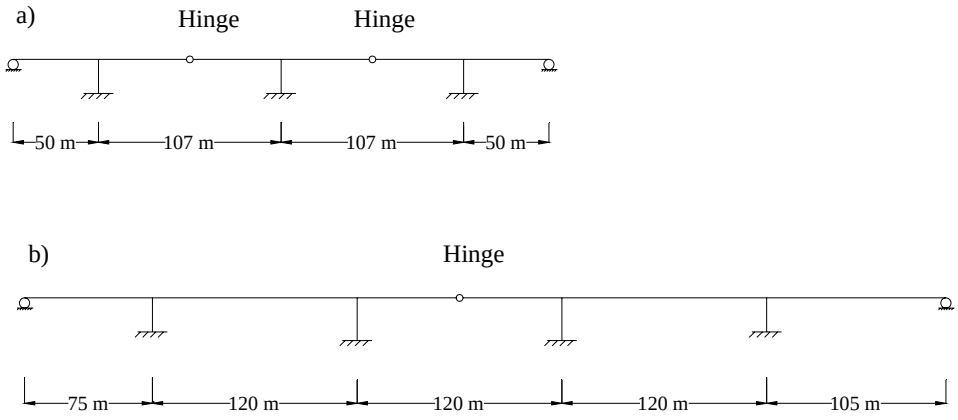

Figure 5.1 *Static system of (a) a bridge with hinge connections in the spans, the Källösund Bridge; and (b) a bridge with continuous spans, the Hammarsund Bridge. Engel and Kong (2008).*

For a hinge connection, the zero moment at the end of each cantilever is achieved by arranging the ends of the prestressing tendons inclined down into the webs; this also increases the shear resistance in these segments, Figure 5.2 (a). Another way of preventing uplift of the cantilever end is to balance the prestressing in the top flange with prestressing also in the bottom flange, Figure 5.2 (b). Due to easier construction, this method has been used in more recent designs in Sweden.

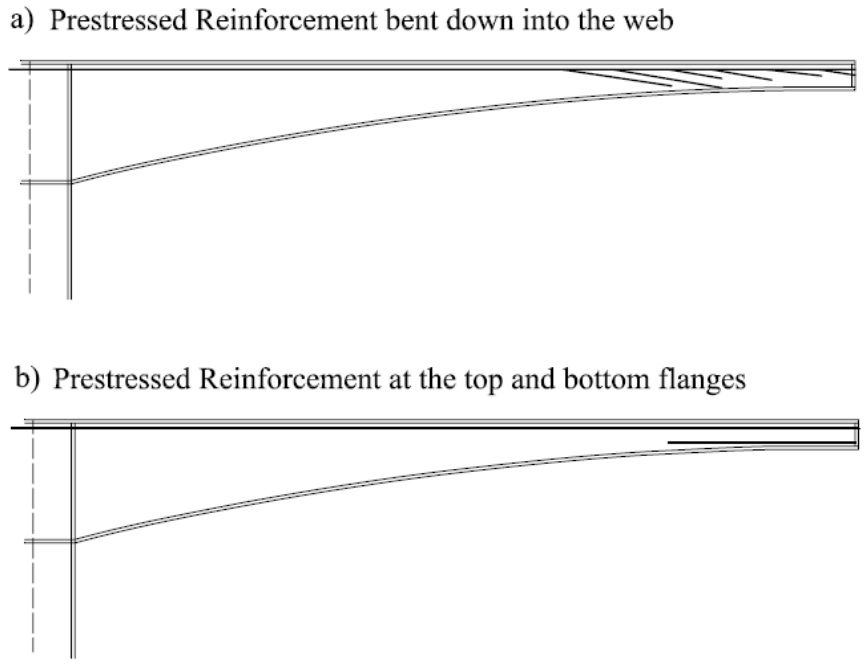

Figure 5.2 Arrangement of prestressing tendons in a box-girder cantilever; (a) in the top flange and with inclined ends down into the web, and (b)both in the top flange and in the bottom flange. Engel and Kong (2008).

Multiple actions govern the design of the box cross-section. The top flange is designed mainly to resist local bending and punching shear from the live load. The web thickness is governed by the shear resistance for vertical shear and torsional moment. The bottom flange is designed to resist the compression caused by the longitudinal moments and the influence from torsional stresses in the box; it is normally thicker towards the support, Chen and Duan (2000).

To satisfy performance in the service state and to prevent problems due to durability it is important to prevent shear cracking or to limit the width of shear cracks. Common models for the estimation of crack widths caused by shear in the serviceability limit state are poor: minimum requirements or simplified approaches are often used. In the Swedish code for bridge design, the requirements for minimum reinforcement in the webs have been changed over the years. The latest change was due to shear cracks discovered in the newly constructed prestressed concrete box-girder bridges in Stockholm, the Gröndal Bridge and the Alvik Bridge, Malm (2006). In the current code, BRO 2004 (2004), the minimum reinforcement amount is 400 mm^2 / m, placed with a maximum spacing of 300 mm. Additionally, when the characteristic concrete tensile strength, f_{ctk}, is higher than 2.0 MPa, the amount of minimum reinforcement should be increased, multiplied by a factor of f_{ctk} / 2.0. If the width of shear cracks is not taken into account, estimated and checked, in the serviceability limit state, a simplified approach can be used; for design in the ultimate limit state, the design strength of the shear reinforcement is limited to 250 MPa.

For prestressed concrete box-girder bridges, the risk of failure due to combined shear and torsion can be a major problem. The box-girder is mainly prestressed in the top flange and the webs are proportionally thin and sparsely reinforced, which make these

webs sensitive to shear. The webs of a box-girder can be idealized as an assembly of membrane elements subjected to in-plane shear and normal stresses, also known as shear panels, see Figure 5.3.

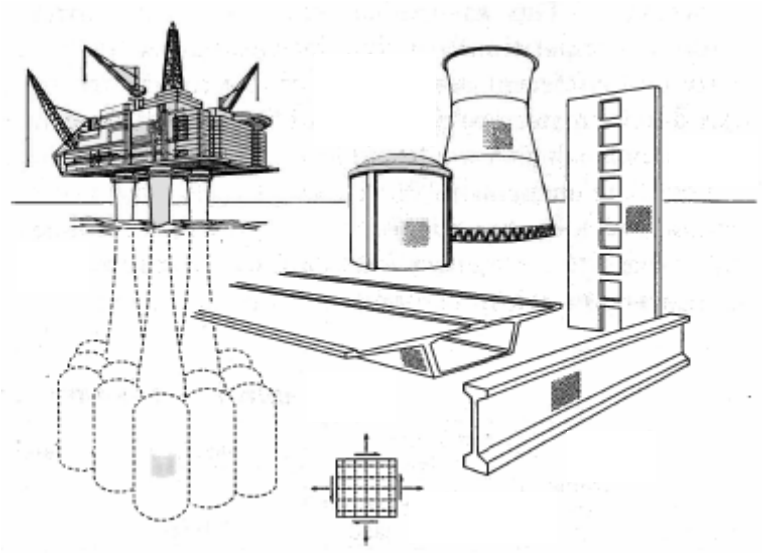

Figure 5.3 Structures that can be idealized as an assembly of membrane elements, Vecchio and Collins (1986).

5.2 A modelling method for large members with shear reinforcement

Paper IV introduces a modelling method worked out to analyse the shear response and shear failure of reinforced and prestressed concrete members. The method should be applicable to large structures, for example box-girder bridges, subjected to various loads. Hence, the concrete was modelled with four-node curved shell elements. Full interaction was assumed between the reinforcement or prestressing tendons and the concrete, by using embedded reinforcement layers. For the concrete a constitutive model, based on non-linear fracture mechanics, and a rotating crack model, based on total strain, were used; see TNO (2004). The hardening of concrete in compression was described by the expression of Thorenfeldt, and the reduction of the strength due to transverse tensile strain was modelled according to Vecchio and Collins, as described in TNO (2004). When a rotating crack model is used and the reinforcement is modelled as perfectly bonded to the concrete, the *concrete contribution* to the shear capacity can be accounted for by modifying the constitutive relations describing the behaviour of the materials, for example the tensile response of concrete (Section 3.2). Therefore, two approaches were compared for the tension softening; see Figure 5.4:

- The curve by Hordijk, as described in TNO (2004), where only the fracture energy of plain concrete is taken into account; and
- a curve modified according to the expression from the MCFT by Collins and Mitchell (1991), which attempts to take into account also the *concrete contribution*, i.e. tension stiffening, aggregate interlock and dowel action.

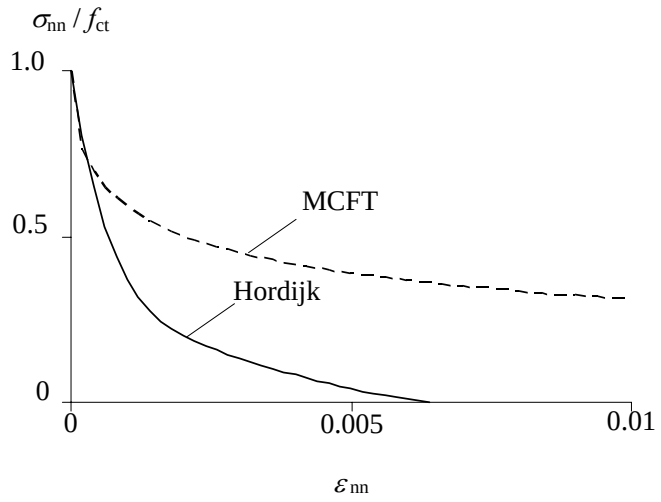

Figure 5.4 Two tension-softening relations compared for the 'Houston panel' A3. For the curve by Hordijk the fracture energy is smeared over a length of 150 mm (the crack band width, h), which corresponds to the calculated average crack spacing.

The modelling method was verified by analysing several tests: orthogonally reinforced shear-panels loaded in pure shear, and reinforced and prestressed beams loaded in bending, shear and torsion, see Paper IV. In the specimens analysed, the amount of shear reinforcement varied from 0.2 % up to 3 %; the thicknesses of the specimens varied from 0.07 m up to 0.189 m. The principles of the test arrangement for the 'Toronto shear panels', tested by Vecchio and Collins (1986), and the 'Houston shear panels', tested by Pang and Hsu (1995), together with the corresponding models used for the finite element analyses are shown in Figure 5.5.

Comparison of results such as shear stress versus shear strain relations, from tests and analyses, showed that four-node curved shell elements combined with embedded reinforcement can describe the shear response, Figures 5.6 and 5.7. Moreover, with only the fracture energy of plain concrete taken into account, the capacity was underestimated and the average strains, i.e. the crack openings, were overestimated. In contrast, when the *concrete contribution* to the shear capacity was included, with a tension-softening curve according to the expression from MCFT, the capacity was overestimated and the average strains underestimated for most panels. It should be mentioned that results from the 'Toronto shear panel' tests were included in the test results used to calibrate the expression in the MCFT. Consequently, the use of the tension-softening curve according MCFT resulted in a better agreement for the 'Toronto shear panel' tests than for the 'Houston shear panels' tests analysed. The results also showed the importance of including the reduction of compressive strength owing to transverse tensile strain. This influenced the response, the capacity and the failure mode.

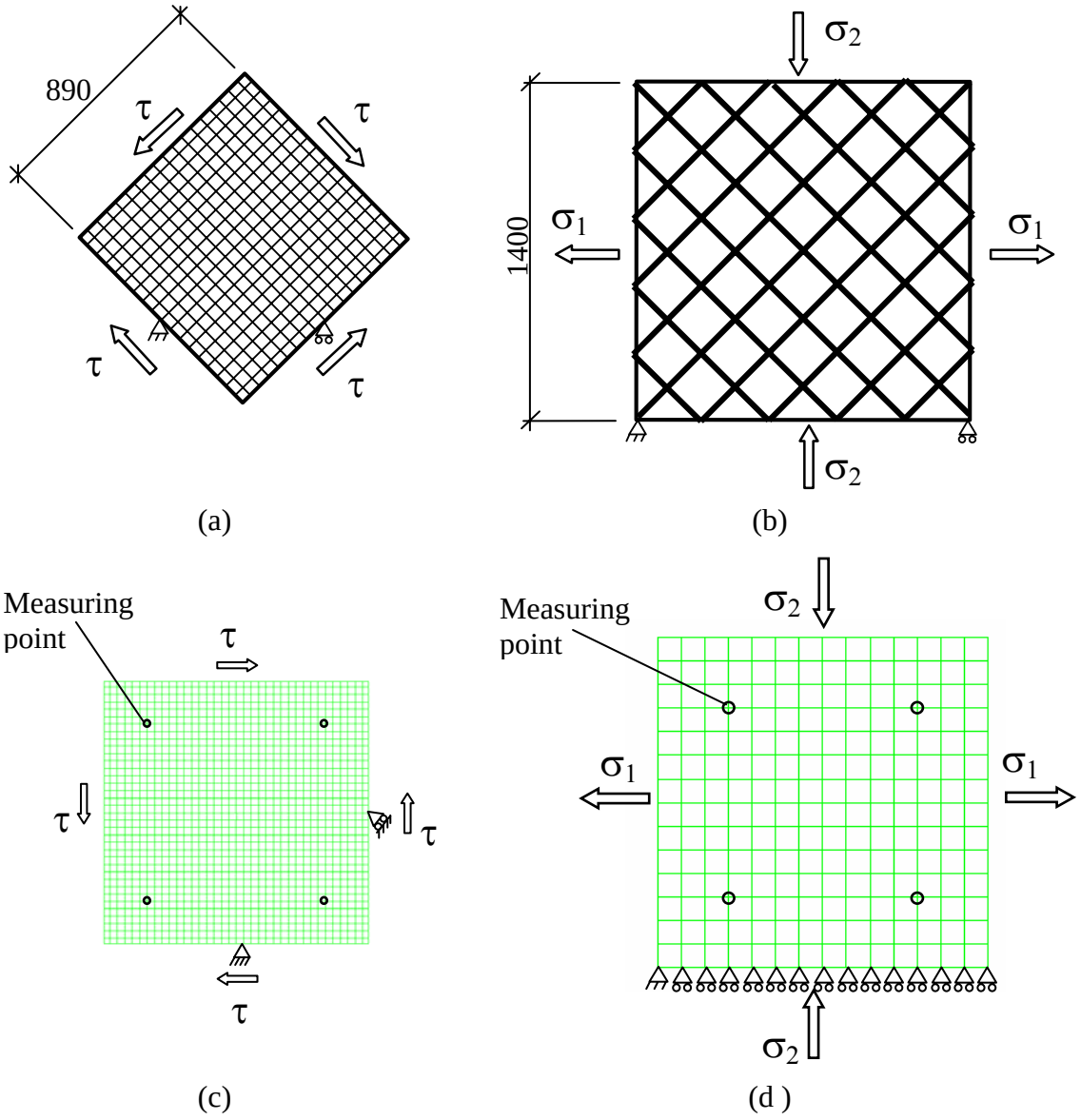

Figure 5.5 *Main principles of the testing arrangement of (a) the 'Toronto shear panels' and (b) the 'Houston shear panels'. The principle of the finite element models used to analyse (c) the 'Toronto panels' and (d) the 'Houston panels'.*

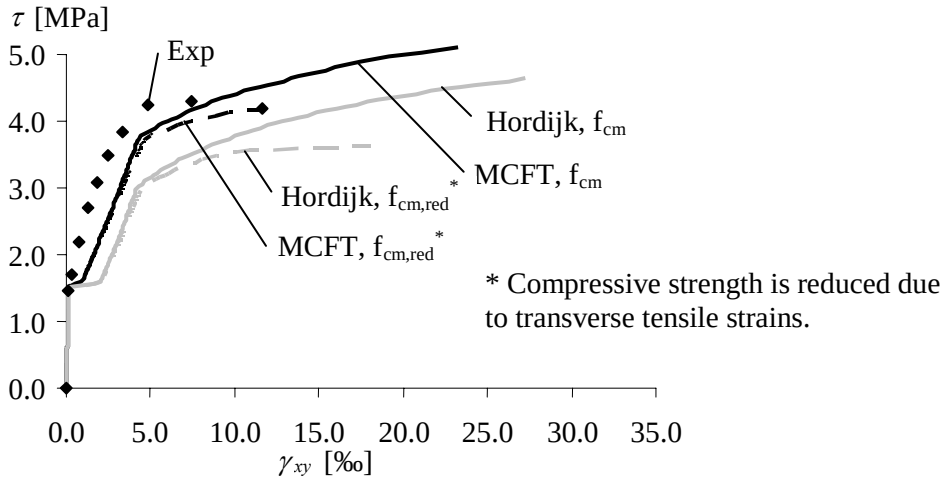

Figure 5.6 Comparison of results from test (Vecchio et al. *(2001)) and analysis of PV20; applied shear stress versus shear strain.*

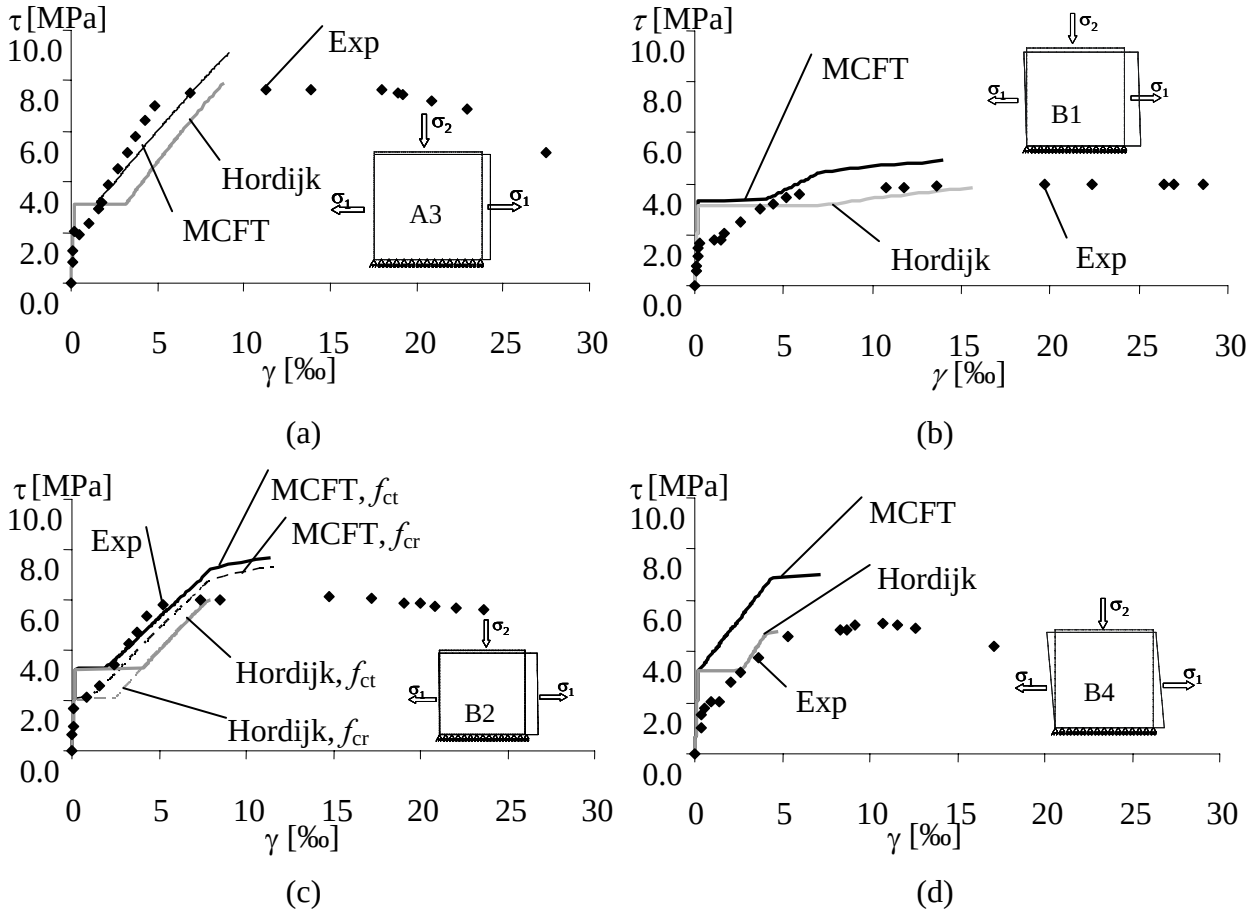

Figure 5.7 Comparison of results from tests and analysis of the Houston panels, applied shear stress versus shear strain: (a) A3; (b) B1; (c) B2; (d) B4. In all the analyses presented in this figure, the concrete compressive strength was reduced owing to transverse tensile strain.

Moreover, the results also showed that the stiffness of the panels decreased and the directions of the principal stresses and the principal strains changed when the cracking was initiated, Figure 5.8. These effects become more pronounced when the reinforcement in the weakest direction started to yield, Figure 5.9

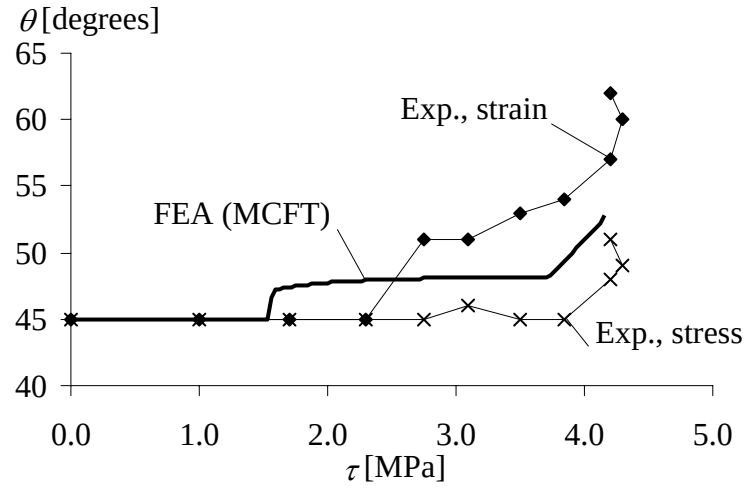

Figure 5.8 Comparison of results from test and analyses for PV20; applied shear stress versus principal strain direction and principal stress direction.

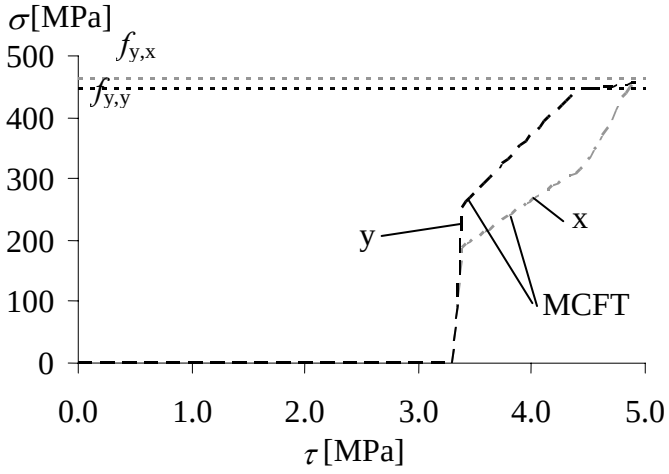

Figure 5.9 Results from FE analyses: applied shear stress versus steel stress in longitudinal (x) and vertical (y) reinforcement for the 'Houston Panels' B1.

The generality of the proposed modelling method was investigated by modelling and analysing two beam tests, a prestressed concrete box-beam, loaded in bending, shear and torsion, and a reinforced concrete beam, loaded in four-point bending, see Paper IV. It was concluded that an analysis of a concrete member with shear reinforcement, subjected to shear, torsion and bending, will be on the safe side when evaluating the load-carrying capacity or crack widths, if the fracture energy alone is

used to define the unloading branch of the concrete in tension. Hence, the load-carrying capacity will probably be slightly underestimated and the crack widths overestimated to some extent.

To further evaluate the methodology proposed, and to verify its applicability and reliability for the assessment of bridges, the load-carrying capacity of a prestressed concrete box girder bridge, the Källösund Bridge, was evaluated in a case study which is given in Paper V; see also Section 5.4.

5.3 A modelling method for small members with shear reinforcement

To reflect, more accurately, the response of reinforced concrete members loaded in shear, all aspects of the *concrete contribution* needs to be taken into account. If a rotating crack model and embedded reinforcement are used to model the member, this can be done approximately by modifying the material response. The *concrete contribution* is influenced by the softening of cracking concrete, the bond between the reinforcement and the concrete, the dowel action of the reinforcing bar, and the friction due to aggregate interlocking. By modelling the reinforced concrete in more detail, some of these effects can be included in the model. The bond between the reinforcement and the concrete can be accounted for by modelling the reinforcement bars separately and then connecting them to the concrete with interface elements describing the bond stress-slip relationship. The dowel action can be included by modelling the reinforcement bars with beam elements. Such a detailed modelling method was worked out by Martin (2007) in a master's thesis project made in connection with this work. This modelling method for detailed analysis was verified by simulating several of the shear panel tests used to verify the previously presented modelling method for large members with shear reinforcement (Section 5.2 and Paper IV).

Only a small interior part of a shear panel was modelled in a more detailed way; see Figure 5.10. The model was loaded with pure shear applied with deformation control along each edge of the model; see Figure 5.10. To satisfy the compatibility of the shear panel, the edges of the model were forced to rotate equally and to be parallel with each other. The edges were also forced to be straight, but the nodes on the edges were free to move along the edge.

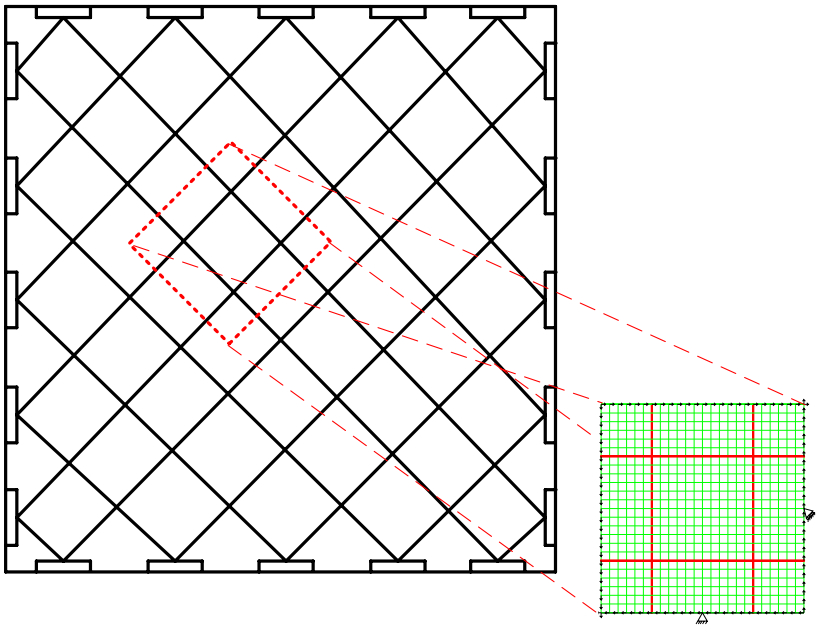

Figure 5.10 Principles of the testing arrangement for the shear panel and the finite element model of an interior part of the tested panel. Martin (2007)

The shear stress versus shear strain relation was compared with those from the previous analysis and the tests; see Figure 5.11.

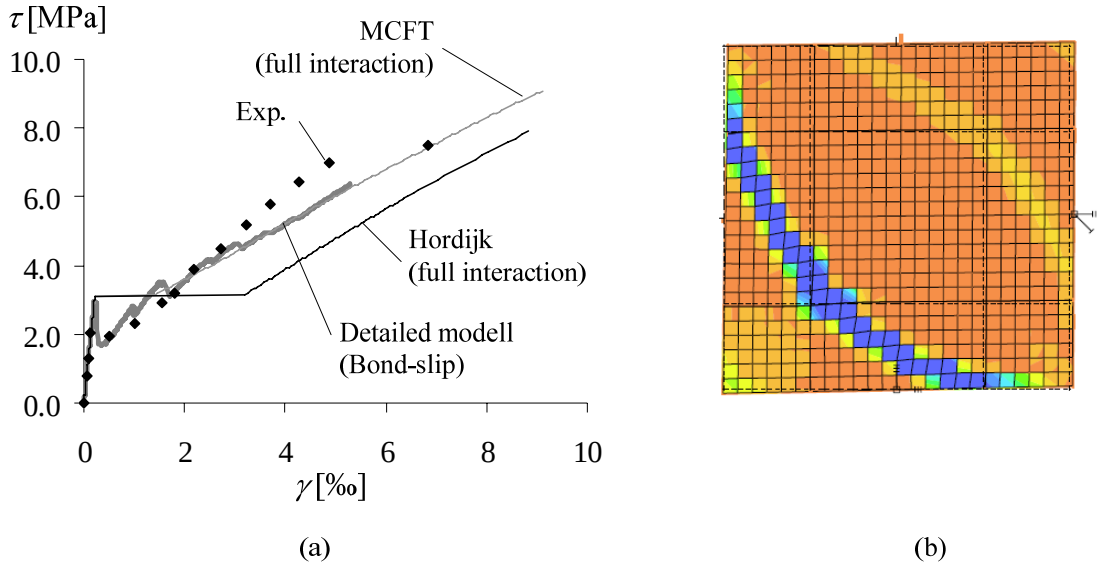

Figure 5.11 The Houston shear panel test A3, (a) comparison of results from test and analyses, shear stress versus shear strain and (b) crack pattern form analysis with detailed model.

The predicted response agreed well with test results for panels with similar or almost similar reinforcement in orthogonal directions. However, for panels in which the amount of reinforcement differed a lot in the two directions, the behaviour was well predicted only for small loads. When the load was increased and the reinforcement in one direction started to yield, the response was unrealistic. The cracks that formed in

the analyses had an unrealistic curved form due to the boundary conditions; see Figure 5.11 (b). This was the main drawback to this modelling method; it was concluded that the boundary conditions influenced the shear response in the analyses. To analyse the shear panel tests on this detailed level, the whole shear panel, including the shear keys used to apply the load, needs to be modelled.

5.4 The modelling method applied to a prestressed concrete bridge

A case study was made to verify the applicability and reliability of the modelling method proposed, for large concrete members with shear reinforcement, (Section 5.2) in analysing concrete bridges. It would have been preferable to have for the case study a prestressed concrete bridge that had been tested to failure due to shear and torsion. However, full-scale tests on concrete bridges are rare; the author has not been able to find any suitably tested bridge on which to use the modelling method. The Källösund Bridge was chosen for the case study since it has previously been extensively assessed and was then judged to have insufficient load-carrying capacity for combinations of shear and torsion. A lot of information regarding the Källösund Bridge was available.

The Källösund Bridge is a prestressed concrete box-girder bridge of the balanced cantilever type, built with the free cantilevering method in the late 1950s. The bridge has a total length of about 325 m, divided into four spans, and is supported on three piers and two abutments. In the top flange of the box girder, there are both longitudinal and transversal prestressing tendons. The ends of the longitudinal tendons in the last segments of the cantilevers are positioned diagonally down into the webs. The webs are reinforced with $\phi 10\ s300$ in both directions and on both sides. This can be considered as a very low amount of shear reinforcement. More detailed descriptions of the bridge can be found in Paper V, Plos *et al.* (2004), Plos (2004), Enochsson *et al.* (2004) and Plos and Gylltoft (2006).

A conventional structural assessment and several enhanced assessments with more advanced methods have been made for the Källösund Bridge. According to the conventional assessment, strengthening was required for combinations of shear and torsion along substantial parts of the bridge. For the critical load combination and the critical section, a more thorough assessment was made; see Plos *et al.* (2004). To try to reveal a higher load-carrying capacity than the one evaluated in the conventional assessment, other more refined methods were used on the bridge. Probabilistic methods taking material properties and the load situation into account were used – see Jeppson *et al.* (2004) – as well as improved methods for combinations of shear, torsion and bending, Enochsson *et al.* (2004). In particular the MCFT (Section 2.3) was used to evaluate the load-carrying capacity. According to these evaluations, the bridge was found to have a lower capacity for bogie loads than required. Furthermore, the load-carrying capacity of the bridge was evaluated by using non-linear finite element analyses, see Plos (2004) and Plos and Gylltoft (2006), with which a substantially higher capacity was found. However, the modelling method used in the FE analyses was not verified against tests, and the results were questioned, see Plos *et al.* (2004). Therefore, the bridge was strengthened with glued fibre-reinforced laminates.

The evaluation conducted in this study was improved, compared with the previously made assessment using non-linear FEM, in several respects:

- the modelling method used was verified;
- long-term effects due to concrete creep were taken into account;
- the reinforcement was modelled more accurately;
- the final loading with traffic point loads was made with displacement control; and
- several analyses were made to study some safety formats, which are suitable for evaluation of the design load capacity, by using non-linear analysis.

To include the effects of force redistribution, the construction history, and the loading sequence, the whole bridge needs to be modelled. A coarse mesh of shell elements with embedded reinforcement for the critical part of the bridge was therefore combined with beam elements for the rest of the bridge, Figure 5.12. For the critical part of the bridge, the modelling method worked out and verified in Paper IV (Section 5.2) was used.

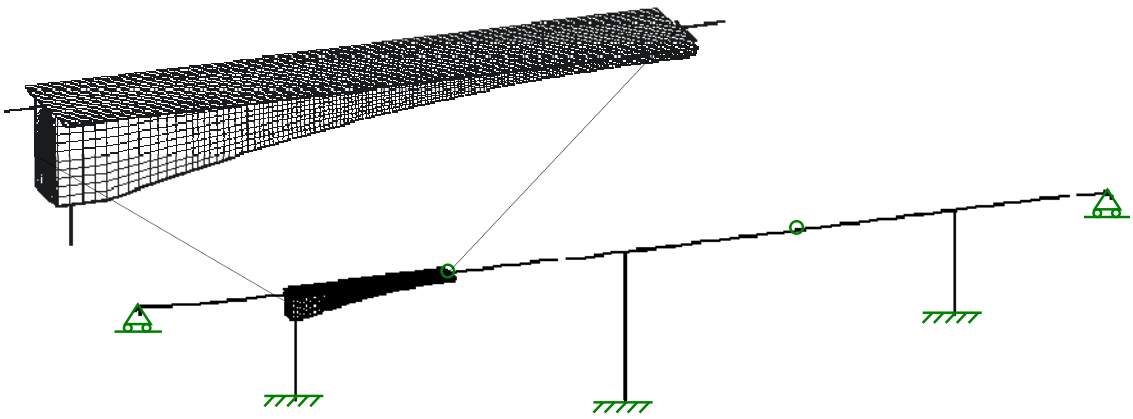

Figure 5.12 FE model of the Källösund Bridge used for the case study. Only the part of the bridge critical for shear and torsion is modelled in detail with curved shell elements, embedded reinforcement and non-linear material properties. The rest of the bridge is modelled with beam elements and linear material properties.

The analyses of the bridge were made in steps to include the construction history and the loading sequence. In the analyses the loads were gradually increased and the supports and tyings for the abutments and the mid-span hinges, respectively, were introduced in stages to represent the construction history. The bridge was loaded with several variable loads simultaneously up to their design value: crowd load on the causeway, distributed traffic load, horizontal and vertical traffic point loads, and wind loads. The failure was reached by increasing, in the last step, the vertical point loads of traffic, defined according to Vägverket (2004), which revealed the load carrying capacity represented by the resistance for a bogie load, B_R. Several point loads were increased simultaneously, using displacement control. This was made possible by a separately modelled statically determinate system of beams; a prescribed displacement was applied at one point and the reaction forces were transferred, in a controlled way, by the beam system to several points in the model.

Although the shear resistance limited the load-carrying capacity in the previously made assessments of the Källösund Bridge, the failure obtained in these non-linear finite element analyses was due to bending, Figure 5.13. However, shear cracks developed in large regions of the webs; thus, a shear response was observed and it could be concluded that the shear capacity of this part of the bridge, for this load combination, is higher than the load-carrying capacity determined in the analysis. Using safety formats more suitable for non-linear analysis (Section 3.3), the finite element analysis performed in this study revealed a load-carrying capacity corresponding to about 80% higher bogie load than in the previously made finite element analysis, Plos (2004), and over 100% higher than in the conventionally made assessment, Enochsson *et al.* (2004). Most of the increased capacity, in comparison with the previous finite element analyses, is probably due to the use of a more stable material model for cracked concrete and to the displacement-controlled loading.

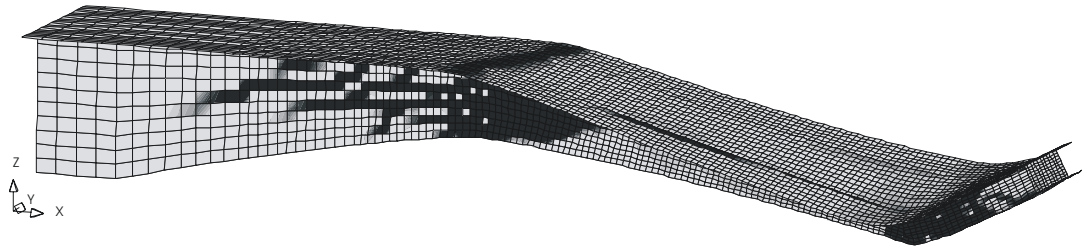

(a)

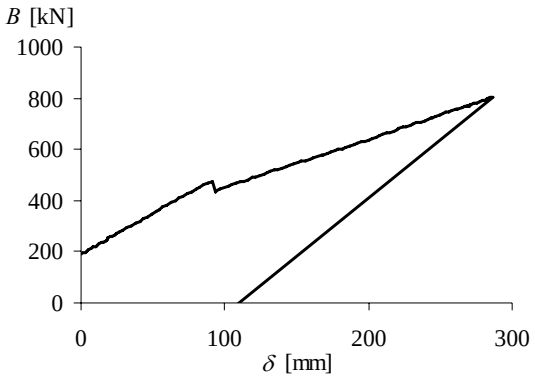

(b)

Figure 5.13 (a) Deformed shape of the detailed modelled cantilever after maximum load. (b) Applied bogie load versus cantilever end deflection.

The higher load-carrying capacity in the non-linear finite element analysis, when compared with conventional methods, is mainly governed by the location and inclination of the main shear crack, Figure 5.14. The web height increases in the direction of shear crack propagation, which influences the length of the shear crack and the amount of reinforcement activated in the crack. This was not taken into account in the conventionally made assessment. With the correct length of the shear crack the reinforcement contribution to the shear capacity of one web increased by 13% or 39% for a crack inclination corresponding to $\cot\theta = 1$ or $\cot\theta = 2.5$, respectively.

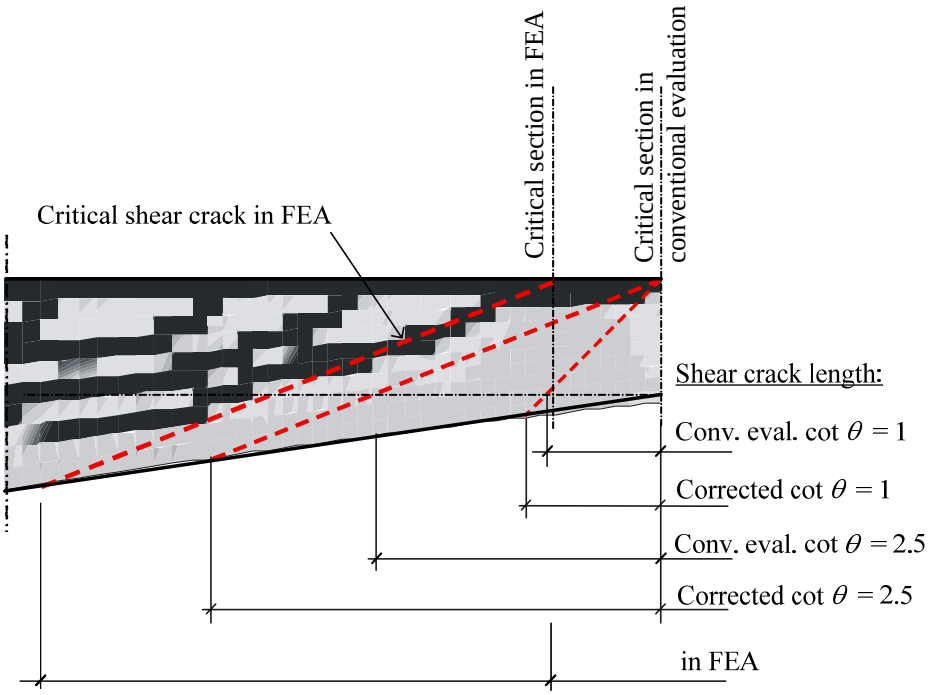

Figure 5.14 Length of shear crack calculated with in the conventional evaluation illustrated on the south web, compared with the length of the critical shear crack from the analysis.

The redistribution of torsional moment due to cracking may also have a positive influence on the capacity. However, the modelling technique of using linear beam elements for parts not critical to failure may have influenced this redistribution. If the load effect in the adjacent beam elements is high enough to cause cracking, the stiffness of this part would decrease and the redistribution would become smaller.

This assessment of the Källösund Bridge was made as a case study to demonstrate how the verified modelling method could be used to evaluate the response and the load carrying capacity of a prestressed concrete bridge subjected to shear and torsion. This assessment was preceded by a conventional assessment taking all possible load combinations and traffic load positions into account. However, in this study only the most critical load combination for the most critical region was evaluated. To verify the load carrying capacity obtained here for the whole bridge with respect to all relevant actions, alternative load cases also need to be evaluated. Nevertheless, the case study shows the ability to use non-linear finite element analysis for assessment or to verify a design of concrete bridges subjected to shear and torsion.

5.5 A parametric study on a box-girder bridge

The bridge model used in the case study (Section 5.4) was further used to investigate the influence of various design parameters for the shear response and the shear capacity, see Paper VI.

Several non-linear finite element analyses were made varying the amount and inclination of web reinforcement, web thickness and longitudinal prestressing level.

Results such as load-displacement relation, cracking load, crack pattern, crack width, failure mode and load-carrying capacity were compared. Most of the results conformed to expectation; both increased amount of web reinforcement and increased web thickness, showed decreased crack widths, decreased stresses in the web reinforcement and, thereby increased load-carrying capacities. Reduced longitudinal prestressing decreased the cracking load and the stiffness but had almost no effect on the load-carrying capacity.

Other results did not conform to expectation; the analysis with inclined web reinforcement did not show reduced widths of shear cracks or higher load-carrying capacity. This could however be explained: results from the analysis revealed that the top flange was separating from the web in the vertical direction. When a bending crack developed in the bottom of the cross-section close to the end of the cantilever, the concrete compressive strength in the top of the web was reduced due to lateral tensile strain. Hence, due to the low remaining compressive strength, the internal lever arm decreased and the moment capacity was reduced. With inclined web reinforcement, the forces that could be carried in the vertical direction by the reinforcement were lower, which is why this separation was more significant. Hence, the moment capacity was more reduced. Due to the low amount of web reinforcement, yielding was initiated in the vertical web reinforcement, as well as in the inclined web reinforcement, when the web cracked. Consequently, there were no major differences regarding crack widths regardless of whether the web reinforcement was vertical or inclined.

As could be expected, the crack widths decreased with increased reinforcement amount. However, with an amount of web reinforcement corresponding to approximately twice the required minimum, according to the current Swedish code for bridge design, the crack widths were still quite large; they exceeded allowable crack widths according to codes, even while forming. It should be noted, however that the crack widths evaluated from the analyses are probably overestimated. The modelling method used was verified for shear response and shear capacity, but not specifically for crack widths, i.e. the global deformations were compared, but not crack spacing or crack widths.

By this study the proposed modelling method was further verified; the analyses with various design parameters revealed expected results in almost all cases. With the information given by the analysis the complex behaviour during the failure could be explained also when unexpected results were revealed. Accordingly, the knowledge and understanding of how various design parameters affect the shear response has been improved, and the ability to use non-linear finite element analysis to verify the designs of box-girder bridges is refined.

6 Conclusions

6.1 General conclusions

This study shows how recognized material models implemented in a commercial finite element code can be used to simulate the non-linear shear response in concrete members with and without shear reinforcement. Modelling methods that can be used for evaluation of the response and the load carrying capacity of (1) hollow core slabs and (2) prestressed concrete bridges were worked out and verified by non-linear analyses of tests. Tests on hollow core units, shear panels, and beams, all subjected to selected combinations of bending, shear and torsion, were modelled. Combining solid elements or shell elements, in the parts of the structure where the failure is expected, with beam elements elsewhere, was shown to be a reasonable modelling level, with regard to desired simplifications. A separate model of a statically determined system of beams made it possible control by displacement the increase of several point loads at a time. With this arrangement it was also easy to vary the ratio between shear and torsion applied on a member. In general, the finite element analyses of the tests could describe the overall behaviour, failure mode, crack pattern, maximum load, and load-displacement relationships quite well.

For members with shear reinforcement, the results imply that the load carrying capacity and the crack widths will be conservatively predicted if the fracture energy alone is used to define the softening branch of the concrete tensile response and if the reduction of the compressive strength due to transverse tensile strain is included. Hence, the load-carrying capacity will probably be slightly underestimated and the crack widths overestimated to some extent. The known increase in shear stiffness and shear capacity due to the *concrete contribution*, i.e. tension softening, tension stiffening, dowel action, and friction due to aggregate interlock, can be accounted for by modifying the constitutive relationships used, e.g. the tension-softening curve describing the concrete behaviour in tension. However, caution is recommended to avoid overestimating the capacity. It is important that the modelling method is general and capable of describing also the response for regions not subjected to shear.

The study also highlighted some problems in using non-linear finite element analyses: if the concrete compressive failure was localised in a small region, the size of which did not correspond to the size of the specimen employed to calibrate the stress-strain relationship used, the model could not predict the response. Furthermore, reducing the compressive strength due to lateral strains in the compressive struts can result in an unreasonable response and a premature failure in other regions of the structure.

6.2 Conclusions about hollow core slabs

For hollow core units, a method for using advanced non-linear finite element analyses to obtain the shear-torsion capacities shown in interaction diagrams is proposed. The finite element analyses revealed a non-linear interaction between shear-torsion capacities in hollow core units, which does not agree with the linear relation between the capacities in the European Standard EN 1168. Moreover, the finite element analyses yielded higher capacities than the calculation method in the current standard,

for most combinations of shear and torsion. The increase was up to 55% for the 200 mm thick unit and up to 30% for the 400 mm thick unit. For several combinations, cracks were observed in the finite element analyses before the maximum load was reached; this indicates a redistribution of stresses. Interaction diagrams, such as those presented here, can be worked out for arbitrary geometries of hollow core units and be used in practical design for specified combinations of shear and torsion.

Furthermore, a global finite element model for complete floors of hollow core units was developed. Each unit was described with beam elements, and the neighbouring units were connected by means of slave nodes in the corners of the cross-section, allowing compression, but not tension, in the joints between the hollow core units. This modelling method gave results that are close to those obtained when the longitudinal joints are modelled as hinges; the difference is that when hinges are used, the torsional moment in the hollow core units becomes greater. When the units are in contact at the corners, the eccentricity of the resulting compressive forces in the corners is included, which reduces the torsional moment. Comparisons with test results showed that, by connecting the units at the corners, torsional moments which correspond better with measurements can be obtained. Further comparisons with test results showed that the model can, with reasonable accuracy, describe the real behaviour of a hollow core floor until shear and torsion cracking occurs.

The more detailed model of a hollow core unit was integrated with the global floor model, to enable the modelling of a failure due to combined shear and torsion in one hollow core unit within a floor system. The boundaries with the adjacent units seem to yield a more favourable stress state, or greater potential for redistribution within the unit. Thus, a hollow core unit placed in a floor system could carry higher amounts of shear and torsion. Good agreement with test results was obtained for failure mode, crack pattern, maximum load, and load-displacement relationships. Hence, it is concluded that the modelling technique used can describe these phenomena satisfactorily.

By combining the global floor model with the method to obtain interaction diagrams from non-linear finite element analyses, it is possible to improve the design process with advanced methods in a simple way in daily practice. Thereby, hollow core floors with arbitrary geometries and loadings can be designed for combined shear and torsion. Modelling of complete floors gives the bending moment, shear force and torsional moment to which each hollow core unit is subjected, while modelling of an individual hollow core unit yields the shear-torsion resistance of the selected region described in an interaction diagram. For the bending moments, the traditional design methods can be used.

With the modelling methods proposed, the design approach for hollow core floors subjected to combined shear and torsion can be improved and applied at three new levels (Level IV represents the traditional approach which designers use today):

I. A model of one hollow core unit integrated with a global floor model gives the load-carrying capacity,

II. A global floor model used with an interaction diagram from finite element analyses of one hollow core unit gives sectional forces that are compared with sectional capacity,

III. A global floor model used with a simplified analytical interaction model of cross-sectional capacity, and

IV. Distribution diagrams used with a simplified analytical interaction model of cross-sectional capacity.

The global floor model resulted in lower torsional moment than the traditional approach, and the modelling method for individual hollow core units offered a higher resistance for most combinations of shear and torsion. Therefore, much can be gained by using these methods instead of the traditional design.

6.3 Conclusions about prestressed concrete bridges

In a case study and a parametric study it was shown that the modelling method proposed for large concrete members with shear reinforcement can be used to evaluate the response and the load-carrying capacity of prestressed concrete bridges loaded in shear and torsion.

The bridge used for the case study, the Källösund Bridge, has previously been evaluated both with conventional assessment methods and with non-linear finite element analysis. The evaluation presented in this study was improved in several respects. The most important improvement was the use of a verified modelling method. Further improvements included the following: the final loading was done in a displacement controlled process, effects of creep and reinforcement hardening were incorporated, and safety formats suitable for non-linear analysis were adopted.

Although the shear resistance limited the load-carrying capacity in the previously made assessment, the failure obtained in these finite element analyses was due to bending. However, shear cracks developed in large regions of the webs; thus, a shear response was observed, and it could be concluded that the shear capacity of this part of the bridge, for this load combination, is higher than the load-carrying capacity determined. The finite element analyses revealed a higher load-carrying capacity than either the previously made finite element analysis or the conventionally made assessment. Most of the increased capacity in comparison with previous finite element analysis can be attributed to the use of a more stable material model for cracked concrete, to the displacement-controlled loading, and to a safety format more suitable for non-linear analysis. The higher load-carrying capacity in these non-linear finite element analyses, when compared to conventional methods, was mainly governed by the location and inclination of the main shear crack. Furthermore, it was shown that the safety format using partial safety factors gave unrealistically conservative results; thus, it is not suitable for non-linear analysis.

By the parametric study of the bridge, the proposed modelling method was further verified; analyses with various design parameters almost always gave the expected results. With the information given by the analysis the complex behaviour during the

failure could be explained also when unexpected results were revealed. Accordingly, the knowledge and understanding of how various design parameters affect the shear response has been improved, and the ability to use non-linear finite element analysis to verify the designs of box-girder bridges is refined.

6.4 Suggestions for future research

The potential of non-linear finite element analysis to reveal higher load-carrying capacities and improved understanding of the mechanical behaviour of concrete structures has been shown in many research projects. To raise the capacity of practicing engineers to use non-linear finite element analysis, for verifications of designs and for assessments of existing structures, guidelines are needed. Guidance is helpful in deciding when non-linear analysis should or can be used and how the safety format should be treated. Further study would increase the ability to use non-linear analysis to evaluate critical load cases and critical regions. Guidance on how to model pre-cracked, damaged, or deteriorated parts is needed to facilitate the evaluation of existing concrete structures under actual conditions.

In this study rough estimations of shear crack widths are made and these predictions are not verified. To satisfy performance demands in the service state and to prevent problems caused by unsatisfying durability, it is important to prevent shear cracking or to limit the width of shear cracks. Further work is needed to propose a verified method for predictions of shear crack widths.

This study shows that the increase in shear stiffness and shear capacity due to tension softening, tension stiffening, dowel action, and friction due to aggregate interlock, also known as the *concrete contribution*, can be accounted for in non-linear finite element analysis by modifying the constitutive relationships used, e.g. the tension-softening curve describing the concrete behaviour in tension. By a more detailed modelling method of the reinforced concrete, some of the effects influencing the concrete contribution could be included in the model. However, analyses showed that the boundaries had a great influence on the shear response. Nevertheless, with further refinements, this modelling method could be used to determine more realistic tension-softening curves for inclined cracked reinforced concrete, which can be used in less detailed non-linear finite element analysis or in combination with numerical models like the MCFT.

The proposed modelling technique combining simplified global models with more detailed ones, where the failure is expected, could be used for investigations of other failure modes, such as punching failure. It could also be used to design or assess other concrete structures.

Due to the lack of vertical reinforcement in hollow core units, the shear-torsion capacity is determined for the actual stress state in the concrete region considered. Outside the support region, the influence of the bending moment imposed on the stress state is more significant than for regions close to the support. This influence on the shear-torsion capacity ought to be further investigated and included in improvements to the design method.

Some of the tests and analyses indicate that a hollow core unit can carry greater amounts of shear and torsion when placed in a floor system; this is not caused only by the transfer between the neighbouring elements. The restraints at the boundaries with the adjacent units seem to yield a more favourable stress state, or greater potential for redistribution within the unit. Future research may reveal whether this conclusion also holds for other floors and, if so, whether it can be taken into account in design.

7 References

ASCE-ACI Committe 445 on Shear and Torsion (1998): Recent approches to shear design of structural concrete. *Journal of Structural Engineering*, Vol. 124, No. 12, December, pp. 1375-1417.

Ayoub A. and Filippou F. C. (1998): Nonlinear Finite-Element Analysis of RC Shear Panels and Walls. *Journal of Structural Engineering*, Vol. 124, No. 3, March, pp. 298-308.

Belarbi A. and Hsu T. T. C. (1995): Constitutive laws of softened concrete in biaxial tension-compression. *ACI Structural Journal*, Vol. 92, No. 5, September-October, pp. 562-573.

Boverket (2004): *Boverkets handbok om betongkonstruktioner BBK 04,* (In Swedish), Karlskrona, Sweden, 2004.

BRO 2004 (2004): *Vägverkets allmänna tekniska beskrivning för nybyggande och förbättring av broar,* (In Swedish). Publikation 2004:56, Vägverket (Swedish Road Administration), Borlänge, Sweden.

CEN/TC229 (2005): *Precast concrete products - Hollow core slabs.*, European Standard EN 1168:2005:E, Brussels.

Cervenka V., Cervenka J. and Pukl R. (2007): Safety assessment in fracture analysis of concrete structures. *The 6th International Conference on Fracture Mechanics of Concrete and Concrete Stuctures*, Catania, Italy, 2007, 1043-1049.

Chen W.-F. and Duan L. (2000): *Bridge Engineering Handbook*, CRC Press, 2000.

Chowdhury M. R. and Ray J. C. (1995): Further Considerations for Nonlinear Finite-Element Analysis. *Journal of Structural Engineering*, Vol. 121, No. 9, September, pp. 1377-1379.

Collins M. P. and Mitchell D. (1991): *Prestressed Concrete Structures*, Prentice Hall, Englewood Cliffs, New Jersey.

EN1992-1-1 C. T. S. (2004): *Eurocode 2: Design of concrete structures - Part 1: General rules and rules for buildings*, European Committee for Standardization, Brussels.

EN1992-2 C. T. S. (2005): *Eurocode 2: Design of concrete structures Part 2: Concrete bridges Design and detailing rules*, European Committee for Standardization, Brussels.

Enochsson O., Puurula A. and Elfgren L. (2004): *Beräkning av betongbroars bärförmåga - Interaktion mellan tvärkraft, vridmoment och böjmoment i Källösundsbron,* (In Swedish). 2004:15, Institutionen för samhällsbyggnad, Luleå tekniska universitet, Luleå, Sweden.

fib (1999): *Structural concrete. Textbook on Behaviour, Design and Performance Updated knowledge of the CEB/FIP Model Code 1990*, International Federation for Structural Concrete (fib), Lausanne, Switzerland.

Hegger J., Sherif A. and Görtz S. (2004): Investigation of Pre- and Postcracking Shear Behavior of Prestressed Concrete Beams Using Innovative Measuring

Techniques. *ACI Structural Journal*, Vol. 101, No. 2, March-April, pp. 183-192.

Ho I.-K. and Shahrooz B. M. (1998): Finite element modeling of deteriorated R.C. slab bridge: lessons learned and recommendations. *Structural Engineering and Mechanics*, Vol. 6, No. 3, pp. 259-274.

Hsu T. T. C. and Zhu R. R. H. (2002): Softened membrane model for reinforced concrete elements in shear. *ACI Structural Journal*, Vol. 99, No. 4, July-August, pp. 460-469.

Huria V., Lee K.-L. and Aktan A. E. (1993): Nonlinear Finite Element analysis of RC Slab Bridge. *Journal of Structural Engineering*, Vol. 119, No. 1, January, pp. 88-107.

Jeppson J., Carlsson F. and Thelandersson S. (2004): *Klassningsberäkning med hjälp av tillförlitlighetsanalys,* (In Swedish). Rapport TVBK - 3050, Avdelningen för konstruktionsteknik, Lunds Tekniska Högskola, Lund, Sweden.

Kaufmann W. and Marti P. (1998): Structural concrete: Cracked membrane model. *Journal of Structural Engineering*, Vol. 124, No. 12, pp. 1467-1475.

Kettil P., Ródenas J. J., Aguilera Torres C. and Wiberg N.-E. (2005): Strength and deformation of arbitrary beam sections using adaptive FEM. *Submitted to Computers & Structures*.

Lackner R. and Mang H. A. (2003): Scale transition in steel-concrete interaction. I:Model. *Journal of Engineering Mechanics*, Vol. 129, No. 4, April, pp. 393-402.

Lindström G. (2004): *Comments on load distribution in prEN 1168*. Unpublished work done within the Holcotors project.

Lundgren K. (1999): *Three-dimensional modelling of bond in reinforced concrete: Theoretical model, experiments and applications*. PhD Thesis, Department of Structural Engineering/Concrete Structures, Chalmers University of Technology, Publication no. 99:1, Göteborg, Sweden, 50 pp.

Maekawa K., Pinmanmas A. and Okmura H. (2003): *Nonlinear mechanics of reinforced concrete*, Spon Press, London.

Malm R. (2006): *Shear cracks in concrete structures subjected to in-plane stresses*. Licentiate Thesis, Structural Design and Bridges, Architecture and the Built Environment, The Royal Institute of Technology (KTH), Stockholm, Sweden, 2006, 136 pp.

Martin M. (2007): *Nonlinear FE analysis of shear behaviour in reinforced concrete - Modelling of shear panel tests*. Master´s Thesis 2007:46, Department of Civil and Environmental Engineering, Divison of Structural Engineering, Concerte Strucures, Chalmers University of Technology, Göteborg, 223 pp.

Pajari M. (2004a): *Shear-torsion interaction tests on single hollow core slabs*. VTT Research Notes 2275, Technical Research Centre of Finland, VTT Building and Transport, Espoo.

Pajari M. (2004b): *Shear torsion test on 400 mm hollow core floor*. VTT Research Note 2274, Technical Research Centre of Finland, VTT Building and Transport, Espoo.

Pang X.-B. D. (1991): *Constitutive laws of reinforced concrete in shear*. Dissertation, The Faculty of the Department of Civil and Environmental Engineering, University of Houston, Houston, TX, 1991, 403 pp.

Pang X.-B. D. and Hsu T. T. C. (1995): Behavior of reinforced concrete membrane elements in shear. *ACI Structural Journal*, Vol. 92, No. 6, November-December, pp. 665-679.

Pang X.-B. D. and Hsu T. T. C. (1996): Fixed angle softened truss model for reinforced concrete. *ACI Structural Journal*, Vol. 93, No. 2, March-April, pp. 197-207.

Plos M. (2002): Improved bridge assessment using non-linear finite element analyses. *First International Conference on Bridge Maintenance, Safty and Management*, Barcelona, 2002, 133-134.

Plos M. (2004): *Structural Assessment of the Källösund Bridge using Finite Element Analysis - Evaluation of the load carrying capacity for ULS*. Rapport 04:1, Concrete Structures, Department of Structural and Mechanical Engineering, Chalmers University of Technology, Göteborg, Sweden.

Plos M. and Gylltoft K. (2002): *Bärighetsutredningar av broar i framtiden,* (In Swedish). Rapport nr. 02:6, Institutionen för konstruktionsteknik, Chalmers tekniska Högskola, Göteborg, Sweden.

Plos M. and Gylltoft K. (2006): Evaluation of shear capacity of a prestressed concrete box girder bridge using non-linear FEM. *Structural Engineering International*, Vol. 16, No. 3, August, pp. 213-221.

Plos M., Gylltoft K., Jeppson J., Carlsson F., Thelandersson S., Enochsson O. and Elfgren L. (2004): *Evaluering av bärförmåga hos broar med hjälp av förfinade analysmetoder Ett samarbetsprojekt mellan LTH, LTU och Chalmers,* (In Swedish). Rapport 04:3, Institutionen för konstruktion och mekanik, Betongbyggnad, Göteborg, Sweden.

Prisco M. d. and Gambarova P. G. (1995): Comprehensive Model for Study of Shear in Thin-Webbed RC and PC Beams. *Journal of Structural Engineering*, Vol. 121, No. 12, December, pp. 1822-1831.

Shahrooz B. M., Ho I. K., Aktan A. E., de Borst R., Blaauwendraad J., van der Veen C., Iding R. H. and Miller R. A. (1994): Nonlinear Finite Element Analysis of Deteriorated RC Slab Bridge. *Journal of Structural Engineering*, Vol. 120, No. 2, February, pp. 422-440.

Soltani M., An X. and Maekawa K. (2003): Computational model for post cracking analysis of RC membrane elements based on local stress-strain characteristics. *Engineering Structures*, Vol. 25, pp. 993-1007.

Song H.-W., You D.-W., Byun K.-J. and Maekawa K. (2002): Finite element failure analysis of reinforced concrete T-girder bridges. *Engineering Structures*, Vol. 24, No. 2, February, pp. 151-162.

Sustainable Bridges (2007): *D4.2 Guideline for Load and Resistance Assessment of Existing European Railway Bridges: Advice on the use of advanced methods.* D4_2-WP4-05-070521, Prepered by Sustainable Bridges - a project within EU FP6. Avialable from: www.sustainablebridges.net.

TNO (2002): *DIANA Finite Element Analysis, User's Manual release 8.1*, TNO Building and Construction Research.

TNO (2004): *DIANA Finite Element Analysis User's Manual release 9*, TNO DIANA BV, Delft, the Netherlands.

Walraven J. and Stroband J. (1999): Shear capacity of high strength concrete beams with shear reinforcement. *5th International Symposium on Utilization of High Strength/ High Performance Concrete*, Sandefjord, Norway, 1999, 693-700.

Walraven J. C. and van der Marel A. P. (1992): *Experiments on hollow core slabs, supported along three edges*. Division of Mechanics and Structures, Delft.

Vecchio F. J. (2000): Disturbed Stress Field Model for Reinforced Concrete: Formulation. *Journal of Structural Engineering*, Vol. 126, No. 9, September, pp. 1070-1077.

Vecchio F. J. and Collins M. P. (1986): The modified compression-field theory for reinforced concrete elements subjected to shear. *Journal of the American Concrete Institute*, Vol. 83, No. 2, March-April, pp. 219-231.

Vecchio F. J. and Collins M. P. (1993): Compression response of cracked reinforced concrete. *Journal of Structural Engineering*, Vol. 119, No. 12, December, pp. 3590-3610.

Vecchio F. J., Lai D., Shim W. and Ng J. (2001): Disturbed Stress Field model for Reinforced Concrete: Validation. *Journal of Structural Engineering*, Vol. 127, No. 4, April, pp. 350-358.

Vecchio F. J. and Shim W. (2004): Experimental and Analytical Reexamination of Classical Beam Tests. *Journal of Structural Engineering*, Vol. 130, No. 3, March, pp. 460-469.

Vägverket (2004): *Bro 2004 Vägverkets allmänna tekniska beskrivning för nybyggande och förbättring av broar*, (In Swedish).

Yamamoto T. and Vecchio F. J. (2001): Analysis of Reinforced Concrete Shells for Transvers Shear and Torsion. *ACI Structural Journal*, Vol. 98, No. 2, March-April, pp. 191-199.

Yang K. H., Chung H. S., Lee E. T. and Eun H. C. (2003): Shear characteristics of high-strength concrete deep beams without shear reinforcements. *Engineering Structures*, Vol. 25, No. 10, Aug, pp. 1343-1352.

Zararis P. D. (1996): Concrete Shear Failure in Reinforced-Concrete Elements. *Journal of Structural Engineering*, Vol. 122, No. 9, pp. 1006-1015.

Paper I

Shear and torsion in prestressed hollow core units:

Finite element analyses of full-scale tests

Broo H., Lundgren K. and Engström B.

Structural Concrete, Vol. 8, No. 2, pp. 87—100, 2007.

Shear and torsion in prestressed hollow core units: finite element analyses of full-scale tests

H. Broo, K. Lundgren and **B. Engström**

The present calculation methods for shear and torsion in prestressed hollow core slabs add stresses from various influences without taking into account deformations and compatibility, the softening of cracking concrete, or restraint at the boundaries; therefore, they are most likely conservative. The main purpose of this work is to establish three-dimensional finite element models, which can be used both to analyse the effect of parameters that influence the shear and torsion response and to be included in global models of complete floors. An important aspect was therefore to simplify the models to avoid time-consuming analyses. Coarse meshes with solid elements were combined with beam elements. The established models were validated by simulating a series of full-scale tests conducted on both 200 mm and 400 mm thick hollow core units subjected to various combinations of shear and torsion. In general, although very coarse meshes were used, the finite element analyses of the tests succeeded in describing the overall behaviour, crack pattern, failure mode, and maximum load, with a reasonably good agreement.
[**doi:** 10.1680/stco.2007.8.2.87]

Helén Broo
Chalmers University of Technology, Göteborg, Sweden

Karin Lundgren
Chalmers University of Technology, Göteborg, Sweden

Björn Engström
Chalmers University of Technology, Göteborg, Sweden

Introduction

Precast prestressed hollow core units are widely used for floors in all kinds of buildings; industrial, offices, apartments and parking garages. The hollow core units are mainly designed to resist bending moments; however, there are many applications in which hollow core units are also subjected to combined shear and torsion. Some examples are three-line supported slabs, slabs carrying a trimmer beam to support interrupted slabs, floors with columns in alternating position at either ends, slabs supported on beams with divergent inclinations and slabs with important skew ends (Figure 1). Concentrated loads on a single hollow core unit are transversely distributed to the surrounding units by the shear keys in the longitudinal joints. Normally, the joints between hollow core units crack and act more or less as hinges. Consequently, load distribution to the neighbouring units always introduces a torsional moment.

Generally, prestressed hollow core units do not have transverse or vertical reinforcement. This, in combination with the cross-sectional geometry, makes the units sensitive to shear and torsion. The most common failure mode for hollow core units subjected to a high shear force is web shear tension failure. The shear strength depends mainly on the tensile strength of the concrete, the prevailing compressive stress in the webs due to prestressing, and the geometry of the particular hollow core unit. Quite a lot of research has been done concerning shear in hollow core units. The shear strength has been investigated experimentally, analytically, or both by Walraven and Mercx,[1] Pisanty,[2] Yang,[3] Jonsson[4] and Becker and Buettner;[5] and, in combination with flexible supports, also by Pajari[6,7]. Procedures for predicting the shear capacity have been presented by Pisanty[2] and Yang.[3] The combination of shear and torsion in hllow core units is, however, not so well investigated. To the authors' knowledge, the publication by Gabrielsson,[8] who focused on experiments and analytical modelling of eccentrically loaded hollow core units, is the only one dealing with this subject.

Torsional loading on a hollow core unit produces shear stresses mainly in the perimetric zone of the unit. In the outermost webs, these shear stresses act upwards in one and downwards in the other. The stresses are added to those resulting from the ordinary vertical shear force, which is uniformly distributed over the webs. This means that one web in the cross-section accumulates much higher stresses than the others; however, close to failure, there might be some redistribution of stresses between the webs. Studies and tests carried out by Gabrielsson[8] indicated that such redistribution exists. The calculation method in the European product standard EN 1168 CEN/TC229[9] for shear and torsion in hollow core units adds stresses from various influences without taking into account deformations and compatibility within the unit, the softening of cracking concrete, or restraint at the boundaries of the element in question.

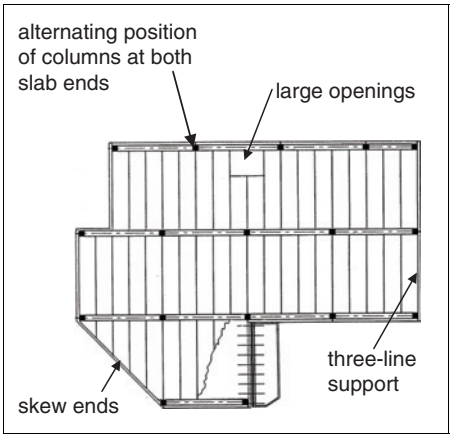

△ **Figure 1 Practical examples where shear forces, bending moments and torsional moment simultaneously are present in hollow core slabs (Modified from sketch by A. Van Acker 2003)**

1464–4177 (Print) 1751–7648 (Online) © 2007 Thomas Telford and *fib*

To improve the current knowledge and understanding of shear and torsion interaction in hollow core floors, a European research project was started in January 2002. The aim of the project is to develop a more accurate design method for shear and torsion interaction in hollow core floors. To reach this goal, experiments are combined with finite element analyses, using non-linear fracture mechanics. This paper presents results from the first part of the project that deals with finite element analyses of hollow core units. The main purpose of this part is to establish three-dimensional finite element models, which can be used both to analyse the effect of various parameters that influence the shear and torsion response and be included in global models of complete floors,[10] which was based on the work presented here. An important aspect was therefore to simplify the models to avoid time-consuming analyses. Coarse meshes with solid elements were combined with beam elements. The established models were validated by simulating a series of full-scale experiments carried out at the Technical Research Centre of Finland, VTT. The development of the finite element models is briefly described here; the main emphasis is laid on the models actually used and on comparison with tests. For more details about how the finite element models were developed, see Broo and Lundgren.[11] The general finite element program DIANA was used for all analyses.[12]

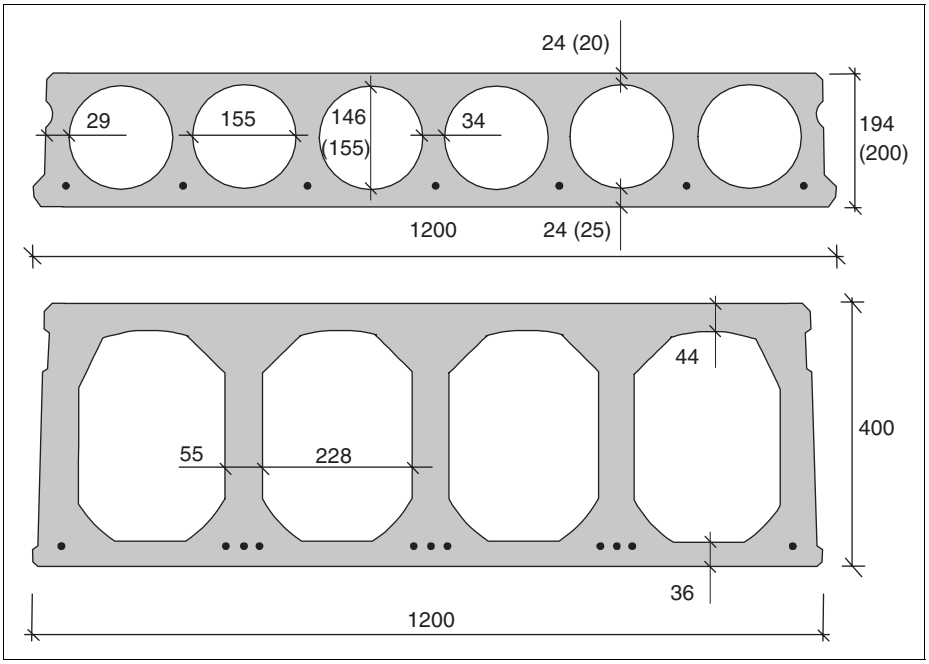

△ **Figure 2 Cross-sections of the hollow core units tested and analysed. Dimensions given in mm. Values in parentheses are nominal if they differ**

Full-scale experiments

The analyses presented in this paper are of full-scale experiments of hollow core units, which were planned cooperatively by VTT, Strängbetong and the authors. The tests, conducted at VTT in 2002 and 2003 (see Pajari[13] for details), are briefly outlined here.

Tests both with and without eccentric loading were conducted on 200 mm and 400 mm thick extruded prestressed hollow core units. The two geometries for the extruded units can be seen in Figure 2. The tests were made to provoke shear tension failures in the webs of the hollow core units, with and without the influence of torsion. To evaluate the effects of torsion in combination with a shear force, the hollow core units were loaded with one or two point loads placed with different eccentricities. To avoid premature failures such as punching, the loads were never placed over two neighbouring webs. The principal testing arrangement for the shear tension tests is shown in Figures 3 and 4. The shear span chosen was $a = 2{\cdot}5h$, according to the test method specified in EN 1168 Annex J.[9] This corresponds to 0·5 m for the 200 mm thick hollow core units and 1·0 m for the 400 mm thick units. Since the length of the span does not affect the shear failure, a span of 7 m was chosen for all tests. The support lengths for the 200 mm thick hollow core units were 60 mm and for the 400 mm thick units 80 mm. The vertical displacement of the hollow core unit was measured at two points above each support and above each web at a distance b from the load. For the 200 mm thick hollow core units $b = 100$ mm, and for the 400 mm thick ones $b = 200$ mm. Identifications and details about the tests are shown in Tables 1, 2 and 3.

Tests were made on hollow core units supported in two ways. In most of the tests the units were simply supported, and a 10 mm thick soft bearing strip of neoprene was

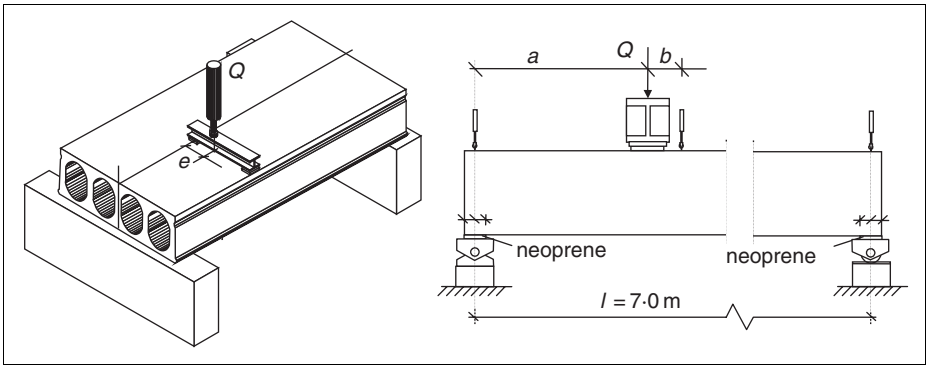

△ **Figure 3 Principal testing arrangement for the tests where the units were supported on a soft bearing strip of neoprene, modified from Pajari[13]**

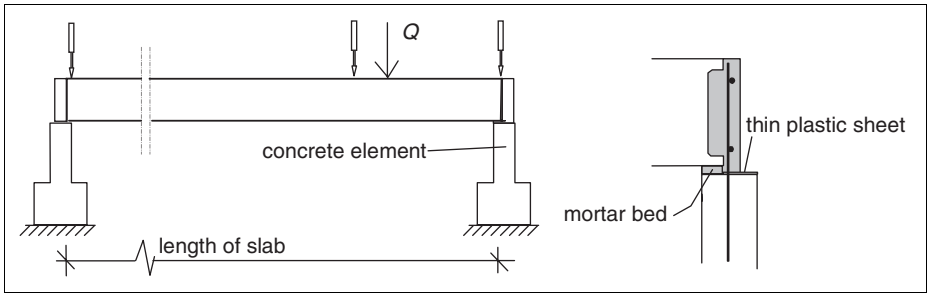

△ **Figure 4 Principal testing arrangement for the tests where the units were supported on a concrete beam with mortar bed and grouted ends, modified from Pajari[13]**

Table 1 Tests on hollow core units

Test identification	Thickness *H*: mm	Number of strands	Diameter of strand Ø: mm	Initial prestress: MPa	Length of slab: m	Length of span *l*: m	Length of shear span *a*: m
ST200	200	7	12·5	900	7·06	7	0·5
ST400	400	11	12·5	1000	7·08	7	1·0

Table 2 Tests on the 200 mm thick hollow core units

Test identification	ST200C	ST200E1, ST200E1b	ST200E2	ST200E1M
	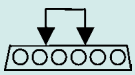	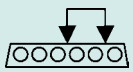	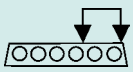	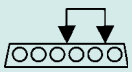
Eccentricity *e*: m	0	0·187	0·374	0·187
Support condition	bearing strip of neoprene	bearing strip of neoprene	bearing strip of neoprene	mortar bearing with grouted ends
Number of tests	1	2	1	1

Table 3 Test on the 400 mm thick hollow core units

Test identification	ST400C1	ST400C2	ST400E1	ST4002E	ST400E1M
	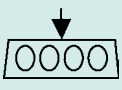	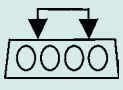	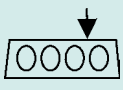	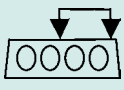	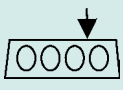
Eccentricity *e*: m	0	0	0·283	0·283	0·283
Support condition	bearing strip of neoprene	bearing strip of neoprene	bearing strip of neoprene	bearing strip of neoprene	mortar bearing with grouted ends
Number of tests	1	1	1	1	1

placed between the support and the hollow core unit to ensure full contact between the unit and the support during loading. However, this soft bearing sometimes had a negative influence on the capacity (see Comparison of tests and analyses). Consequently, two additional tests, one on a 200 mm thick unit (ST200E1M) and one on a 400 mm thick unit (ST400E1M) with grouted ends supported on a mortar bed on a concrete beam, were conducted. The support conditions for these tests are shown in Figure 4. Except for the support conditions, these tests were arranged the same as ST200E1 and ST400E1. The supporting concrete beams were not fixed in any way to the floor of the laboratory; when the hollow core unit was loaded, the supporting beams tilted (Figure 5). The supporting concrete beam used for the 400 mm thick unit was so heavy that it caused a horizontal reaction force that influenced the results.

Finite element analyses

The finite element analyses described here were made at Chalmers University of Technology. Hollow core units subjected to different combinations of shear and torsion were modelled with various levels of detailing, using the non-linear finite element program DIANA 8·1. The work started with the modelling of tests of hollow core units subjected to shear and torsion, which are available in the literature.[8] The information and knowledge gained from this was used for preliminary analyses for planning purposes, made to determine a test plan. Some conclusions from these early analyses were as follow.

(*a*) As beam elements are not capable of describing failure due to shear stresses, solid elements had to be used.
(*b*) Modelling the whole slab with solid elements resulted in a very large model and time-consuming analyses. Simplifications of the model were necessary.
(*c*) If the response after maximum load was of interest, a realistic interaction between the prestressing steel and the concrete had to be assumed, for example by using a bond–slip relation.

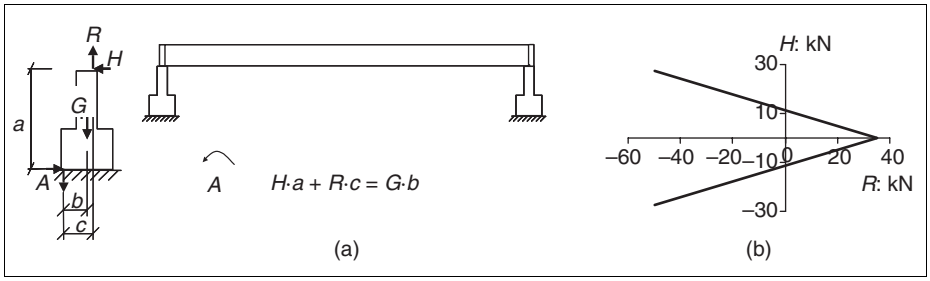

△ **Figure 5 (a) Horizontal restraint at the supports is limited by tilting of the support beams in the test of a 400 mm thick hollow core unit supported on a mortar bed. (b) Input for the friction layer**

(*d*) It was not enough to apply supports on one node line only; the extension of the support had to be modelled.
(*e*) When the loading is eccentric, lifting of the slab at the support must be allowed.
(*f*) The deformation of the supports was large in the tests, due to the neoprene strips used. The neoprene had to be modelled with solid elements to describe both the vertical displacement and the lateral dilation in the neoprene strip.
(*g*) The actual geometries for the cross-section had to be modelled if differences between these and the nominal values were large.
(*h*) To improve the convergence, deformation controlled loading was used instead of load controlled.

In this paper only the models actually used are described. More about how the models were developed can be found in Broo and Lundgren.[11]

Finite element model

The analyses given in this paper were made for models with relatively coarse meshes. The modelling technique used was with eight-node solid elements only for the part of the hollow core unit where the failure was expected, closest to the load and the active support. The rest of the slab was modelled with three-node beam elements, as shown in Figure 6. For the 200 mm unit the part with solid elements was 1·03 m long, and for the 400 mm unit, 1·54 m. In this part the strands were modelled with two-node bar elements, combined with interface elements and a predefined bond–slip relation, to simulate the interaction between the prestressing steel and the concrete. In reality, the bond–slip differs for the release of the prestressing force and for the loading stage, due both to the changes in the concrete strength and to the effect of the radial normal stresses. This can be modelled by the use of solid elements for both the strands and the concrete, with a special frictional layer between them.[14,15] However, this modelling technique was judged to be too time-consuming for these analyses, and a bond–slip relation was considered to give a sufficient level of modelling.

The solid elements were connected to the beam elements by assuming a stiff rotation of the cross-section and that the plane cross-section remained plane. To describe the cross-section of the beam elements, the program offered 20 four-point zones to define the arbitrary cross-section shape of one hollow core unit. The beam elements were assigned the properties of a 200 mm high and 1200 mm wide hollow core unit by defining the cross-section with 16 zones; for the 400 mm high and 1200 mm wide hollow core units 17 zones were used (Figure 7). In the part of the model with beam elements, the strands were modelled as embedded reinforcement. This choice means that in the beam elements, full interaction between the prestressing steel and the concrete was assumed.

The loading plates were modelled with four eight-node solid elements, which would spread the applied load over several nodes to avoid local failure. Between the loading plates and the concrete, full interaction was assumed. The loads were applied with deformation control. To enable loading with deformation control for the eccentric loading, a three-node beam element with hinged ends was modelled between the centre nodes of the loading plates (Figure 6). Loading was then applied as a prescribed deformation of the centre node of the beam element. These

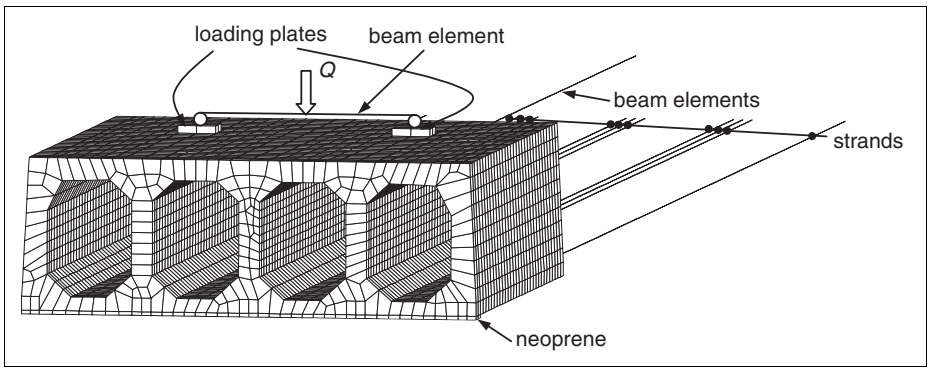

△ **Figure 6 Mesh used in the analyses of the tests on 400 mm thick hollow core units carried out at VTT**

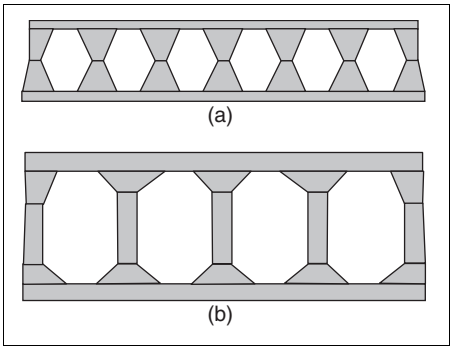

△ **Figure 7 The cross-section of the beam elements defined with zones. (a) 200 mm unit, and (b) 400 mm unit**

analyses had to be carried out in two phases. In the first phase, the centre node of the beam element was not supported; then the prestressing force was released and the self-weight was applied. In the second phase, the centre node of the beam element was supported vertically at the location obtained from the first phase. Due to the syntax of the program, the self-weight had to be applied again. Thereafter, the loading was applied by increasing the displacement of the centre node of the beam element.

As the development of the model progressed, the analyses showed that the support conditions were of great importance. Hence, the support itself was modelled in detail. The support conditions used can be seen in Figures 8 and 9. In the analyses of tests on units supported on a roller bearing, with a thick soft bearing strip between the unit and the support, the bearing strip was modelled with eight-node solid elements. This was done to describe the effect of the lateral dilation in the bearing strip and to include the effects of large settlement. In the tests there was a Teflon layer between the soft bearing strip and the supporting steel plate. In the model this was simulated by supports only in vertical direction. The nodes on the line in the centre of the soft bearing strip were supported vertically, while the nodes at the edges were tied to have the same vertical displacement but in opposite directions, thus enabling a rotation and simulating a free support (Figure 8). The opposite support, the end of the beam elements, was supported for displacements in transversal and vertical directions and for rotation around the longitudinal and vertical axes. The model was supported for longitudinal displacements only at the node where the load was applied.

In the models used to analyse the tests made on a mortar bed, the bed was modelled with eight-node solid elements. In the first phase of the analysis, release of the prestressing force and application of dead load, the nodes on the centre line of the mortar bed were supported vertically, transversally and longitudinally. In phase two, application of the load, all bottom nodes of the mortar bed were supported the same way (Figure 9). To simulate the grouted end of the unit, the nodes on the end cross-section were tied, to keep the cross-section in plane and to have a stiff rotation. In the analysis of ST400E1M, a friction layer at the opposite support (at the end of the beam element) applied the horizontal force (the restraint of the heavy support beams) to the hollow core unit. Input for the friction layer is shown in Figure 5(b). The horizontal force acted on the lower edge of the unit of the hollow core cross-section, therefore a stiff link as long as half of the unit height was modelled between the end of the beam element and the support node.

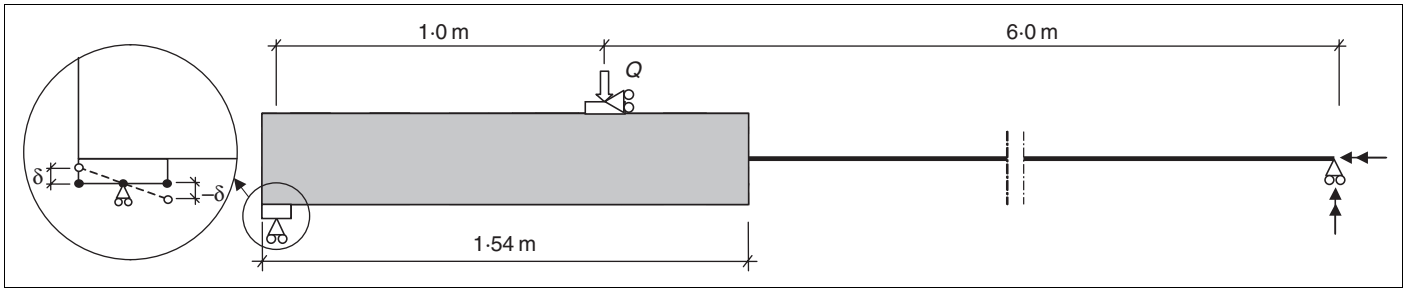

△ **Figure 8 Support conditions in the analyses of ST400C1, ST400E1, ST400C2 and ST4002E tests carried out at VTT. Double arrow indicates support for rotation**

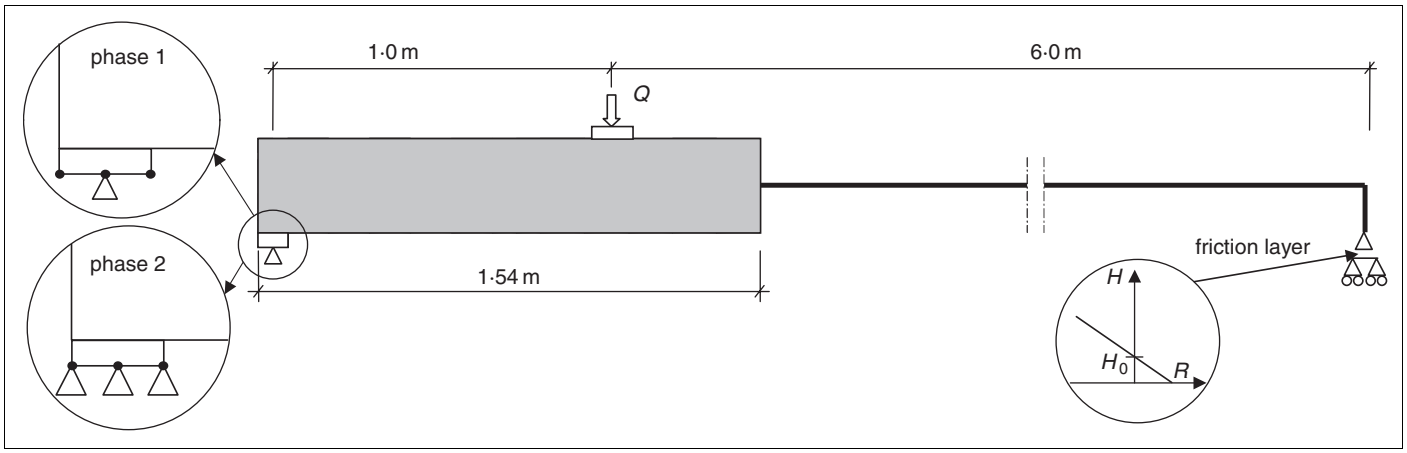

△ **Figure 9 Support conditions in the analysis of ST400E1M, test carried out at VTT**

Modelling of material

In all of the analyses, the concrete was modelled with a constitutive model based on non-linear fracture mechanics. A rotating crack model based on total strain was used for the concrete.[12] The hardening in compression was described by the expression of Thorenfeldt; for the tension softening, the curve by Hordijk was chosen, as described in TNO.[12] Material data for the concrete were calculated from compressive cylinder tests carried out by VTT, on 50 mm cores drilled from the test specimens.[13,11] To obtain correct torsional stiffness of the beam elements, two factors, which TNO[12] designates 'shear factors', were adjusted. The torsional stiffness was evaluated from pure torsion tests.[16] The constitutive behaviour of the prestressing steel was modelled by the von Mises yield criterion, with an associated flow law and isotropic hardening, using the strength and modulus of elasticity measured in tensile tests carried out at VTT.[13] All material properties used for the models are shown in Table 4.

The pre-defined bond–slip relationship between seven wire strands and the concrete was taken from pull-through tests carried out at Chalmers[17] (Figure 10). In reality, the bond–slip relation depends on the surrounding structure. For example, the bond stress decreases if splitting of the concrete occurs, while it increases on release of the prestressing force and at the support region due to the higher normal stresses between the concrete and the steel. However, it was accepted as a reasonable simplification to use the same bond–slip relation for all load cases.

The stiffness of the 10 mm thick neoprene was determined from two loading tests, one with and one without neoprene, performed at VTT. The loaded area in these tests was $80 \times 500\ mm^2$. The Poisson's ratio was assumed to be $\nu = 0{\cdot}49$, and Young's modulus was $E = 15$ MPa.

Verification of the mesh

To evaluate the established model and the modelling technique used, a series of linear analyses was made. For the 400 mm thick hollow core units the established model was checked against other models in which the complete unit was modelled with solid elements, one with a coarse mesh and one with a more dense mesh. The linear analyses showed that the substitution of beam elements in a part of the model or a refined mesh had very little or no influence on the resulting displacements and stresses. The section where beam elements were connected to the solid elements in the non-linear analyses was closely investigated in the linear analyses. The resulting displacements in this section showed very little transverse bending. This justified the assumption that this section had a stiff rotation. For both the 200 mm and the 400 mm units, the torsional stiffness of the part with solid elements was evaluated for the meshes used and for the refined ones. These linear analyses showed that using a more dense mesh made only a small difference in the result.

Comparison of tests and analyses

Comparison of results from tests and analyses showed that the established FE models described quite well the behaviour of hollow core units subjected to various combinations of shear and torsion. The load–displacement relationship, maximum obtained load, deformation of cross-section, and crack pattern, from the tests and the analyses, were compared to evaluate the FE models and to explain the differences between the tests. All of the analyses showed the same failure mode as in the tests, namely, shear tension failure. Although the differing behaviour and capacity caused by different support conditions could be described for the 400 mm thick hollow core unit, this could not be done for the 200 mm unit.

In the tests on the hollow core units supported on a thick soft bearing strip, the sequence was as follows. The load was increased until the first cracking appeared. For all 400 mm thick units and for the eccentrically loaded 200 mm units, the first cracking was diagonal in one of the outermost webs and some longitudinal cracks in the bottom

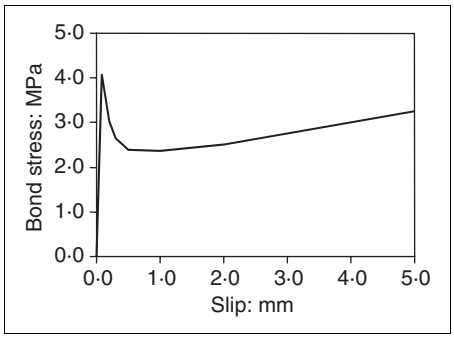

△ **Figure 10 Bond–slip relationship used between seven-wire strand and concrete, from pull-through tests by Lundgren[17]**

Table 4 Material properties used in the analyses of the tests carried out at VTT

	ST200	ST400	ST200M	ST400M	Mortar in ST200M	Mortar in ST400M
Mean concrete compression strength f_{ccm}: MPa	56·4	52·4	57·6	64·3	29·8	29·9
Mean concrete tensile strength f_{ctm}: MPa	3·57	3·42	3·62	3·87	2·43	2·44
Fracture energy G_F: Nm/m^2	100·7	95·6	102·2	110·4	64·4	64·6
Young's modulus of concrete E_{ci}: GPa	38·3	37·3	38·6	40·0	30·9	31·0
Shear factors: - (only beam elements)	10·39	4·06	10·39	4·06	–	–
Tensile strength of prestressing steel $f_{0{\cdot}1u}/f_{pu}$: MPa	1680/1910	1680/1910	1680/1910	1680/1910	–	–
Young's modulus of prestressing steel E_p: GPa	198	198	198	198	–	–

or top flange or both. For the centrically loaded 200 mm unit, the first cracking was a longitudinal crack in the top flange. These first cracks increased in width and length, while the load was decreased and the vertical deflection of the hollow core unit increased. The load was then increased again, and at maximum load diagonal cracks arose in several webs. After the maximum load was reached, the load was decreased and the deflection of the cracked parts of the unit increased significantly. These tests showed that redistribution of the load between the webs after cracking is possible and that the load could be further increased. However, it is worth noting that for all 400 mm thick units, even the centrically loaded, the first cracking occurred in one of the outermost webs. When the units supported on mortar beds were tested, they failed suddenly at the maximum load. A diagonal crack could be seen in the outermost web and longitudinal cracks in the top flange.

In Figure 11, the maximum loads from the analyses are compared with the measured ones for all tests. As can be seen there is a rather good agreement with the exception of the centrically loaded 200 mm thick unit and the 200 mm thick unit supported on a mortar bed. Some attempts were made to improve the agreement between the tests and analyses for the 200 mm unit and to find an explanation for the increased capacity of the unit supported on a mortar bed (Figure 12).

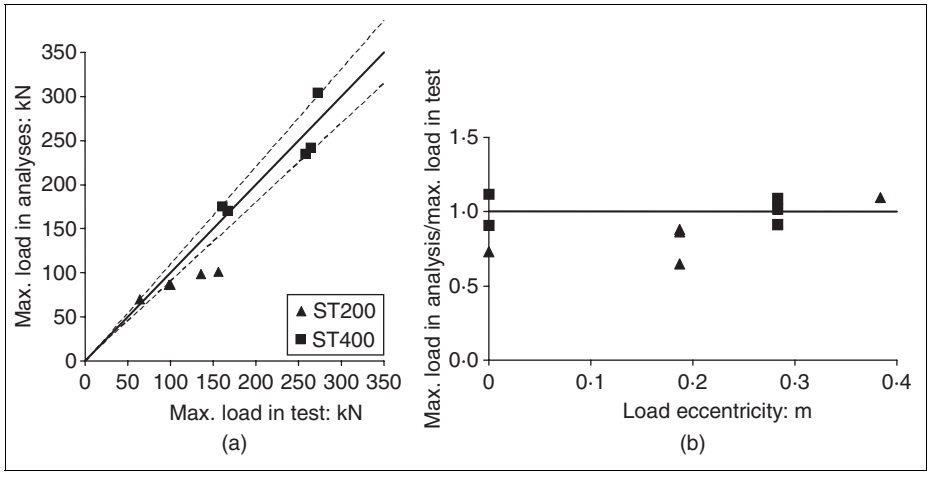

△ **Figure 11 (a) Evaluated maximum loads in analyses compared with the measured ones in the tests. The dashed lines show 10% deviation. (b) Evaluated maximum loads in analyses compared with the measured ones in the tests plotted versus the load eccentricity**

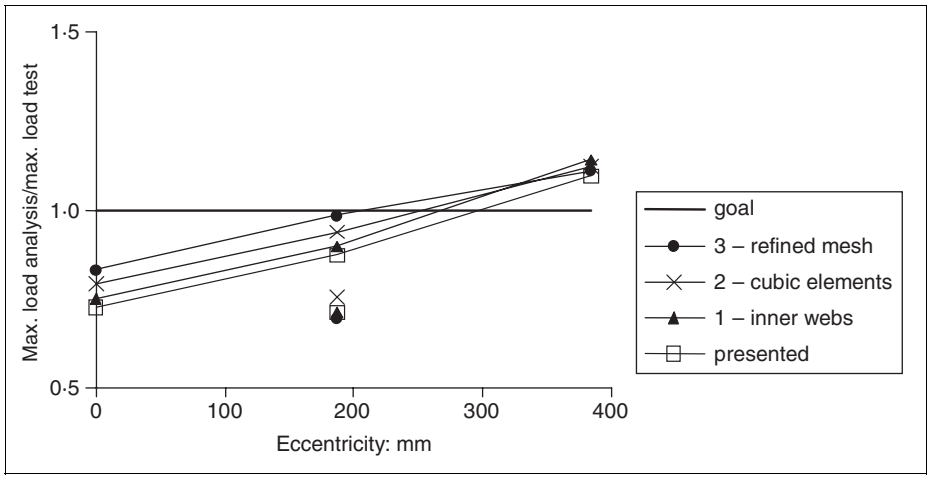

△ **Figure 12 Comparison of results from various analyses of the 200 mm thick units. Evaluated maximum loads from the analyses compared with the measured ones**

(*a*) The thickness of the inner webs was increased by 1 mm in the model, to better correspond with the measured values. This was only a minor change in geometry, and thus had no major influence on the results.

(*b*) The part of the model with solid elements was subdivided into more elements in the longitudinal direction, to better represent the cubic form of the concrete elements. This led to slightly increased maximum loads in all of the analyses. Thus, the agreement for tests ST200C, ST200E1 and ST200E1b was slightly improved, while the overestimation of test ST200E2 became slightly larger. The high capacity of the unit with grouted ends, ST200E1M, could not be described.

(*c*) The mesh was refined again, which led to slightly increased maximum loads in the analyses of units on thick soft bearings, for those analyses that were previously underestimated. Thus, the agreement for tests ST200C, ST200E1 and ST200E1b was slightly improved, while the overestimation of test ST200E2 remained almost the same. However, the maximum load in the analysis of the test with grouted ends, ST200E1M, did not change, and thus this test was still underestimated. Furthermore, these analyses became rather time-consuming, due to the dense mesh.

As none of these attempts managed to describe the increased capacity for the test on a mortar bed or to sufficiently improve the agreement for the other tests, it was decided to present the results from the original analyses. It is noteworthy that when the measured capacities were compared with the expected ones calculated according to EN1168 CEN/

TC229[9,13] the conclusions were as follows: for the 200 mm thick units supported on a thick soft bearing strip and for the 400 mm thick unit supported on a mortar bed the agreement was good. However, for the 400 mm thick units supported on a thick soft bearing strip, the measured capacities were much lower than the predicted ones; for the 200 mm thick unit supported on a mortar bed, the capacity was greatly underestimated. This suggests that the experimental result of the 200 mm unit on mortar bed is exceptionally high or that the 200 mm units are more difficult to predict.

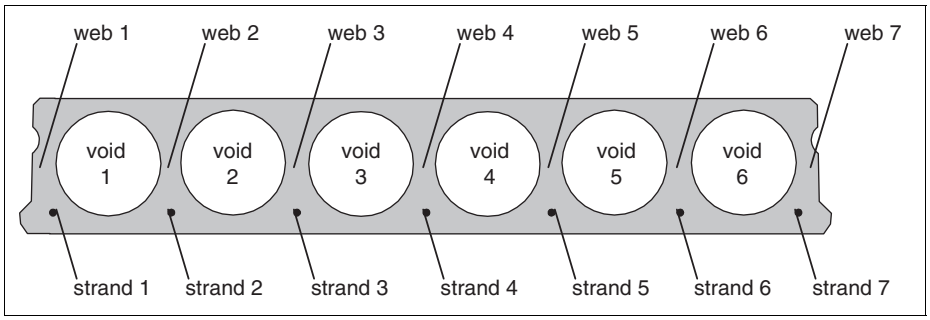

△ **Figure 13 Notations used to describe the tests and analyses of the 200 mm thick hollow core slab. Section seen from active end**

Analyses of tests on 200 mm thick units

The results from each of the tests and analyses of the 200 mm thick units are compared more in detail here, see also Broo.[18] Notations used to describe the tests and the analyses are shown in Figure 13. The load versus vertical displacement relations from the tests and the analyses of ST200E1 and ST200E1b are shown in Figure 14(a). In the analyses of ST200E1 and ST200E1b, the first cracking appeared at a load of $Q = 82$ kN in the form of a shear tension crack in the sixth web. At the maximum load, $Q = 86$ kN, shear tension cracks in the fourth and fifth webs arose.

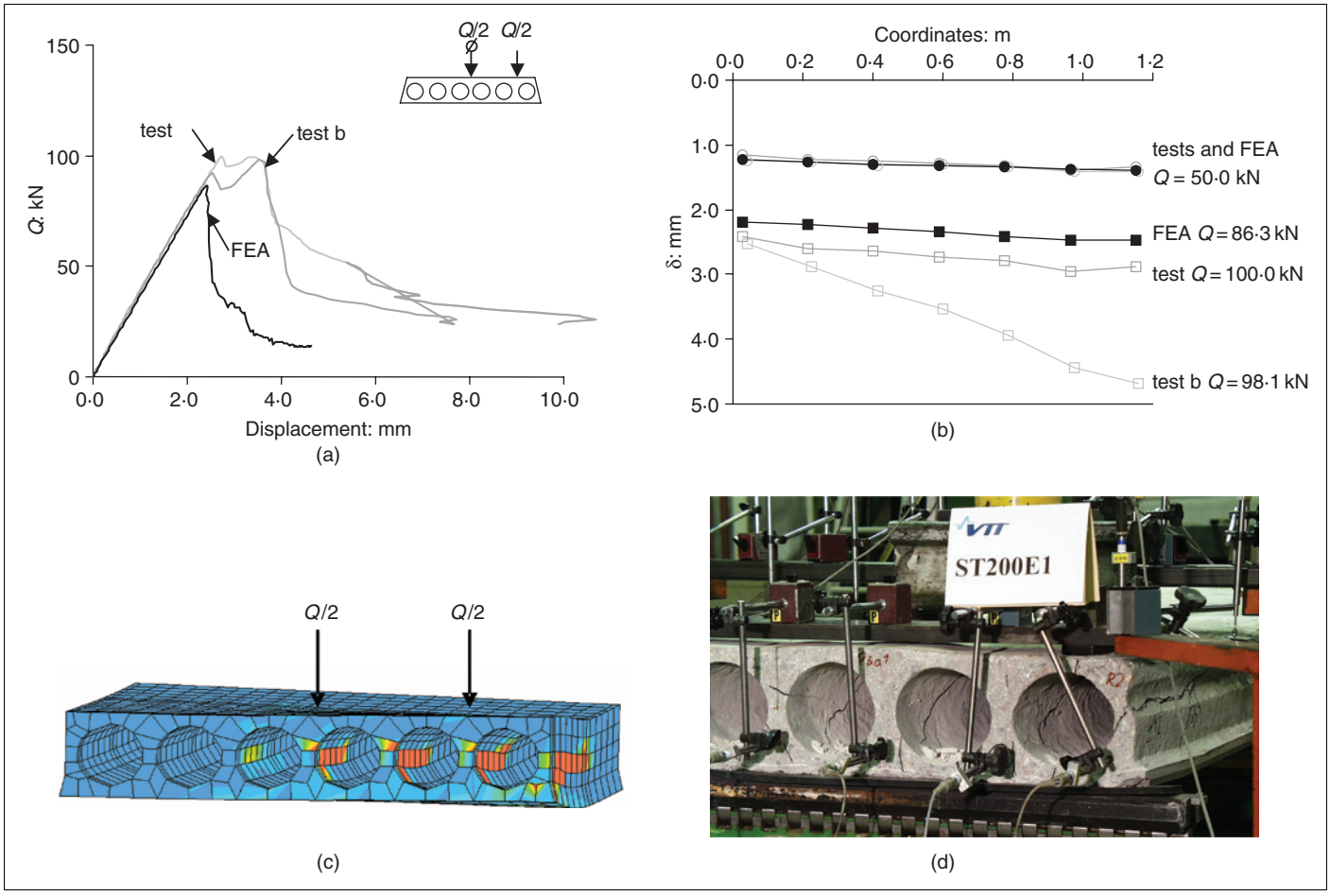

△ **Figure 14 Comparison of results from tests and analysis of ST200E1 and ST200E1b; (a) load versus vertical displacement, (b) deflection measured above the cross-section at each web, filled marks for the analysis and unfilled marks for the tests, (c) crack pattern from the analysis, (d) crack pattern from the test ST200E1**

After the maximum load, the outermost web also failed in shear tension (Figure 14(c)). The final crack pattern agrees well with those from the tests (Figure 14(d)). However, in the tests the first cracking occurred in the form of a diagonal crack in the outermost web and a longitudinal crack in the flange above the sixth void. Shear tension cracks in the fourth to sixth webs then occurred at maximum load for test ST200E1b and after maximum load was reached for test ST200E1. The measured displacements over the cross-section, at each web, show that the bending in the transversal direction of the unit is quite small (Figure 14(b)). The corresponding displacement from the analyses agrees well with the measured one until cracking; thereafter the rotation of this section increased in the test of ST200E1b.

The load versus vertical displacement relations from the tests and analyses of ST200C and ST200E2 are shown in Figure 15(a). In the analysis of ST200C, shear tension cracks appeared in the third and fifth webs before maximum load was reached. At the maximum load there were shear tension cracks in the second to the sixth webs. In the ST200C test the first cracking occurred in form of a longitudinal crack in the flange above and below the fifth void. At the maximum load shear tension cracks occurred in the webs, but the first, sixth and seventh webs remained uncracked.[13]

In the analysis of ST200E2, the first cracking occurred at maximum load in the form of shear tension cracks in the outermost web. After maximum load, shear tension cracks also appeared in the fifth and sixth webs. This can be compared with the ST200E2 test, where a diagonal crack in the outermost web and a longitudinal crack in the flange above the outermost void had occurred before the sixth web failed in shear tension at maximum load. The measured displacements above the cross-section, at each web, for the test and analysis of ST200E2 are shown in Figure 15(b). These show that the bending in the transversal direction of the unit is quite small; however, after cracking, the rotation of the section increased significantly.

A test similar to the ST200E1 one was also conducted: ST200E1M with grouted ends and on a mortar bed. This resulted in a much higher capacity for shear and torsion (Figure 16). This difference could not be described in the analysis. In the test of ST200E1M the first cracking occurred at the maximum load, in the form of diagonal cracks in the fourth to seventh webs and a longitudinal crack in the flange.[13] In the analysis the first cracking occurred in the sixth web at a load of $Q = 90$ kN. At what could be considered to be the maximum load, $Q = 101$ kN, there were cracks in the fifth, sixth and seventh webs. After this point, there were large errors in the solution, therefore this was considered as the maximum load. After the maximum load there were cracks in all webs except the first and a transversal crack in the top and bottom flanges along the support. No longitudinal cracks occurred in the analysis. No reasonable explanation was found for the increased capacity or why the analysis could not describe this.

To conclude, the sequence in cracking was well described by the analyses except for the longitudinal cracking, which occurred only in the tests. The displacements above the cross-section in the analyses corresponded well with the measured ones until cracking. The maximum load was, however, underestimated for the tests of ST200C and ST200E1M, while it was slightly overestimated for ST200E2.

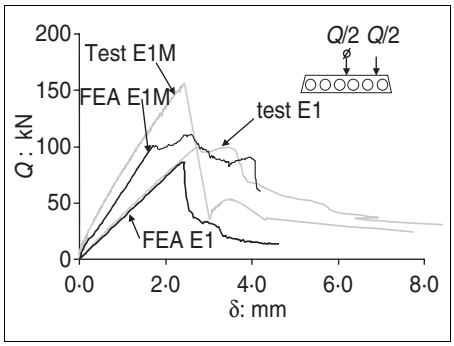

△ **Figure 16 Comparison of results from tests and analyses of ST200E1M and ST200E1; load versus vertical displacement**

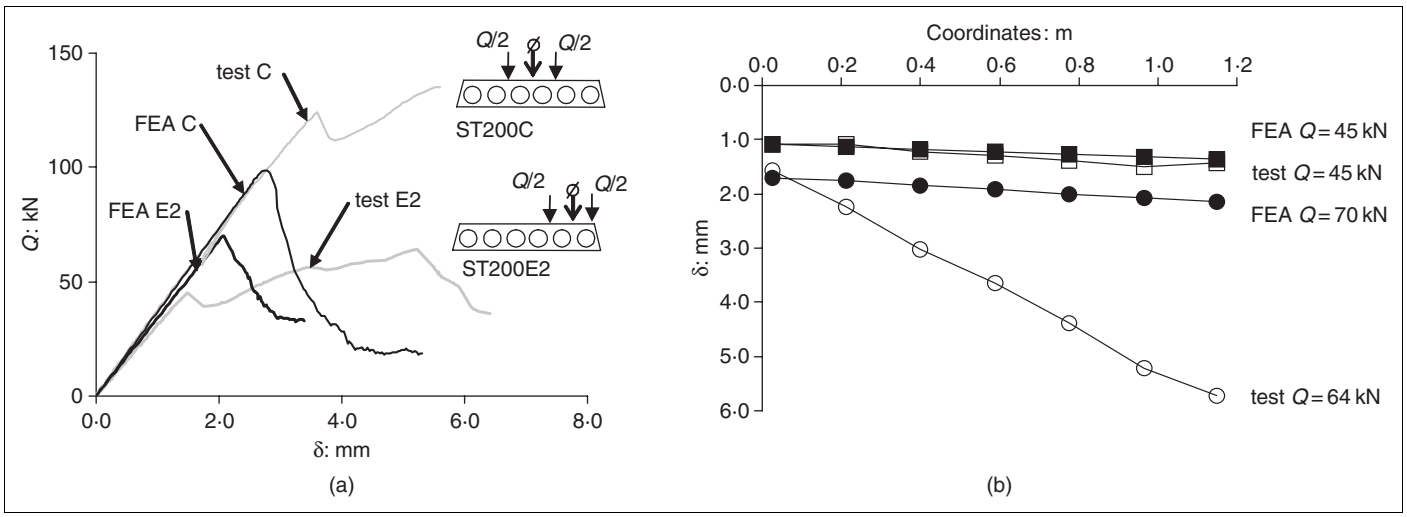

△ **Figure 15 Comparison of results from tests and analyses of ST200C and ST200E2; (a) load versus vertical displacement, (b) deflection measured above the cross-section at each web, ST200E2, filled marks for the analysis and unfilled marks for the test**

Analyses of tests on 400 mm thick units

In all tests on 400 mm units, there was a thin longitudinal crack above one of the outermost voids at both slab ends before the loading started. For the eccentrically loaded units, the surroundings of these cracks remained un-cracked during the tests; most likely these cracks did not influence the results of the tests. For the two centrically loaded units, these cracks did influence the results of the tests.[13] as they were a part of the final crack pattern. In the following, the results from each of the tests and analyses of the 400 mm thick units are compared and evaluated in more detail, see also Broo.[18] Notations used to describe the tests and the analyses are shown in Figure 17.

The load versus vertical displacement relations from the tests and the analyses of ST400C and ST400C2 are shown in Figure 18(a). In the analyses of the centrically loaded units the shear tension failure occurred in the centre webs, while the outermost webs remained un-cracked (Figures 18(d) and (f)). In the tests the first shear tension crack arose in one of the outermost webs before the maximum load was reached, when the centre webs failed in shear tension (Figures 18(e) and (g)). This could be explained by the initial longitudinal crack, above one of the outermost voids, observed before loading, which was a part of the final crack pattern. The measured displacements above the cross-section, at each web, show that the hollow core unit also bends in the transverse direction (Figure 18(b) and (c)). The differences in the displacements above the cross-section are smaller in the analysis. An explanation could be that the coarse mesh is less accurate in describing bending. Due to the first crack in the outermost web, which occurred in the tests but not in the analyses, the stiffness of the hollow core section was changed (lowered) in the tests and the displacements of the whole section increased.

The load versus vertical displacement relations from the tests and analyses of ST400E1 and ST4002E are shown in Figure 19(a). At first, the maximum load appears to be overestimated in the analyses. It should be noted, however, that because of the modelling technique with a pre-defined bond–slip relationship between the strand and the surrounding concrete elements, the transverse strain in a concrete element would not influence the bond versus slip of the strand in the analyses. In reality, a crack in the concrete cover below a strand would decrease the bond-stress and increase the slip of the strand, which would decrease the effect of the prestressing. Thus, cracking below a strand would most likely lead to anchorage failure, resulting in shear tension cracking in the web. To evaluate the effect of the lateral dilation in the soft bearing strip, the strain in the concrete elements below the strands was checked against the concrete tensile strain at cracking, $\varepsilon_{ct} = f_{ct}/E_c$. The load versus tensile strain in the concrete elements below the strand in web 5, from the analysis of ST400E1, are shown in Figure 19(b). If the calculated tensile strain in the element exceeds ε_{ct}, the element could be considered cracked and the slip of the strand would increase. This line of argument means that the load at which ε_{ct} is reached could be considered as the maximum load; in this case the maximum load for ST400E1 would be 170 kN, and for ST400E2 175 kN. This could be compared with the maximum loads 166·9 kN and 160·7 kN, respectively, reached in the experiments (Figure 19(a)). In the analysis of ST400C1 and ST400C2 and the 200 mm thick units, the ε_{ct} was never exceeded in the concrete elements under the strands at the support.

The tests with one eccentric load were made on hollow core units supported in two ways: on a thick soft bearing strip (ST400E1), and on a mortar bed with grouted ends (ST400E1M). The latter resulted in a much higher capacity for shear and torsion (Figure 20(a)). This difference was reflected in the analyses by anchorage failure due to cracks in the concrete cover below the strands, caused by the dilation in the soft bearing strip; the difference was also caused by the longitudinal cracks that arose in the top and bottom flanges before ultimate failure. These cracks occurred in both the test and the analysis of ST400E1 as well as of ST400E1M. However, for ST400E1M, the grouting prevented the cracks from reaching the support region (Figures 20(c) and (d)). This confirms that the grouting is of great importance to ensure the anchorage of the prestressing strands in the short support lengths that are common for hollow core units. In both the test and the analysis of ST400E1M, a shear tension crack and a longitudinal crack in the bottom flange below the load occurred at the maximum load. In the test also a diagonal crack in the outermost web could also be seen, but in the analysis the outermost web remained un-cracked. The measured displacements above the cross-section, at each web, show that the hollow core unit also bends in the transversal direction, even if the support is stiff (Figure 20(b)).

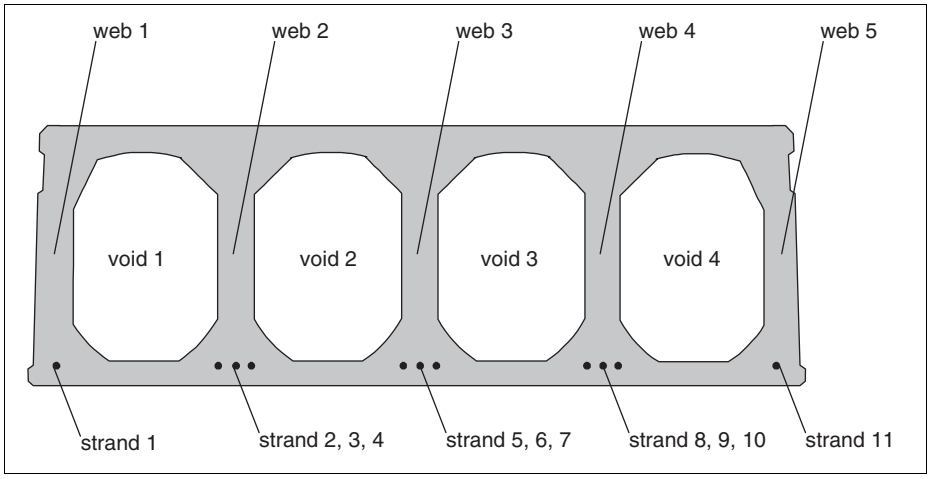

△ **Figure 17 Notations used to describe the tests and analyses of the 400 mm thick hollow core units. Section seen from active end**

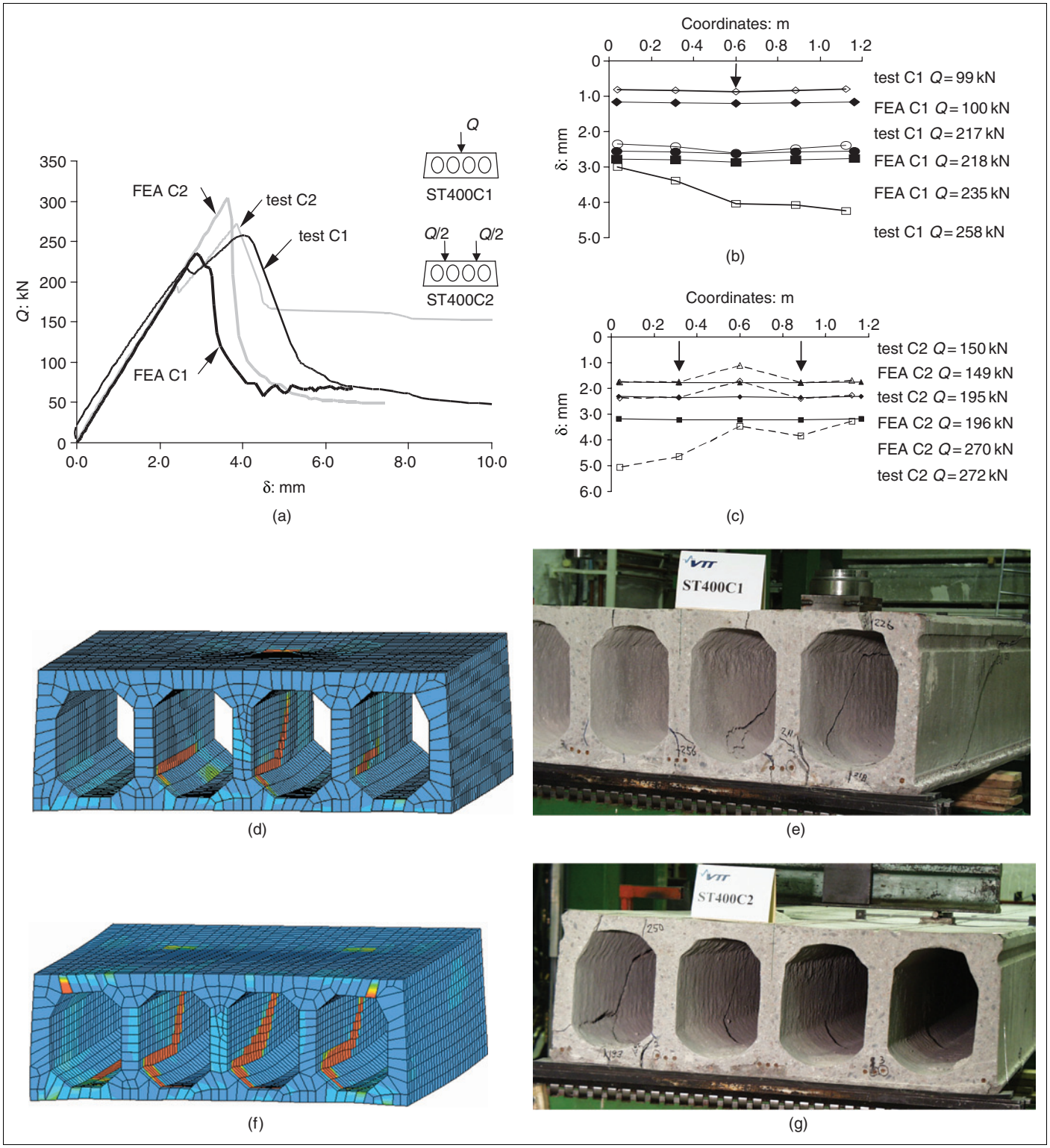

△ **Figure 18 Comparison of results from tests and analyses of ST400C1 and ST400C2. (a) Load versus vertical displacement. Deflection measured above the cross-section at each web, filled marks for the analysis and unfilled marks for the test: (b) ST400C1, (c) ST400C2. Crack pattern after maximum load: (d) analysis ST400C1, (e) test ST400C1, (f) analysis ST400C2, (g) test ST400C2**

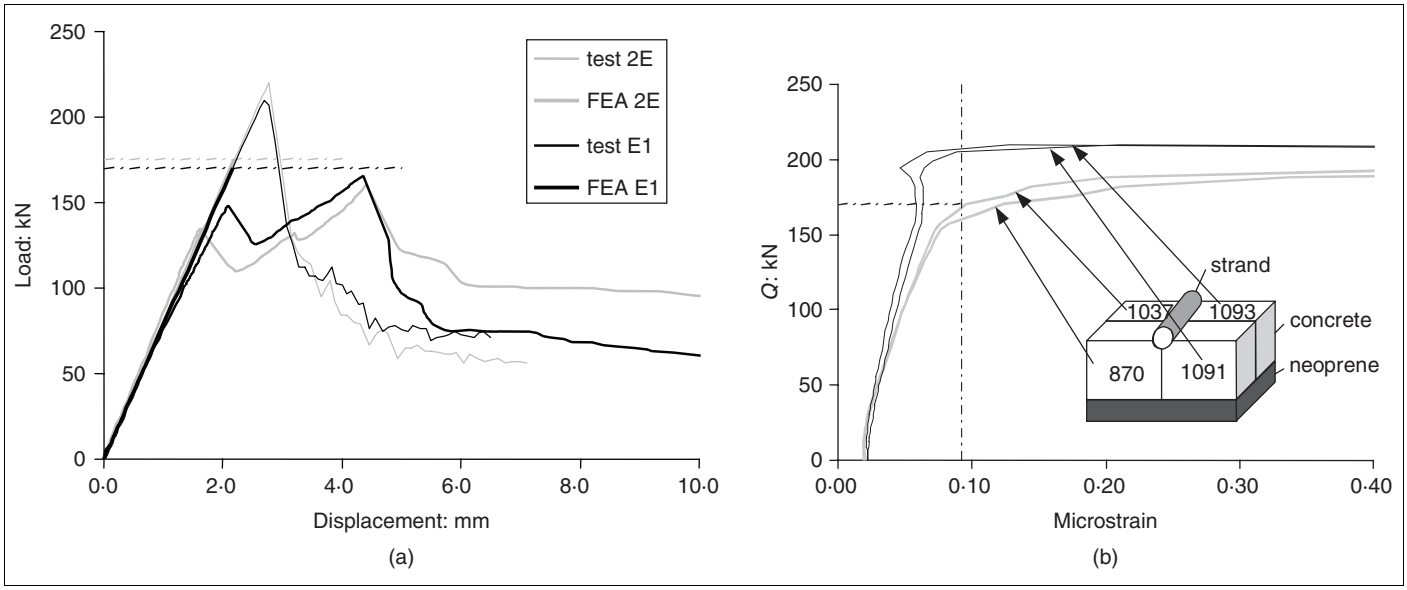

△ **Figure 19 Comparison of results from tests and analyses of ST400E1 and ST4002E: (a) load versus vertical displacement; (b) load versus strain in the concrete elements below the strand in web 5 from the analysis of ST400E1**

Conclusions

Three-dimensional finite element models of hollow core units were worked out and verified by non-linear finite element analyses of full-scale experiments. Combining coarse solid elements for critical parts with beam elements for the rest was shown to be a reasonable modelling level, with regard to desired simplifications. Tests on 200 mm and 400 mm thick hollow core units subjected to various combinations of shear and torsion were modelled. In general, the finite element analyses of the experiments could describe the overall behaviour, failure mode, crack pattern, maximum load, and displacements quite well, with exception of the centrically loaded 200 mm thick unit and the 200 mm unit supported on a mortar bed. All of the analyses showed the same failure mode as in the tests, namely, shear tension failure.

Both tests and analyses revealed that the support conditions were of great importance for the capacity; thus, the support detailing must be included in the model. The modelled tests were made on hollow core units supported in two ways: (a) on a roller bearing with a thick soft bearing strip between the unit and the support, and (b) with grouted ends and a mortar bed between the unit and the supporting concrete beam. The latter exhibited a much higher capacity for shear and torsion. For the 400 mm thick units, this difference lay in the dilation of the soft bearing strip, which caused cracks in the concrete cover below the strands, and led to anchorage failure. The cracks formed in both the tests and the analyses. For the hollow core unit with grouted ends, the grouting prevented these cracks. This confirms that the grouting is of great importance to assure the anchorage of the prestressing strands with the short support lengths that are common for hollow core units. For the 200 mm thick units, no such cracks were observed, either in the tests or in the analyses, and there was no reasonable explanation for the higher capacity obtained in the test with grouted ends.

The tests on a thick soft bearing strip showed that a redistribution of the load between the webs after cracking is possible, and that the load could be further increased. However, it is worth noting that for all 400 mm thick units, even the centrically loaded, the first cracking occurred in one of the outermost webs. The tests showed that the 400 mm thick units also bend transversely when concentrated loads are applied. It does not matter whether the support is stiff or soft. The mesh used in the models was too coarse to describe this accurately.

The models presented will be used to analyse the effect of parameters that influence the shear and torsion response. In finite element analyses of hollow core floors,[10] these models have been included in global models to enable modelling of shear and torsion failure.

Acknowledgements

The photographs in this paper are used with kind permission of VTT. The authors would like to thank Dr Matti Pajari at VTT for letting us attend the tests and use the data collected directly after the tests were carried out. The research was financed by the 5th Framework of European Commission, the International Prestressed Hollow Core Association, the 'Bundesverband Spannbeton-Hohlplatten' in Germany, and also by the cooperating partners, which were Chalmers University of Technology, VTT, Consolis Technology, Strängbetong, Castelo and Echo.

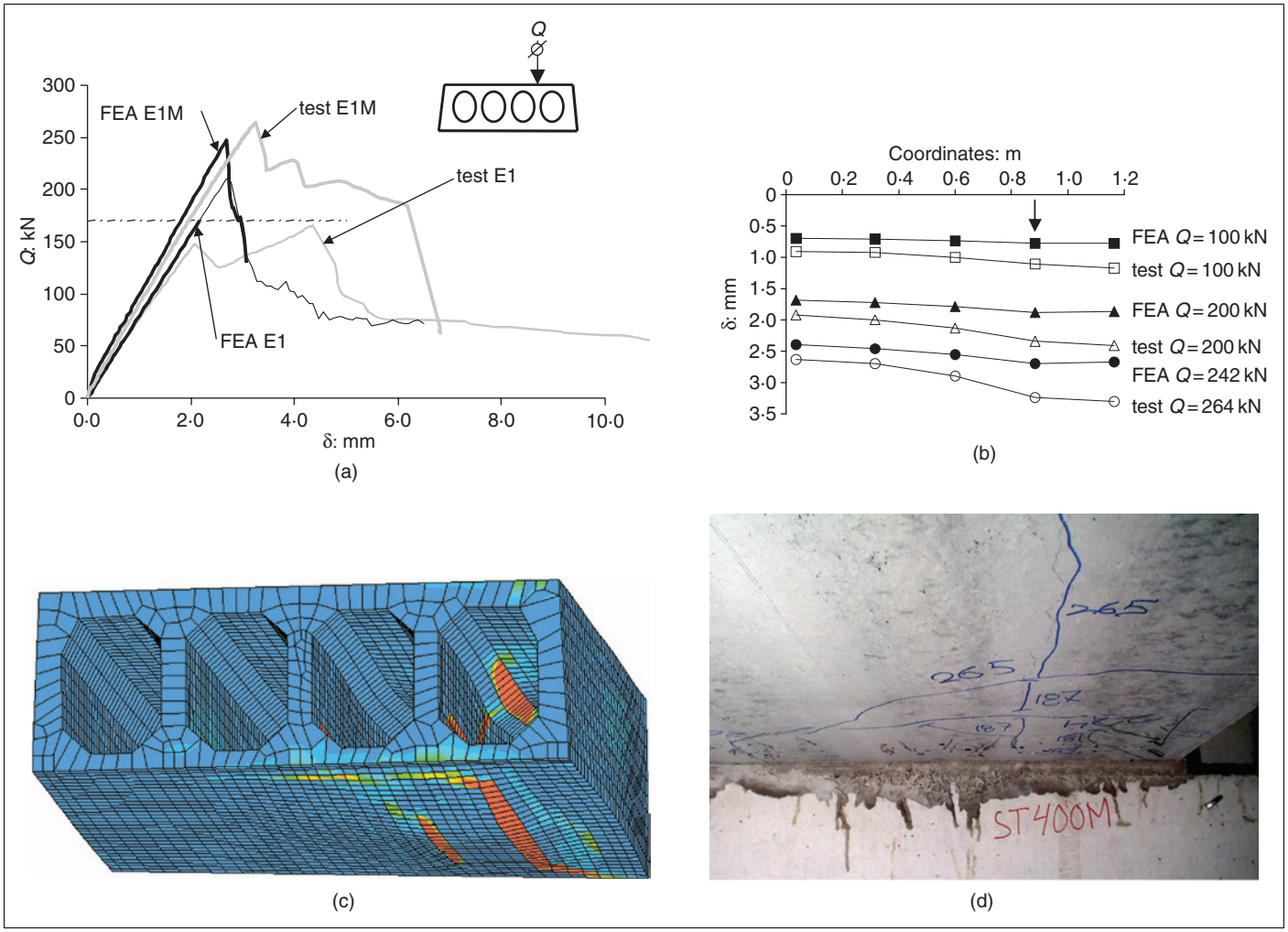

△ **Figure 20 Comparison of results from tests and analyses of ST400E1 and ST400E1M: (a) load versus vertical displacement; (b) deflection measured over the cross-section at each web, ST400E1M, filled marks for the analysis and unfilled marks for the test; (c) crack pattern from the analysis of ST400E1M after maximum load; (d) crack pattern from the test ST400E1M**

References

1. Walraven, J. C. and Mercx, W. P. M. The bearing capacity for prestressed hollow core slabs. *Heron*, 1983, **28**, No. 3, 3–46.
2. Pisanty, A. The shear strength of extruded hollow-core slabs. *Materials and Structures*, 1992, **25**, No. 148, 224–230.
3. Yang, L. Design of prestressed hollow core slabs with reference to web shear failure. *Journal of Structural Engineering - ASCE*, 1994, **120**, No. 9, 2675–2696.
4. Jonsson, E. Shear capacity of prestressed extruded hollow-core slabs. *Nordic Concrete Research*, 1988, No. 7, 167–187.
5. Becker, R. J. and Buettner, D. R. Shear tests of extruded hollow-core slabs. *PCI Journal*, 1985, **30**, No. 2, 40–54.
6. Pajari, M. *Shear resistance of prestressed hollow core slabs on flexible supports*. PhD Thesis, VTT, Technical Research Centre of Finland, Espoo, 1995.
7. Pajari, M. Shear resistance of PHC slabs supported on beams. II: Analysis. *Journal of Structural Engineering - ASCE*, 1998, **124**, No. 9, 1062–1073.
8. Gabrielsson, H. *Ductility of high performance concrete structures*. PhD Thesis, Division of Structural Engineering, Luleå University of Technology, Luleå, Sweden, 1999.
9. CEN/Tc229. *Precast concrete products – hollow core slabs.* European Standard EN 1168:2005:E, Brussels, 2005.
10. Lundgren, K., Broo, H., and Engström, B. Analyses of hollow core floors subjected to shear and torsion. *Structural Concrete*, 2004, **5**, No. 4, 1464–4177.
11. Broo, H. and Lundgren, K. Finite element analyses of hollow core units subjected to shear and torsion. Chalmers University of Technology, Department of Structural Engineering, Concrete Structures, Göteborg, Report 02:17, December 2002.
12. TNO. *DIANA Finite Element Analysis, User's Manual release 8.1*. TNO Building and Construction Research, 2002.
13. Pajari, M. Shear–torsion interaction tests on single hollow core slabs. Technical Research Centre of Finland, VTT Building and Transport, Espoo VTT research notes 2275, 2004.
14. Lundgren, K. and Gylltoft, K. A model for the bond between concrete and reinforcement. *Magazine of Concrete Research*, 2000, **52**, No. 1, 53–63.

15. Gustavson, R. and Lundgren, K. Modelling of bond between three-wire strands and concrete. *Magazine of Concrete Research*, 2006, **58**, No. 3, 123–133.
16. Pajari, M. Pure torsion tests on single slab units. Technical Research Centre of Finland, VTT Building and Transport, Espoo, Internal report VTT research notes 2273, December 2004.
17. Lundgren, K. Steel-encased pull-through tests of seven-wire strands. Department of Structural Engineering, Concrete Structures, Chalmers University of Technology, Göteborg, Sweden, Report 02:13, 2002.
18. Broo, H. *Shear and torsion interaction in prestressed hollow core slabs*. Licentiate thesis, Department of Civil and Environmental Engineering, Division of Structural Engineering, Chalmers University of Technology, Göteborg, 2005.

Paper II

Analyses of hollow core floors subjected to shear and torsion

Lundgren K, Broo H.. and Engström B.

.*Structural Concrete*, Vol. 5, No. 4, pp. 161—172, 2004.

Analyses of hollow core floors subjected to shear and torsion

K. Lundgren, H. Broo and **B. Engström**

Hollow core units are commonly subjected to shear and torsion, for example when placed in floors with openings or skew ends. Present design codes give rough estimations for how the torsional moment can be estimated. The aim of this work was to increase the understanding of torsion in hollow core floors, and to develop a modelling strategy suited to model complete hollow core floors subjected to shear and torsion, using the non-linear finite element method. In a simplified global model, the cross-section of each hollow core unit was represented by one beam element, and the neighbouring hollow core units were coupled by means of slave nodes in the corners, allowing compression but not tension. Comparisons with test results showed that the simplified global model can, with reasonable accuracy, describe the real behaviour of hollow core floors. Furthermore, the simplified global model was used together with solid elements in a part of a hollow core unit, to enable modelling of a shear and torsion failure. Good agreement with test results was obtained concerning failure mode, crack pattern, maximum load, and displacements. Thus, the modelling technique used appears to describe the actual situation in a good way.

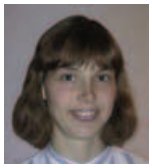

Karin Lundgren
Chalmers University of Technology, Göteborg, Sweden

Helén Broo
Chalmers University of Technology, Göteborg, Sweden

Björn Engström
Chalmers University of Technology, Göteborg, Sweden

Introduction

Hollow core units are precast products commonly used for floors. The cores reduce the dead weight and this, in combination with prestressing, enables long spans. The hollow core units are mainly designed to resist bending moments. However, there are many applications in which hollow core units are subjected to combined torsion and shear, for example three-line supported slabs, floors with openings, alternating position of columns at both slab ends, and slabs with significant skew ends. The hollow core units are in practice connected to each other with longitudinal joints that are grouted in situ. Load on a single hollow core unit is transversely distributed to the surrounding units by the shear keys in the longitudinal joints. Normally, the joints between hollow core units crack and, in the design, are assumed to act as hinges. Consequently, load distribution to the neighbouring units always introduces a torsional moment.

Present design codes give rough estimations for how the torsional moment can be estimated. There has been only a small amount of work done concerning hollow core units or floors subjected to torsion and shear. The behaviour of single units has been studied by Gabrielsson,[1] who did tests and analytical work. More experimental work on single units has been done by Pajari,[2,3] and the potential for the use of the non-linear finite element method for analyses of single units subjected to combined shear and torsion was studied by the authors.[4] However, in the practical applications where shear and torsion prevail, the hollow core units are grouted together to form a complete floor. There exists some research on complete floors. For example, Walraven and van der Marel[5] have carried out tests on floors supported on three-sides. Load distribution has been investigated by Stanton[6] (see also Stanton[7]), and also by Van Acker[8] and Pfeifer and Nelson.[9]

The aim of the work described in this paper was to increase the understanding of torsion in hollow core floors, and to develop a modelling strategy suitable to describe the behaviour up to failure of complete floors of hollow core units subjected to shear and torsion. The described work was part of a European project called Holcotors, in which both single hollow core units and complete floors were tested and analysed. This paper focuses on modelling of complete floors: various modelling techniques are discussed and compared with experimental results.

Modelling technique for complete floors

As the intention with this work was to model complete floors, the first question that arises is the level of detail that it is reasonable to choose. The aim was to avoid excessively time-consuming analyses, and to focus on a modelling level which enables one to establish and carry out analyses of several floor types within a moderate period. To be able to describe a shear and torsion failure in a hollow core element, however, it is necessary to model each web, either with solid elements or with shell elements. For both choices, it was judged that several elements over the height would be needed in order to describe the bending adequately. In particular, when modelling slabs that have a geometry which includes circular holes, it was considered easier to choose solid elements. Analyses carried out on single hollow core units also showed that it is necessary to incorporate the interaction between the strands and the concrete through a bond–slip relation.[10] However, this modelling technique was judged to be inapplicable for complete floors, as the resultant analyses

1464–4177 © 2004 Thomas Telford and *fib*

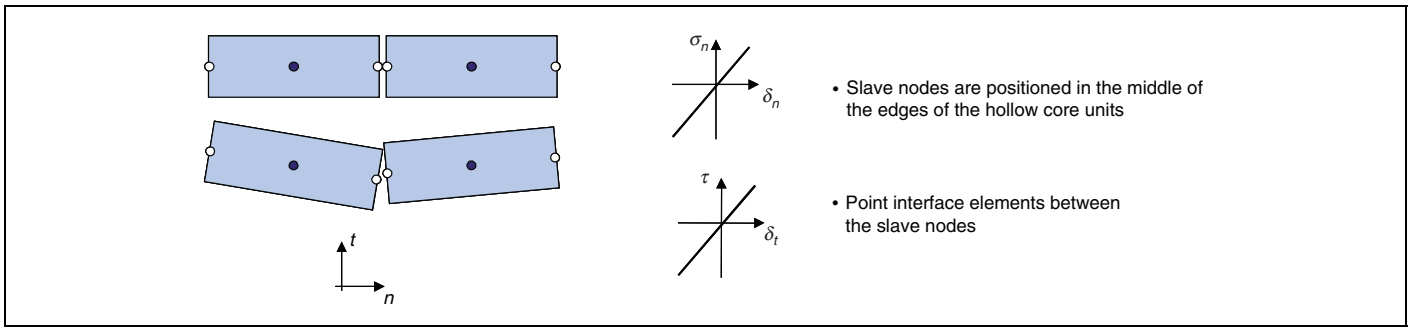

△ **Figure 1 Modelling of joints, alternative (a)**

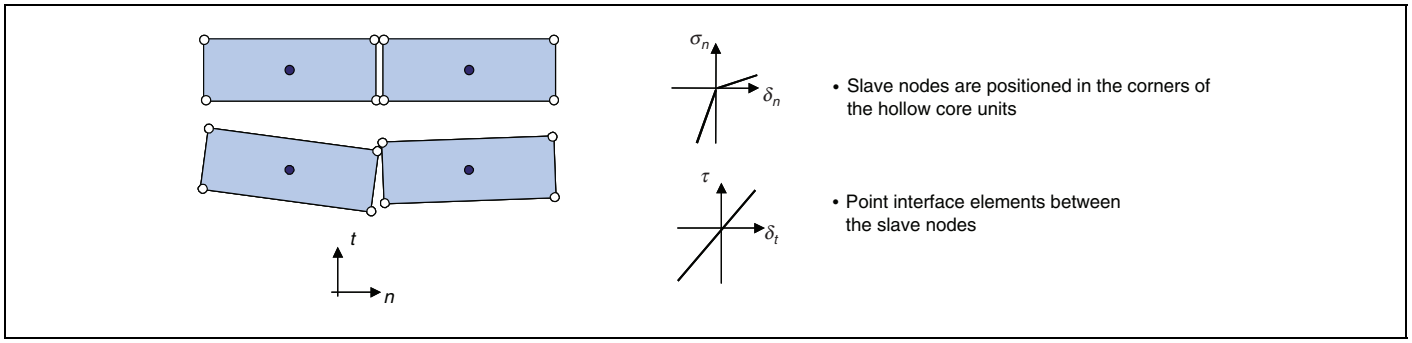

△ **Figure 2 Modelling of joints, alternative (b)**

would be too time-consuming. A simplified global model for the part of the floor where failure was not expected was necessary. The intention was to combine this global model with solid elements in the part of the floor where failure was expected. The simplified global model is thus not intended to be able to describe the shear and torsion failure of a floor, only its behaviour until shear/torsion cracking occurs. However, as non-linear material models are used, the global model is capable of describing bending cracks as well as bending failure. The general finite element program Diana was used in all analyses.[11]

Simplified global models for complete floors

According to CEN/TC229,[12] shell elements connected with hinges to model the behaviour of the longitudinal joints are recommended for analyses of complete floors. This was considered as one alternative. Another alternative was to use beam elements, each representing the whole cross-section of one hollow core unit.

The hollow core units are in practice connected to each other with longitudinal joints that are grouted in situ. Two alternatives were tested for the description of these joints as shown in Figures 1 and 2. In both alternatives, point interface elements were used between slave nodes that were tied to the nodes describing the hollow core units. One difference between the two alternatives was the position of the slave nodes: in alternative (a) the slave nodes are positioned in the middle of the edges of the hollow core units, whereas in alternative (b) the slave nodes are positioned in the corners of the hollow core units. In alternative (a), the point interface was assumed to carry both tensile and compressive forces in both the normal and transverse directions. The stiffness in the normal direction was chosen as 3×10^{10} N/m^3, and the transverse stiffness was 1×10^9 N/m^3. This modelling is very close to a hinge, as the stiffness in the normal direction is high, although with shear deformations added, as the transverse stiffness is relatively low. In alternative (b), tensile and compressive forces were still allowed in the transverse direction, whereas, in the normal direction, compressive forces were allowed but a very small stiffness was used for the tensile side, thus reducing the tensile stresses. The same transverse stiffness as in alternative (a) was used, and the same stiffness for compression in the normal direction (3×10^{10} N/m^3). The stiffness in tension was only 1×10^4 N/m^3, in order to represent cracked concrete in the joint. The reason for using both these alternatives for the joints was that hinges are normally assumed, and therefore can be regarded as a reference. However, it can be argued that the modelling alternative (b) corresponds better with physical reality, as the effect of the height of the slab is included.

Modelling of material

Several experiments were modelled, two floors that have been tested at VTT (Technical Research Centre of Finland),[13,14] and three floors that have been tested in Delft.[5] In these experiments, the compressive strength

Table 1 Input data used in the analyses

Parameter/analysis	(1)	(2) Hollow core no.				(3)	(4)
		1	2	3	4		
Young's modulus: GPa	38·0	39·1	39·2	38·1	38·3	39·8	36·9
Compressive strength: MPa	–	60·4	60·8	55·7	56·5	63·6	50·8
Tensile strength: MPa	–	3·72	3·74	3·54	3·58	3·84	3·35
Fracture energy: N/m	–	95·6	95·6	95·6	95·6	109·5	93·5
Shear factors	4·06	4·06	4·06	4·06	4·06	4·06	6·2
(only for beam elements)	4·06	4·06	4·06	4·06	4·06	4·06	6·2

(1) Comparison beam/shell elements
(2) Floor VTT[13]
(3) Floor Pajari[14]
(4) Floors Walraven and van der Marel[5]

was tested on cylinders—cores drilled from the tested specimens. The drilled cores from the tests carried out at VTT had a diameter of 50 mm and a height of 50 mm, whereas those that were tested in Delft had a diameter of 60 mm and a height of 120 mm. It was assumed that the strength of cylinders with diameter 150 mm and height 300 mm, f_{ccm}, corresponds to 85% of the strength of the tested drilled cores. This value was used as compressive strength in the analyses. Furthermore, from this value, the mean tensile strength, f_{ctm}, was calculated according to Comité Euro-International du Béton (CEB);[15] the fracture energy, G_F, and Young's modulus, E_{ci}, were calculated according to CEB.[16] Poisson's ratio for the concrete was set to 0·15 in all analyses. The values used for the different analyses are shown in Table 1. In all analyses of experiments, a constitutive model based on non-linear fracture mechanics, using a rotating crack model based on total strain, was used for the concrete.[11] The deformation of one crack was smeared over a length corresponding to the size of one element in the part modelled with solid elements. In beam or shell elements, the deformation of one crack was smeared over an assumed crack distance of 300 mm. For the tension softening, the curve by Hordijk *et al.* was chosen, as described in TNO.[11] The hardening in compression was described by the expression of Thorenfeldt *et al.*[17]

The constitutive behaviour of the pre-stressing steel was modelled by the Von Mises yield criterion with associated flow and isotropic hardening. The material properties in the pre-stressing steel used in the floor test by Pajari[14] were measured in tensile tests.[3] For the other tests, no measurements of the steel could be found; due to lack of better data the same material behaviour was therefore assumed. The stress in the steel was well below the yield stress in all analyses. The pre-stressing steel was modelled as 'embedded' in the simplified global models, which means that complete interaction between the concrete and the pre-stressing steel was assumed. In the part modelled with solid elements, a bond–slip relation was used to model the interaction between the pre-stressing steel and the concrete. The bond–slip relation used as input was taken from results in pull-through tests by Lundgren,[18] and is shown in Figure 3.

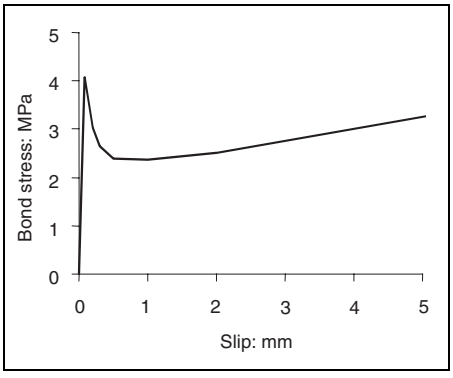

△ **Figure 3 Bond stress versus slip used as input**

Development and verification of a simplified global model

Comparison between shell elements and beam elements

Some analyses were carried out to determine the difference in use between shell and beam elements to model the behaviour of a complete floor. A floor consisting of five hollow core units, loaded with a point load in the centre of the span, was modelled (Figure 4). The span length was varied in the analyses. The floors were modelled using both beam elements (Figure 5) and shell elements (Figure 6). The beam elements used were three-node and three-dimensional, using a two-point Gauss integration scheme; see TNO.[11] The beam elements were assigned the properties of a 400 mm high and 1200 mm wide hollow core unit by defining the cross-section with 17 zones (Figure 7). To obtain correct torsional stiffness of the beam elements, two factors which in TNO[11] are called 'shear factors' were adjusted. The torsional stiffness was evaluated from pure torsion tests carried out on 400 mm hollow core units.[2]

The shell elements used were four-node quadrilateral isoparametric curved shell elements, based on linear interpolation and Gauss integration. They were assigned a thickness of 354 mm, which gives the same bending stiffness as a 400 mm hollow core slab in the main direction. The bending stiffness in the transverse direction was assumed to be the same.

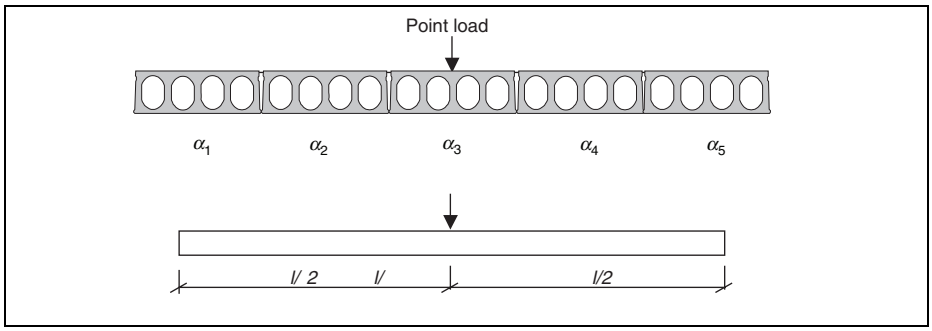

△ **Figure 4 Analysed load case: a floor consisting of five hollow core units loaded with a point load in the centre of the span**

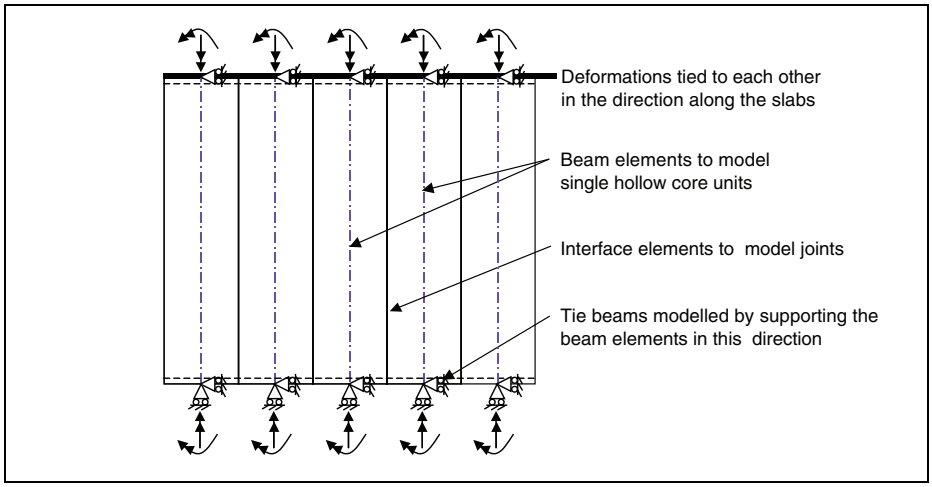

△ **Figure 5 Model using beam elements**

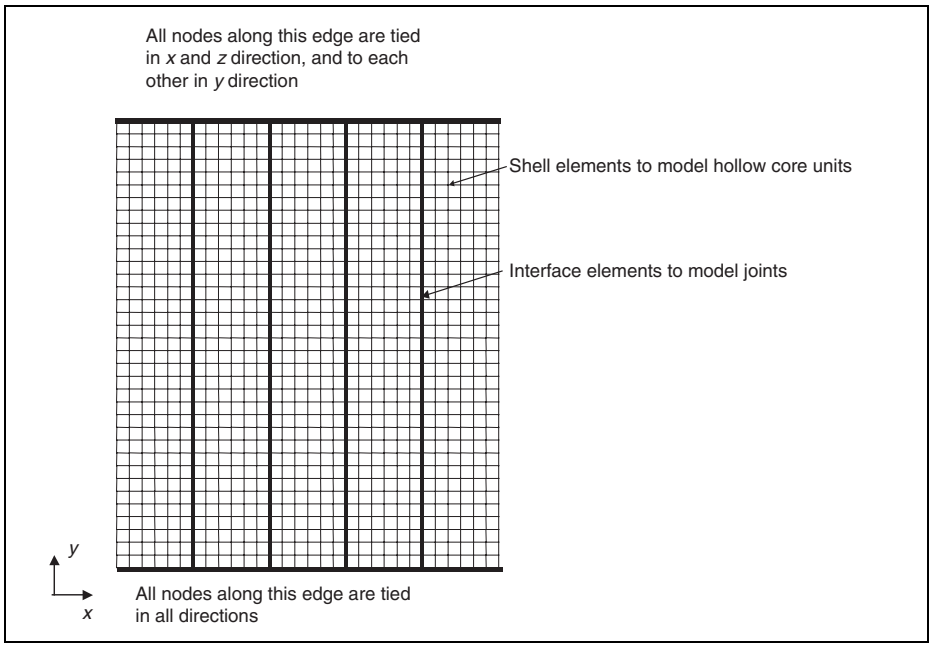

△ **Figure 6 Model using shell elements**

The joints were modelled using alternative (b) in Figure 2, namely with slave nodes in the corners of the hollow core units, connected with point interface elements that allow compressive stresses but only low tensile stresses.

Some results from these analyses are shown in Figures 8 to 11. In Figure 8(a), the transverse distribution of the bending moment at mid-span in the analyses is compared with curves given in Fédération Internationale de la Précontrainte (FIP).[19] The results from the different kinds of analyses are close to each other, and also close to the curves given in FIP.[19] It is interesting to note, however, that in the curves given in FIP,[19] there is a safety factor of 1·25 on the loaded element (No. 3) included in the curves; one could expect a higher moment factor for this element than in the analyses. It is important to note that the transverse distribution of the shear at the supports was not the same as the transverse distribution of the bending moment at mid-span; compare Figures 8(a) and 8(b). The shear at the supports was more distributed among the hollow core units than the bending moment. Note, however, that the maximum shear force in the loaded hollow core unit was not at the support: as part of the shear force is transferred to the neighbouring hollow core units, the maximum shear force in the loaded hollow core unit was at the position of the point load (Figure 9(a)).

The transverse distribution of the support reaction along the support line in the analyses with shell elements is shown in Figure 10. The use of beam elements does not result in any distribution of the support reaction, but only in supporting force and supporting torsional moment at each hollow core unit. Here the support reaction was assumed to be linearly distributed along the support length of each

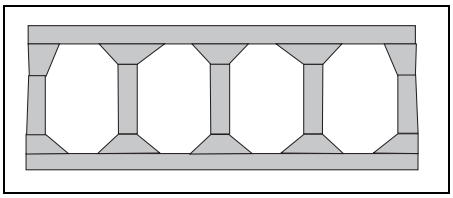

△ **Figure 7 The cross-section of the beam elements defined with zones**

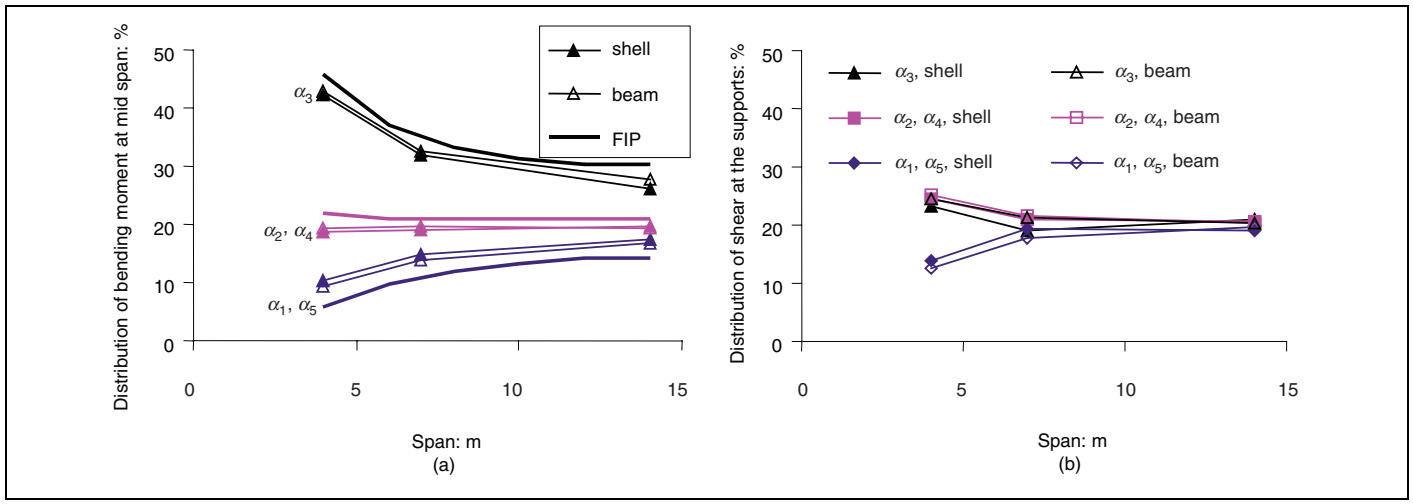

△ **Figure 8 (a) Transverse distribution of bending moment at mid-span; results from analyses with beam elements and shell elements are compared with curves given in FIP.[19] (b) Transverse distribution of shear at the supports. The subscripts indicate the number of the hollow core slab; see Figure 4**

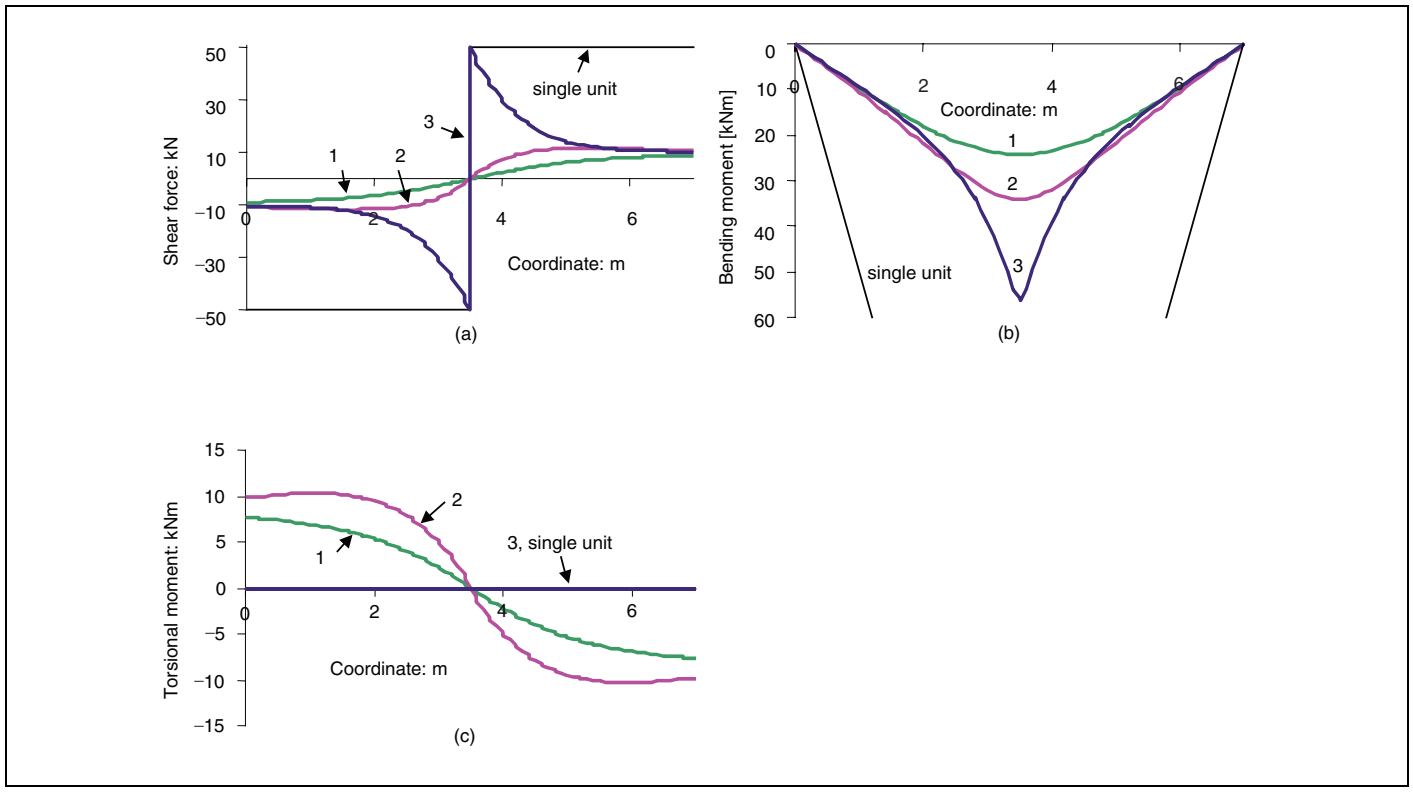

△ **Figure 9 (a) Shear force, (b) bending moment, and (c) torsional moment in the hollow core units due to a point load of 100 kN; results from analysis with beam elements with 7 m span. The numbers indicate the number of the hollow core unit; see Figure 4**

hollow core unit, to enable a comparison with the shell elements; see Figure 10. As can be seen, the use of shell elements led to an uneven distribution, with high peaks at the corners of the hollow core units that were loaded in torsion and, in addition, the loaded hollow core unit had an uneven distribution of the support reaction.

The displacements at mid-span are compared in Figure 11. As can be seen, the results differed slightly; the displacements were more evenly spread over the floor when shell elements were used. The main reason for this difference is that the torsional stiffness of the hollow core units becomes too large when the

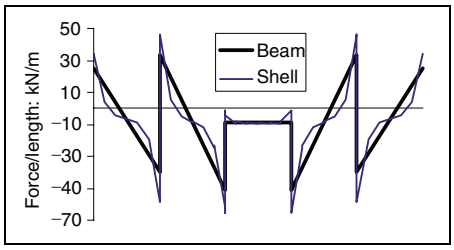

△ **Figure 10 Comparison of the distribution of support reaction along the support for an applied load of 100 kN; results from analyses of 7 m span**

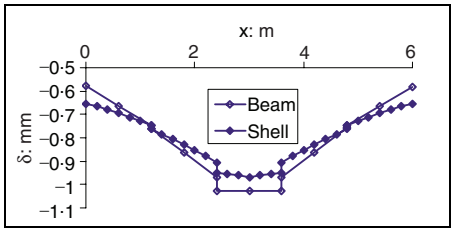

△ **Figure 11 Comparison of displacements at mid-span for an applied load of 100 kN; results from analyses of 7 m span**

shell elements are used, because the shell elements are too stiff in torsional behaviour.

Due to these results, it was decided to work mainly with beam elements, for several reasons. First, this makes it possible to obtain a correct relation between bending and torsional stiffness, and to model the geometry of the cross-section with zones. Thereby, and through using a non-linear material model for the concrete and including the pre-stress of the reinforcement, it is possible to describe the cracking in bending in a correct way. Moreover, beam elements are slightly less time-consuming than shell elements, and it was considered easier to couple beam elements to a part with solid elements.

Analyses of a floor tested at VTT in 1990

To check the modelling, some floor tests found in the literature were modelled. One floor with four 400 mm hollow core units grouted together that has been tested in Finland was analysed; see VTT[13] or Suikka and Parkkinen.[20] Loads have been applied to the floor at two different points, in two stages, and the support reactions and displacements at several spots have been measured. The floor was analysed using the same type of beam elements as described in the previous section. Input data used in these analyses are listed in Table 1. The joints were modelled using both alternatives (a) and (b) in Figures 1 and 2, namely with slave nodes either in the middle of the edges or in the corners of the hollow core units.

The measured support reactions are compared with the ones obtained in the analyses in Figure 12. The results show that the supporting forces from the analyses corresponded rather well with the measured ones, and that they were not influenced by the modelling of the joints. However, for the torsional moment, the modelling technique of the joints has an influence. As can be seen in Figure 12, the modelling technique alternative (b), with slave nodes in every corner of the hollow core elements, shows reduced values of the torsional moments in comparison with the modelling technique (a). These reduced torsional moments corresponded better to the measured ones. This is to be expected, as the effect of the height of the slab is included in modelling alternative (b) and therefore corresponds better with physical reality. This is the main reason why modelling technique alternative (b) for the joints is preferable.

The displacements for a load of 161 kN at a point close to one of the supports are shown in Figure 13. As can be seen, the displacements were larger in the test than in the analysis. However, when the displacements for a point

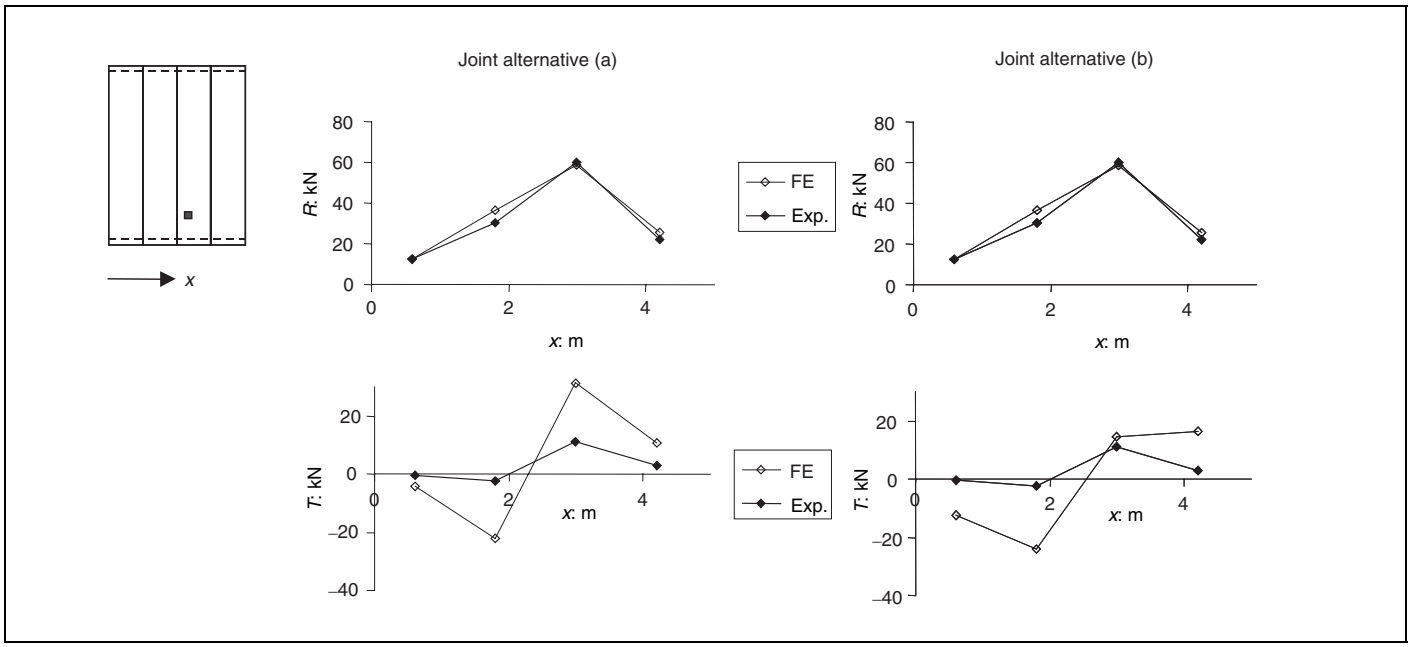

△ **Figure 12 Support reactions at a load of 161 kN in the marked point. The filled markers are experimental, from VTT[13]**

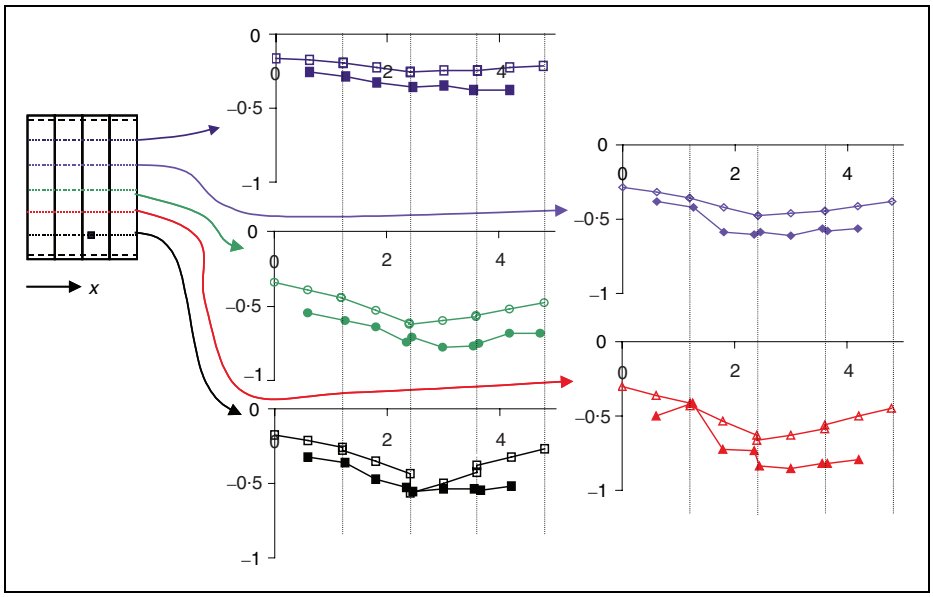

△ **Figure 13 Displacement (in mm) plotted against *x*-coordinate (in m) at a load of 161 kN in the marked position. The filled markers are experimental, from VTT,[13] and the unfilled are from the analysis with the joints modelled as in alternative (b)**

load in the centre of the span were compared (Figure 14), they corresponded rather well. It is worth noting that the displacements were very small. The choice of how the joints were modelled did not have any large influence on the displacements.

Analyses of floors supported along three edges

Hollow core floors supported along three edges are rather often used in reality. The hollow core units will then be loaded in torsion. Three such floors were tested in Delft.[5] The floors consisted of two hollow core units that had been grouted together. The floors had supports along three of their edges; the differences between the tests were the loading points and some detailing of the support arrangements. The floors were analysed using the same kind of beam elements as in the analyses described earlier. In these tests, however, the height of the hollow cores was only 260 mm compared with 400 mm in the analyses described earlier. Thus, the geometry of the cross-section was still described with zones in a similar way as shown in Figure 7, but considering the actual cross-section. The torsional stiffness of the cross-section was calculated according to the methods described in Murray,[21] and the input 'shear factors' were adjusted to fit this. Input data are listed in Table 1. The joints were modelled using alternative (b); that is with slave nodes in the corners of the hollow core units. As it was not possible to apply supports to the slave nodes, stiff links were used between the beam nodes and the edge nodes where the third support line was applied. This is equivalent to the use of slave nodes. The symmetry line was used in the analyses, so that only half the floor was modelled.

The displacements in two of these tests (no. 1 and 2) are compared with results from analyses in Figures 15 and 16. As can be seen, there is good agreement for low loads. When the load is close to the maximum load obtained in the tests, the displacement in the analyses was too small. This is to be expected, as the simplified global model is not intended to be able to describe the shear and torsion failure of a floor; but only its behaviour until shear/torsion cracking occurs.

Analyses of a floor tested at VTT in 2002

Within the European project Holcotors, one floor consisting of four 400 mm thick hollow core units was tested at VTT in 2002. The hollow core units were grouted together on supports made of concrete beams. The joints were pre-cracked to simulate shrinkage and normal use. The floor was first loaded with one point load of about 100 kN at 12 different points

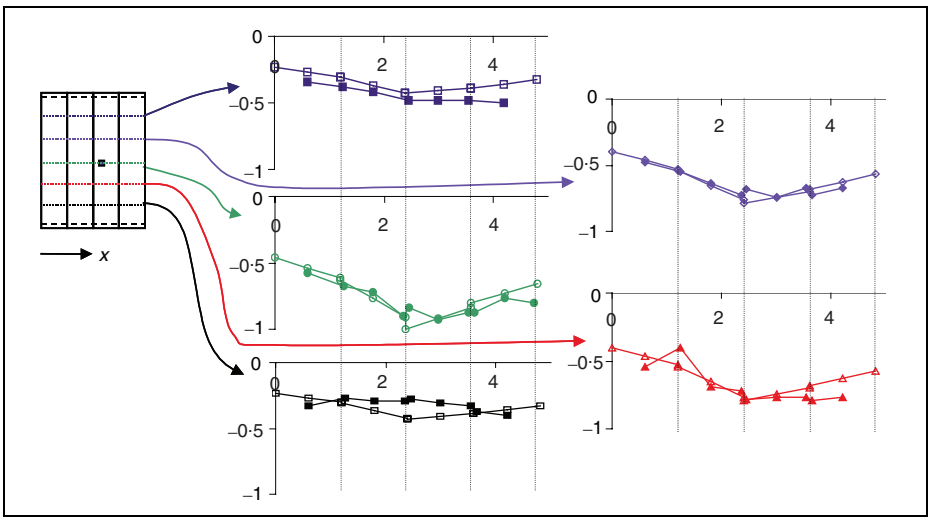

△ **Figure 14 Displacement (in mm) plotted against *x*-coordinate (in m) at a load of 110 kN in the marked position. The filled markers are experimental, from VTT,[13] and the unfilled are from the analysis with the joints modelled as in alternative (b)**

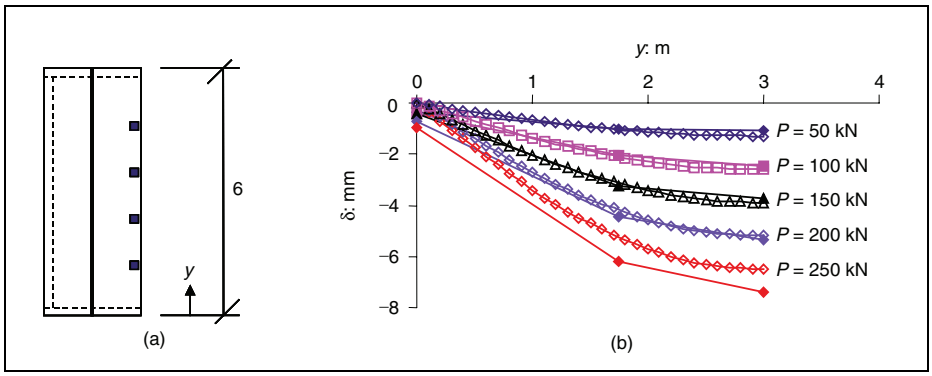

△ **Figure 15 (a) Test set-up in a three-edged supported floor, test no. 1 by Walraven and van der Marel;[5] point loads were applied in the marked positions. (b) The displacements measured in this test (filled markers) are compared with analysis results**

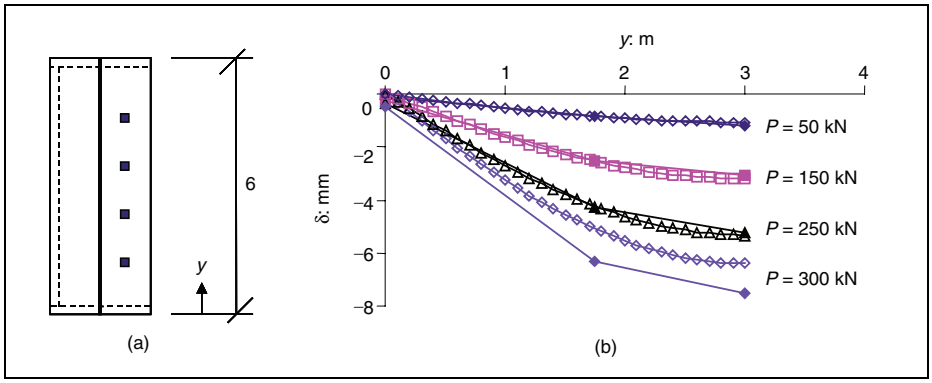

△ **Figure 16 (a) Test set-up in a three-edged supported floor, test no. 2 by Walraven and van der Marel;[5] point loads were applied in the marked positions. (b) The displacements measured in this test (filled markers) are compared with analysis results**

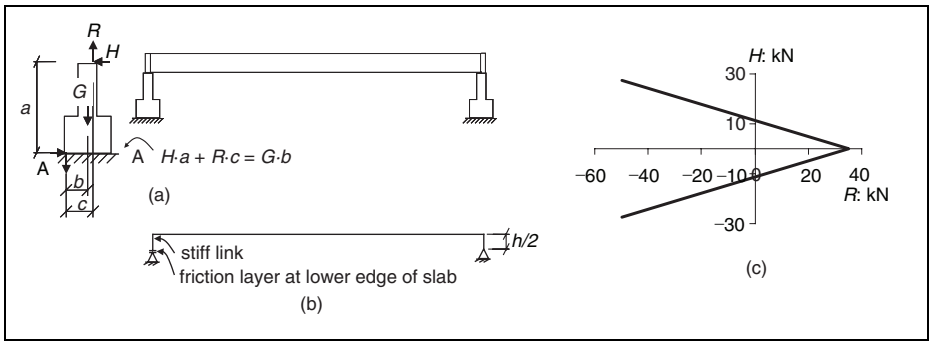

△ **Figure 17 (a) Horizontal restraints at the supports limited by tilting of the support beams in the floor test by Pajari;[14] (b) modelling of horizontal restraint with stiff links and friction layer; and (c) input for the friction layer**

across the floor and the vertical displacement of the floor was measured at 47 points. Afterwards the floor was loaded with one point load until failure, and since local failure occurred, two more failure loadings were possible, each of them including two point loads at different positions. For more information about this test, see Pajari.[14]

This floor was analysed in two steps. At first, the developed simplified global model was used for the whole floor, and results were checked with measured displacements from the first 12 loadings. In the second step, the three final ultimate loadings of the floor were modelled using solid elements in a part of the loaded hollow core unit and the simplified global model describing the rest of the floor. The model with solid elements was verified against tests on single hollow core units.[4]

Analyses using the simplified global model

The floor was analysed using the same beam elements as in the analyses of the floor tested at VTT in 1990. The joints were modelled using alternative (b) in Figure 2, that is with slave nodes in the corners of the hollow core units. Preliminary analyses showed that there was horizontal longitudinal restraint due to the dead weight of the supporting concrete beams, which had a rather large influence on the displacements. The horizontal restraint was limited by tilting of the support beams (Figure 17). This effect was included in the analyses by adding stiff links from the outer beam node to the bottom of the hollow core units. Furthermore, a friction layer was introduced at one of the support lines, where the horizontal force depends on the reaction force. The cohesion and coefficient of friction used as input for this friction layer are shown in Figure 17(c). An additional required input is the dilatancy angle, which was set to zero. The support at the friction layer (on the left side in Figure 17(b)) was free to move in the direction along the slab when the pre-stress and the dead weight were applied, but was locked for further loading.

Measured displacements are compared with results from the analyses in Figure 18. As can be seen, the displacements agree rather well; however, slightly larger displacements were obtained in the analyses than in the tests. This is in contrast to what was obtained for the similar loading point in the floor in the previous section. Again, the displacements are rather small.

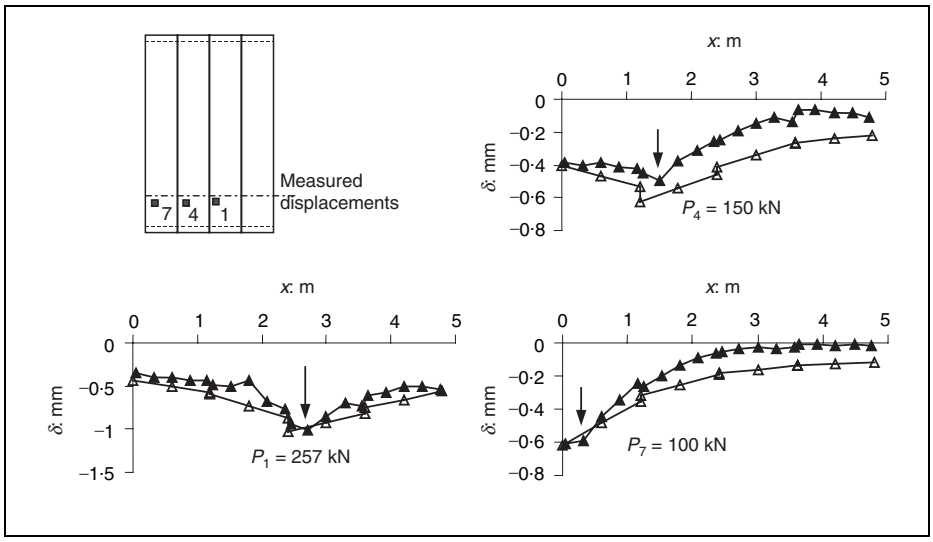

△ **Figure 18 Measured displacements in the floor tested by Pajari[14] (filled markers) compared with results from the analyses. The different numbers refer to the actual load positions**

Combination of simplified global model and solid elements

As stated before, the intention was to combine the simplified global model with solid elements in the part of the floor where failure was expected. The three final ultimate loadings of the floor (see Pajari[14]) were modelled using solid elements in a part of the loaded hollow core unit, and using the developed simplified global model for the rest of the floor. For information about the simplified global model, and the modelling of the horizontal restraint provided by the support beams, see the previous section.

The finite element mesh used for the analysis of loading in position no. 14 is shown in Figure 19. Point interface elements were applied between the upper and lower edges of the solid element part and the slave nodes of the neighbouring hollow core units, similarly to alternative (b) in Figure 2. The edge sections of the part modelled with solid elements (at the support and towards the beam elements) were forced to remain plane. At the support, this was done to simulate the effect of the grouting of the edge joint. Towards the beam elements, this section was tied to the beam node in the same cross-section.

In the part modelled in greater detail, eight-node isoparametric solid brick elements were used for the concrete. The strands were modelled with two-node, directly integrated (one-point) truss elements. The interaction between the steel and the concrete was modelled with $2 + 2$ node line interface elements, describing a bond–slip relation. In reality, the bond–slip differs between the release of the pre-stress and in the loading stage, both due to the change in concrete strength and due to the effect of the normal stresses that result at the release of the pre-stress. This can be modelled by the use of solid elements for both the strands and the concrete and a special frictional layer between them. However, that modelling technique was judged to be too time-consuming for the analyses here, and a bond–slip relation was considered to be a sufficient level of modelling.

Whereas the analyses described earlier could be run in load control, these analyses converged only when displacement control was applied. The analyses were run in two phases: in phase 1, the pre-stressing force was released and the dead weight was applied. Horizontal longitudinal tying was introduced only at the support line without friction layer during this phase (Figure 17). In phase 2, horizontal longitudinal tying was applied also at the friction layer, and the point interface elements between the hollow core units were activated. The dead weight had to be applied again, and thereafter the loading was applied by increasing the displacement at the loaded position. To enable displacement control when there were two points loaded, a stiff beam between the two loading plates was introduced (Figure 19) in a similar way as in the test.

The load versus displacement curves obtained in the analyses of the three different loadings are compared with experimental results in Figure 20. As can be seen, the agreement is rather good; the load capacity increased, in the experiments as well as in the analyses, when the load was applied on two webs instead of one. Load in position no. 13 (on one web) resulted in a punching failure, both in the test and in the analysis (Figure 21). The crack pattern corresponds

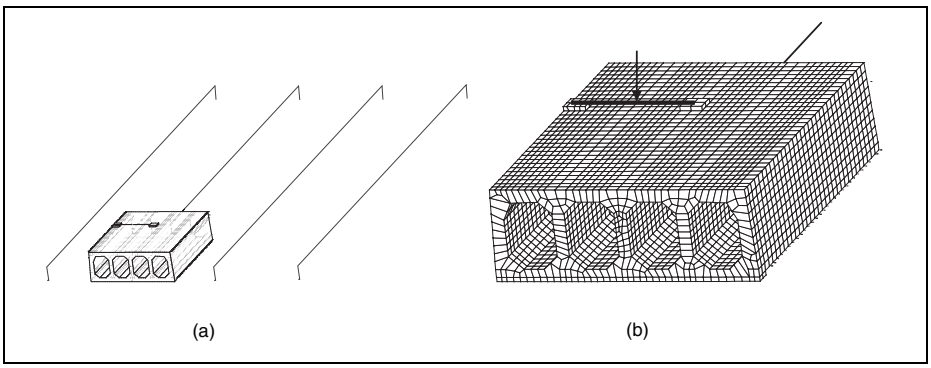

△ **Figure 19 (a) Finite element mesh with solid elements combined with simplified global model, used in analysis of the floor tested by Pajari,[14] load in position no. 14. (b) Part with solid elements enlarged**

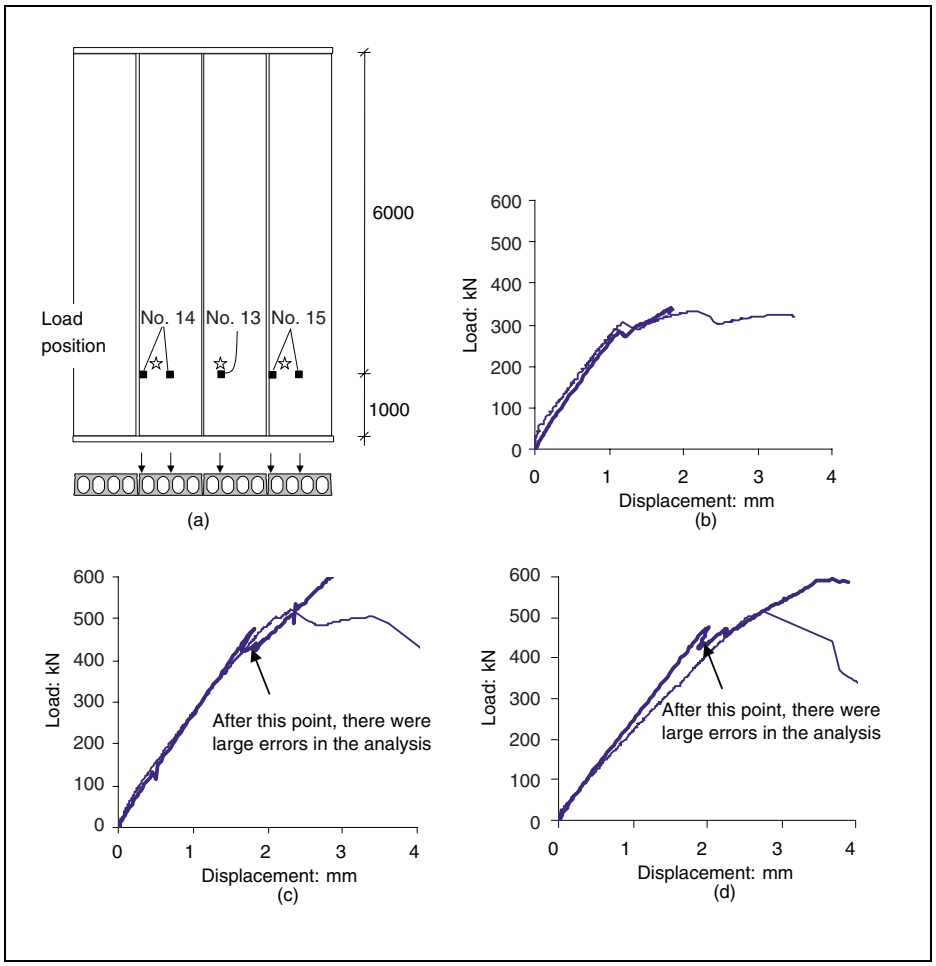

◁ **Figure 20 (a) Loading positions in the three final ultimate loadings of the floor tested by Pajari.[14] Load versus displacement in positions 200 mm from the loads, marked with stars; thick lines are analysis results and thin lines are experimental results in loading position (b) no. 13, (c) no. 14, and (d) no. 15**

well between the test and the analysis. For both of the loadings in positions no. 14 and no. 15, local crushing at the loading plate at the outermost web, combined with inclined cracking of the webs, occurred at a load of about 480 kN, which can be seen as a load drop in the load versus displacement curves in Figure 20(c) and (d). Thereafter, it was possible to increase the load in the analyses. However, for the continued analyses, there were rather large errors in the solutions, and they are therefore not to be trusted. The maximum load in the analyses should thus not be considered to be as high as in the curves shown in Figure 20(c) and (d), but rather slightly above

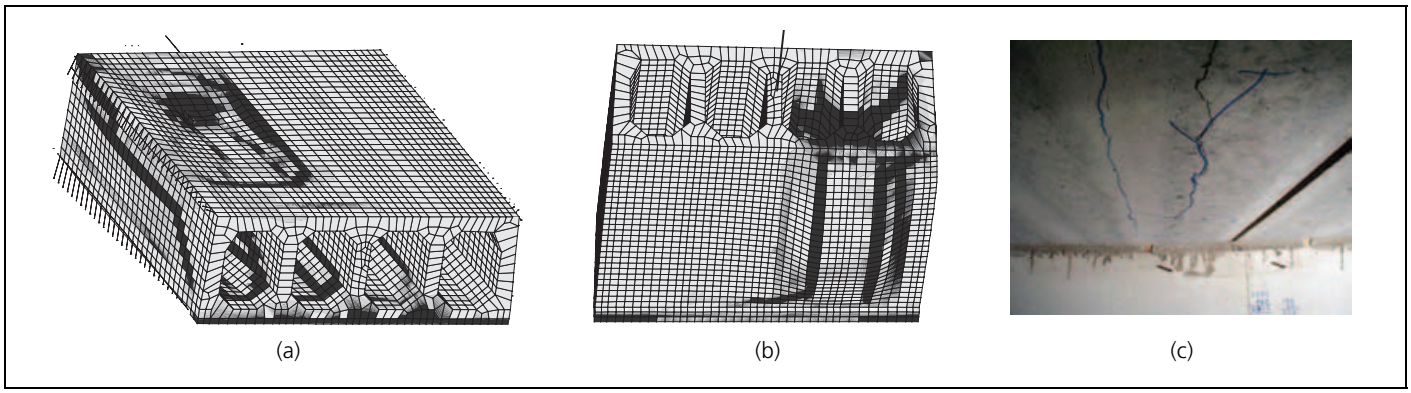

△ **Figure 21 Load in position no. 13 results in a punching failure. (a) and (b) Deformed mesh after maximum load, with dark areas indicating cracks; (a) seen from above, from the support, and (b) seen from below, towards the support. (c) Photograph from VTT, taken after the test, seen from below, towards the support**

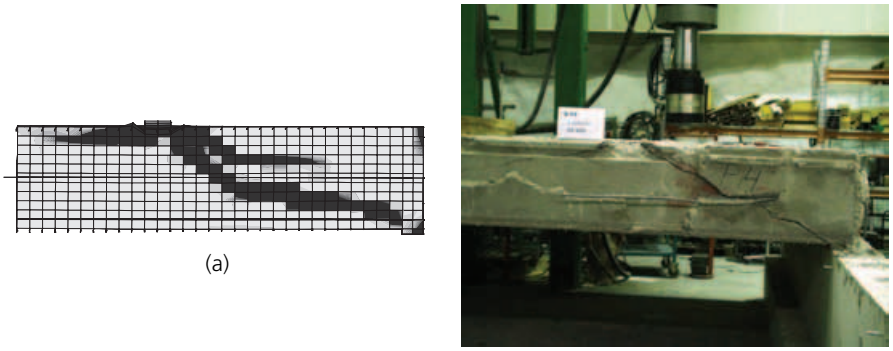

(a) (b)

△ **Figure 22 Load in position no. 14 results in local crushing at the loading plate at the outermost web, combined with inclined cracking of the webs. (a) From analysis, with dark areas indicating cracks. (b) Photograph from VTT, loaded unit after the test, during demounting of the floor**

480 kN, which corresponds fairly well with the measured maximum loads, which were 522 and 518 kN in the no. 14 and no. 15 loadings, respectively. In Figure 22, the crack pattern on the loaded hollow core unit for the load in position no. 14 from the analysis is compared with the experimental pattern. Again, the agreement is good.

Shear and torsion at maximum load

Within the project, several tests of single hollow core units were also carried out; see Pajari.[3] In one of these tests (denoted ST400E1M), a similar hollow core unit and detailing of the supports were used, and a point load was applied with the same shear span and eccentricity as in all three ultimate loadings of the floor. First, it is worth taking note of the high increase in capacity that was obtained in the floor test. In the floor test, the maximum load was as high as 522 and 518 kN in the no. 14 and no. 15 loadings, respectively, where punching failure was avoided; whereas it was only 265 kN in the corresponding single element test. To check whether this high increase can be explained by the distribution of the load to the neighbouring units, the shear and torsional moment in the loaded hollow core unit, obtained in the analyses, were checked. Slightly different results were obtained when only the simplified global model was used, compared with when it was used in combination with solid elements. In Figure 23(a), the shear and torsional moments in the loaded hollow core unit in floor loading no. 14 are shown to be larger than the corresponding values at ultimate load in the single unit test. In Figure 23(b), it can be seen that the shear and the torsional moments at a loading corresponding to the maximum load in the floor test, 522 kN, were larger in the analysis with the simplified global model than in the corresponding single unit test at ultimate load.

Thus, from these tests and analyses it appears that a hollow core unit can carry higher amounts of shear and torsion when placed in a floor system. The reason might be that the stress state in a unit placed in a floor differs from that in a single unit, even if the action effects, namely the shear and the torsional moment, are the same. Hence, the boundaries with the adjacent units seem to result in a more favourable stress state, or better possibilities for redistribution within the unit. One question for future research, then, is whether this conclusion also holds for other floors and, if so, whether it can be taken into account in design.

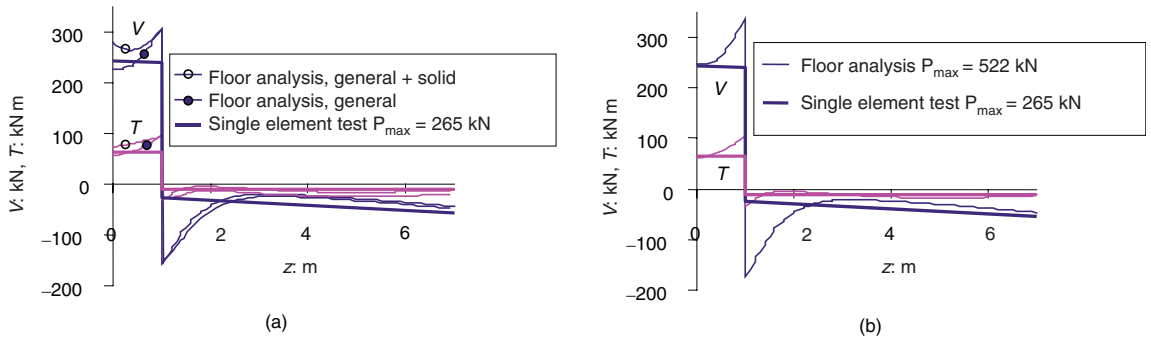

△ **Figure 23 Shear and torsional moment in the loaded hollow core element in floor loading no. 14 are compared with the ones at ultimate load in a single element test. (a) Loading in floor analyses equals 477 kN, when local crushing under one loading plate occurred in the analysis with simplified global model combined with solid elements. (b) From analysis with simplified global model; loading equals the ultimate load in the test**

Conclusions

A simplified global model for complete floors of hollow core units was developed, in which the cross-section of each unit was described with one beam element, and where the neighbouring units were coupled by means of slave nodes in the corners, allowing compression but not tension in the joints between the hollow core elements. This modelling method gives results that are close to those obtained when the longitudinal joints are modelled with hinges; the difference is that when hinges are used, the torsional moment in the hollow core units becomes larger. This is due to the eccentricity of the resulting compressive forces in the corners, which is included when the units are coupled at the corners. Comparisons with test results showed that by coupling the units at the corners, torsional moments that correspond better with measurements are obtained. Further comparisons with test results showed that the model can, with reasonable accuracy, describe the real behaviour of a hollow core floor. The simplified global model was used together with solid elements in a part of a hollow core unit, to enable modelling of shear and torsion failure of a hollow core unit within a floor system. Good agreement with test results was obtained concerning failure mode, crack pattern, maximum load, and displacements. It is therefore concluded that the modelling technique used appears to describe these phenomena properly.

Some of the tests and analyses indicate that a hollow core unit can carry higher amounts of shear and torsion when placed in a floor system, and not only due to the transfer to the neighbouring elements. The explanation could be that the stress state in a unit placed in a floor differs from that in a single unit, even if the action effects, namely the shear and the torsional moment, are the same. Consequently, the boundaries with the adjacent units seem to yield a more favourable stress state, or better possibilities for redistribution within the unit. Future research may reveal whether this conclusion also holds for other floors and, if so, whether it can be taken into account in design. The intention is to use the modelling technique described here to analyse typical cases occurring in reality, in which both torsion and shear present a problem. The results will improve the understanding of the shear and torsion behaviour of hollow core units in a floor system, and form a basis for design recommendations.

Acknowledgements

The photographs in this paper are used with kind permission of VTT. The authors would like to thank Dr Matti Pajari at VTT for letting us use the data collected during the tests directly after the tests were carried out. The research was financed by the Fifth Framework of European Commission, the International Prestressed Hollow Core Association, the 'Bundesverband Spannbeton-Hohlplatten' in Germany, and also by the co-operating partners, which were Chalmers University of Technology, VTT, Consolis Technology, Strängbetong, Castelo and Echo.

References

1. Gabrielsson, H. *Ductility of high performance concrete structures*. PhD thesis, Division of Structural Engineering, Luleå University of Technology, Luleå, 1999.
2. Pajari, M. *Pure Torsion Test on Single Slab Units*. Technical Research Centre of Finland, Espoo, VTT Building and Transport, Internal report RTE50-IR-25/2002, 2003.
3. Pajari, M. *Shear-torsion Interaction Tests on Single Slab Units*. Technical Research Centre of Finland, Espoo, VTT Building and Transport, Internal report RTE50-IR-1/2003, 2003.
4. Broo, H., Lundgren, K. and Engström, B. Shear and torsion in prestressed hollow core units: Finite element analyses of full-scale tests. Submitted to *Structural Concrete*.
5. Walraven, J. C. and van der Marel, A. P. *Experiments on Hollow Core Slabs, Supported along Three Edges.* Division of Mechanics and Structures, Delft 1992.
6. Stanton, J. F. Response of hollow-core slab floors for concentrated loads. *PCI Journal*, 1992, **37**, No. 4, 98–113.
7. Stanton, J. F. Proposed design rules for load distribution in precast concrete decks. *ACI Structural Journal*, 1987, **84**, No. 5, 371–382.
8. Van Acker, A. Transversal distribution of linear loadings in prestressed hollow core floors. *Calgary Symposium*. Federation Internationale de la Precontrainte, Commission on Prefabrication, 1984.
9. Pfeifer, D. W. and Nelson, T. A. Tests to determine the lateral distribution of vertical loads in a long-span hollow core floor assembly. *PCI Journal*, 1983, **28**, No. 6, 42–57.
10. Broo, H. and Lundgren, K. *Finite Element Analyses of Hollow Core Units Subjected to Shear and Torsion*. Chalmers University of Technology, Department of Structural Engineering, Concrete Structures, Göteborg, Report 02:17, 2002.
11. TNO. *DIANA Finite Element Analysis, User's Manual release 8.1*. TNO Building and Construction Research, Delft, Netherlands, 2002.
12. CEN/TC229. *Precast Concrete Products Hollow Core Slabs for Floors*. European Prestandard prEN 1168, 2002.
13. VTT. *Variax 4-laataston pistekuormakokeet* (in Finnish). Technical Research Centre of Finland, Espoo, RAT12503/91, 1991.
14. Pajari, M. *Shear-torsion Interaction Tests on 400 mm Floor*. Technical Research Centre of Finland, VTT Building and Transport, 2003.
15. Comité Euro-International du Béton. *High Performance Concrete, Recommended Extension to the Model Code 90*. Bulletin d'Information 228. CEB, Lausanne, Switzerland, 1995.
16. Comité Euro-International du Béton. *CEB-FIP Model Code 1990*. Bulletin d'Information 213/214. CEB, Lausanne, Switzerland, 1993.
17. Thorenfeldt, E., Tomaszewicz, A. and Jensen, J. J. Mechanical properties of high-strength concrete and application in design. *Utilization of High Strength Concrete*, Symposium in Stavanger, Norway, 1987. Tapir N-7034 Trondheim.
18. Lundgren, K. *Steel-Encased Pull-Through Tests of Seven-Wire Strands*. Department of Structural Engineering, Concrete Structures, Chalmers University of Technology, Göteborg, Sweden, Report 02:13, 2002.
19. Fédération Internationale de la Précontrainte. *Precast prestressed hollow core floors*. Thomas Telford, London, 1988.
20. Suikka, A. and Parkkinen, I. Load distribution in 400 mm deep hollow-core floor. *IECA Conference*, Paris, 1991.
21. Murray, N. W. *Introduction to the Theory of Thin-walled Structures*. Clarendon Press, Oxford, 1985.

Paper III

Shear and torsion interaction in prestressed hollow core units.

Broo H., Lundgren K. and Engström B.

Magazine of Concrete Research, Vol. 57, No. 9, pp. 521—533, 2005.

Magazine of Concrete Research, 2005, **57**, No. 9, November, 521–533

Shear and torsion interaction in prestressed hollow core units

H. Broo,* K. Lundgren* and B. Engström*

Chalmers University of Technology, Sweden

Hollow core units are mainly designed to resist bending and shear. There are, however, many applications in which they are also subjected to torsion. The present calculation method for shear and torsion in the European Standard EN 1168 adds stresses from multiple influences without taking into account the softening of cracking concrete; therefore it is probably conservative. The main purpose of this work is to investigate the response of prestressed hollow core units subjected to selected combinations of shear and torsion by using non-linear finite element (FE) analyses. In previous work by the present authors, three-dimensional FE models of hollow core units were developed and validated by full-scale experiments. This paper shows how similar models were analysed for several load combinations of shear and torsion ratios. One load combination was validated by full-scale tests. The results from the FE analyses made it possible to present shear and torsion capacities in interaction diagrams useful in practical design. Moreover, the influences of the shear span and the prestressing transfer zone on the shear and torsion capacity were evaluated. It was concluded that the boundaries affected the capacity: shorter shear span gave higher capacity. The curved interaction diagrams obtained from the FE analyses were compared with linear diagrams from the analytical model in EN 1168. For most combinations the FE analyses showed higher capacities, except for combinations close to pure torsion, and pure shear for one of the geometries investigated.

Notation

A	total cross-sectional area (including inner hollow areas) of the transformed cross-section (m^2)
A_c	cross-sectional area (m^2)
b	width at the centroidal axis (m)
$b_{w,out}$	thickness of the outermost web (m)
$\sum b_w$	the sum of the widths at the centroidal axis of all webs (m)
d	effective depth (m)
E_{ci}	modulus of elasticity of concrete
E_p	modulus of elasticity of prestressing steel
e	eccentricity of the strands (m)
f_{ct}	concrete tensile strength (Pa)
I_c	second moment of area (m^4)
l_{pt}	transmission length of the prestressing strand (m)
l_x	distance between the section studied and the starting point of the transmission length (m)
M	imposed moment (Nm)
P	prestressing force (Pa)
S	first moment of area above and around the centroidal axis (m^3)
T	applied torsional moment (Nm)
$T_{R,top}$	torsional capacity for the top flange (Nm)
$T_{R,web}$	torsional capacity for the outermost web (Nm)
t	thickness (m)
t_{bottom}	thickness of the bottom flange (m)
t_{top}	thickness of the top flange (m)
u	outer circumference of the transformed cross-section (m)
V	applied shear force (N)
$V_{R,c}$	shear capacity (N)
$V_{Rd,c}$	design value of shear capacity (N), given in EN 1168
V_{Rdn}	design value of the shear capacity for simultaneous torsion (N), given in EN 1168
V_{Rn}	shear capacity for simultaneous torsion
V_{ETd}	design value of acting shear force in the web owing to torsion (N), given in EN 1168
V_T	shear force in the web owing to torsion (N)
W_t	sectional modulus for torsion (m^3)

* Division of Structural Engineering, Concrete Structures, Chalmers University of Technology, SE-412 96 Göteborg, Sweden.

(MCR 41353) Paper received 22 December 2004; accepted 21 April 2005.

0024-9831 © 2005 *Thomas Telford Ltd*

$W_{t,top}$	sectional modulus for torsion for top flange (m^3)
$W_{t,web}$	sectional modulus for torsion for outermost web (m^3)
z	z-coordinate of the point considered (origin at centroidal axis) (m)
α	quotient of l_x/l_{pt}
σ_c	normal stress (Pa)
σ_{cp}	normal stress owing to prestress (Pa)
τ	shear stress (Pa)
τ_V	shear stress from shear force (Pa)
τ_T	shear stress from torsional moment (Pa)

Introduction

The use of precast prestressed hollow core units for floors is common in all kinds of buildings, especially where large spans are required. The hollow core units are designed mainly to resist bending moment and shear: owing to the production methods, there is no transverse or vertical reinforcement. This, in combination with the prestress and the cross-section geometry, with large voids to save material and reduce self-weight, makes the units sensitive to shear and torsion. There are, however, many applications in which hollow core units are subjected to combined shear and torsion, for example in floors supported on three edges, in floors with openings and in floors with skew ends.

A significant amount of research has been done on shear in hollow core units. The shear strength has been investigated experimentally, analytically, or both by Walraven and Mercx,[1] Pisanty,[2] Yang,[3] Jonsson,[4] Hoang,[5] Becker and Buettner[6] and, in combination with flexible supports, also by Pajari.[7,8] Procedures for predicting the shear capacity have been presented by Walraven and Mercx,[1] Pisanty,[2] Yang[3] and Hoang[5]. The combination of shear and torsion in hollow core units is, however, not so well investigated. To the authors' knowledge, the publication by Gabrielsson,[9] who focused on experiments and analytical modelling of eccentrically loaded hollow core units, and the work done within this project, by Pajari[10,11] and by the authors,[12–14] are the only pieces of work dealing with this subject.

Torsion on a hollow core unit generates shear stresses that act mainly in the perimetric zone. In the outermost webs, these stresses act upwards in one and downwards in the other. A vertical shear force, on the other hand, produces shear stresses that are uniformly distributed over all webs. When vertical shear and torsion act simultaneously on one hollow core unit, the stresses from these influences interact. This means that one of the outermost webs in the cross-section receives much higher stresses than the others. The current calculation method for shear and torsion in EN 1168,[15] adds stresses from shear and from torsion linearly, without taking into account deformations and compatibility within the hollow core unit. Earlier research indicates, however, that there is a redistribution within the hollow core unit.[9,10,12,13,15]

To improve the current knowledge and understanding of shear and torsion interaction in hollow core floors, a European research project called Holcotors was started in January 2002. The aim of the project is to develop an improved design procedure for shear and torsion interaction in hollow core floors. To reach this goal, experiments were combined with finite element (FE) analyses, using non-linear fracture mechanics, for hollow core units as well as for whole floors.

The aim of the analyses reported here is to evaluate the load-carrying capacity and the response of the hollow core units investigated when they are subjected to various combinations of shear and torsion. An additional goal is to establish shear and torsion interaction diagrams that could be used in practical design when the shear force and torsional moment are given.

In a previous part of the project, three-dimensional FE models of 200 mm and 400 mm thick hollow core units were developed and validated by full-scale tests.[13] This paper analyses similar FE models for several load combinations with various ratios of shear and torsion, from pure torsion to pure shear. One of the load combinations was validated against full-scale experiments done within the project at VTT, Technical Research Centre of Finland.[10] Moreover, the effects of the shear span and the influence of the prestressing transfer zone on the shear and torsion capacity were evaluated. Finally, the interaction diagrams obtained from the FE analyses are compared with the analytical model in EN 1168.

Analytical method

The possible failure modes for simply supported hollow core units have been summarised.[1,16] As regards the behaviour for loading close to the support, the following failure modes are distinguished. The failure could start by a flexural crack that becomes an inclined shear crack and results in failure either by crushing or splitting of the compression zone or by shear sliding along the inclined crack. A flexural crack close to the support could result in failure owing to slipping of the strands. Another possible failure mode is shear tension failure that occurs in regions not cracked in bending; this starts in the webs with an inclined crack, which propagates both upwards and downwards until failure. A hollow core unit subjected to torsion could start cracking in the top flange, in the bottom flange or in one of the outermost webs. Whether this cracking results in failure or not depends on the possible redistribution of the stresses.

Shear

In a prestressed hollow core cross-section subjected to vertical shear, it is assumed that the shear stresses

produced are uniformly distributed over all webs. A shear tension crack is formed when the principal tensile stress in the concrete reaches a critical value, that is the concrete tensile strength, f_{ct}. Thus, cracks usually form, according to Walraven and Mercx,[1] where the plane inclined at 45° from the edge of the support intersects with the mid-depth plane, see Fig. 1. Here the prestressing force is not fully developed and the web width is at a minimum. In the critical section the normal stress, σ_c, owing to the pre-stressing and bending moment, and shear stress, τ_V, owing to vertical shear, are superimposed. The normal stress can be estimated as

$$\sigma_c(z) = \frac{-\alpha P}{A_c} + \frac{-\alpha P e + M}{I_c} z \tag{1}$$

where P is the prestressing force, $\alpha = l_x/l_{pt} \leqslant 1$ where l_x is the distance between the section considered and the starting point of the transmission length, and l_{pt} is the transmission length of the prestressing strand. Here, A_c is the cross-sectional area, e is the eccentricity of the strands, z is the z-coordinate of the point considered (origin at centroidal axis), M is the imposed moment and I_c is the second moment of area. The critical stress combination is, however, assumed to be in a section at mid-depth ($z \approx 0$) and, therefore, it is independent of the flexural moment.

$$\sigma_c(0) = \frac{-\alpha P}{A_c} = -\alpha \sigma_{cp} \tag{2}$$

Theoretically, therefore, if the shear force is constant between the support and the load, the shear capacity is independent of the shear span. The shear stress owing to load is

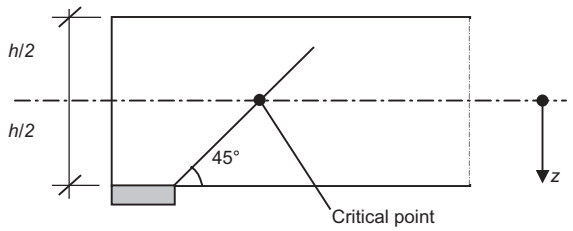

Fig. 1. Most probable point for a shear tension crack to start

$$\tau_V = \frac{VS}{\sum b_w I} \tag{3}$$

where V is the applied shear force, S is the first moment of area above and around the centroidal axis and $\sum b_w$ is the sum of the widths at the centroidal axis of all webs.

In the ultimate limit state, the principal tensile stress is equal to the tensile strength of the concrete, and thus

$$f_{ct} = \frac{\sigma_c}{2} + \sqrt{\left[\left(\frac{\sigma_c}{2}\right)^2 + \tau^2\right]} \tag{4}$$

Then, with $\tau = \tau_V$ and by inserting equations (2) and (3) into equation (4) and assuming that cracking results in failure, it follows that the shear capacity for web shear tension failure can be estimated as

$$V_{R,c} = \frac{I \sum b_w}{S} \sqrt{\left(f_{ct}^2 + \alpha \sigma_{cp} f_{ct}\right)} \tag{5}$$

This formula corresponds to the formula for shear capacity, $V_{Rd,c}$, given in EN 1168.

Torsion

The torsional loading causes shear stresses, τ_T, acting mainly in the perimetric zone of the cross-section. In the outermost webs and in the flanges, these stresses act together with the normal stresses, σ_c, introduced by the prestressing and by the bending moment. The actual stress combination and the thickness of the flanges and the outermost webs determine whether the cracking starts in a web or in one of the flanges. The shear stress owing to torsion is calculated as

$$\tau_T = \frac{T}{W_t} \tag{6}$$

where W_t can be calculated by transforming the cross-section of the hollow core unit into a tubular cross-section, see Fig. 2

$$W_t = 2t\left[h - \frac{(t_{top} + t_{bottom})}{2}\right](b - b_{w,out}) \tag{7}$$

where $t = t_{top}$ in calculations for the top flange and $t = b_{w,out}$ in those for the outermost web. However, the thickness, t, may not be larger than A/u, where A is the total cross-sectional area (including inner hollow areas)

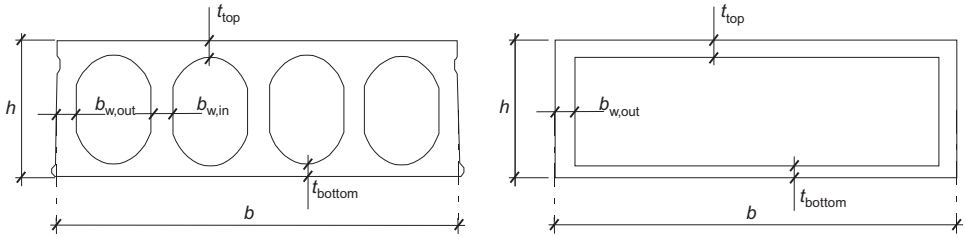

Fig. 2. The cross-section of one hollow core unit transformed into a tubular cross-section for calculations of the torsional resistance

and u is the outer circumference of the transformed cross-section.

In the ultimate limit state the tensile strength again limits the tensile stresses. Accordingly, by inserting τ_T as τ in equation (4) and combining it with equation (6), the torsion capacity, assuming that cracking of the top flange results in failure, is

$$T_{R,\text{top}} = W_{\text{t,top}}\sqrt{\left(f_{\text{ct}}^2 + \sigma_c f_{\text{ct}}\right)} \tag{8}$$

and the torsion capacity assuming that cracking in the outermost web results in failure is

$$T_{R,\text{web}} = W_{\text{t,web}}\sqrt{\left(f_{\text{ct}}^2 + \alpha\sigma_{cp} f_{\text{ct}}\right)} \tag{9}$$

Shear and torsion

For a component loaded simultaneously with vertical shear and torsion, the shear stresses from each action are added in one of the outermost webs

$$\tau = \tau_V + \tau_T \tag{10}$$

by including τ_V from equation (3) and τ_T from equations (6) and (7) calculated for $t = b_{\text{w,out}}$. Thus, the shear stress in the outermost web is

$$\tau = \frac{VS}{I\sum b_{\text{w}}} + \frac{T}{b_{\text{w,out}}2(b - b_{\text{w,out}})(h - (t_{\text{top}} + t_{\text{bottom}})/2)} \tag{11}$$

The shear capacity then becomes

$$V = \frac{\tau I\sum b_{\text{w}}}{S} - \frac{T\sum b_{\text{w}} I}{b_{\text{w,out}}2(b - b_{\text{w,out}})(h - (t_{\text{top}} + t_{\text{bottom}})/2)S} \tag{12}$$

By assuming that $I/S \approx d$ and $h\text{-}(t_{\text{top}} + t_{\text{bottom}})/2 \approx d$, and identifying $V_{R,c}$ from equation (5), the reduced shear capacity for simultaneous torsion, assuming web shear tension failure at cracking, can be written as

$$V_{R\text{n}} = V_{R,\text{c}} - \frac{T\sum b_{\text{w}}}{b_{\text{w,out}}2(b - b_{\text{w,out}})} = V_{R,\text{c}} - V_{\text{T}} \tag{13}$$

where V_T is the shear force in the web owing to torsion

$$V_{\text{T}} = \frac{T\sum b_{\text{w}}}{b_{\text{w,out}}2(b - b_{\text{w,out}})} \tag{14}$$

These equations correspond to the formulae for the net value of the shear capacity, $V_{R\text{dn}}$, and the design value of acting shear force, $V_{E\text{Td}}$, caused by the torsional moment given in EN 1168.[15]

As the shear stresses from shear and torsion are simply added together, there is a linear interaction between shear and torsion. According to the standard it is not necessary to check cross-sections closer to the support edge than half the height of the hollow core unit. It is worth noting that the method in EN 1168[15] takes into account only the web shear tension failure of the outermost web: no other possible failure mode is considered to be critical.

FE analyses

This study investigates two geometries of hollow core units, the dimensions of which are shown in Fig. 3. One was a 200 mm thick unit with six circular voids and with seven prestressing strands in the bottom flange. The other was 400 mm thick, had four almost rectangular voids and was provided in the bottom flange with 11 prestressing strands. All strands were seven-wired with a diameter of 12·5 mm. The initial prestress was 900 MPa for the 200 mm thick units and 1000 MPa for the 400 mm thick units.

In Broo *et al.*[13] three-dimensional FE models of these two geometries of hollow core units were developed and validated by full-scale tests. Here, similar FE models, changed only with regard to support and loading conditions, were used for analyses of several load combinations with various shear–torsion ratios, from pure torsion to pure shear. All of the FE analyses described in this paper were made using the general FE program Diana, version 8·1·2.[17] One of the load combinations was validated against full-scale experiments conducted at VTT.[11]

FE analyses of full-scale tests

The same test was made twice on the 400 mm thick hollow core unit, denoted ST400G1 and ST400G2. Fig. 4 shows the arrangements for these full-scale experiments. The torsion was applied by twisting one end of the hollow core unit and keeping the other end fixed. In the tests this was accomplished by allowing the support at one end to rotate around a longitudinal axle, and applying a point load at each support. For stability, the point loads had slightly different eccentricities in the transversal direction. A line load was applied with

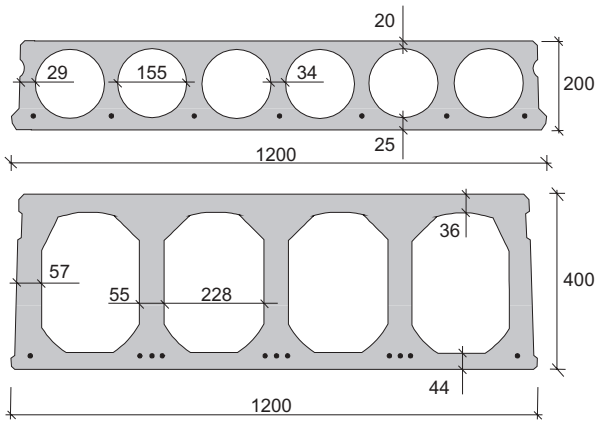

Fig. 3. Cross-sections of the hollow core units tested and analysed. Dimensions are given in mm

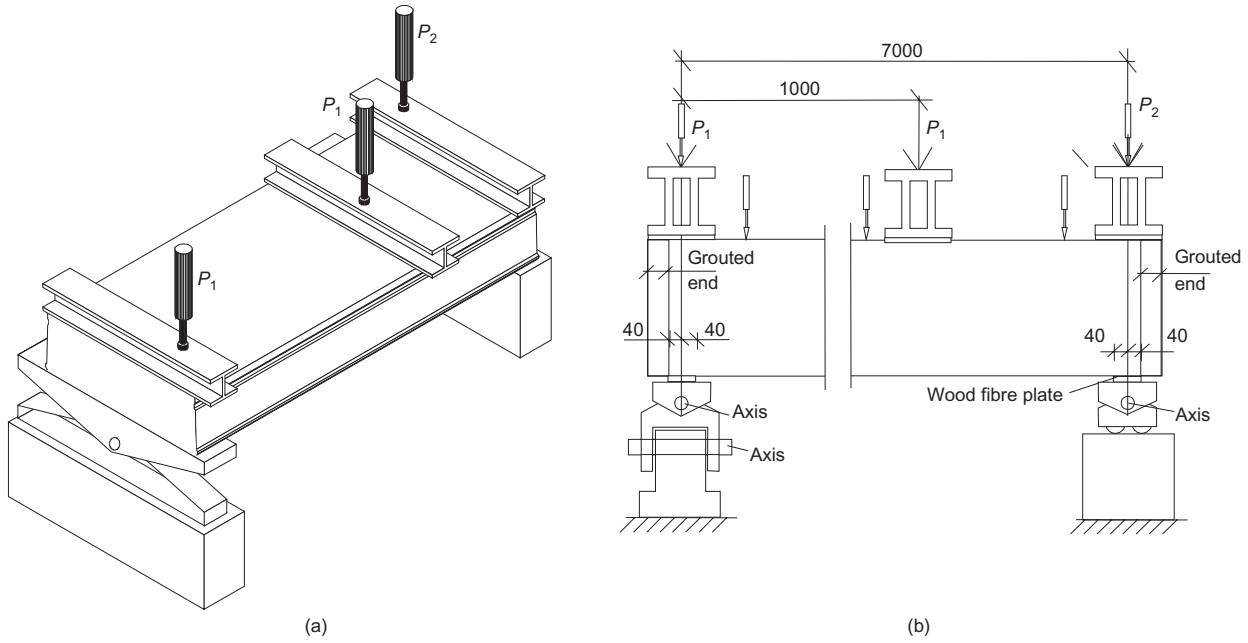

Fig. 4. Overview of test arrangements. Dimensions are given in mm. Modified from Pajari[10]

a shear span of 1·0 m. The relation between shear and torsion was kept constant throughout the test.

Modelling technique. A sketch of the FE model used to analyse the 400 mm thick hollow core unit is given in Fig. 5. Eight-node solid elements were used only for the part of the hollow core unit where the failure was expected, close to the load in the span. The rest of the unit was modelled with three-node beam elements. The solid elements were connected to the beam elements by assuming a stiff rotation of the cross-section and that the plane cross-section remained plane. The beam elements were assigned the properties of a 400 mm high and 1200 mm wide hollow core unit by defining the cross-section with 17 zones, see Fig. 5(b). To obtain correct torsional stiffness of the beam elements, two factors, which TNO (the Netherlands Organisation for Applied Scientific Research)[17] designates 'shear factors', were adjusted. The torsional stiffness was evaluated from pure torsion tests carried out within the project.[11]

In the analysis, the concrete was modelled with a constitutive model based on non-linear fracture mechanics. A rotating crack model based on total strain was used for the concrete.[17] The hardening in compression was described by the expression suggested by Thorenfeldt; for the tension softening, the curve proposed by Hordijk was chosen, as described in TNO.[17] Material data for the concrete were calculated from the compressive strength, evaluated from cylinder tests carried out by VTT, on 50 mm cores drilled from the test specimens, see Pajari.[10] The mean tensile strength, f_{ctm}, was calculated according to the Comité Euro-International du Béton (CEB),[18] the fracture energy, G_F, and the Young's modulus, E_{ci}, were calculated according to CEB.[19] All material properties used for the concrete in the model are shown in Table 2.

In the part with solid elements, the strands were modelled with two-node bar elements, combined with interface elements and a pre-defined bond–slip relation, to simulate the interaction between the prestressing steel and the concrete. The pre-defined bond–slip relationship between the seven-wire strands and the concrete was taken from pull-through tests carried out at Chalmers, by Lundgren,[20] see Fig. 6. In the part of the model with beam elements, the strands were modelled as embedded reinforcement. This choice means that, in the beam elements, full interaction between the prestressing steel and the concrete was assumed. The constitutive behaviour of the prestressing steel was modelled by the von Mises yield criterion, with an associated flow law and isotropic hardening. For the analysis, the strength and modulus of elasticity measured in tensile tests carried out at VTT were used, see Pajari.[10] The 0·1% proof stress, $f_{p0\cdot1}$, was 1680 MPa, the ultimate tensile strength, f_{pu}, was 1910 MPa and Young's modulus, E_p, was 198 GPa.

In the analysis the torsion was applied by twisting the hollow core unit with eccentric point loads at the ends. At the end with beam elements, a stiff link was used, see C in Fig. 5(b), and at the end with solid elements, the eccentric point load was distributed over the whole width of the hollow core unit, see B in Fig. 5(b). The span was loaded with a centric point load that was also distributed over the whole width of the hollow core unit. In the tests the loads were distributed by 200 mm wide stiff steel beams. In the analysis this was simulated by tying the nodes of the loading area to the

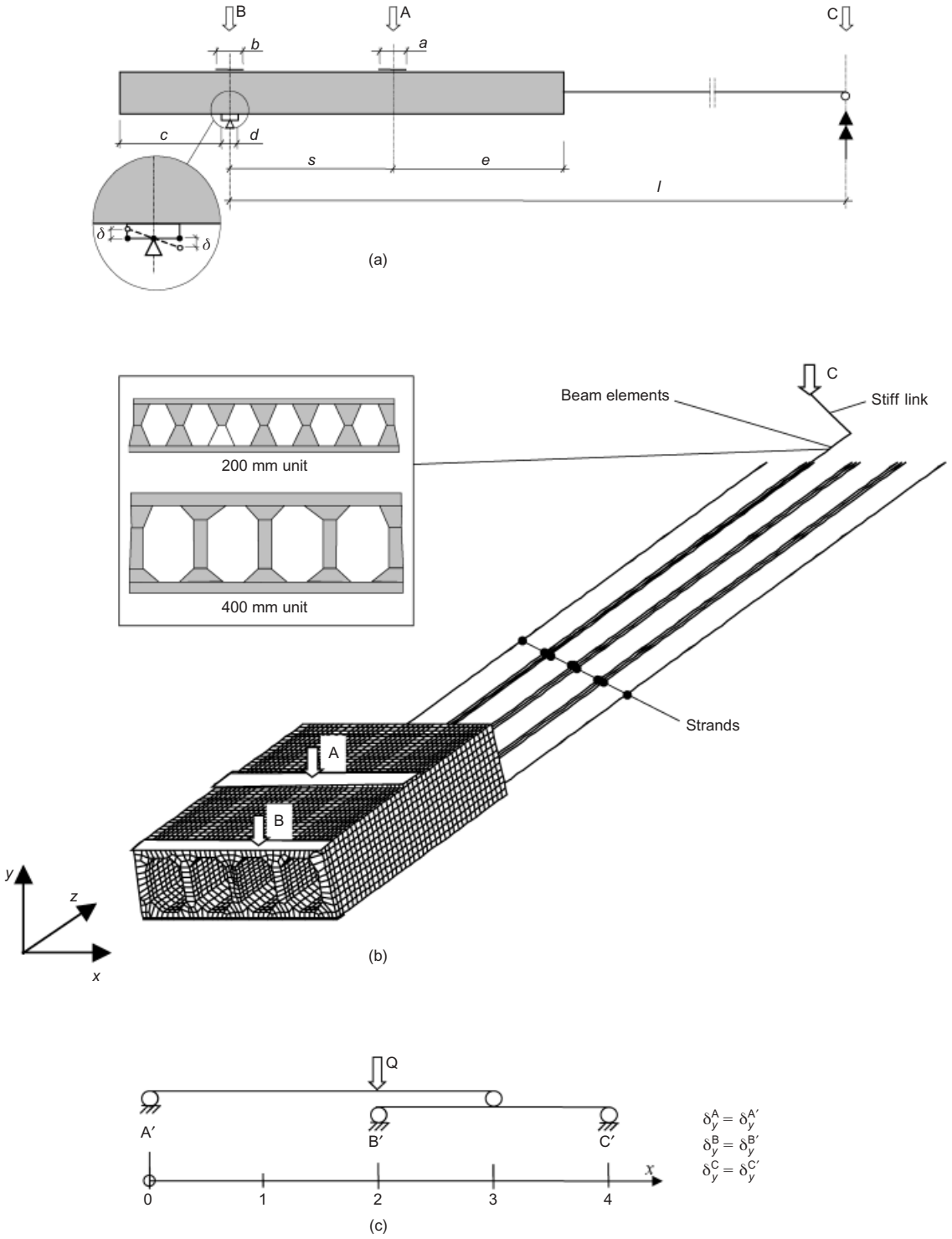

Fig. 5. (a) The principle of the FE models, see Table 1 for measurements; (b) FE model of the 400 mm thick unit, used to calculate the shear and torsion resistance; (c) loading arrangement of beams by which various combinations of shear end torsion were obtained by varying the position of the load Q

loaded node to keep this area in the vertical plan, see A in Fig. 5(b). In the analysis the load was distributed above the support over a 140 mm wide area. In the tests there were sheets of wood fibre between the unit and the steel beams. In the analysis these sheets of wood fibre were modelled with eight-node solid elements; full interaction was assumed between the concrete and the wood fibre. The tensile strength of the wood fibre was assumed to be 0·05 MPa, the Poisson ratio $\nu = 0{\cdot}15$, Young's modulus $E = 2$ GPa, and the fracture energy $G_F = 10{\cdot}0$ Nm/m^2. For the tension softening, the curve proposed by Hordijk was chosen, as described in reference 17.

In the tests the hollow core units were supported on

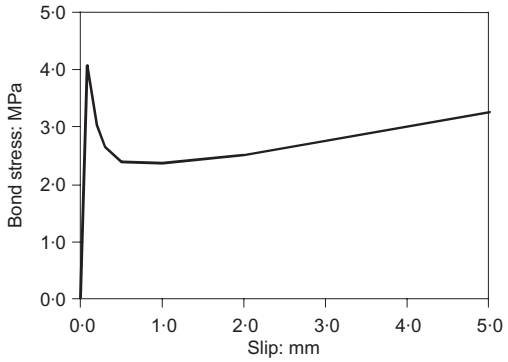

Fig. 6. Bond–slip relationship used between a seven-wire strand and concrete, from pull-through tests by Lundgren[20]

roller bearings. At each support there was a 10 mm thick sheet of wood fibre under the hollow core unit. In the analysis this sheet was modelled in the same way and had the same material properties as the sheet of wood fibre used under the steel beams. The nodes along the centre line of the modelled plate were supported vertically, transversally and longitudinally. The nodes at the edges were, however, tied to obtain the same vertical displacement, but in opposite directions, thus enabling a rotation and simulating a free support, see Fig. 5(a). In practice, and also in the tests, the end section of the hollow core units is grouted. To simulate this in the analysis, the nodes on the end cross-section were tied to keep the cross-section in plane and to have stiff rotation. In the analysis the end of the beam elements was supported for transversal and vertical displacement and for rotation around the vertical axis.

To enable deformation-controlled loading with a constant relation between shear and torsion, a separate loading arrangement of beams was modelled, see Fig. 5(c). The loading beams were modelled with three-node beam elements that have the properties of stiff beams without dead weight. The beams were supported as shown in Fig. 5(c). The nodes where loads were applied on the hollow core unit (A, B and C) in Fig. 5(b) were tied so they would have the same vertical displacement as the supporting nodes (A′, B′ and C′) in Fig. 5(c) on the loading arrangement. The hollow core unit could be loaded by applying Q anywhere along the x-axis on the loading beam; $x = 0$ m for pure shear and $x = 3{\cdot}0$ m for pure torsion. In this analysis the load, Q, was positioned at $x = 2{\cdot}0$ m to obtain the same ratio of shear and torsion as in the full-scale experiments.

Deformation-controlled analysis had to be carried out in two phases. In the first phase, the loading beam arrangement was not active; then the prestressing force was released and the self-weight was applied. In the second phase, all of the elements were active. Owing to the syntax of the program, the self-weight had to be applied again. Thereafter, the loading was applied by increasing the vertical displacement of the chosen node ($x = 2{\cdot}0$ m) along the loading beam.

Results. The load versus vertical displacement from the tests is compared with FE analysis results in Fig. 7. In both tests the first crack was an inclined flexural crack below the loading point at a load of approximately $Q = 300$ kN. After the load dropped slightly, it could be increased until failure at $Q = 334$ kN for ST400G1 and $Q = 357$ kN for ST400G2. In the analysis there were no cracks before failure at a load of $Q = 356$ kN. In Fig. 8 the crack pattern from the tests and the analysis are shown. Although the load versus vertical displacement relation for the two tests was similar and the capacities were almost the same, the crack patterns did not reveal the same failure modes. The ST400G1 test failed in web shear tension, see Fig. 8(a). For the ST400G2 test, however, the failure mode was not completely clear, see Fig. 8(b). Pajari classifies it as a shear–torsion anchorage failure.[10] In the analysis of the tests, the crack pattern

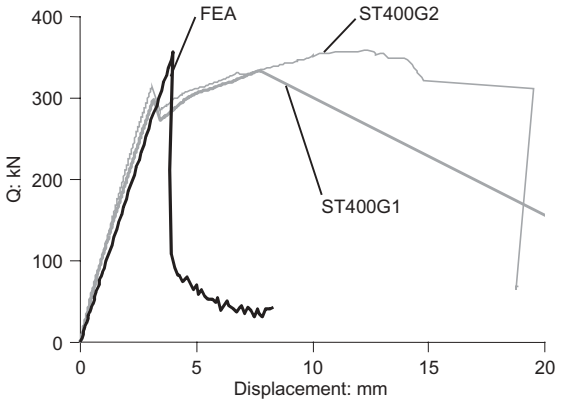

Fig. 7. Load versus displacement: comparison of FE analysis and test

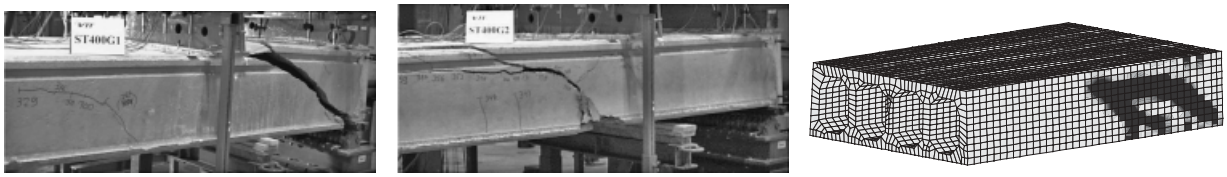

(a) (b) (c)

Fig. 8. Crack pattern from tests: (a) ST400G1; (b) ST400G2; (c) the corresponding FE analysis

as shown in Fig. 8(c), indicated a web shear tension failure.

FE analyses for shear and torsion interaction diagrams

FE analyses for several load cases with different relations between shear and torsion were made for both the 200 mm and the 400 mm thick hollow core units to establish shear and torsion interaction diagrams. To evaluate the effects of shear span and the influence of the prestressing transfer zone on the shear and torsion capacities, three set-ups were analysed for the 200 mm thick hollow core unit, see Fig. 5(a). In Table 1 the measurements for the set-ups are given. Two set-ups had the prestress transfer region inside the shear span: the shear spans were 0·8 m and 0·5 m, denoted VT2-IN-0·8 and VT2-IN-0·5. The third set-up, denoted VT2-OUT-0·8, had the transfer region outside the shear span of 0·8 m. For the 400 mm thick unit, the shear span chosen was 1·0 m for the set-up with the transfer region inside the shear span, VT4-IN-1·0, as well as for the set-up with the transfer region outside the shear span, VT4-OUT-1·0. To have the prestress transfer region outside the shear span, one end of the hollow core units was cantilevered 1·0 m from the support at the loaded end.

Modelling technique. To analyse the 400 mm thick hollow core unit, principally the same FE model as in the analysis of the tests was used. The mesh for the analyses of the 200 mm thick units was established by the same principle. The width of the loading area, see A in Fig. 5, was half of the thickness of the hollow core unit. In these analyses, the loading area over the support, see B in Fig. 5, had the same width as the support. The sheets of wood fibre at these places were not included. The concrete compressive strength used here was a mean value from all of the tests on each of the geometries included in this project.[10] All material properties used for the concrete in the models are shown in Table 2. For all other material properties the same values were used as in the analysis of the tests.

The separate loading arrangement of beams made it possible easily to vary the relation between shear and torsion. This was done in the analyses to establish the interaction curves. For all set-ups, an analysis was made for each ratio of shear and torsion chosen. In total, 57 analyses were made.

Results. With results from FE analyses, it was possible to establish shear and torsion interaction diagrams for the geometries investigated, see Figs 9–11. Each solid mark in the diagrams is the result from one analysis: the actual shear force and the torsional moment are calculated for the maximum load. The open marks with dashed curves show the shear force and torsional moment from the analyses when it was estimated that the first crack would be visually observed in a corresponding test.

Figure 9 shows the interaction diagram for VT4-IN-1·0. For some load combinations, the crack pattern just after the maximum load is shown. In the diagram the results from the two tests, ST400G1 and ST400G2, are also included. The diagram shows that the interaction between shear and torsion is non-linear. The failure mode changed gradually with the shear–torsion ratio. As can be seen from the crack patterns, the failure mode varied from a diagonal crack in the upper flange for combinations close to pure torsion, to shear tension cracks in the webs and also bending cracks in the bottom flange, for combinations close to pure shear. When the shear force is less than approximately 200 kN, the curve is almost horizontal and the torsional capacity is not affected by the increased shear force.

Table 1. Measurements for the set-ups. Notation as shown in Fig. 5(a)

Identification	ST4G	VT4-IN-1·0	VT4-OUT-1·0	VT2-IN-0·8	VT2-IN-0·5	VT2-OUT-0·8
Shear span (s): m	1·0	1·0	1·00	0·80	0·50	0·80
Cantilever (c): m	—	—	0·96	—	—	0·97
Extension (e): m	0·9	0·9	0·90	0·75	0·75	0·75
Support length (d): mm	80	80	80	60	60	60
Loading plate A (a): mm	200	200	200	100	100	100
Loading plate B (b): mm	140	80	80	60	60	60

Table 2. Material properties used for the concrete in the FE analyses

	Mean concrete compressive strength f_{ccm}: MPa	Mean concrete tensile strength f_{ctm}: MPa	Fracture energy G_F: Nm/m^2	Young's modulus of concrete E_{ci}: GPa	Shear factors [—] (beam elements only)
ST4G	61·2	3·75	106·6	39·33	4·06
VT4	61·0	3·74	106·3	39·28	4·06
VT2	53·2	3·45	88·7	37·54	10·39

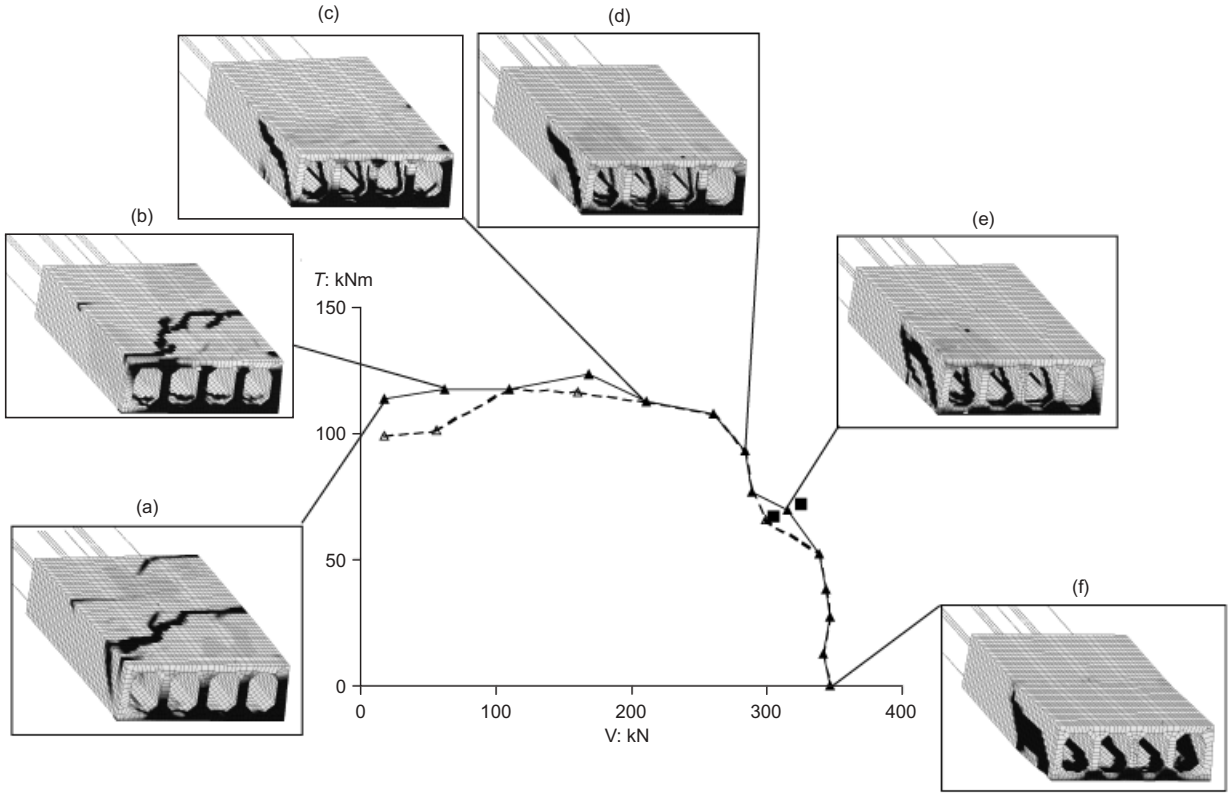

Fig. 9. Shear and torsion interaction diagram for the 400 mm thick hollow core unit with the prestress transfer region within the shear span, VT4-IN-1·0. Each solid mark is the result from one analysis: the shear force and torsional moment are calculated at the maximum load. The open marks with dashed curves show the shear force and torsional moment when it was estimated that the first crack would be visually observed in a corresponding test. (a)–(f) Crack pattern just after maximum load for some load combinations

Nevertheless, the crack patterns show that the relations between shear and torsion affect the failure modes. For some combinations, as the dashed curve shows, cracks were observed before the maximum load was reached in the analyses. This indicates some stress redistribution. For combinations with a shear capacity less than 200 kN, these cracks were observed in the top flange. For the combination shear/torsion $\approx$ 300/70, the crack was observed in the second web.

The interaction diagram for VT4-OUT-1·0 is shown in Fig. 10 together with the crack pattern just after the maximum load from some of the analyses. Outside the transfer region the prestress is fully developed; this explains why the capacities are higher than in the previous diagram. For a shear force less than approximately 200 kN, the capacity for torsional moment increases with the shear force. This is the result of increased bending moment and, therefore, the tensile stresses in the top flange decrease and a higher torsional moment can be carried. These stresses, in combination with the thickness of the top flange and the outermost webs, will determine if the failure starts in the web or in the top flange, see equations (8) and (9). As long as the critical point for failure is in the top flange the decrease of tensile stresses owing to increased bending moment will lead to a higher capacity for torsional moment, see Figs 10 and 11. This line of argument is valid also for VT4-IN-1·0. The negative moment owing to the prestress is smaller within the anchorage region; the positive effects on the torsional capacity resulting from increased bending moment are, therefore, smaller, see Fig. 9. For all combinations with a torsional capacity higher than about 100 kN/m, cracks in the top flange were visually observed before the maximum loads were reached. For the combination with pure shear and the one closest to it, flexural cracks in the bottom flange were observed before the maximum load. After the maximum load was reached, however, shear tension cracks occurred in the webs.

Figure 11 shows the interaction diagram for VT2-IN-0·5 and VT2-IN-0·8. As can be seen, the capacity was higher when the load was applied closer to the support. This indicates that the failure is affected by the loading arrangement. It is hard (nearly impossible) to predict a shear capacity that is not affected by the boundaries. For a shear force less than approximately 50 kN, the capacity for torsional moment increases with the shear force, owing to increased bending moment. Cracks were observed before the maximum loads were reached for several combinations. For combinations with tor-

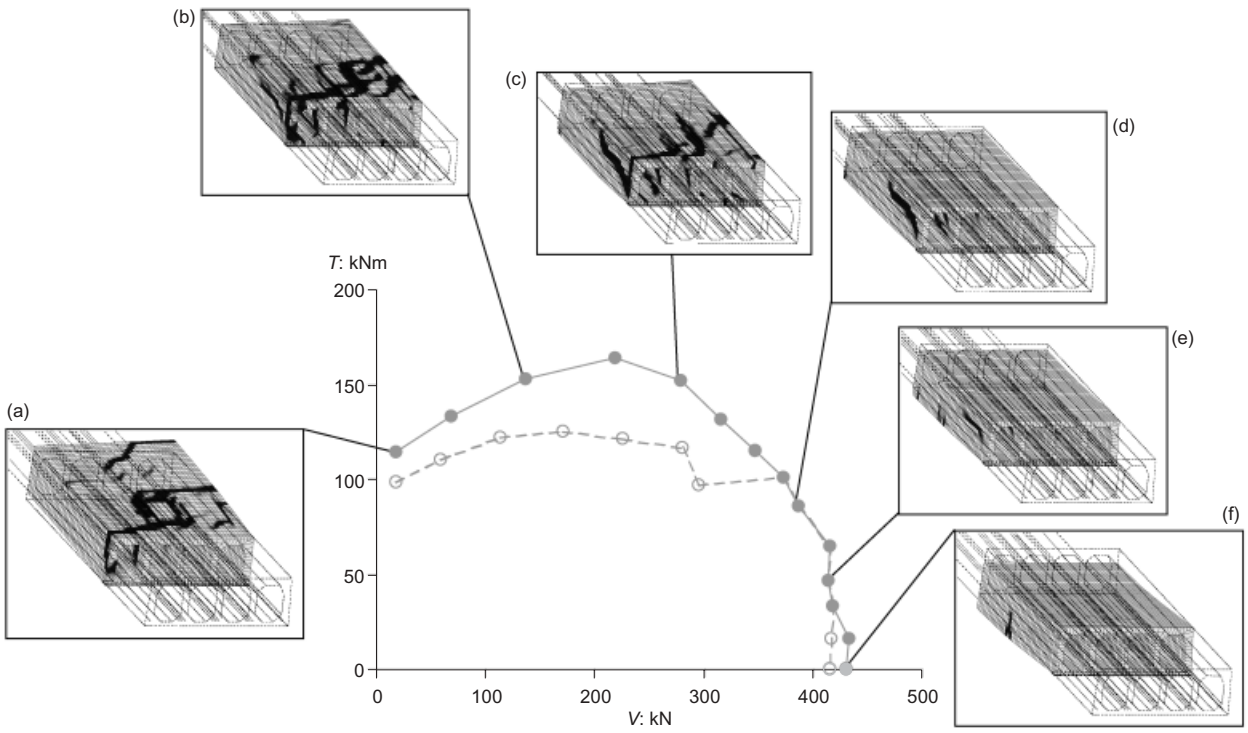

Fig. 10. Shear and torsion interaction diagram for the 400 mm thick hollow core unit with the prestress transfer region outside the shear span, VT4-OUT-1·0. Each solid mark is the result from one analysis: the shear force and torsional moment are calculated for the maximum load. The open marks with dashed curves show the shear force and torsional moment when it was estimated that the first crack would be visually observed in a corresponding test (a)–(f) Crack pattern just after maximum load for some load combination

sional capacity higher than 30 kN/m, these cracks were observed in the top flange, marked with open circles in Fig. 11. For the combinations marked with open diamonds, flexural cracks in the bottom flange were observed before or at the maximum load. In combination with large slips of the strands and no cracks in the webs after maximum load, see Fig. 11 (i) and (j), this indicates anchorage failures. The shear and torsion capacity were thus obtained by anchorage failure, not by a web shear tension failure.

Comparison of FE analyses and the analytical method

The capacities from the FE analyses are compared with those predicted by the formulae given in the present standard, EN 1168,[15] in shear and torsion interaction diagrams, see Figs 12 and 13. The same mean tensile strength as in the FE analyses was used in the calculations, that is the mean tensile strength calculated according CEB,[18] which gives a slightly lower tensile strength than EN1992.[21] Altogether the FEA results from various combinations of shear and torsion gave non-linear convex interaction curves compared with the linear relation given in EN 1168, see equation (13). As can be seen, the FE analyses gave higher capacity than the method in EN 1168 for most combinations of shear and torsion, both for the 200 mm and the 400 mm thick hollow core unit. The increase in capacity is large when the transfer region is inside the shear span (IN) as well as outside (OUT) the shear span, up to 55% and 30%, respectively, for the 200 mm thick hollow core unit, Fig. 12. For the 400 mm thick hollow core unit, Fig. 13, the increase is up to 30% when the transfer region is inside the shear span and up to 25% when it is outside.

As the prevailing stresses owing to the prestressing are of great importance for where the failure starts, the transmission lengths resulting from the FE analyses are compared with those calculated with the method in the standard, see Fig. 14. In the FE analyses, no adjustment of the initial prestress was made to account for relaxation, creep or shrinkage. After release of the prestressing force, the resulting steel stress in the FE analyses of the 200 mm thick hollow core units was 855 MPa and 946 MPa for the 400 mm thick units; the strands were fully anchored within approximately 0·8 m and 0·9 m, respectively. The hand calculations of the anchorage length were made by assuming that the hollow core units were sawn (release of prestressing force) one day after grouting; the initial prestressing level was reduced by 50 MPa. The resulting anchorage length was 0·69 m for the 200 mm thick units and 0·80 m for the 400 mm thick units. The small differences in trans-

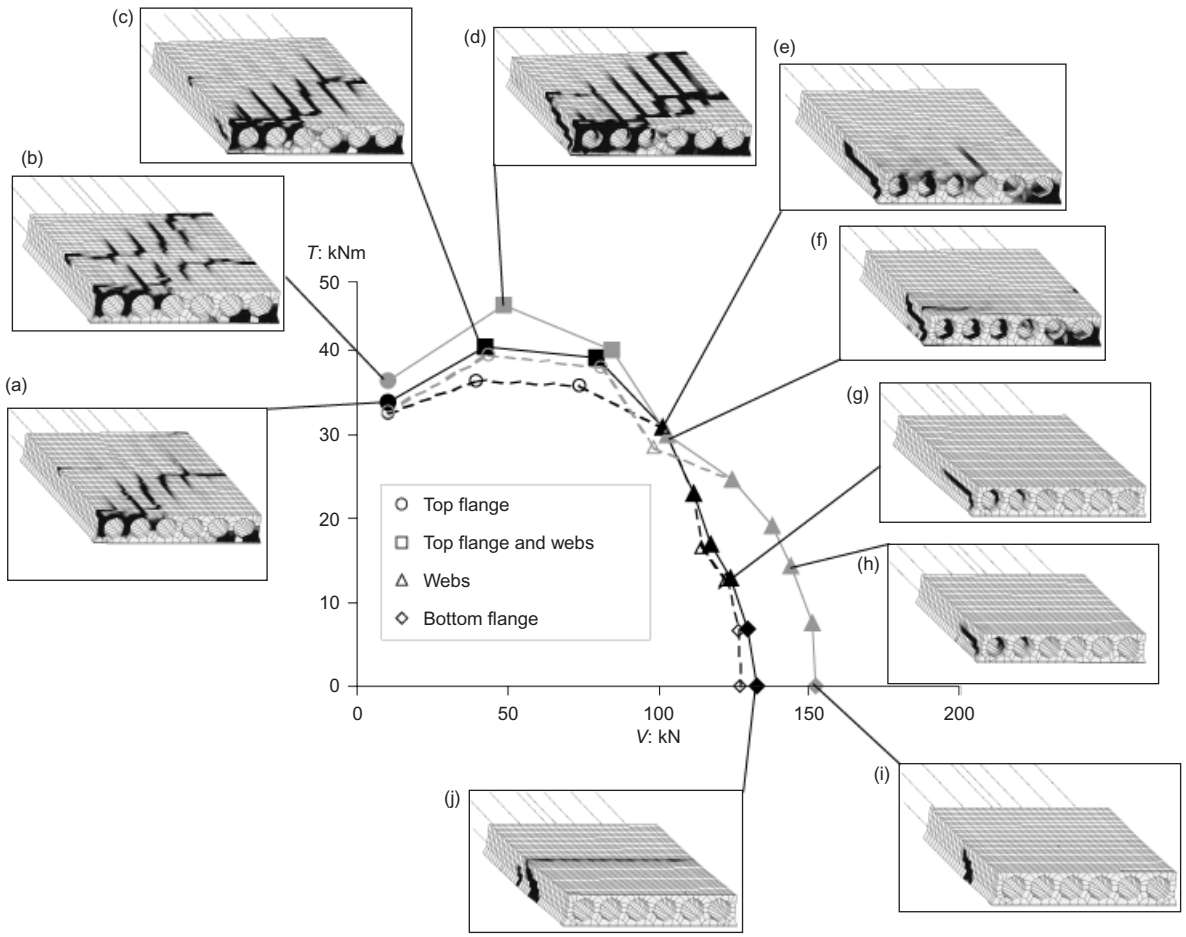

Fig. 11. Shear and torsion interaction diagrams for the 200 mm thick hollow core unit with the prestress transfer region within the shear span: black for shear span 0·8 m and grey for shear span 0·5 m. Each solid mark is the result from one analysis: the shear force and torsional moment calculated for the maximum load. The open marks with dashed curves show the shear force and torsional moment from the analyses when it was estimated that the first crack would be visually observed in a corresponding test. The marks show where cracks occurred. (a)–(j) Crack pattern just after maximum load for some load combinations

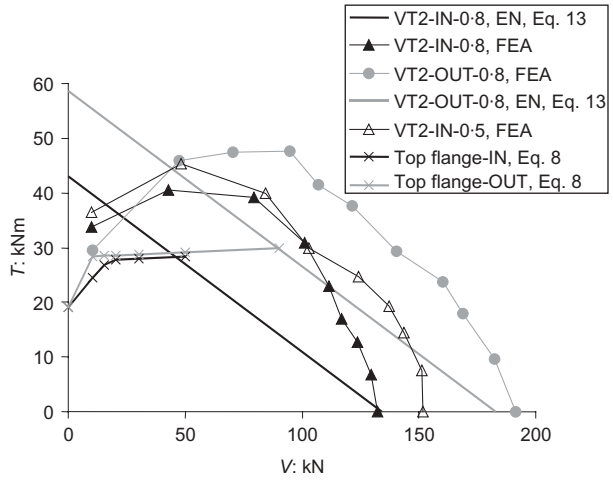

Fig. 12. Shear and torsion interaction diagram for the 200 mm thick unit

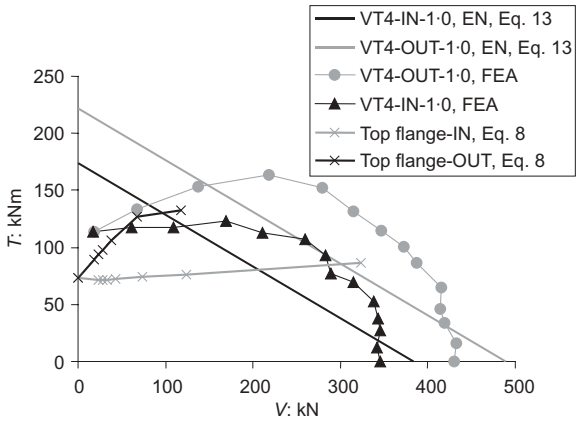

Fig. 13. Shear and torsion interaction diagram for the 400 mm thick unit

mission length cannot explain the higher capacities obtained in the FE analyses.

The FE analyses also showed that, for the cross-sections studied, the method in EN 1168[15] is not valid for loading close to pure torsion, where the failure took place in the upper flange of the hollow core unit. This failure mode is not taken into account in EN 1168; here, however, it has been calculated from equation (8) and included in the diagram. Note that, in the analytical

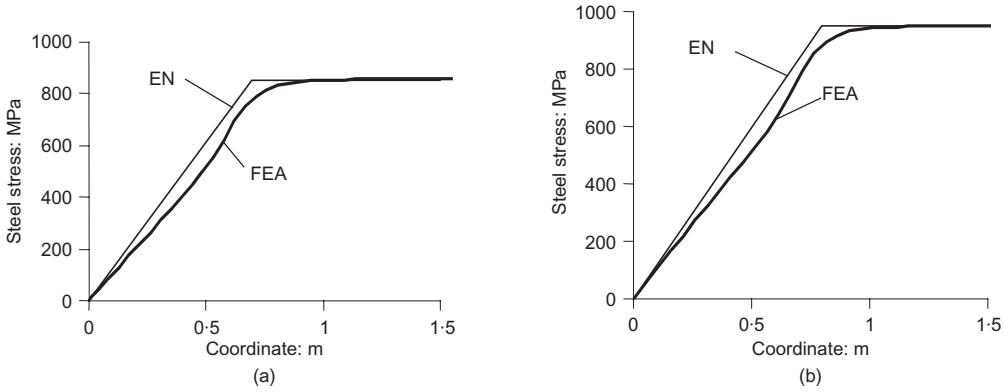

Fig. 14. Results from analysis compared with the predicted results, calculated by the method in EN 1168; steel stress in strands after release of prestressing force: (a) VT2; (b) VT4

model, the failure criterion is based on the crack load. The FE analyses showed, however, that after cracking in the upper flange, an additional load could be carried before failure occurred; hence, the structure could still be used owing to redistribution of stresses.

For the 400 mm thick hollow core unit, the method in EN 1168 slightly overestimates the capacity for pure shear. This difference may stem from the analytical model in which it is assumed that the cracking starts where the plane inclined at 45°, from the edge of the support, intersects with the mid-depth plane, see Fig. 1. At this intersection the prestressing force is not fully developed and, for cross-sections with circular voids, the web width is minimum; thus, this is the most critical section. This does not, however, seem to be true for cross-sections with constant web widths,[3,7] as the critical section can be elsewhere than in the mid-depth plane, depending on the transfer of the prestress. Furthermore, the transfer of the prestressing force introduces not only compressive stress but also shear stresses in the structure, which influence the stress state in the webs. A calculation method to take this into account was proposed by Yang.[3] In the FE analysis of the 400 mm thick unit subjected to pure shear, the shear tension crack starts in the middle web, lower than mid-depth and closer to the support than half the depth away (the critical point assumed in the analytical model), which is the same result obtained by Pajari.[7]

Conclusions

A method to use advanced non-linear FE analyses to obtain shear and torsion interaction diagrams is proposed. Two cross-sections were investigated: a 200 mm thick hollow core unit with six circular voids; and a 400 mm thick unit with four almost rectangular voids.

The FE analyses revealed a non-linear interaction between shear and torsion capacity in hollow core units rather than the linear one in EN 1168.[15] Moreover, the FE analyses gave higher capacities than the calculation method in the present standard for almost all combinations of shear and torsion. The increase was up to 55% for the 200 mm thick unit and up to 30% for the 400 mm thick unit. For several of the combinations, cracks were visually observed in the FE analyses before the maximum load was reached; this indicates a redistribution of stresses.

For load situations close to pure torsion, the analyses resulted in less resistance than that predicted by the method in EN 1168.[15] This is attributed to the failure mode in the FE analyses, that is cracking of the upper flange, which is not taken into account in the present standard. For pure shear, the difference was small; still, for the 400 mm unit, the analyses showed slightly lower resistance than the method in EN 1168. This divergence may be caused by the fact that, in the present standard, only the cross-section at a distance of half of the depth away from the support (the critical point assumed in the analytical model) is used. For cross-sections with circular voids this is the most critical point, although it may not apply cross-sections with constant web widths.

The effects of shear span and the influence of the prestressing transfer zone on the shear and torsion capacities were also evaluated. As could be expected, the capacities were higher when the shear span was outside the prestressing transfer zone, except for loading close to pure torsion. The shear spans influenced the capacities; shorter shear span gave higher capacities. This indicates that it is hard to predict a shear–torsion capacity that is not influenced by the boundaries. This problem is similar, however, when using analytical methods: one assumed crack pattern is used for all load cases.

Interaction diagrams, such as those presented here, could be established for different geometries of hollow core units and used in practical design when the shear force and torsional moment are known. These action effects could be evaluated from diagrams used in practical design today,[15] or by FE analyses using a simplified model of the whole floor, such as the model developed in Lundgren *et al.*[14]

Acknowledgements

The photographs in this paper are used with kind permission of VTT. The authors would like to thank Matti Pajari, DSc(tech), at VTT for allowing us to attend the tests and to use the data collected directly after the tests were carried out. The research was financed by the 5th Framework of European Commission, the International Prestressed Hollow Core Association, the 'Bundesverband Spannbeton-Hohlplatten' in Germany and by the partners involved, which were Chalmers University of Technology, VTT, Consolis Technology, Strängbetong, Castelo and Echo.

References

1. Walraven J. C. and Mercx W. P. M. The bearing capacity for prestressed hollow core slabs. *Heron*, 1983, **28**, No. 3, 3–46.
2. Pisanty A. The shear strength of extruded hollow-core slabs. *Materials and Structures*, 1992, **25**, No. 148, 224–230.
3. Yang L. Design of prestressed hollow-core slabs with reference to web shear failure. *Journal of Structural Engineering, ASCE*, 1994, **120**, No. 9, 2675–2696.
4. Jonsson E. Shear capacity of prestressed extruded hollow-core slabs. *Nordic Concrete Research*, 1988, No. 7, 167–187.
5. Hoang L. C. *Shear Strength of Non-Shear Reinforced Concrete Elements Part 3. Prestressed Hollow-Core Slabs*. Institut for baerende konstruktioner og material, Department of Structural Engineering and Materials, Technical University of Denmark, Lyngby Series R No 30, 1997.
6. Becker R. J. and Buettner D. R. Shear tests of extruded hollow-core slabs. *Precast/Prestressed Concrete Institute Journal*, 1985, **30**, No. 2, 40–54.
7. Pajari M. *Shear resistance of prestressed hollow core slabs on flexible supports*. PhD Thesis, VTT, Technical Research Centre of Finland, Espoo, 1995.
8. Pajari M. Shear resistance of PHC slabs supported on beams. II: Analysis. *Journal of Structural Engineering, ASCE*, 1998, **124**, No. 9, 1062–1073.
9. Gabrielsson H. *Ductility of high performance concrete structures*. PhD Thesis, Division of Structural Engineering, Luleå University of Technology, Luleå, 1999.
10. Pajari M. *Shear–Torsion Interaction Tests On Single Slab Units*. Technical Research Centre of Finland, VTT Building and Transport, 2004, Internal report RTE50-IR-1/2003.
11. Pajari M. *Pure torsion tests on single slab units*. Technical Research Centre of Finland, VTT Building and Transport, December 2003, Internal report RTE50-IR-25/2002.
12. Broo H. and Lundgren K. *Finite Element Analyses of Hollow Core Units Subjected to Shear and Torsion*. Chalmers University of Technology, Department of Structural Engineering, Concrete Structures, Göteborg, December 2002, Report 02:17.
13. Broo H., Lundgren K. and Engström B. Shear and torsion in prestressed hollow core units: Finite element analyses of full-scale tests. *Structural Concrete* (submitted for publication).
14. Lundgren K., Broo, H. and Engström B. Analyses of hollow core floors subjected to shear and torsion. *Structural Concrete*, 2004, **5**, No. 4, 1464–4177.
15. Comité Européen de Normalisation. CEN/TC229: *Precast concrete products—Hollow core slabs. Final draft prEN 1168*, CEN, Brussels, 2004.
16. Pajari M. *Design of prestressed hollow core slabs*. Technical Research Centre of Finland, 1989, Espoo Research Reports 657.
17. TNO. *DIANA Finite Element Analysis, User's Manual release 8·1*. Nederlandse Organisatie voor Toegepast-natuurwetenschappelijk Onderzoek, Building and Construction Research, Delft, The Netherlands, 2002.
18. Comité Euro-international du Béton. *High Performance Concrete, Recommended Extension to the Model Code 90. Bulletin d'Information 228*, CEB, Lausanne, Switzerland, 1995.
19. Comité Euro-international du Béton. *CEB-FIP Model Code 1990. Bulletin d'Information 213/214*, CEB, Lausanne, Switzerland, 1993.
20. Lundgren K. *Steel-Encased Pull-Through Tests of Seven-Wire Strands*. Department of Structural Engineering, Concrete Structures, Chalmers University of Technology, Göteborg, Sweden, 2002, Report 02:13.
21. Comité Européen de Normalisation. CEN/TC250/SC2. *Eurocode 2: Design of concrete structures—Part 1: General rules and rules for buildings*, *prEN 1992-1-1 Draft for Stage 49 ed*. CEN, Brussels, 2002.

Discussion contributions on this paper should reach the editor by 1 May 2006

Paper IV

Simulation of shear-type cracking and failure with non-linear finite element method.

Broo H., Plos M., Lundgren K. and Engström B.

Magazine of Concrete Research, Vol. 59, No. 9, pp. 673—687, 2007.

Magazine of Concrete Research, 2007, **59**, No. 9, November, 673–687
doi: 10.1680/macr.2007.59.9.673

Simulation of shear-type cracking and failure with non-linear finite-element method

H. Broo, M. Plos, K. Lundgren and B. Engström

Chalmers University of Technology

Today, the non-linear finite-element (FE) method is commonly used by practising engineers. Simulating the shear behaviour and shear failure of reinforced concrete structures, using three-dimensional non-linear finite-element methods, has shown higher load-carrying capacity due to favourable load distribution, compared to conventional analyses. However, the modelling method for reinforced and prestressed concrete members subjected to shear and torsion has not been generally verified. Therefore, the method needs to be investigated further and confirmed to be practically reliable. The aim of this project is to develop, improve and verify a method to simulate the shear response of reinforced and prestressed concrete members. The method should be applicable for large structures, for example box-girder bridges, subjected to various load actions. Experiments with panels loaded in shear and beams loaded in bending, shear and torsion are simulated by using non-linear FE analysis. The results showed that four-node curved shell elements with embedded reinforcement could simulate the shear response. It is well known that the shear sliding capacity is larger than that which can be explained by the reinforcement contribution determined from a truss model. This increase is due to dowel action and aggregate interlock, and has been accounted for in the past by modifying the concrete tension response in models—for example, according to the modified compression field theory (MCFT). Results from the analyses show that without any modification, the capacity was underestimated and the average strains—that is, the crack widths—were overestimated. On the other hand, if the concrete contribution to the shear capacity was considered with the expression from MCFT, the capacity was in many cases overestimated and the average strains underestimated.

Notation

A_c concrete area (m^2)
E_c concrete modulus of elasticity (Pa)
E_s reinforcement modulus of elasticity (Pa)
f_{cm} mean compressive cylinder concrete strength (Pa)
f_{ct} concrete tensile strength (Pa)
f_{ctm} mean tensile concrete strength (Pa)
f_u reinforcement ultimate strength (Pa)
f_y reinforcement yield strength (Pa)
G_f concrete fracture energy
h characteristic length (m)
s_m mean crack spacing (m)
γ shear strain
ε_1 average principal tensile strain
ε_2 average principal compressive strain
ε_x average strain in x-direction
ε_y average strain in y-direction
ρ reinforcement amount
σ_1 principal tensile stress (Pa)
σ_2 principal compressive stress (Pa)
σ_{c1} average principal concrete tensile stress (Pa)
σ_s steel stress (Pa)
τ shear stress (Pa)
ϕ diameter or reinforcement bar (m)

Department of Civil and Environmental Engineering, Structural Engineering, Concrete Structures, Chalmers University of Technology, SE-412 96 Göteborg, Sweden

(MCR 700012) Paper received 11 January 2007; last revised 25 April 2007; accepted 4 June 2007

Introduction

For structural design and assessment of reinforced concrete (RC) members, the non-linear finite-element (FE) analysis has become an important tool. However, design and assessment for shear and torsion are still made today with simplified analytical or empirical design methods. In some cases, more enhanced methods are used, such as the modified compression field theory (MCFT) of Vecchio and Collins.[1] These methods all use sectional forces and moments, which usually are determined through elastic beam or frame analysis or

www.concrete-research.com 1751-763X (Online) 0024-9831 (Print) © 2007 *Thomas Telford Ltd*

linear FE analysis. The current calculation method for RC members subjected to combined shear and torsion, in the European Standard EC2 CEN/TC250/SC2,[2] adds stresses from shear and from torsion linearly without taking into account deformations and compatibility within the member. However, earlier research indicates that there is a redistribution within concrete members lacking transverse reinforcement,[3,4] and that this could be modelled with non-linear FE analyses.[5,6] It is also well known that the shear capacity is larger than what can be explained by the reinforcement contribution determined from a truss model. Non-linear FE analyses of concrete members with transverse reinforcement subjected to shear have been reported by several researchers, for example Ayoub and Filippou,[7] Yamamoto and Vecchio,[8] Vecchio and Shim[9] and Kettil *et al.*[10] In recently conducted research projects, failures owing to shear and torsion were successfully simulated with non-linear FE analyses, also for members with transverse reinforcement (see Plos[11]). A higher load-carrying capacity compared with conventional analysis was shown. This can be explained by a more favourable load distribution, when the structure has been analysed in three dimensions and by including the fracture energy associated with concrete cracking. Here, though, the modelling method used for reinforced and prestressed concrete members subjected to shear and torsion had not been verified. The modelling method therefore requires further study and verification in order to be reliable and practically applicable.

The aim of this project is to develop a method to model and simulate shear-type cracking and shear failure of reinforced and prestressed concrete members. It should be possible to use the method for analyses of more complex structures, for example box-girder bridges, subjected to bending, shear, torsion and combinations of these load actions. Engineers using commercial non-linear FE programs, not specially designed for shear analysis, should be able to use the method in their daily practice. Further aims are to examine and determine the most important parameters that need to be accounted for in the material model or in the material properties used. The mechanisms contributing to the shear resistance of cracked concrete are explained and various ways to model these are briefly presented. Tests of panels loaded in shear and beams loaded in bending, shear and torsion are simulated by using the non-linear finite-element method (FEM) and the results are compared.

The non-linear response in shear

Both shear forces and torsional moments cause shear stresses that can result in cracks in a concrete member. Cracks owing to shear stresses are usually inclined relative to the direction of the reinforcement. To satisfy the new equilibrium after shear cracking, longitudinal reinforcement and transverse reinforcement or friction in the crack is required. After cracking, the shear force is transmitted by compression in the concrete between the inclined cracks, tension in the transverse reinforcement crossing the inclined cracks, tension in the longitudinal reinforcement, compression and shear in the compressive zone and stresses transferred over the crack, for example through aggregate interlocking along the crack. The visual shear cracks are preceded by the formation of micro-cracks. The micro-cracking and the following crack formation change the stiffness relations in the member, and a redistribution of stresses can occur resulting in strut inclinations smaller than 45° (see Hegger *et al.*[12]). Owing to the rotation of the struts, more transverse reinforcement can be activated. This behaviour becomes more pronounced when the transverse reinforcement starts to yield. The rotation of the compressive struts can continue until failure. Possible failure modes in shear are: (a) sliding along a shear crack; (b) crushing of the concrete between two shear cracks; or (c) crushing of the concrete in the compressive zone. In the case of transverse reinforcement, shear sliding cannot take place before the transverse reinforcement yields. It is well known that the shear capacity is larger than what can be explained by the reinforcement contribution determined from a truss model. This increase in shear capacity is caused by tension stiffening, compression and shear in the compressive zone and stresses transferred over the crack, for example tension softening, dowel action and aggregate interlocking. This increase is also known as the 'concrete contribution'.

After cracking, concrete can transmit tensile stresses owing to tension softening, and for RC also owing to tension stiffening. Tension softening is the capability of plain concrete to transfer tensile stresses after crack initiation. In an RC member subjected to tensile forces, tensile stresses are transferred by bond from the reinforcement to the concrete in between the cracks, which contributes to the stiffness of the member. This is known as the tension stiffening. The tension stiffening effect increases the overall stiffness of the RC member in tension compared with that of the bare reinforcement. Owing to both tension stiffening and tension softening, there are still significant transverse tensile stresses in the compressive struts. Cracked concrete subjected to tensile strains in the direction transverse to the compression is softer and weaker in compression than concrete in a standard cylinder test.[1,13,14]

The complex behaviour of RC after shear crack initiation has been explained in several papers (see for example References 1 and 15–20). The equilibrium conditions can be expressed in average stresses for a region containing several cracks, or in local stresses at a crack. The local stresses normal to the crack plane are carried by the reinforcement and by the bridging stresses of plain concrete (tension softening). Along the crack plane, the shear stresses are carried by aggregate

interlocking and dowel action. The stresses will depend on the shear slip, the crack width, the concrete composition (strength, grading curve and maximum aggregate size) and of course the reinforcement (type, diameter and spacing).[21]

Modelling of the non-linear shear behaviour

Several analytical models that are capable of predicting the non-linear response in shear have been presented, for example the MCFT of Vecchio and Collins,[1] the distributed stress field model (DSFM) of Vecchio,[22] the cracked membrane model (CMM) of Kaufmann and Marti,[23] the rotating-angle softened truss model (RA-STM) of Pang and Hsu,[16] the fixed-angle softened truss model (FA-STM) of Pang and Hsu,[24] and the softened membrane model (SMM) of Hsu and Zhu.[25] All these models are based on the smeared crack approach—that is, the influences of cracks are smeared over a region and the calculations are made with average stresses and average strains. Stress equilibrium, strain compatibility and constitutive laws are used to predict the shear force for chosen strains. Some models use a rotating crack concept and thus no relationship between shear stress and shear strain is needed for the concrete. Others are based on a fixed crack concept including a relationship for average shear stresses and average shear strains. Most of the models are also implemented in FE programs. Soltani *et al.*[20] propose a model based on formulations of local stresses and strains at the crack plane, separating the contributions from tension softening, tension stiffening, aggregate interlocking and dowel action, to predict the non-linear shear response.

If the shear-type cracking and shear failure are modelled and simulated with the non-linear FEM, with an FE program not specially designed for shear analysis, parts of the concrete contribution need to be accounted for by modifying the constitutive relationships used. The modifications needed depend on the modelling method, material model, and how the interaction between reinforcement and concrete is modelled.

Modelling of reinforcement and the interaction between reinforcement and concrete can be made more or less detailed. When modelling larger structures—that is, box-girder bridges—a simple approach is needed and the reinforcement can be modelled as embedded in the concrete elements. Embedded reinforcement can be applied to any type of FE that represents the concrete. The embedded reinforcement adds stiffness to the FE representing the concrete, but the reinforcement has no degree of freedom of its own. Hence, the reinforcement is perfectly bonded to the surrounding concrete and no slip can occur. In this case the effects of the concrete contribution, described above, must be taken into account in the constitutive relations describing the materials' behaviour, for example the concrete in tensile response or in the reinforcement response. Ways of doing this for the tension stiffening have been proposed by Kaufmann and Marti[23] and Lackner and Mang.[26] Relationships between tensile stress and crack opening in plain concrete are based on fracture mechanics and related to the fracture energy, G_f; an example is the relation proposed by Hordijk, as described in Reference 27. For RC members subjected to shear, the contribution from dowel action and aggregate interlocking can also be accounted for in the constitutive relations. Such relationships that link the average tensile stress to the average tensile strain for orthogonally reinforced concrete have been established on the basis of shear panel tests. Vecchio and Collins[1] suggested

$$\sigma_{c1} = \frac{f_{ctm}}{1 + \sqrt{200\varepsilon_1}} \tag{1}$$

after several tests on thin panels reinforced with smooth welded wire meshes with close spacing—the 'Toronto panels'. Here σ_{c1} is the average principal tensile stress, f_{ctm} is the mean tensile concrete strength and ε_1 is the average principal tensile strain. Following tests on thicker panels reinforced with coarser reinforcement this was changed to

$$\sigma_{c1} = \frac{f_{ctm}}{1 + \sqrt{500\varepsilon_1}} \tag{2}$$

which is the relationship used in the MCFT of Collins and Mitchell.[28] Bentz[29] compared these relationships with

$$\sigma_{c1} = f_{ctm}\left(\frac{0{\cdot}00008}{\varepsilon_1}\right)^4 \tag{3}$$

which was suggested for the softened truss model of Pang and Hsu,[16] and evaluated from tests on thick panels reinforced with widely spaced coarse bar reinforcement. In Fig. 1 the relationships by Vecchio and Collins,[1] Pang and Hsu[16] and Hordijk[27] are compared for one particular shear panel. By adjusting the expression by Vecchio and Collins[1] to depend on reinforcement ratio and rebar diameter, Bentz[29] proposed

$$\sigma_{c1} = \frac{f_{ctm}}{1 + \sqrt{3{\cdot}6M\varepsilon_1}} \tag{4}$$

where

$$M = \frac{A_c}{\Sigma\phi\pi} \tag{5}$$

Here A_c is the concrete area and ϕ is the diameter of the reinforcement bar. These relationships should be limited so that no concrete tensile stress is transmitted after the reinforcement has started to yield. This is a problem when modifying the relationship for concrete in tension in an FE program, since there is no obvious link between the steel strain in the reinforcement direction and the concrete strain in the

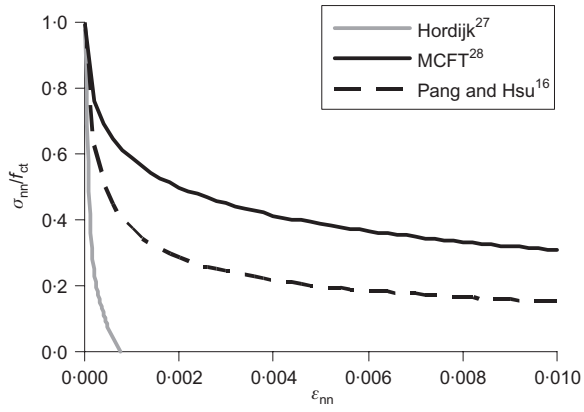

Fig. 1. Different tension-softening relations compared for Houston panel A3. For the curve by Hordijk the fracture energy is smeared over a length of 150 mm (the crack band width, h), which corresponds to the calculated average crack spacing

principal stress direction. Hence, the cracked concrete can transfer tensile stresses in the principal stress direction even when the reinforcement in any direction yields.

The relationships by Vecchio and Collins,[1] Collins and Mitchell,[28] Pang and Hsu[16] and Bentz[29] were established for analysis of orthogonally reinforced concrete panels subjected to shear. However, more general applicability for members with deviating reinforcement or specimens subjected to, for instance, bending or tension is not shown and is rather doubtful. In the following analyses, the use of the tension–softening curve by Hordijk and a curve modified according to MCFT are compared for several RC members.

Modelling technique

The non-linear FE program DIANA and the following modelling approach were used to simulate tests of RC and prestressed concrete members subjected to bending, shear, torsion or combinations of these. This included tests on shear panels, the 'Toronto panels' of Vecchio and Collins[1] and the 'Houston panels' of Pang and Hsu,[16] and beams with various cross-sections and various load actions according to Karlsson and Elfgren[30] and Magnusson.[31]

In all analyses the concrete was modelled with four-node curved shell elements. For the specimens modelled here, plane-stress elements would have been more appropriate to use, but the aim was to develop an analysis method that could be used also for more complex structures, for which curved shell elements are more suitable. Full interaction was assumed between the reinforcement and the concrete. The concrete was modelled with a constitutive model based on non-linear fracture mechanics. In most of the analyses a rotating crack model based on total strain[27] was used. For some of the analyses this was compared with the use of a fixed crack model.[27] For most analyses the hardening of concrete in compression was described by the expression of Thorenfeldt and the reduction of the strength owing to transverse tensile strains was modelled according to Vecchio and Collins, as described in TNO;[27] when something else is used, this is specifically pointed out. For the tension softening, two approaches were compared

(*a*) the curve by Hordijk,[27] where only the fracture energy of plain concrete is taken into account
(*b*) a curve modified according to the expression from the MCFT of Collins and Mitchell,[28] which attempts to take into account also the concrete contribution when subjected to shear, see Fig. 1. For the curve by Hordijk, the fracture energy is smeared over a length, h, the crack band width, which corresponds to the mean crack spacing obtained in the test or calculated according to Collins and Mitchell.[28]

The concrete material properties used in all analyses are presented in Table 1. The concrete tensile strength, f_{ct}, the concrete modulus of elasticity, E_c, and the fracture energy G_f were calculated according to fib[21] from the mean cylinder compressive strength, f_{cm}, reported from the tests. The constitutive relations of the reinforcement and the prestressing steel were modelled by the von Mises yield criterion with an associated flow law

Table 1. Material properties for concrete used in the analyses of the Toronto panel tests, the Houston panel tests and the beam tests

Test		f_{cm}: MPa	f_{ctm}: MPa	E_c: GPa	G_f: Nm/m^2	s_m: mm	h: m
Toronto panel	PV10	14·5	1·04	24·30	32·4	50·0	0·050
	PV19	19·0	1·48	26·60	39·2	50·0	0·050
	PV20	19·6	1·58	26·90	44·0	50·0	0·050
Houston panel	A3	41·6	3·12	34·58	67·8	151·2	0·150
	B1	45·2	3·34	35·55	71·9	194·7	0·195
	B2	44·0	3·27	35·24	70·6	163·7	0·165
	B4	44·7	3·31	35·42	71·3	173·2	0·175
Beams	Beam 5	24·9	1·97	29·14	47·3		
	NSC 3	27·3	2·16	30·05	88·9	107·0	0·107

and isotropic hardening. In Fig. 2, definitions of the mechanical properties for the reinforcement are presented. The material properties used for the reinforcement in the Toronto panels and the Houston panels are presented in Table 2. From the test of the Toronto panel only the reinforcement strength was reported and the modulus of elasticity was chosen as 200 GPa for all reinforcement. In Table 3, the material properties of the reinforcement used for the beam analyses are presented. No hardening parameters were presented for the reinforcement used in the box-beam test. Instead, the values presented in Table 3 are mean values taken from several other test reports using the same kind of reinforcement, from the same laboratory and the same time period.

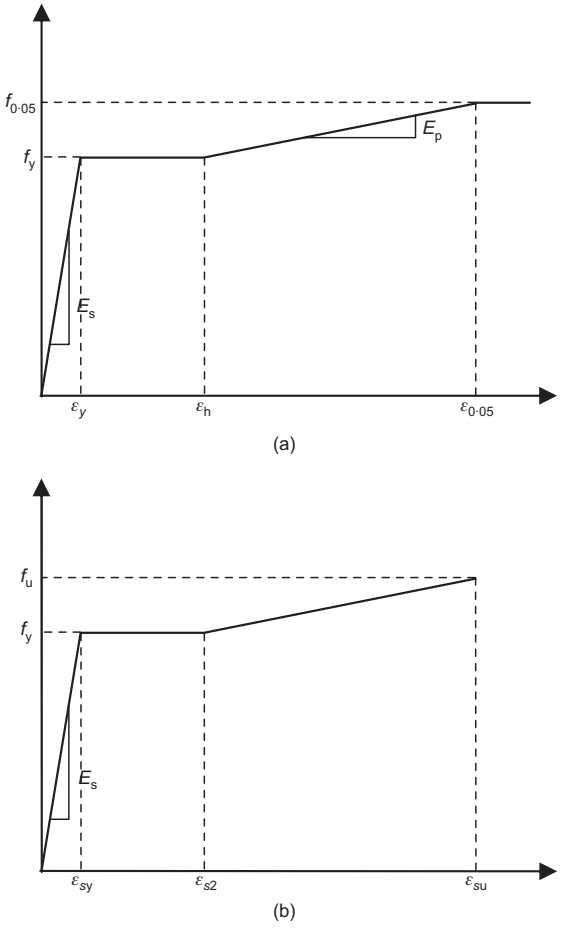

Fig. 2. Typical stress–strain relationships for reinforcement. Definitions of mechanical properties: (a) panels; (b) beams

Finite-element analyses of shear panel tests

Tests

Three shear panel tests were simulated out of 30 of the Toronto panels by Vecchio and Collins,[1] labelled PV10, PV19 and PV20. From the Houston panels by Pang and Hsu[16] and Pang,[32] four tests were simulated, labelled A3, B1, B2 and B4. The specimens tested in Toronto were 0·89 m square and 0·07 m thick; they were reinforced with two layers of smooth welded wire mesh. The specimens analysed here were loaded in pure shear; see Fig. 3(a). The specimens tested in Houston were 1·4 m square and 0·178 m thick. They were reinforced in two layers of deformed bars spaced at 0·189 m in two directions. The loading, equal in compression and in tension, was applied in the principal directions and the reinforcement was orientated with 45° inclination, resulting in the same stress situation as in the Toronto panels; see Fig. 3(b). In the Toronto panel tests as well as in the Houston panel tests, the loads were applied by hydraulic jacks connected to shear keys that were welded to the reinforcement. It is worth noting that the reinforcement ratios in the two test series are quite similar, see Table 2. The Toronto panels are thin with closely spaced reinforcement of small bar diameters and of a low-strength con-

Table 2. Material properties for reinforcement used in the analyses of the Toronto panel tests (PV10, PV19 and PV20) and the Houston panel tests (A3, B1, B2 and B4)

Test		ρ	f_y: MPa	E_s: GPa	$f_{0\cdot05}$: MPa	ε_y	ε_h	E_p: GPa
PV10	Long (x-)	0·01790	276	200	—	—	—	—
	Trans (y-)	0·01000	276	200	—	—	—	—
PV19	Long (x-)	0·01790	458	200	—	—	—	—
	Trans (y-)	0·00710	299	200	—	—	—	—
PV20	Long (x-)	0·01790	460	200	—	—	—	—
	Trans (y-)	0·00890	297	200	—	—	—	—
A3	Long (x-)	0·01789	446	200	625	0·0022	0·0111	4·60
	Trans (y-)	0·01789	446	200	625	0·0022	0·0111	4·60
B1	Long (x-)	0·01193	462	192	609	0·0024	0·0144	3·73
	Trans (y-)	0·00596	444	181	579	0·0044	—	2·69
B2	Long (x-)	0·01789	446	200	625	0·0022	0·0111	4·60
	Trans (y-)	0·01193	462	192	609	0·0024	0·0144	3·73
B4	Long (x-)	0·02982	469	200	629	0·0023	0·0073	3·76
	Trans (y-)	0·00596	444	181	579	0·0044	—	2·69

Table 3. Material properties for reinforcement used in the analyses of the beam tests

Test	Dimension and quality	f_y: MPa	f_u: MPa	ε_{sy}: ‰	ε_{s2}: ‰	ε_{su}: ‰	E_s: GPa
Beam 5	$\frac{1}{2}$ in. St 150/170	1840	—	—	—	—	207·0
	ϕ 8 Ks40s	456	600*	2·09	—	150*	218·0
	ϕ 16 Ks60	710	900*	3·05	—	110*	233·0
NSC 3	ϕ 8 K500 ST	574	670	3·10	29·3	99	199·8
	ϕ 20 K500 ST	468	600	2·40	21·5	132	195·6

*Values taken as a mean value of test values from several other reports using same kind of reinforcement.

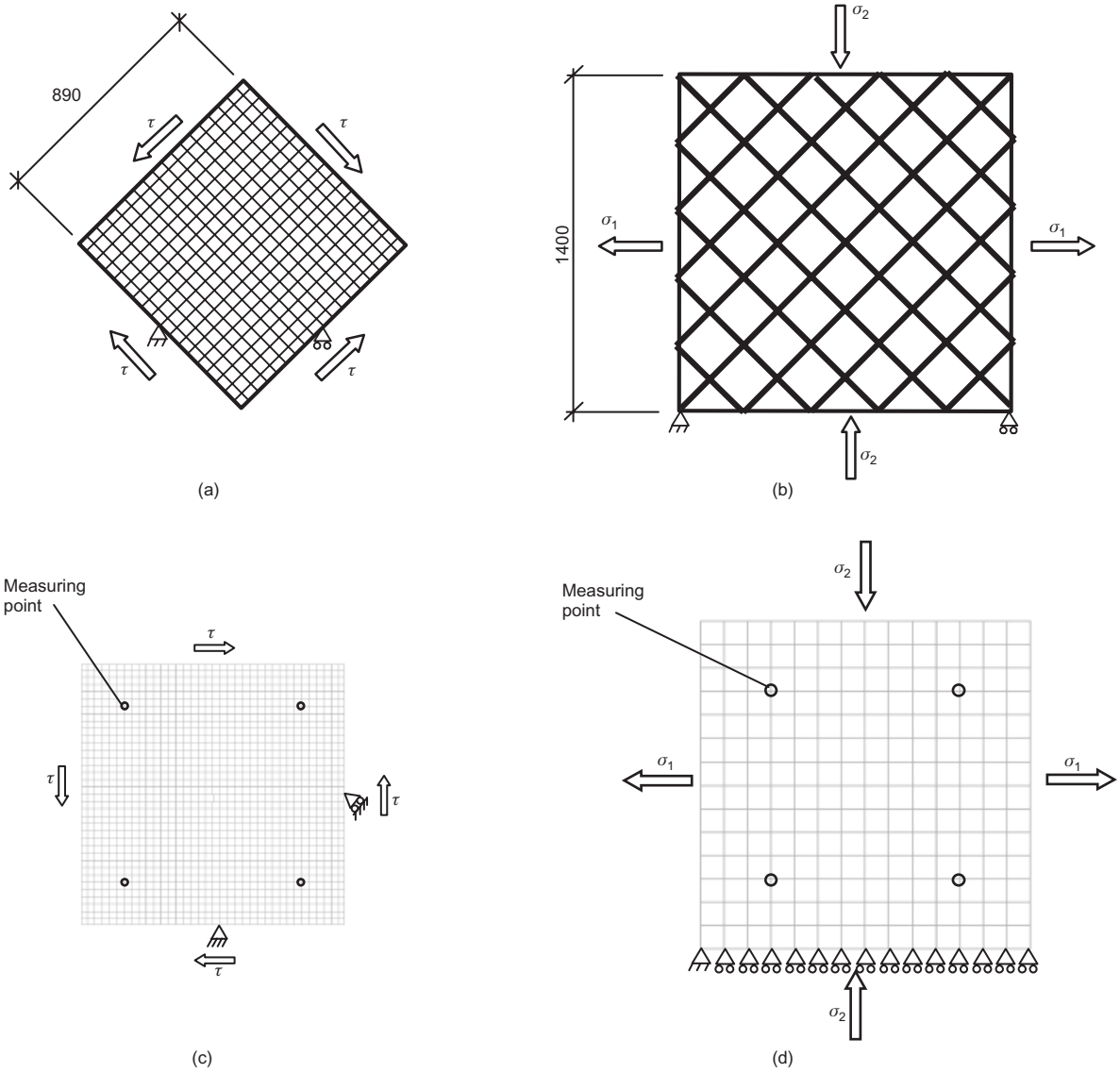

Fig. 3. Principal testing arrangement of (a) the Toronto shear panels PV10, PV19 and PV20; (b) the Houston shear panels A3, B1, B2 and B4. The principle of the FE models used to analyse (c) the Toronto panels; (d) the Houston panels

crete and could thus be seen as made in a model scale compared with the Houston panels. This is reflected in the FE analyses since measured concrete compressive strength and estimated crack distances determined the concrete properties used, see above section on modelling technique.

FE models

Diagrammatic representations of the FE models used to analyse the Toronto panels and the Houston panels are given in Fig. 3. The loads were equally distributed on each side and applied at each node as shear, tension or compression in accordance with each

test procedure respectively. The panels were supported as shown in Fig. 3. In the analyses, the self-weight was applied in one step and then the load was applied in steps of 1 kN for the Toronto panels and 5 kN for the Houston panels. This corresponds to a shear stress of approximately 16 Pa and 20 Pa respectively.

Results

From the analyses, the shear strains, γ, were calculated from ε_x and ε_y or from ε_1 and ε_2 in accordance with how they were calculated in the Toronto panel tests and the Houston panel tests respectively; see Fig. 4. In the tests and in the analyses, the elongation between the measuring points (see Fig. 3) was used to calculate the average strains. In Figs 5–9, results from the analysis of tests PV10, PV19 and PV20 are compared with results from the tests as presented in Vecchio *et al.*[33] and Vecchio and Lai.[34] In Figs 10 and 11, the results from the analysis of tests A3, B1, B2 and B4 are compared with results from the tests as presented in Pang.[32]

Comparing results such as the applied shear stress plotted against shear strain shows that four-node curved shell elements combined with embedded reinforcement can describe the shear response. Furthermore, with only fracture energy of plain concrete taken into account, the capacity was underestimated and the average strains—that is, the crack widths—were overestimated. On the other hand, if the concrete contribution was modelled with a tension-softening curve modified according to the expression from MCFT, the capacity was overestimated and the average strains were underestimated for most panels, except for the Toronto panels. It should be mentioned that results from the Toronto panel tests have been included in the test results used

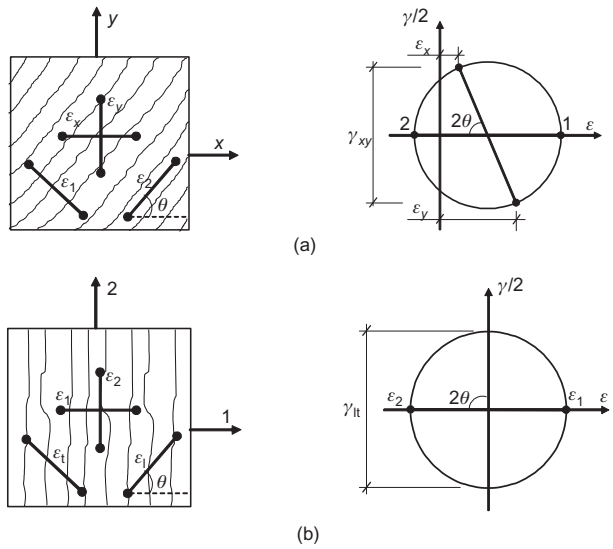

Fig. 4. The shear strains from the analyses, γ_{xy} and γ_{lt}, were calculated from ε_x and ε_y or from ε_1 and ε_2, respectively, with Mohr's strain circle in accordance with how they were calculated in (a) the Toronto panel tests and (b) the Houston panel tests

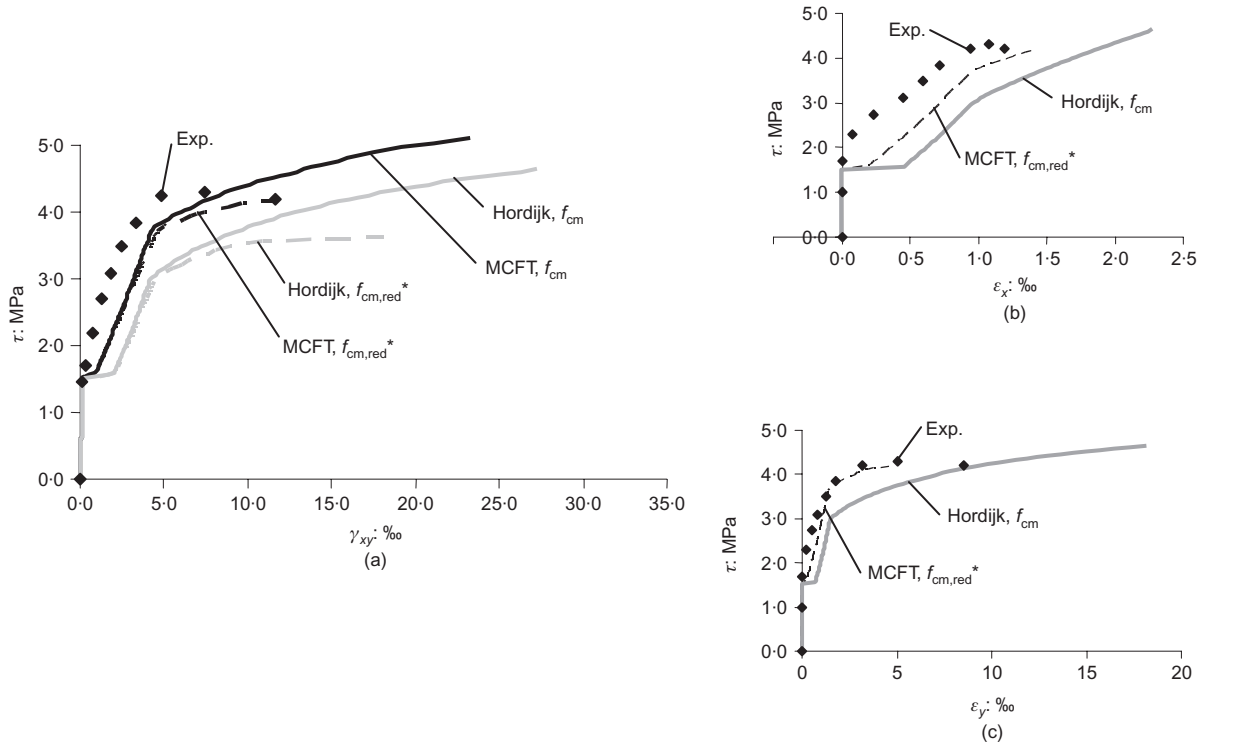

*Fig. 5. Comparison of results from test and analysis of PV20, applied shear stress plotted against (a) shear strain, (b) longitudinal strain, ε_x, (c) transversal strain, ε_y. *The compressive strength is reduced owing to transverse tensile strains*

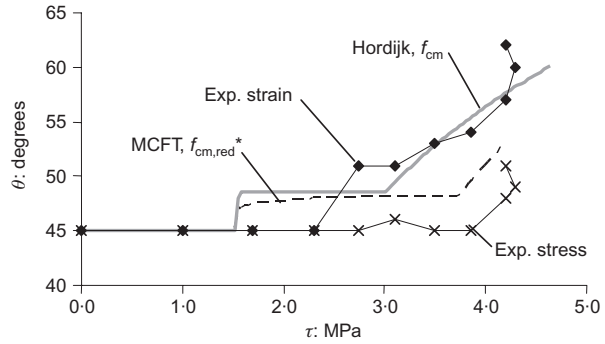

*Fig. 6. Comparison of results from test and analyses for PV20, applied shear stress against principal strain direction and principal stress direction. *The compressive strength is reduced owing to transverse tensile strains*

to calibrate the expression in the MCFT. This means that the concrete contribution to the shear capacity can be accounted for by modifying the constitutive relationship used for concrete in tension. However, caution is recommended in order not to overestimate the capacity. The modification needs to take the reinforcement (type, diameter and spacing) and possibly also the concrete composition (strength, grading curve and maximum aggregate size) into account. If no modification of the tension-softening curve is performed, the shear capacity will at least not be overestimated. Moreover, it was found that it is important to include the reduction of compression strength owing to transverse tensile strain. This influenced the behaviour and, if the failure mode was crushing of the concrete between the shear cracks, also the capacity; see Fig. 8.

When the cracking was initiated, the concrete shear strain started to increase just like the steel stress in the reinforcement. The steel stresses in the transverse reinforcement, which is in the direction with the lowest reinforcement amount, increased faster than the steel stresses in the longitudinal reinforcement, see Figs 7–9 and 11. In the tests and the analyses before cracking, the applied shear stress was equal to the principal tensile stress. Thus, the cracking was expected to start when the principal tensile stress reached the concrete tensile strength. This was also the case for the Toronto panel tests. However, for the Houston panel tests, cracking started for a much lower concrete principal tensile stress than could be expected from the mean compressive cylinder strength according to fib.[21] The analyses by Soltani *et al.*[20] show much better agreement, since here the concrete tensile strength was chosen as the cracking strength obtained in the tests. In Fig. 10(c), results from analyses using the cracking strength instead of the calculated tensile strength are shown. The tensile strength is an important material property for prediction of when the cracking starts, but it is less important for the capacity. The low cracking

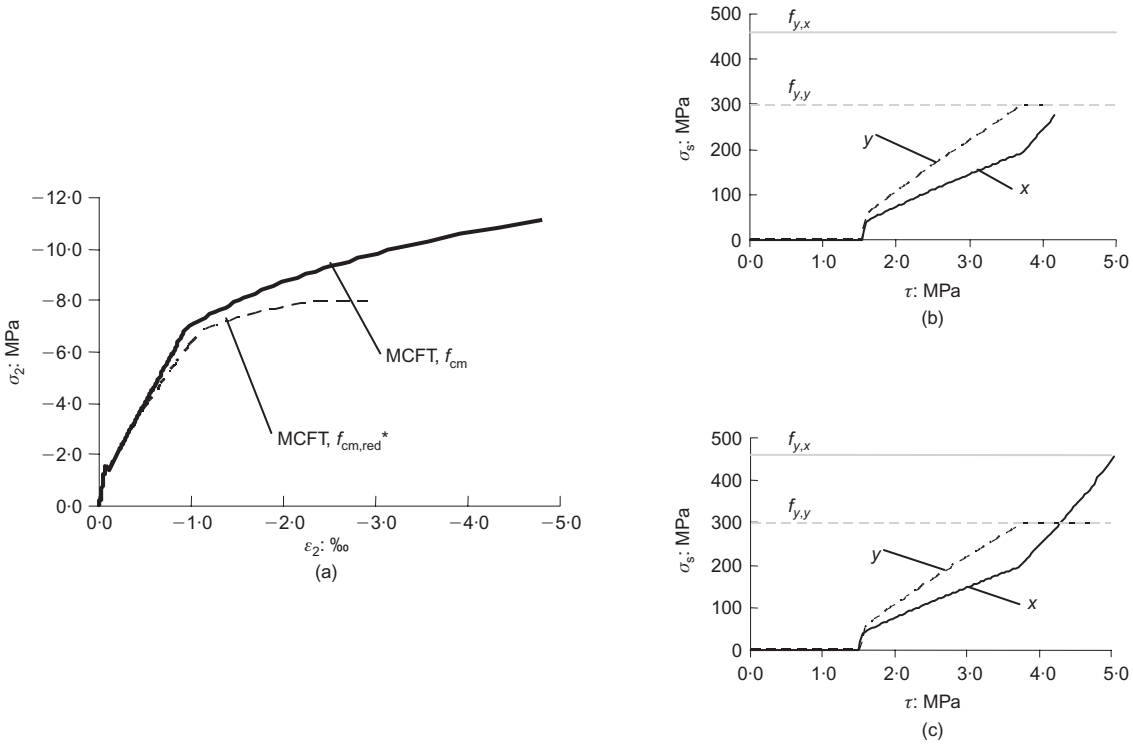

*Fig. 7. Results from FE analyses of PV20: (a) principal compression stress plotted against principal compression strain in one element; (b) and (c) applied shear stress plotted against steel stress in longitudinal (x-) and vertical (y-) reinforcement, MCFT (b) with and (c) without reduction of the concrete compressive strength owing to transverse strain respectively. *The compressive strength is reduced owing to transverse tensile strains*

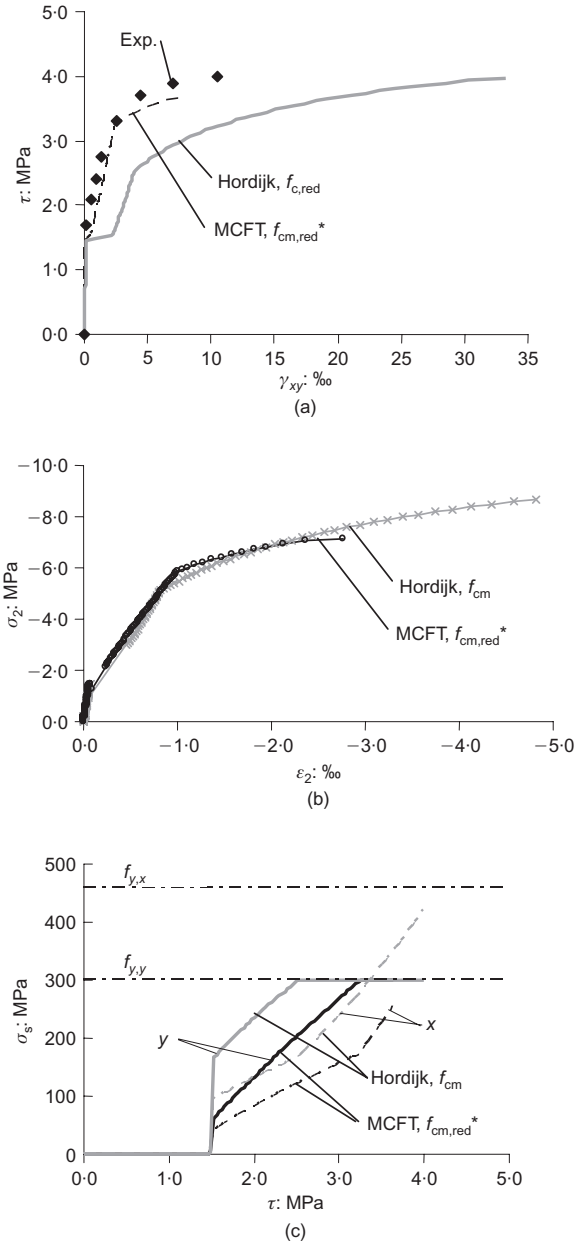

*Fig. 8. Results from FE analyses of PV19: (a) applied shear stress plotted against shear strain; (b) principal compressive stress plotted against principal compression strain; (c) applied shear stress plotted against steel stress in longitudinal (x-) and vertical (y-) reinforcement. *The compressive strength is reduced owing to transverse tensile strains*

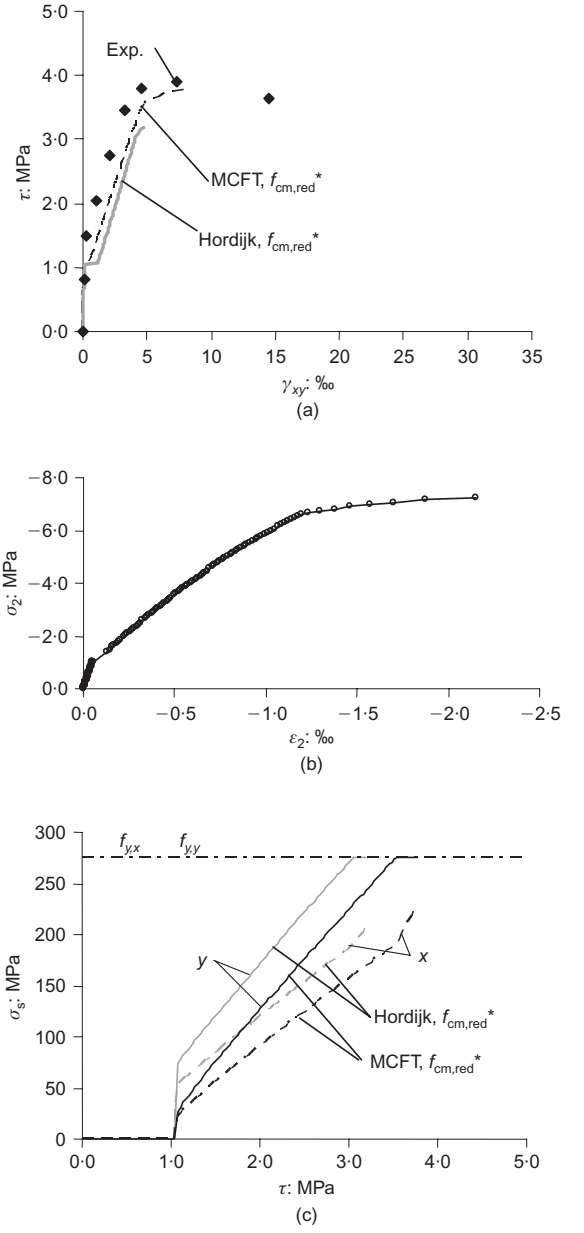

*Fig. 9. Results from FE analyses of PV10: (a) applied shear stress plotted against shear strain; (b) principal compression stress plotted against principal compression strain; (c) applied shear stress plotted against steel stress in longitudinal (x-) and vertical (y-) reinforcement. *The compressive strength is reduced owing to transverse tensile strains*

strengths reported from the tests may be attributed to initial internal stresses caused by shrinkage, or to local effects introduced by the shear keys.

The stiffness of the panel decreased and the direction of the principal stress and the principal strain changed when the panel started to crack. This became even more pronounced when the weakest reinforcement started to yield. From the Toronto panel test it was found that the principal strain direction deviated from the principal stress direction; see Fig. 6. The direction of the principal compressive stress in concrete was calculated from the applied loads and the measured steel strains. In a rotating crack model that was used here, the principal strain direction and the principal stress direction are the same by definition.

Finite-element analyses of a box-beam

FE model

To investigate the general applicability of the above-used analysis method for members with non-orthogonal

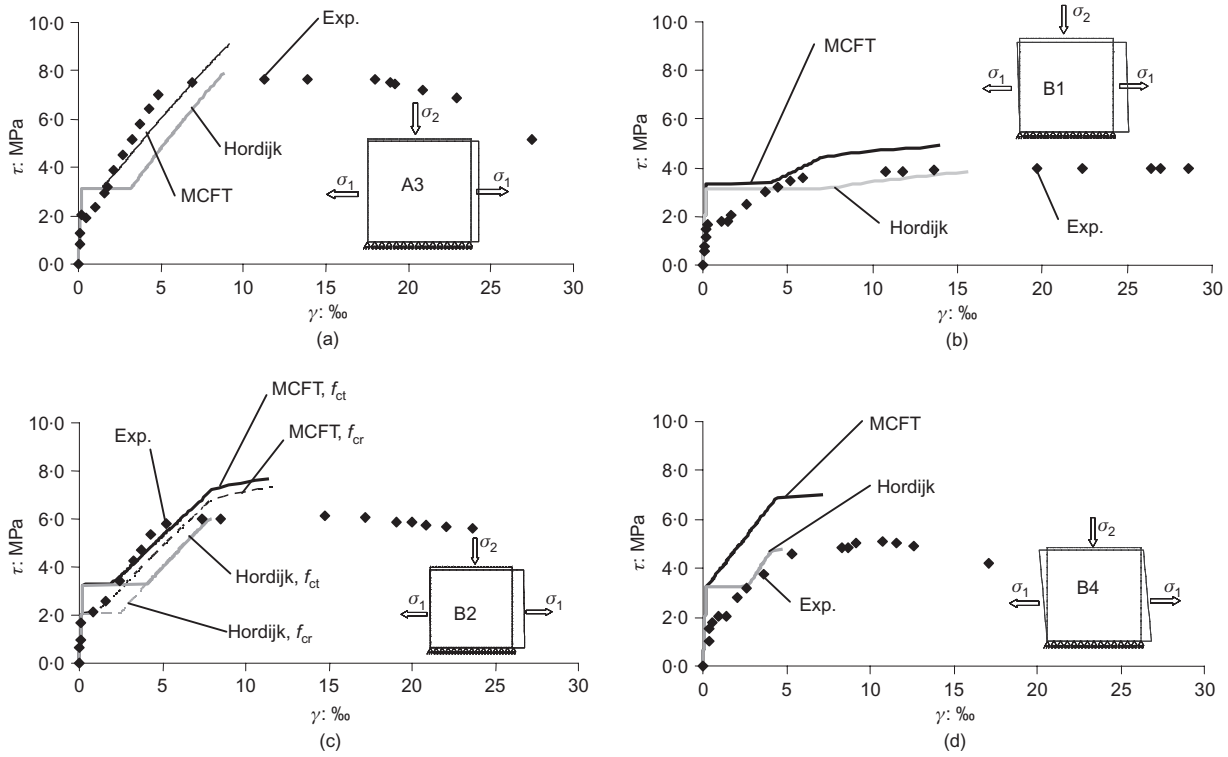

Fig. 10. Comparison of results from test and analysis of the Houston panels, applied shear stress plotted against shear strain: (a) A3; (b) B1; (c) B2; (d) B4. In all the analyses presented in this figure, the concrete compressive strength was reduced owing to transverse tensile strain

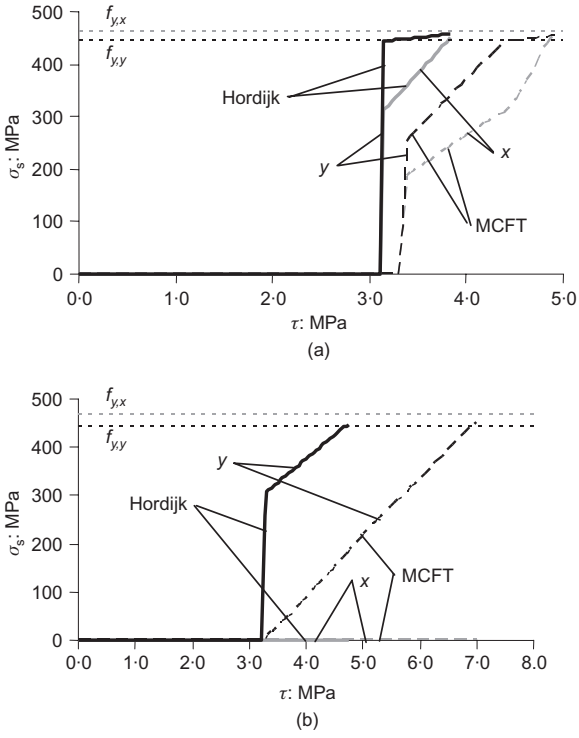

Fig. 11 Results from FE analyses: applied shear stress plotted against steel stress in longitudinal (x-) and vertical (y-) reinforcement for the Houston panels; (a) B1; (b) B4

reinforcement and subjected to mixed loading effects, a reinforced and prestressed box-beam, beam 5, tested by Karlsson and Elfgren,[30] was analysed. The box-beam was subjected to bending, shear and torsion and the final failure was attributed to large opening of a shear and torsion crack in the loaded web. Fig. 12 shows the principal arrangement, the dimensions, the support conditions and the FE model of the simulated box-beam.

Owing to symmetry only half of the beam was modelled, as shown in Fig. 12, using curved shell elements and material properties according to Tables 1 and 3. The box-beam was reinforced as shown in Fig. 12. The prestressing strands and the 8 mm longitudinal reinforcement bars were modelled as embedded bars, while the rest of the reinforcement was modelled as embedded grids; see TNO.[27]

In the test, the box-beam was supported on roller bearings with a load-distributing support plate. In the analyses, the nodes in the centre of the supports were fixed in the vertical direction. The nodes on each side of this node were forced to have the same vertical displacement but in opposite directions, thus enabling a rotation and simulating a free support with a distribution length equal to the support plate in the test.

Stiffeners at the support, and at the mid-span where the load was applied, were taken into account as fol-

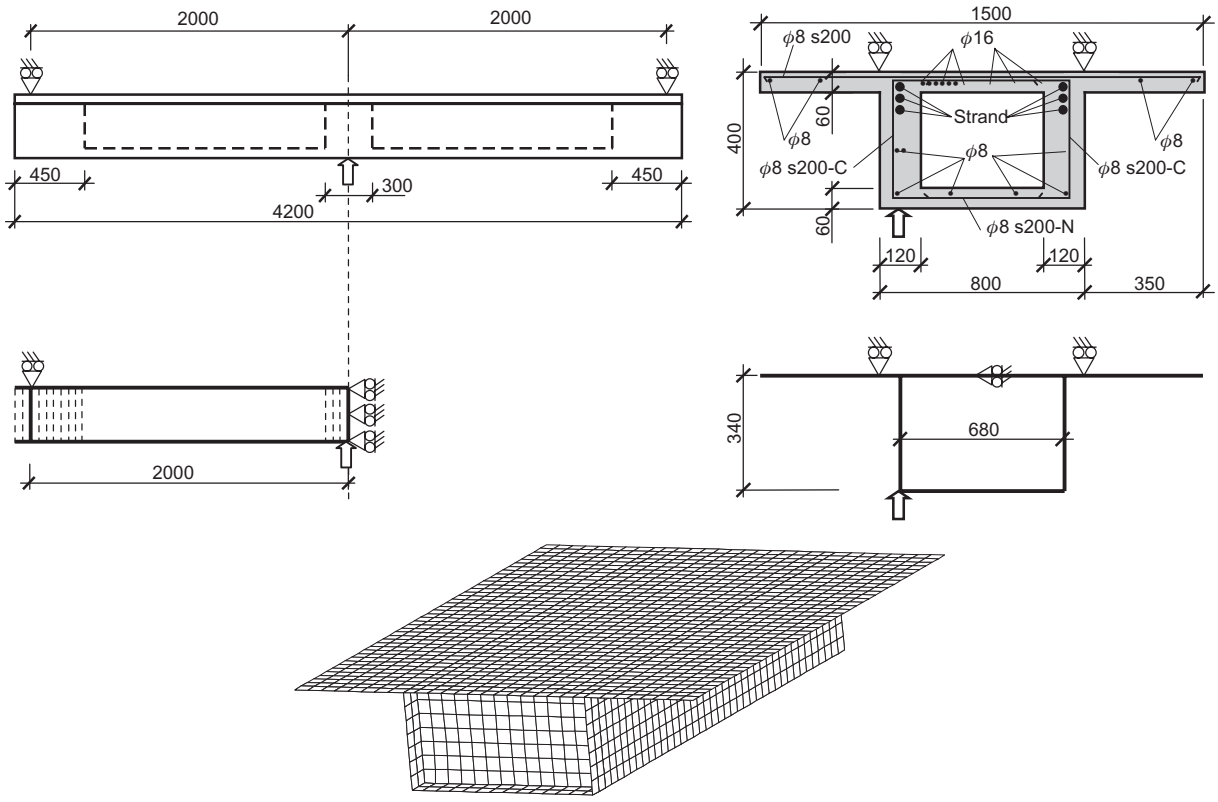

Fig. 12. Principal testing arrangement and FE model of the prestressed box-beam, beam 5

lows. All shell elements for the box wall and flanges in the area of the stiffeners were given a thickness twice the thickness of the elements outside these parts. The density of the concrete was also modified to maintain the correct self-weight of the box-beam. Furthermore, all nodes in each cross-section of the stiffened areas were tied to keep the cross-section plane.

In the box-beam test, the load was applied in steps of 40 kN up to 320 kN. Thereafter, the load was increased by controlling the mid-deflection in steps of 1–2·5 mm. In the analyses, the load was applied as a prescribed deformation of the loading node—that is, the bottom corner node in the symmetry section. The box-beam analysis had to be performed in two phases. In the first phase, the loading node was not supported; here the prestressing force (110 kN) was released and the self-weight was applied. In the second phase, the loading node was supported vertically at the location obtained in the first phase. Thereafter, the loading was applied by increasing the vertical displacement of the loading node.

In the analyses of the box-beam, concrete compressive failure was localised into one element. The size of this element does not correspond to the size of the specimens used to calibrate the compression relationship by Thorenfeldt as described in TNO.[27] Consequently, if the relationship by Thorenfeldt was used, the model could not predict the response. This disadvantage was overcome by modelling the concrete in compression with an elastic–ideal plastic relationship instead.

Results

The applied load plotted against vertical displacements from the analyses and the test are compared in Fig. 13. The results show, as expected, that if only the fracture energy of plain concrete was taken into account, the capacity was underestimated and the vertical deflections were overestimated. However, when the concrete contribution was modelled with the expression from MCFT, the capacity was still underestimated but the vertical deflections agreed well.

In the test, the first crack, going in the transverse direction across the top flange, occurred at a load of

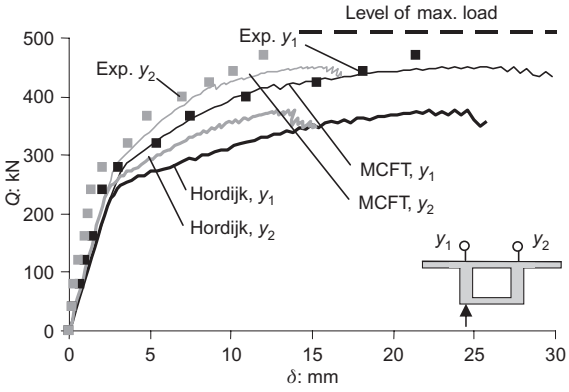

Fig. 13. Comparison of results from test and analyses of a prestressed concrete box-beam subjected to bending, shear and torsion; applied load plotted against mid-deflections

240 kN owing to bending. This crack propagated down in the most loaded web at a load of 280 kN. At a load of 320 kN the first shear and torsion crack appeared near the support. The final failure, at a load of 510 kN, was attributable to large opening of a shear and torsion crack in the loaded web. The angle of the cracks in the most loaded web varied between 45 and 60°, while they remained vertical in the other web. The crack propagation and the crack pattern from both analyses agreed well with those observed in the test.

In Fig. 14, the load plotted against steel strains for one strand and one stirrup, from the test and the analyses, are compared. The steel strain increased first when the box-beam started to crack. In the analysis with the tension softening modelled according to MCFT, the steel strain increase was slower, which corresponds better with the steel strains measured in the test.

FE analysis of a bending beam

FE model

To investigate the general applicability of the above analysis method for members that do not fail due to shear cracks, a four-point bending beam, NSC3, tested by Magnusson,[31] was simulated. The bending beam was subjected to bending and shear, and failed in bending owing to yielding of the longitudinal reinforcement and crushing of the concrete in the compressive zone in the mid-span part of the beam. Fig. 15 shows the dimensions and support conditions of the simulated bending beam.

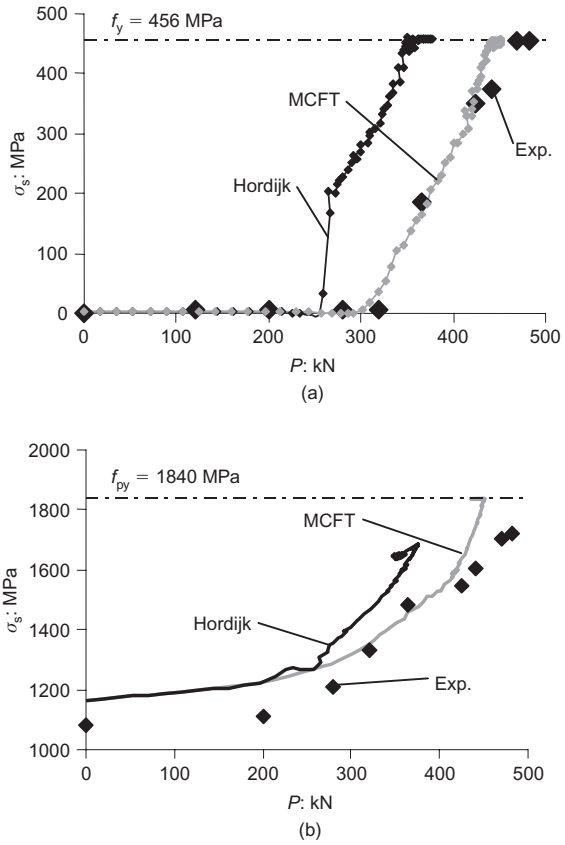

Fig. 14. Comparison of results from test and analyses of a prestressed concrete box-beam subjected to bending, shear and torsion; applied load plotted against steel stresses in loaded web; (a) stirrup 400 mm from load, (b) top prestressing strand

Owing to symmetry, only half of the beam was modelled, as shown in Fig. 16, using curved shell elements and material properties according to Tables 1 and 3. The beam was reinforced as shown in Fig. 15. The longitudinal reinforcement and the stirrups between the support and the load were modelled as embedded bars, while the stirrups in the middle part of the beam were modelled as an embedded grid, see TNO.[27] The supports were modelled in the same way as for the box-beam.

The loading of the bending beam was controlled by displacement both in the test and in the analysis. In the analysis, the loading was applied by increasing the vertical displacement of the loading node in steps of 0·1 mm. In the test, the load was distributed by a loading plate. In the analyses, this was simulated in the same way as for the box-beam.

Also in the bending beam analyses, compressive failure was localised in one element. Therefore, the concrete in compression was modelled with an elastic–ideal plastic relationship instead of the curve by Thorenfeldt. The element in which high compressive strains were localised was also subjected to large lateral strains owing to a flexural shear crack. This flexural shear crack was also observed in the test, but there it did not go into the compressive zone. Consequently, reducing the compressive strength owing to lateral strains resulted in an unreasonable response. Therefore, for these analyses, the compressive strength was not reduced.

Results

The relations between the applied load and the vertical displacements from the analyses and the test are compared in Fig. 17. With only the fracture energy of plain concrete taken into account, the capacity is very well estimated and the behaviour is just a little bit too stiff. However, when the tension softening was modelled according to MCFT, the behaviour was too stiff and the capacity was overestimated. The reason was that, in this case, the cracked concrete transferred tensile stresses over the bending cracks even after the longitudinal reinforcement had started to yield.

The conclusion is that if a tension-softening curve including the concrete contribution to shear capacity is used, it needs to be modified, so that no tensile stresses are transferred when the reinforcement yields. Otherwise the capacity will be overestimated for the parts of a member which are subjected to tension or bending. Furthermore, even if the curve is modified with respect to reinforcement yielding, it will lead to a too stiff response after cracking and before yielding.

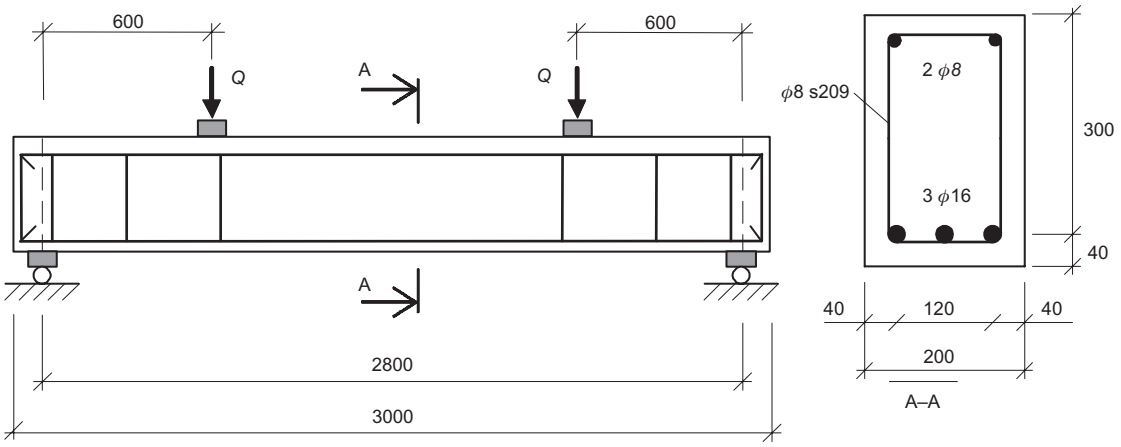

Fig. 15. Principal testing arrangement of the four-point bending beam, NSC3

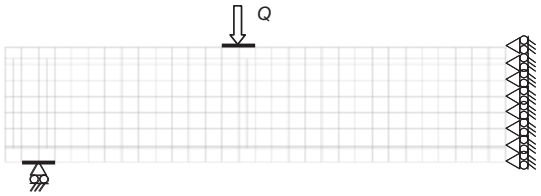

Fig. 16. FE model of the four-point bending beam, NSC3

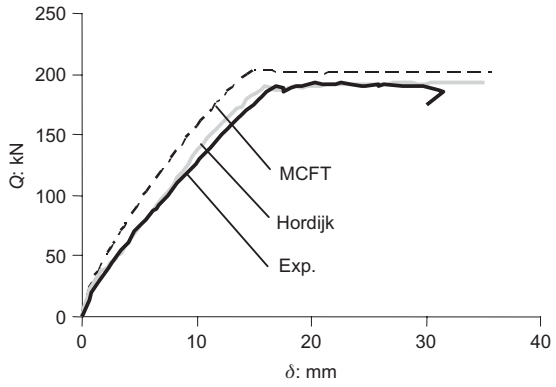

Fig. 17. Comparison of results from test and analyses of a reinforced concrete beam subjected to bending; applied load plotted against mid-deflection

Conclusions

It is well known that the shear capacity determined by sliding along inclined cracks is larger than can be explained by the reinforcement contribution determined from a truss model. This increase in shear stiffness and shear capacity is attributable to tension stiffening, dowel action and friction owing to aggregate interlock, and is also known as the concrete contribution. If the shear response is simulated with non-linear FEM, with a model not specially designed for shear analysis, the concrete contribution has in the past been accounted for by modifying the constitutive relationships used, for example the tension-softening curve describing the concrete behaviour in tension.

In the present study, the commercial FE program DIANA was used to simulate the non-linear response in experiments of several shear panels, a prestressed box-beam subjected to shear, torsion and bending, and an RC beam subjected to bending and shear. It was shown that four-node curved shell elements with embedded reinforcement could describe the non-linear shear response for panels loaded in shear and also for prestressed members loaded in bending, shear and torsion. Results from the analyses showed that, if only the fracture energy of plain concrete was taken into account, the capacity was well predicted and the average strains—that is, the crack widths—were well reflected for the bending beam and one shear panel. For all other specimens studied, the shear capacity was underestimated and the average strains were overestimated. On the other hand, if the concrete contribution to the shear capacity was considered with the expression from MCFT, the capacity was in many cases overestimated and the average strains underestimated, except for the Toronto panels. It should be mentioned that results from the Toronto panel tests have been included in the test results used to calibrate the expression in the MCFT. This means that the concrete contribution to the shear capacity can be accounted for by modifying the constitutive relationship used for concrete in tension. However, caution is recommended in order not to overestimate the capacity. If no modification of the tension-softening curve is undertaken, the shear capacity will at least not be overestimated.

The analysis results from the shear panels showed that it was important to include the reduction of the compression strength due to transverse tensile strain for the behaviour, and also for the capacity if the failure mode was crushing of the concrete between the shear cracks. Furthermore, it was shown that the stiffness of the panel decreased and the direction of the principal stress and the principal strain changed when the panel started to crack. This became even more pronounced when the weakest reinforcement started to yield.

The analyses of the box-beam showed that if only

the fracture energy of plain concrete was taken into account, the capacity was underestimated and the vertical deflections were overestimated. However, when the concrete contribution was considered with the expression from MCFT, the capacity was still underestimated but the vertical deflections agreed well.

By simulating a test of a four-point bending beam that failed in bending, it was found that when the concrete contribution was considered according to MCFT, the behaviour was too stiff and the capacity was overestimated. Hence, the cracked concrete transferred tensile stresses even when the longitudinal reinforcement yielded. In the analyses of the box-beam and the bending beam, concrete compressive failure was localised into one element, whose size did not correspond to the size of the specimens used to calibrate the compression relationship used—that is, the non-linear tension-softening curve by Thorenfeldt. Hence, if the relationship by Thorenfeldt was used, the model could not predict the response. This disadvantage was overcome by modelling the concrete in compression with an elastic–ideal plastic relationship instead. In the bending beam analyses, the element in which high compressive strains were localised was also subjected to large lateral strains owing to a flexural shear crack. This flexural shear crack was also observed in the test, but there it did not go into the compressive zone. Consequently, reducing the compressive strength owing to lateral strains resulted in an unreasonable response. Therefore, for these analyses, the compressive strength was not reduced.

In summary, the present study implies that an analysis of a concrete member subjected to shear, torsion and bending will be on the safe side when evaluating the load-carrying capacity or crack widths, if only the fracture energy is used to define the unloading branch of the concrete in tension.

Acknowledgements

The research was financed by the Swedish Road Administration (Vägverket), the Swedish Rail Administration (Banverket) and Chalmers University of Technology.

References

1. Vecchio F. J. and Collins M. P. The modified compression-field theory for reinforced concrete elements subjected to shear. *Journal of the American Concrete Institute*, 1986, **83**, No. 2, 219–231.
2. Comité Européen de Normalisation. *CEN/TC250/SC2. Eurocode 2: Design of concrete structures—Part 1: General rules and rules for buildings, prEN 1992-1-1*. CEN Brussels, 2004.
3. Gabrielsson H. *Ductility of High Performance Concrete Structures*. PhD thesis, Luleå University of Technology, Luleå, Sweden, 1999.
4. Pajari M. *Shear–torsion Interaction Tests on Single Hollow Core Slabs*. Technical Research Centre of Finland, Espoo, 2004, VTT Research Notes 2275.
5. Broo H., Lundgren K. and Engström B. Shear and torsion interaction in prestressed hollow core units. *Magazine of Concrete Research*, 2005, **57**, No. 9, 521–533.
6. Broo H. *Shear and Torsion Interaction in Prestressed Hollow Core Slabs*. Thesis for the degree of Licentiate of Engineering, Chalmers University of Technology, Göteborg, 2005.
7. Ayoub A. and Filippou F. C. Nonlinear finite-element analysis of RC shear panels and walls. *Journal of Structural Engineering*, 1998, **124**, No. 3, 298–308.
8. Yamamoto T. and Vecchio F. J. Analysis of reinforced concrete shells for transverse shear and torsion. *ACI Structural Journal*, 2001, **98**, No. 2, 191–199.
9. Vecchio F. J. and Shim W. Experimental and analytical reexamination of classical beam tests. *Journal of Structural Engineering*, 2004, **130**, No. 3, 460–469.
10. Kettil P., Ródenas J. J., Aguilera Torres C. and Wiberg N.-E. Strength and deformation of arbitrary beam sections using adaptive FEM. *Computers and Structures*, 2007, **85**, No. 1, 15–29.
11. Plos M. *Structural Assessment of the Källösund Bridge Using Finite Element Analysis: Evaluation of the Load Carrying Capacity for ULS*. Concrete Structures, Department of Structural and Mechanical Engineering, Chalmers University of Technology, Göteborg, Report 04:1, March 2004.
12. Hegger J., Sherif A. and Görtz S. Investigation of pre- and postcracking shear behavior of prestressed concrete beams using innovative measuring techniques. *ACI Structural Journal*, 2004, **101**, No. 2, 183–192.
13. Vecchio F. J. and Collins M. P. Compression response of cracked reinforced concrete. *Journal of Structural Engineering*, 1993, **119**, No. 12, 3590–3610.
14. Belarbi A. and Hsu T. T. C. Constitutive laws of softened concrete in biaxial tension–compression. *ACI Structural Journal*, 1995, **92**, No. 5, 562–573.
15. ASCE–ACI Committee 445 on Shear and Torsion. Recent approaches to shear design of structural concrete. *Journal of Structural Engineering*, 1998, **124**, No. 12, 1375–1417.
16. Pang X.-B. D. and Hsu T. T. C. Behavior of reinforced concrete membrane elements in shear. *ACI Structural Journal*, 1995, **92**, No. 6, 665–679.
17. Prisco M. D. and Gambarova P. G. Comprehensive model for study of shear in thin-webbed RC and PC beams. *Journal of Structural Engineering*, 1995, **121**, No. 12, 1822–1831.
18. Walraven J. and Stroband J. The behaviour of cracks in plain and reinforced concrete subjected to shear. *Proceedings of the 5th International Symposium on Utilization of High Strength/High Performance Concrete, Sandefjord, Norway*, 1999, pp. 701–708.
19. Zararis P. D. Concrete shear failure in reinforced-concrete elements. *Journal of Structural Engineering*, 1996, **122**, No. 9, 1006–1015.
20. Soltani M., An X. and Maekawa K. Computational model for post cracking analysis of RC membrane elements based on local stress–strain characteristics. *Engineering Structures*, 2003, **25**, No. 8, 993–1007.
21. International Federation for Structural Concrete (FIB). *Structural Concrete. Textbook on Behaviour, Design and Performance Updated Knowledge of the CEB/FIP Model Code 1990*, Vol. 2. fib, Lausanne, Switzerland, 1999.
22. Vecchio F. J. Disturbed stress field model for reinforced concrete: formulation. *Journal of Structural Engineering*, 2000, **126**, No. 9, 1070–1077.
23. Kaufmann W. and Marti P. Structural concrete: cracked membrane model. *Journal of Structural Engineering*, 1998, **124**, No. 12, 1467–1475.
24. Pang X.-B. D. and Hsu T. T. C. Fixed angle softened truss model for reinforced concrete. *ACI Structural Journal*, 1996, **93**, No. 2, 197–207.

25. Hsu T. T. C. and Zhu R. R. H. Softened membrane model for reinforced concrete elements in shear. *ACI Structural Journal*, 2002, **99**, No. 4, 460–469.
26. Lackner R. and Mang H. A. Scale transition in steel–concrete interaction. I: Model. *Journal of Engineering Mechanics*, 2003, **129**, No. 4, 393–402.
27. TNO. *DIANA Finite Element Analysis, User's Manual Release 8·1*. TNO Building and Construction Research, Delft, the Netherlands, 2002.
28. Collins M. P. and Mitchell D. *Prestressed Concrete Structures*. Prentice Hall, Englewood Cliffs, New Jersey, 1991.
29. Bentz E. C. Explaining the riddle of tension stiffening models for shear panel experiments. *Journal of Structural Engineering*, 2005, **131**, No. 9, 1422–1425.
30. Karlsson I. and Elfgren L. *Prestressed Box-beams Loaded in Combined Torsion, Bending and Shear*. Chalmers University of Technology, Göteborg, Sweden, Report 76:10, September 1976 (in Swedish).
31. Magnusson J. *Anchorage of Deformed Bars over End-supports in High-strength and Normal-strength Concrete Beams: An Experimental Study*. Division of Concrete Structures, Chalmers University of Technology, Göteborg, Sweden, Report 98:7, August 1998.
32. Pang X.-B. D. *Constitutive Laws of Reinforced Concrete in Shear*. Dissertation, Faculty of the Department of Civil and Environmental Engineering, University of Houston, Houston, TX, USA, 1991.
33. Vecchio F. J., Lai D., Shim W. and Ng J. Disturbed stress field model for reinforced concrete: validation. *Journal of Structural Engineering*, 2001, **127**, No. 4, 350–358.
34. Vecchio F. J. and Lai D. Crack shear-slip in reinforced concrete elements. *Journal of Advanced Concrete Technology*, 2004, **2**, No. 3, 289–300.

Discussion contributions on this paper should reach the editor by 1 May 2008

Paper V

Non-linear finite element analysis of the shear response in prestressed concrete bridges.

Broo H., Plos M., Lundgren K. and Engström B.

Submitted to *Magazine of Concrete Research*, February, 2008.

Non-linear finite element analysis of the shear response in prestressed concrete bridges

Helén Broo	Mario Plos	Karin Lundgren	Björn Engström
Research Assistant	Assistant Professor	Associate Professor	Professor
helen.broo@chalmers.se	mario.plos@chalmers.se	karin.lundgren@chalmers.se	bjorn.engstrom@chalmers.se

Department of Civil and Environmental Engineering
Structural Engineering, Concrete Structures
Chalmers University of Technology
SE-412 96 Göteborg, Sweden
Telephone: +46 31 772 00 00
Fax: +46 31 772 22 60

Abstract

For structural assessment of concrete bridges the non-linear finite element method has become an important and increasingly used tool. The method has shown a great potential to reveal higher load-carrying capacity compared to conventional assessment methods. However, the modelling method used for reinforced and prestressed concrete members subjected to shear and torsion has been questioned.

The aim of this study is to present an analysis method for evaluation of the load-carrying capacity of prestressed concrete bridges, when failure due to shear and torsion is the main problem. The modelling method used was previously worked out and verified for shear-type cracking and shear failure. Here, shell elements with embedded reinforcement were used together with non-linear material models, taking into account the fracture energy of cracking plain concrete and the reduction of the concrete compression strength due to lateral tensile strain. Analyses with the method proposed have shown to predict the shear response and the shear capacity on the safe side.

In the work presented here, the load-carrying capacity of a box-girder bridge was evaluated as a case study. The whole bridge was modelled, but only the part that was most critical to shear and torsion was modelled according to the method previously worked out and was combined with beam elements for the rest of the bridge. The case study showed a substantially higher load-carrying capacity for the bridge compared to assessment with conventional methods. In the evaluation, several possible safety formats was used in combination with the non-linear finite element method. It was shown that the format using partial safety factors gave unrealistic conservative results; it is more correct to use the semi-probabilistic formats for non-linear FE analysis.

Introduction

Large investments have been made in infrastructure, and the present stock of bridges represents a huge asset for society. Therefore, maintenance and upgrading of bridges are very important. Since most concrete bridges were designed and constructed, the traffic loads have increased and many bridges are subjected to higher loads than originally designed for. In the future, it is likely that the traffic load demands will further increase. The bridges' condition has also deteriorated due to the environment or accidents. Hence, it is important to be able to upgrade the existing bridges and to ensure that they perform properly under the increased loads with respect to their actual condition. Today, many bridges are strengthened or replaced because their reliability cannot be guaranteed based on the structural assessments made. Large savings, both economic and environmental, would be possible if more correct and reliable assessments were made.

The principal aims of design and assessment of concrete bridges are the same: to demonstrate that the bridge has the required load-carrying capacity and performance under service conditions. However, in design, there are large uncertainties in the overall behaviour, the material properties and the loads, and a conservative design can be made without great cost. In assessment of existing bridges, some of the uncertainties can be reduced by measurements, testing and monitoring. A too conservative assessment may give a misapprehension that the requirements are unfulfilled, with unnecessary strengthening or demolition as a consequence. Therefore, it is important to predict the load-carrying capacity as appropriately as possible by using more enhanced assessment methods. There are several advanced methods suitable for bridge design or assessment; see for example Mokhtar and Ghail[1], Shushkewich[2], Picard and Massicotte[3], Shushkewich[4] and Sustainable Bridges[5].

Advanced simulations by means of non-linear finite element (FE) analysis of concrete structures are now well established for research within structural engineering. It is also increasingly used in engineering practice for assessment of existing concrete bridges. An overview of structural assessment of bridges with the finite element method (FEM) is presented in Sustainable Bridges[5]. The number of references within the area is rather limited: Huria *et al.*[6], Chowdhury and Ray[7], Shahrooz *et al.*[8], Ho and Shahrooz[9] and Song *et al.*[10]. The assessments made by Plos[11], Plos and Gylltoft[12], and Plos and Gylltoft[13] have shown a great potential to reveal higher load-carrying capacities compared to conventional assessment methods. It is also stated in Sustainable Bridges[5] that non-linear analysis is the analysis method with the highest potential for discovering any additional sources for load-carrying capacity of concrete bridges. Non-linear analysis gives the possibility to resemble the redistribution of sectional forces in statically undetermined structures. Also the redistribution of internal stresses can be simulated by including the fracture energy associated with cracking concrete. Both govern the higher load-carrying capacity shown. The structural effects utilized to achieve a higher capacity for previously assessed bridges have mainly been associated with bending moment and normal forces.

Plos and Gylltoft[13] have shown a higher load-carrying capacity also for a bridge where shear and torsion governed the failure. However, the modelling method used in these FE analyses was not verified and the results were brought into question. Non-

linear FE analyses of concrete members with vertical shear reinforcement subjected to shear have been reported by several researchers, for example Ayoub and Filippou[14], Yamamoto and Vecchio[15], Vecchio and Shim[16] and Kettil *et al.*[17]. These analyses were made to verify established material models or developed FE programs. A commercial FE program, usable by engineers in daily practice, has not been adopted. Therefore, in a previous study by the authors, tests of shear panels and beams were analysed with such a non-linear FE program to examine the reliability of the methods and to develop a verified methodology that gives a lower bound value of the load-carrying capacity in cases of shear and torsion; see Broo *et al.*[18]. To further evaluate the methodology proposed, and to verify its applicability and reliability for assessment of bridges, the load-carrying capacity of a prestressed concrete box girder bridge was evaluated in a case study and is presented in this paper.

The aim of this study is to show how the modelling method, worked out in Broo *et al.*[18], can be used for assessment of a prestressed concrete bridge subjected to shear and torsion. The objective was not only to evaluate the load-carrying capacity, but also to follow the response and to estimate the failure mode. Engineers using commercial non-linear FE programs, not particularly designed for shear analysis, should be able to use the method in their daily practice. The Källösund Bridge, used for the case study, has previously been evaluated by Plos and Gylltoft[13]. The evaluation presented here was, compared to the previous one, improved in several respects. For instance, the modelling method used has been verified, the final loading was made in a deformation-controlled process, and long-term effects such as creep were taken into account.

A general problem when using non-linear FE analysis for structural assessment is how to determine the reliability of the load-carrying capacity. Possible alternative safety formats suitable for non-linear analysis are presented in EN1992-2[19], in Sustainable Bridges[5] and by Cervenka *et al.*[20]. In this study semi-probabilistic formats according to Sustainable Bridges[5] were used and compared with deterministic formats.

Structural assessment of the shear response in concrete bridges

Shear response and shear failure

Both shear forces and torsional moments cause shear stresses that can result in cracks in a concrete member. Cracks due to shear stresses are usually inclined relative to the direction of the reinforcement. To satisfy the new equilibrium after shear cracking, longitudinal reinforcement and transverse reinforcement or friction in the crack are required. The visual shear cracks are preceded by the formation of micro-cracks. The micro-cracking and the following crack formation change the stiffness relations in the member, and a redistribution of stresses can occur resulting in strut inclinations smaller than 45°; see Hegger *et al.*[21]. Due to the rotation of the struts, more transverse reinforcement can be activated. This behaviour becomes more pronounced when the transverse reinforcement starts to yield. The rotation of the compressive struts can continue until failure. Possible failure modes in shear are (1) sliding along a shear crack and (2) crushing of the concrete between two shear cracks. In the case of

transverse reinforcement, shear sliding cannot take place before the transverse reinforcement yields. An important objective of shear and torsion design, in addition to providing the required load-carrying capacity, is to avoid a sudden failure of the structural member. It is also necessary to predict the behaviour in the serviceability limit state (SLS), i.e. deformations and crack widths under service load conditions.

Structural assessment

The objective of a structural assessment of an existing bridge is to assess whether the requirements of serviceability and load-carrying capacity are fulfilled with sufficient reliability. Assessment of a bridge usually means to determine, by calculations, a theoretical value of the axle load *A* and bogie load *B* for a type vehicle – see e.g. Vägverket[22] – that the bridge can resist. The assessment can also be used to determine regions with insufficient load-carrying capacities, as a basis for design of strengthening.

Sustainable Bridges[5] presents an assessment strategy for enhanced evaluation of load-carrying capacity of existing bridges. The assessment of an existing bridge is preferably made by using analysis methods on different levels with increasing accuracy and complexity. In an initial assessment, a linear analysis of the structural system is usually made to determine cross-sectional forces and moments. In this analysis, all possible load combinations, type vehicles and traffic load positions are evaluated. For each cross-section the maximum cross-sectional forces are presented and the resistance of the cross-section is calculated with conventional design methods.

Today, design and assessment for shear and torsion are still commonly made by using simplified analytical or empirical design methods. For members with shear reinforcement these are based on the truss model; see Figure 1. It is well known that, for shear-reinforced concrete members, the shear capacity is larger than what can be explained by the reinforcement contribution determined from a truss model. The truss model can be combined with a *concrete contribution*, compensating for the difference in shear capacity found in tests and theoretically calculated capacities. The *concrete contribution* is empirical, but accounts for the shear transferred in the compression zone and across the crack. The influencing parameters are the softening of cracking concrete, the bond between reinforcement and concrete, the aggregate interlocking in the crack, and the dowel action provided by the reinforcement; see Figure 1. The methods based on the truss model are only valid in the ultimate limit state (ULS), i.e. they can only predict the ultimate shear capacity.

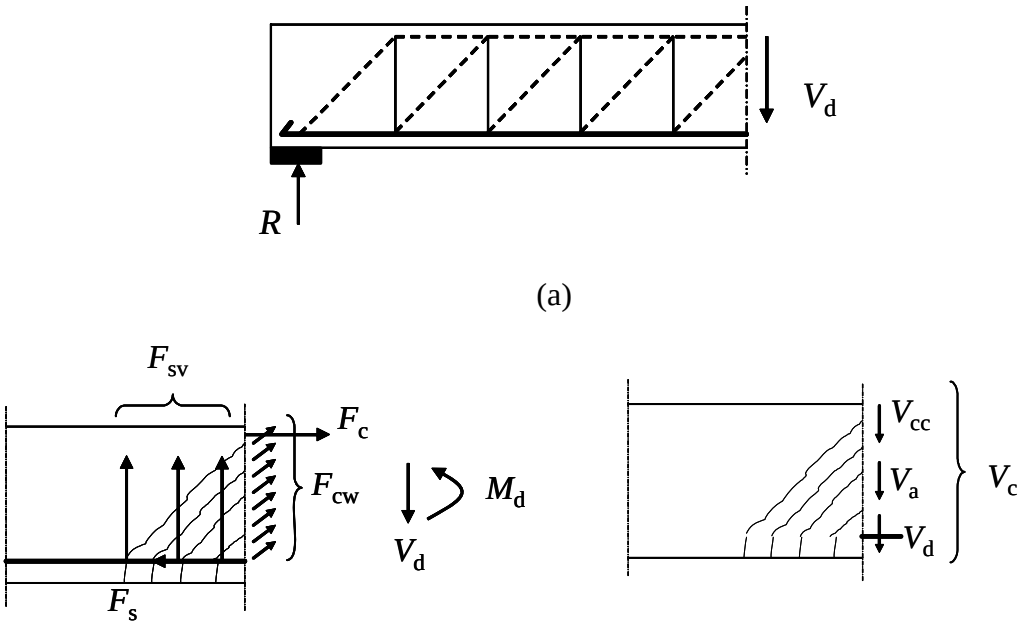

Figure 1 *Models describing the transition of shear force after cracking. (a) and (b) The truss model. (c) The concrete contribution term V_c is empirical but accounts for the shear transferred in the compression zone and in the crack: the softening of cracking concrete, the tension stiffening, the aggregate interlocking and dowel action.*

To predict also the shear response, more enhanced methods are needed, such as the modified compression field theory, MCFT, of Vecchio and Collins[23], or the softened-truss models of Pang and Hsu[24,25]. These methods are based on a smeared approach, i.e. the influences of cracks are smeared over a region and the calculations are made with average stresses and average strains. Stress equilibrium, strain compatibility and constitutive laws are used to predict the shear force for chosen strains. The constitutive laws needed for the concrete response are established from shear panel tests. These constitutive relationships can be seen as a way of including the *concrete contribution*. However, both the truss models and these more enhanced methods use sectional forces determined from an independent overall structural analysis.

If needed, the assessment can be refined with more accurate analysis methods, improved input data and more appropriate safety formats. In Plos *et al.*[26] the use of probabilistic analysis, FE analysis, alternative design methods and combinations of these were presented for two prestressed box-girder bridges, including the bridge used for the case study presented here.

Safety format

The design resistance R_d, i.e. the load-carrying capacity with sufficient reliability, can be estimated according to various safety formats; see Sustainable Bridges[5] and Cervenka *et al.*[20]. The safety format can be fully probabilistic, semi-probabilistic or

deterministic. Some of the formats presented in Sustainable Bridges[5] were used and compared in this study and are therefore briefly presented below.

A commonly used method to estimate the design resistance is to use safety formats presented in codes, such as the partial safety factor method. These formats are generally developed for section analysis with the sectional forces often determined through linear analysis. However, reducing the material strength properties with partial safety factors will, in a non-linear analysis, influence not only the resistance of the structure but also the distribution of sectional forces and internal stresses. The design resistance is determined by an analysis using material properties calculated with partial safety factors, for all input material parameters.

$$R_d = r(f_d, ...) \tag{1}$$

This format gives a deterministic value of the load-carrying capacity. As previously stated, this is a conceptually doubtful method in combination with non-linear analysis. This method is likely to give conservative results, but it may also be an unsafe method, at least in some theoretical cases. Furthermore, it may cause deviations in structural response – e.g. the failure mode may change compared to if more realistic material properties were used.

The most appropriate way to determine the design resistance for an existing bridge would be to perform a fully probabilistic non-linear analysis. This requires several deterministic non-linear analyses for random sets of input variables such as material properties, geometry, support conditions and loading. A less demanding way is to use a semi-probabilistic format. In Sustainable Bridges[5] and Cervenka *et al.*[20] a format based on semi-probabilistic estimation of the variation coefficient of resistance, the ECOV method, is proposed. For this method two non-linear analyses are needed, one with mean and one with characteristic material properties, f_m and f_k respectively. The load-carrying capacities determined with the analyses are used to evaluate a global safety factor, γ_0, according to Equation 2 and 3.

$$\gamma_0 = \exp(\alpha_R \cdot \beta \cdot V_R) \approx \exp(0{,}8 \cdot 4{,}7 \cdot V_R) \approx \exp(3{,}76 \cdot V_R) \tag{2}$$

Here, α is the sensitivity factor for resistance reliability and β is the reliability index. Typical values are α = 0.8 and β = 4.7 according to Cervenka *et al.*[20].

$$V_R = \frac{1}{1{,}65} \ln\left(\frac{R_m}{R_k}\right) \tag{3}$$

where

$$R_m = r(f_m, ...) \tag{4}$$

$$R_k = r(f_k, ...) \tag{5}$$

The design resistance, R_d, is then estimated by dividing the resistance evaluated with mean material properties, R_m, by the global safety factor.

$$R_d = \frac{R_m}{\gamma_0} \tag{6}$$

Another semi-probabilistic format is presented in EN1992-2[19]. Here, fictive material properties (see Equations 7-10) are used in one analysis to determine the load-carrying capacity, which then is divided by a global safety factor, γ_0 = 1,27, to estimate the design resistance.

$$R_d = r(\tilde{f}_{ym}, \tilde{f}_{cm}, ...)/\gamma_0 \tag{7}$$

where

$$\tilde{f}_{ym} = 1{,}1 f_{yk} \text{ , for reinforcing steel yield strength,} \tag{8}$$

$$\tilde{f}_{pm} = 1{,}1 f_{pk} \text{ , for prestressing steel yield strength,} \tag{9}$$

$$\tilde{f}_{cm} = 1{,}1 \cdot \frac{\gamma_s}{\gamma_c} f_{ck} = 0{,}843 \cdot f_{ck} \text{ , for concrete compressive strength.} \tag{10}$$

This method is limited to cases where the tensile strength of concrete is not a major parameter influencing the limit state; see Sustainable Bridges[5].

A structure such as a bridge is subjected to several actions, permanent and variable loads, and creep and temperature deviations. In a non-linear analysis the loads are applied sequentially, in a way similar to a load test. For example, permanent loads and other variable loads than the point loads of traffic are applied before the point loads are increased successively up to failure. Consequently, the axle or bogie load resistance is determined for the bridge subjected to the other loads acting on it, i.e. the effects of these loads are included in the resistance calculated. Also the actions on a bridge have variations, but this has not been taken into account in the analyses performed in this study.

The modelling method for simulating shear response and shear failure

To include effects of force redistributions, the construction history, and the loading sequence, the whole bridge needs to be modelled. Beam elements are often suitable for modelling of a complete concrete bridge structure. However, beam elements are not capable of describing shear cracking and shear failure or a reduced torsional stiffness due to cracking. When modelling the shear response with non-linear FEM, it is important to understand, as far as possible, the non-linear shear response of reinforced concrete. This is in order to choose the proper level of detailing, element types, material models etc. to use in the model. To be able to simulate the shear

response and shear failure, continuum elements, Broo *et al.*[27], or shell elements, Broo *et al.*[18], are needed. At the same time it is important to simplify the model to avoid too time-consuming analyses. Continuum or shell elements for critical parts of the structure can be combined with beam elements for parts that are not critical; see Plos and Gylltoft[13] and Lundgren *et al.*[28]. However, the modelling of the critical part also needs to be simplified, i.e. coarse mesh and full interaction between reinforcement and concrete need to be used. These simplifications will govern the choice of material models and material properties needed.

In Broo *et al.*[18], a modelling method was worked out to analyse the shear response and shear failure of reinforced and prestressed concrete members. The method was verified for members subjected to shear, torsion, bending, and combinations of these load effects. The FE program Diana, TNO[29], was used to analyse several shear panel tests, orthogonally reinforced and loaded in pure shear, and reinforced and prestressed beam tests loaded in bending, shear and torsion. In the specimens analysed, the shear reinforcement amount varied from 0.2 % up to 3 % and the thicknesses of the specimens varied from 0.07 m up to 0.189 m.

In the analyses, the concrete was modelled with four-node curved shell elements. Full interaction was assumed between the reinforcement or prestressing strands and the concrete, by using embedded reinforcement layers. The concrete was modelled with a constitutive model based on non-linear fracture mechanics, and a rotating crack model based on total strain was used; see TNO[29]. The hardening of concrete in compression was described by the expression of Thorenfeldt, and the reduction of the strength due to transverse tensile strains was modelled according to Vecchio and Collins, as described in TNO[29]. For the tension softening, two approaches were compared; see Figure 2:

- The curve by Hordijk, as described in TNO[29], where only the fracture energy of plain concrete is taken into account.
- A curve modified according to the expression from the MCFT by Collins and Mitchell[30], which attempts to take into account also the *concrete contribution*, i.e. tension stiffening, aggregate interlock and dowel action.

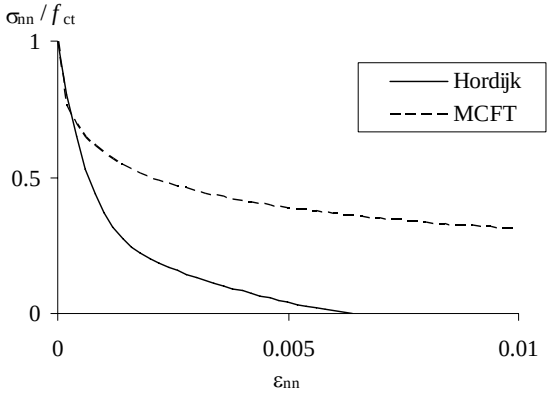

Figure 2 *Comparison of tension-softening relationships according to Hordijk as described in TNO[1], only fracture energy of plain concrete, and according to MCFT ,Collins and Mitchell[2] including the concrete contribution when subjected to shear.*

The constitutive relations of the reinforcement and the prestressing steel were modelled by the von Mises yield criterion with an associated flow rule and isotropic hardening.

It was shown that four-node curved shell elements with embedded reinforcement could describe the non-linear shear response and predict the shear capacity. Further, this study implied that an analysis of a reinforced or prestressed concrete member subjected to shear, torsion and bending will predict the load-carrying capacity and the crack widths on the safe side, if:

- The fracture energy alone is used to define the softening branch of the concrete tensile response.
- The reduction of the compression strength due to transverse tensile strain is included.

Also some problems were highlighted. If the concrete compressive failure was localised into a small region, whose size did not correspond to the size of the specimens used to calibrate the compression relationship used, i.e. the non-linear tension-softening curve of Thorenfeldt, the model could not predict the response. Furthermore, reducing the compressive strength due to lateral strains can result in an unreasonable response and a premature failure.

A case study

The Källösund Bridge

The Källösund Bridge, a prestressed concrete box-girder bridge, was built in 1958-1959 on the Swedish west coast; see Figure 3. The bridge was constructed with the free cantilevering method and cast in-situ concrete. The total length of the bridge is about 325 m, divided in four spans with theoretical span widths of 50 m, 107 m, 107 m and 50 m. It is supported on three piers and two end abutments. Elevation and plan of the bridge are shown in Figure 4. In 1982 the bridge was complemented with a causeway for pedestrians and bicycles. This causeway is constructed in steel and mounted on the south side of the bridge; see Figure 5, which shows the bridge girder cross-section over the pier and in the mid-span region. The main part of the longitudinal reinforcement in the bridge girders is prestressed, and is mostly positioned in the top flange. A part of the longitudinal prestressed reinforcement is bent down diagonally in the webs in the outer parts of the cantilevers; see Figure 6. The bridge slab is also prestressed in the transversal direction with a reinforcement spacing of 500 mm. The prestressing reinforcement consists of bars with a diameter of 26 mm in grouted ducts. The level of the prestressing is, after long-term losses, about 530 MPa and 620 MPa for the longitudinal and the transversal prestressed reinforcement respectively. The bridge girders have a quite low amount of non-prestressed reinforcement, generally $\phi 10$ s 300; see Figure 7. More detailed descriptions of the bridge can be found in Plos *et al.*[26], Plos[31], Enochsson *et al.*[32] and Plos and Gylltoft[13].

Figure 3 *The Källösund Bridge, seen from Stenungsön (in west direction).*

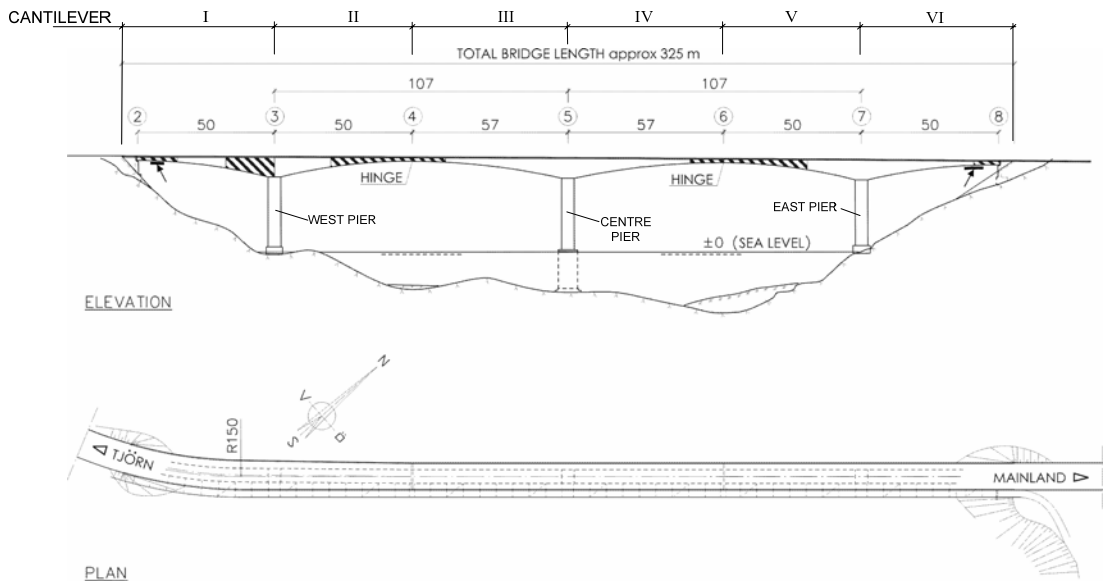

Figure 4 *Elevation and plan of the Källösund Bridge. (Regions with insufficient capacity and critical cross-sections according to the initial assessment are indicated.) Modified from Enochsson* et al.[32].

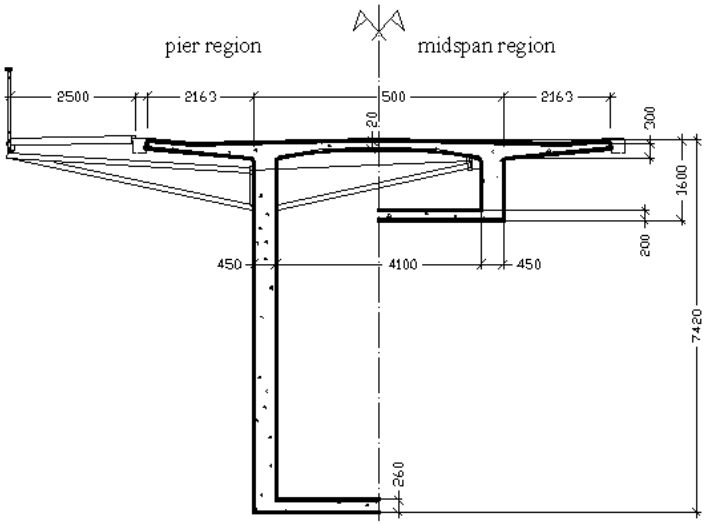

(a) (b)

Figure 5 *a) The bicycle and pedestrian causeway on the south side of the bridge. b) Bridge girder cross-section, including the causeway, in the pier and mid-span region.*

Total number of prestressing bars:

156 148 140 132 124 116 108 100 90 78 76 66 48 30 20 8

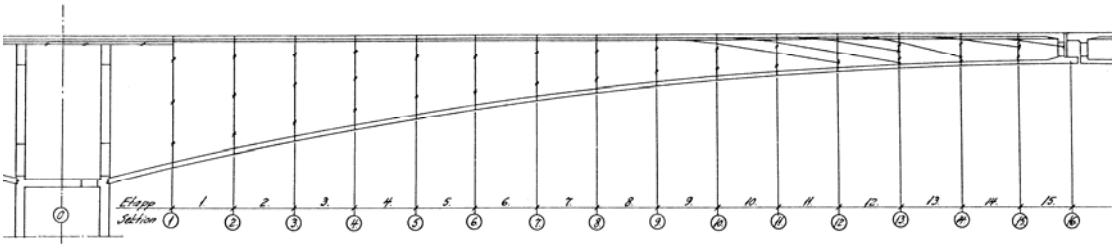

Figure 6 *Main prestressing reinforcement in the cantilever II. From drawing O497ap.*

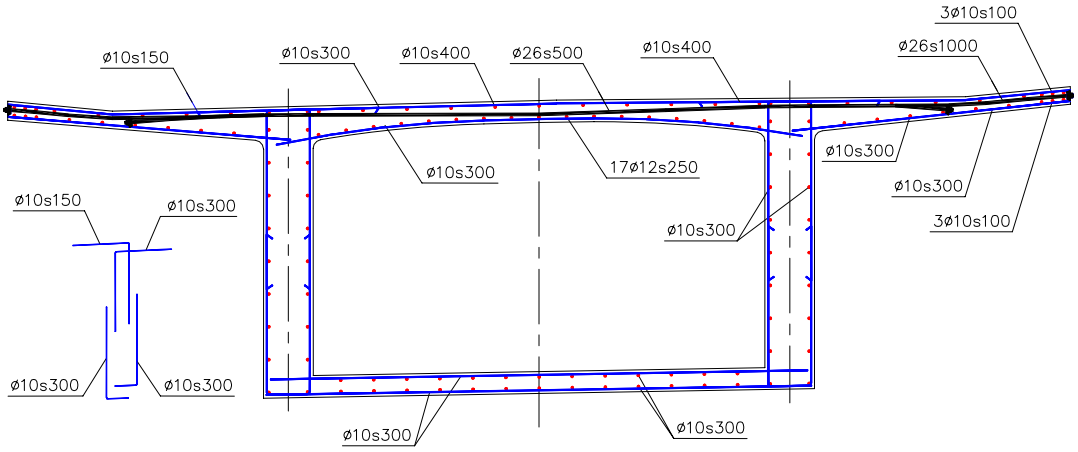

Figure 7 *Cross-section and reinforcement layout in the critical section (29.5 m from the west pier, in the cantilever II).Longitudinal prestressing tendons not included. Modified from Plos*[31].

Previous assessments

In this study the Källösund Bridge was analysed as a case study, using the modelling method previously worked out. It would have been preferable to make the case study on a prestressed concrete bridge that has been tested to failure due to shear and torsion. However, full-scale tests on concrete bridge are rare and the authors have not been able to find any suitable tested bridge to use the modelling method on. The Källösund Bridge has previously been extensively assessed and was judged to have insufficient load-carrying capacity for combinations of shear and torsion.

In connection with a maintenance and repair intervention, both a conventional structural assessment and several enhanced assessments with more advanced methods were performed. In the conventional assessment, linear structural analyses were made and all possible load combinations, type vehicles and traffic load positions were evaluated. For each cross-section the maximum cross-sectional forces were presented. The required reinforcement amount for each cross-section was calculated according to the design methods for concrete structures in the Swedish code BBK 94, Boverket[33]. According to this assessment, strengthening was required for combinations of shear and torsion along substantial parts of the bridge; see Figure 8. The most critical sections were found to be in cantilever II, 26.5 m and 29.5 m from the centre of the west pier. Figure 8 shows the critical load combination and the location of the critical section. Figure 7 shows the critical cross-section with reinforcement. For the critical load combination and the critical section, a more enhanced assessment was performed in a project aiming at showing how more advanced methods can be used for more accurate assessments of concrete bridges; see Plos *et al.*[26]. In order to try to reveal a higher load-carrying capacity than the one evaluated in the convectional assessment, different more enhanced methods were used on the bridge. Probabilistic methods taking material properties and load situation into account were used – see Jeppson *et al.*[34] – as well as improved methods for combinations of shear, torsion and bending, Enochsson *et al.*[32]. In particular the MCFT was used to evaluate the load-carrying capacity. According to these evaluations, the bridge was found to have lower bogie load capacity than required. Furthermore, the load-carrying capacity of the bridge was

evaluated by using non-linear FE analyses; see Plos[31] and Plos and Gylltoft[13]. Here, a substantially higher capacity was found. However, the modelling method used in the FE analyses was not verified against tests and the results were questioned; see Plos *et al.*[26]. Therefore, the bridge was strengthened with glued fibre-reinforced laminates.

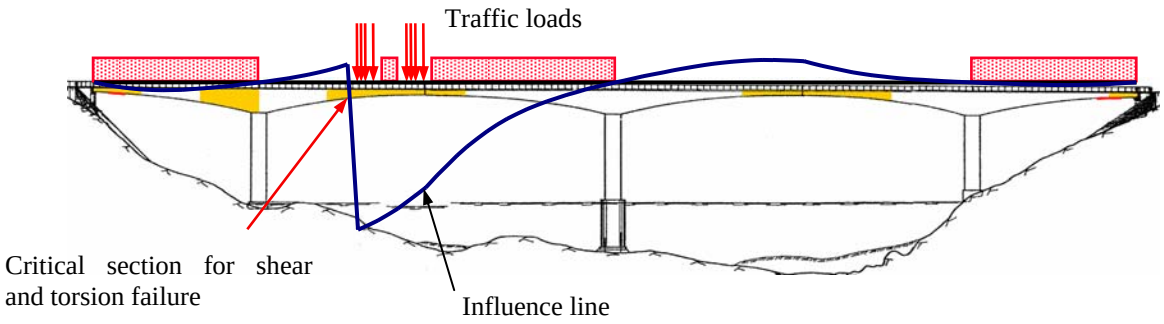

Figure 8 *Influence line for the shear force in the critical cross-section and corresponding critical traffic load position. Modified from Plos and Gylltoft[3].*

The evaluation performed in this study is improved, compared to the previously made assessment with non-linear FEM, in several respects:

- the modelling method used is verified,
- long-term effects due to concrete creep are taken into account,
- the reinforcement is modelled more accurately,
- the final loading with traffic point loads is made with displacement control, and
- several analyses are made to study some safety formats that are suitable for evaluation of the design load capacity by using non-linear analysis.

FE model of the bridge

The non-linear FE program Diana, TNO[29], and the modelling approach presented above were used to simulate the shear and torsion response of the Källösund Bridge. The model was built up with the same information and with the same simplifications as the model used by Plos[31], if nothing else is stated. The whole bridge was modelled, but only the part that was most critical to shear and torsion failure was modelled in detail; see Figure 9. Cantilever II (see Figure 4) was modelled with shell elements and embedded reinforcement according to the modelling method presented. For the shell elements in the top and bottom flange, seven integration points over the thickness were used in order to describe bending properly. For the shell elements in the webs, only three integration points were used in order to save computational time. The rest of the bridge was modelled with two-node beam elements and linear material properties. The bridge was cast in segments that were about 3 m long. In the model there is one beam element for each segment. The geometric properties of the beam elements, moment of inertia and eccentricity were given the mean values for each segment. The reinforcement and the prestress were not included in the parts modelled with beam elements.

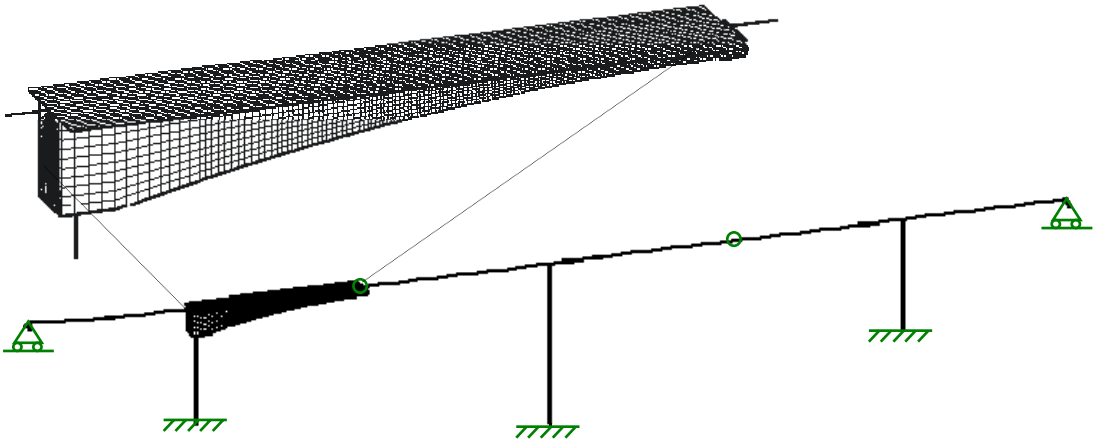

Figure 9 *FE model of the Källösund Bridge used for the case study. Only the part of the bridge critical for shear and torsion is modelled in detail with curved shell elements, embedded reinforcement and non-linear material properties. The rest of the bridge is modelled with beam elements and linear material properties.*

The piers were assumed to be fixed at the bottom end. The end spans were simply supported at the abutments. From the node at each end, two inclined stiff links were used to model the boundary conditions at the correct positions of the abutments. Here, the ends of the stiff links were supported in vertical and transversal direction; see Figure 10 b.

(a) (b)

Figure 10 *Stiff links, i.e. beams with high stiffness and no density, connecting a) the non-linear modelled part with the linear modelled parts at the west pier connection, b) the linear modelled cantilever VI with the abutments.*

At the mid-span hinges, the vertical and transversal displacements as well as the torsional rotations were kept equal for the nodes on each side. However, the longitudinal displacements and the bending rotations of the connected cantilever ends were uncoupled. The west end of the detailed part was connected to the linear parts, i.e. the west end span and the west pier, through stiff links; see Figure 10 a. Three-node beam elements with high stiffness and no density were used to constrain displacements and rotations between the detailed part and the linear part. All nodes at the end section of the detailed part were forced to remain in the plane given by the end rotation of the connected beam element. Moreover, the nodes on the part of the cross-section forming the closed box were forced to keep their relative distance to each other, in order to simulate the cross-wall in this section. At the section connected to the pier, the same type of constraints was used.

Material properties

The material properties used in the analyses are listed in Table 1 and graphically presented in Figures 11 and 12. For non-linear FE analysis the non-linear responses of the materials are needed. Material models are used to describe these responses; however, characteristics like tensile strength, compressive strength, Young's modulus and fracture energy are needed as input for these material models.

Table 1 Material properties used in the analyses

Material			f_m	f_k	$f_{m,EN}$	$\eta\gamma_m$	f_d
Concrete	Piers	E_c [GPa]	32.6	32.6	27.5	1.2	22.6
	Cant	f_{cc} [MPa]	52.7	44.7	37.7	1.5	24.8
		f_{ct} [MPa]	3.80	2.58	2.17	1.5	1.43
		E_c [GPa]	37.4	37.4	31.5	1.2	26.0
		G_f [Nm/m2]	186	126	106	-	70
Reinforcing steel	ϕ 10	f_y [MPa]	450	392	431	1.15	284
		f_u [MPa]	630	549	603	1.15	398
		ε_u [–]	0.15	0.15	0.15		0.15
		E_s [GPa]	204	200	220	1.05	159
Prestressing steel	ϕ 26	f_p [MPa]	860	770	847	1.15	558
		f_u [MPa]	1110	1000	1100	1.15	725
		ε_g [–]	0.07	0.07	0.07	-	0.07
		E_p [GPa]	178	174	191	1.05	138

When the bridge was designed, the concrete classes used were K35 for the piers, K55 for the 50-m cantilevers, and K50 for the central 57-m cantilevers. In the analyses, the concrete in the piers was assigned the characteristic concrete strength, f_{ck}, used in the conventional assessment, FB_Engineering[35]. The concrete in the cantilevers has been tested and evaluated more extensively; see Jeppson *et al.*[34], Enochsson *et al.*[32] and Plos *et al.*[26]. However, the values available in Jeppson *et al.*[34] were considered too incomplete to evaluate the properties statistically. Instead, in the analyses, the concrete in the cantilevers was given the characteristic concrete strength, f_{ck}, statistically evaluated from field tests and reported in Plos *et al.*[26]. All other mean and characteristic concrete material properties were determined from f_{ck} according to CEB-FIP Model Code, fib[36]. The design values used in the analysis are calculated from the characteristic values according to Boverket[37], with partial safety factors $\gamma_n = 1.2$ and $\eta\gamma_m$ for each material, as presented in Table 1. The mean fracture energy was evaluated by assuming a maximum aggregate size of 32 mm. The corresponding values were calculated by choosing a crack band width $h = 0.3$ m and the same ultimate crack strain $\varepsilon^{cr}_{enn,ult}$, for the Hordijk tension-softening curve; see Figure 11a. The crack band width corresponds approximately to the mean crack spacing calculated according to EN1992-1-1[38].

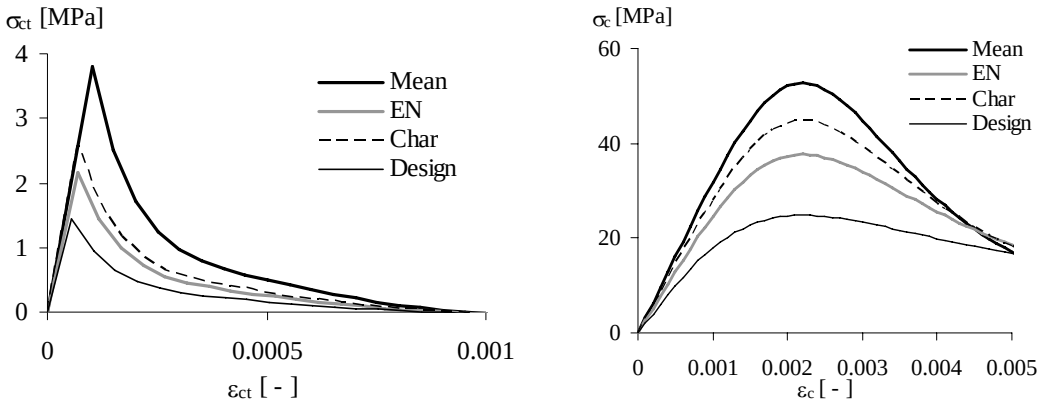

(a) (b)

Figure 11 *The concrete uni-axial response for mean, characteristic, EN, and design material properties used in the analyses. (a) the tension softening curves according to Hordijk as described in TNO[1] (b) The compressive softening curve according to Thorenfeldt as described in TNO[1].*

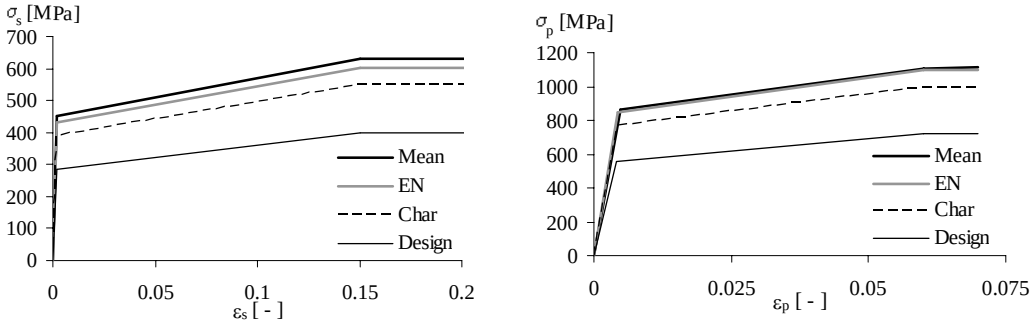

(a) (b)

Figure 12 *The steel response for mean, characteristic, EN, and design material properties used in the analyses. (a) Ordinary reinforcement and (b) prestressed reinforcement.*

The material properties used for the non-prestressed and the prestressed reinforcement are in accordance with the ones reported as statistically evaluated in Plos *et al.*[26]. No hardening parameters were presented for the non-prestressed reinforcement. Instead, the values presented in Table 1 are mean values taken from several other test reports using the same kind of reinforcement, from the same time period.

FE analyses of the bridge

The model was used to make four non-linear FE analyses, in order to evaluate the safety formats presented, one for each set-up of material properties; see Table 1. The analysis procedure was the same in all analyses if nothing else is stated. The loads were the same as in the analysis by Plos[31]. However, here the traffic point loads in the last step were applied with deformation control instead of load control as in Plos[31].

The bridge response was evaluated for design loads in the ULS according to the Swedish assessment regulations for road bridges, Vägverket[22]. The ULS load case includes permanent loads, traffic loads and wind loads. Long-term effects on the prestressing were taken into account. The overall redistribution of stresses in the bridge due to concrete creep was accounted for in an approximate way, by applying prescribed displacements to the end supports. These displacements were calibrated against measured support reactions in FB_Engineering[35]; see Table 2. Temperature effects were not taken into account in the analyses.

Table 2 Measured support reactions at the abutments and calculated pre-described deformations to the model.

	West abutment		East abutment	
	North	South	North	South
Support reaction [kN]	-401	-367	-375	-535
Deformation [mm]	7.4	6.5	34.5	34.2

The analyses were made in steps to include the construction sequence and the loading history; see Figure 13. In the analyses, the loads were gradually increased and the abutments and the mid-span hinges were introduced at certain stages during the construction. The gravity load of the parts included in the model was accounted for by the density of reinforced concrete, $\rho = 25$ kN/m^3. The gravity load of parts not included in the model was applied as external loads. The bridge was loaded with several variable loads simultaneously: crowd load on the causeway, distributed traffic load, horizontal and vertical traffic point loads, and wind loads. The vertical point loads of traffic in the critical load combination consist of four type vehicles, with eight point loads of $0.22B$ for each vehicle; see Vägverket[22]. Hence, the vertical point loads of traffic were applied to 32 nodes; see Figure 14. To enable deformation-controlled loading for several point loads, a separate statically determined arrangement of stiff beams was modelled. The nodes, where the vertical traffic point loads were applied on the bridge, were tied to have the same vertical displacements as the corresponding bottom end nodes of the loading arrangement. The vertical point loads of traffic were applied by increasing the vertical displacement of one node at the top beam element in the loading structure. The resulting vertical reaction force in this node was used to calculate the applied bogie load B according to:

$$B = 190 + \frac{P}{32 \cdot 0.22 \cdot \xi} \quad \text{[kN]} \tag{11}$$

where a dynamic multiplication factor $\xi = 1.06$ evaluated in Plos[31] was used.

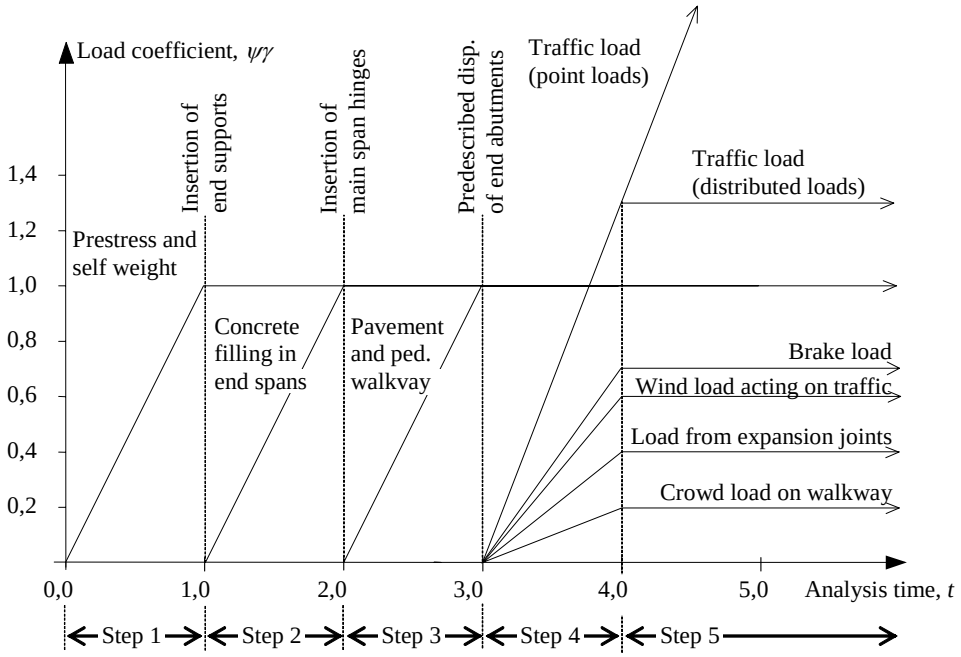

Figure 13 *Loading sequence and construction history of the bridge for analysis in the ULS, modified from Plos and Gylltoft[3].*

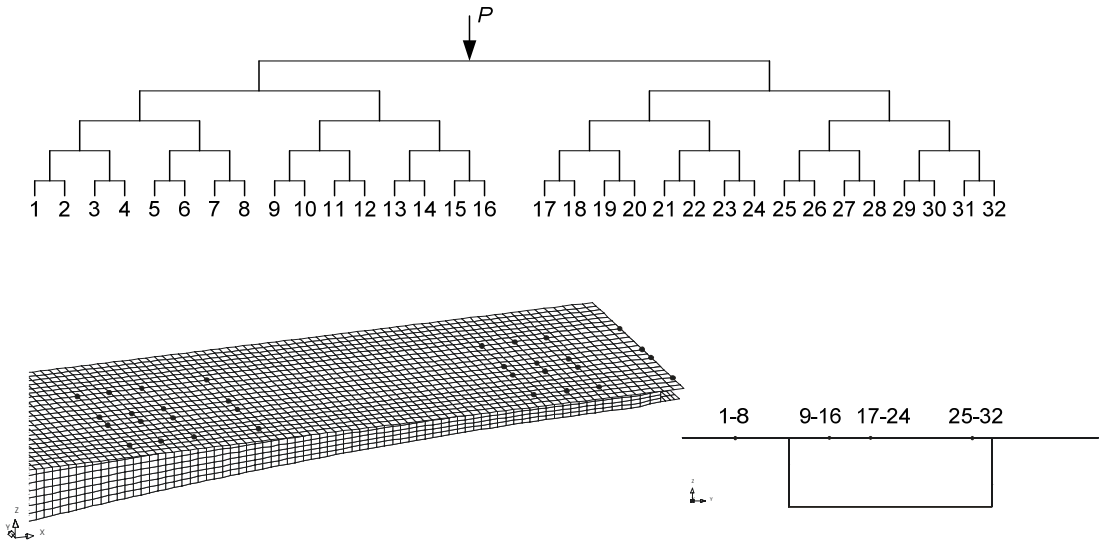

Figure 14 *The point loads of the vertical traffic load were applied in 32 points (on 32 nodes) on the top flange, using a statically determined arrangement of stiff beams*

In the first step of the analyses (see Figure 13), the prestressing forces were released and the gravity load of the structure was applied. At this stage, only the piers were supported. In the next step, the end abutments were introduced, i.e. the nodes were supported in the vertical direction, before a gravity load from concrete filling in the end spans was applied. In the third step, the hinges in the mid-spans were introduced. The remaining parts of the permanent loads were then applied, e.g. the gravity load from the pavement and the causeway, which completed the construction phase. In the

next step, the pre-described deformations of the end abutments were introduced, to account for the effects of concrete creep; see Table 2. Thereafter, the variable loads were applied up to their design values, which included the point loads of the vertical traffic load up to the bogie load B = 190 kN. The final failure was reached, in the last step, by increasing the vertical point loads of the traffic to obtain the bogie load resistance, B_R.

In the FE analyses, an implicit solving method was used. In the final step, the loading was made with constant deformation increments of 1.0 mm. For each increment, equilibrium was found by using the BFGS secant iteration method, TNO[29]. A line search algorithm guided with default values, TNO[29], was used to increase the convergence rate in the iteration process. The analysis was continued if the specified displacement convergence criterion was fulfilled, according to default value; see TNO[29]. If the convergence criterion was not fulfilled within two hundred iterations, the analysis was stopped.

Results from the analyses

The results shown are from the analysis with mean material properties if nothing else is stated. The response was linear for the whole bridge when subjected to all permanent loads. This can be seen in Figure 15, showing the vertical support reaction in the west pier versus deflection of the cantilever II-end. Figure 15 also indicates which part of the loading each part of the response emanates from.

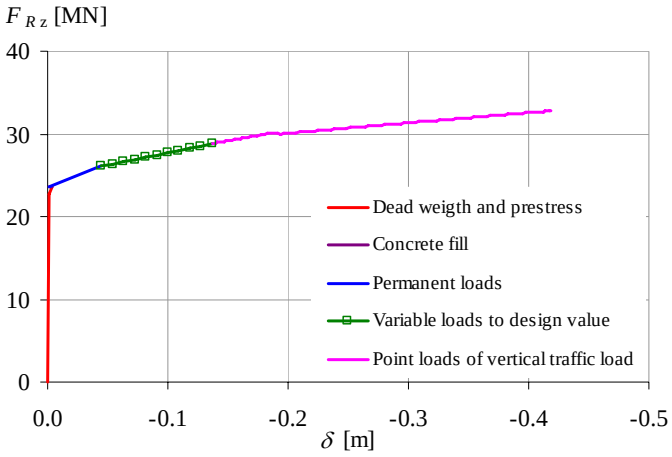

Figure 15 Vertical support reaction in the west pier versus vertical displacement of the cantilever II end.

In Figure 16 the increase of the bogie load B versus the applied deformation is shown for the analyses with: mean material properties, characteristic material properties, and the material properties according to the method in EN1992-2, respectively. The maximum bogie loads obtained from these analyses were B_{Rm} = 806 kN, B_{Rk} = 626 kN and B_{REN} = 631 kN, respectively. As can be seen from the results, the response in the analyses was similar and all three analyses showed the same failure mode.

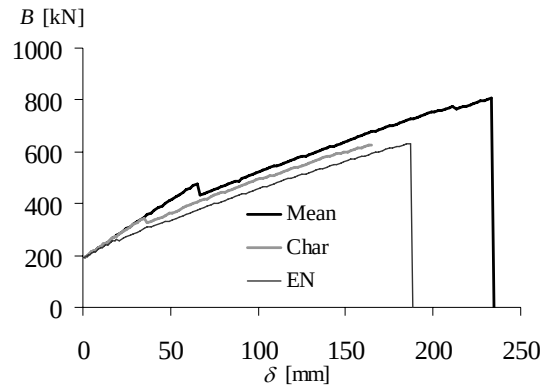

Figure 16 *The vertical traffic point load (Bogie load) versus the applied deflection as result from analyses with mean, characteristic and material parameters according to EN1992-1, respectively.*

Even if the shear resistance limited the load-carrying capacity in the evaluations previously performed, the failure obtained in these FE analyses was due to bending, see Figure 17. However, shear cracks were developed in large regions in the webs, so a shear response was still observed. In the analysis with mean material properties, the cracking of the concrete started at $B = 476$ kN, with flexural-shear cracks, going through the top flange and down into the webs; see Figure 18. The cracks occurred in the sections where the prestressing tendons are anchored in the top flange. When the web cracked, yielding was initiated in the vertical web reinforcement due to the low reinforcement amount, 0.16 %; see Figure 19. More cracking occurred, both in the top flange and in the webs, when the load was increased. In the part of the cantilever where the bending mode changed from tension in the top to tension in the bottom, the top element row of the south web cracked in shear; see Figure 20. Thereafter, when a bending crack developed in the bottom of the cross-section close to the end of the cantilever, the concrete compressive strength in the top of the web was reduced due to lateral tensile strains. Hence, the concrete in the compressive zone crushed when the tensile reinforcement in this section yielded due to the low remaining compressive strength; see Figures 21 and 22.

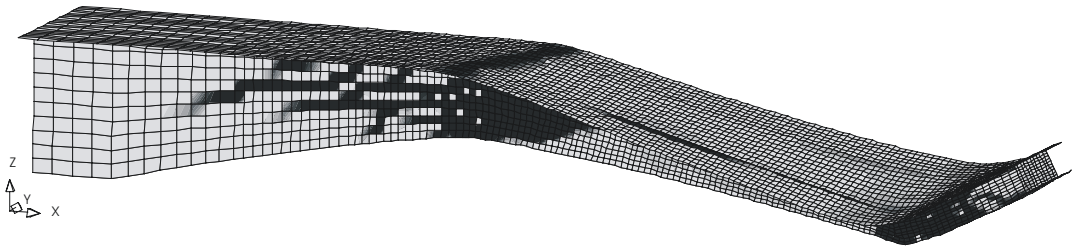

Figure 17 *Deformed shape of cantilever II after maximum load. Result from analysis with mean material properties.*

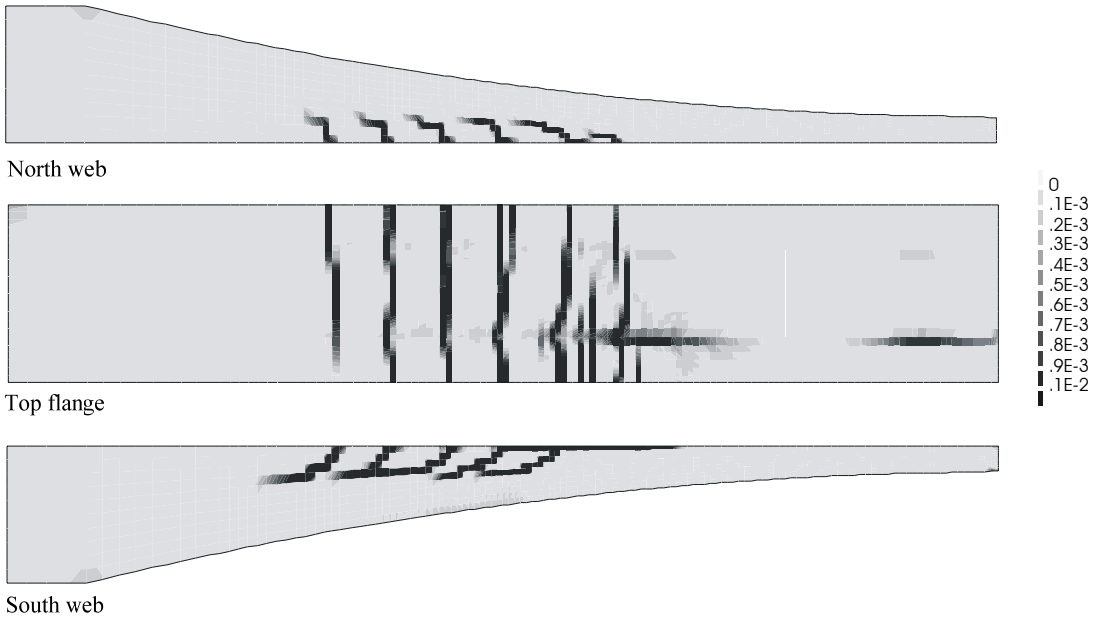

Figure 18 *Cantilever II north web, top flange and south web, principal tensile strain when the cracking starts, load B = 476 kN. Result from the analysis with mean material properties.*

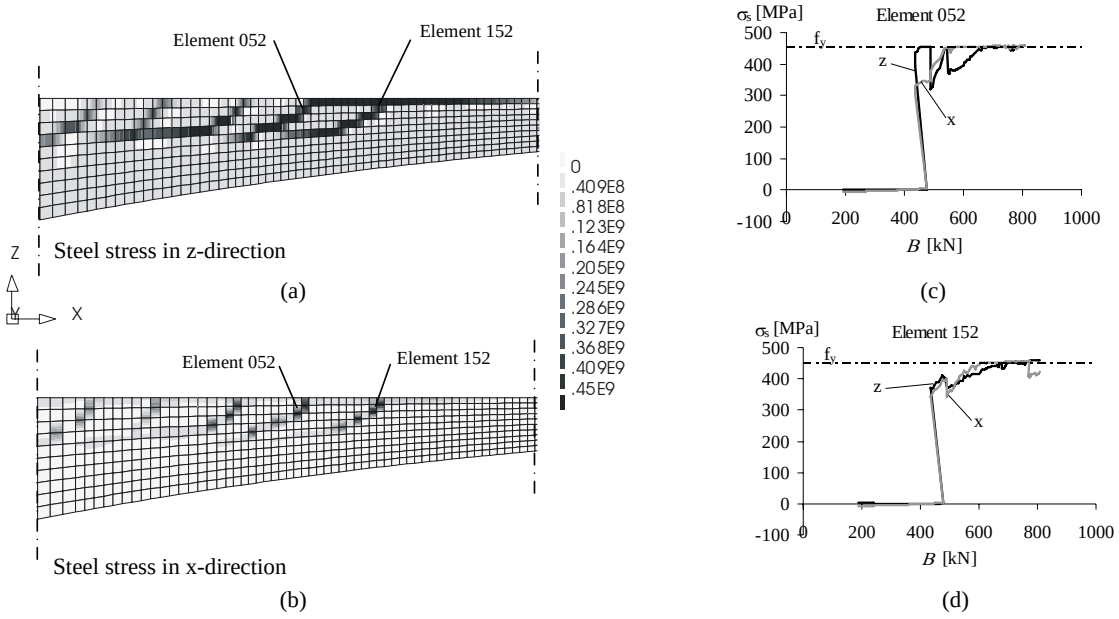

Figure 19 *Results from the analysis with mean material properties. Steel stress in the outer reinforcement in the south web when the concrete crack (a) vertical (z-direction), (b) longitudinal (x-direction). (c) and (d) steel stress versus bogie load for reinforcement element 052 and 152, respectively.*

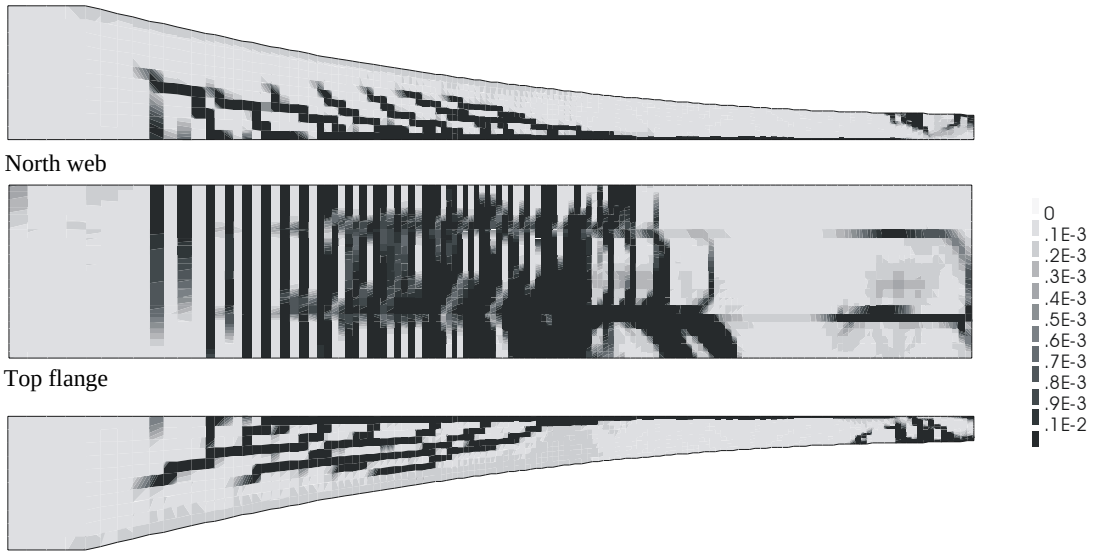

Figure 20 *Cantilever II north web, top flange and south web, principal tensile strain at maximum load from analysis with mean material properties.*

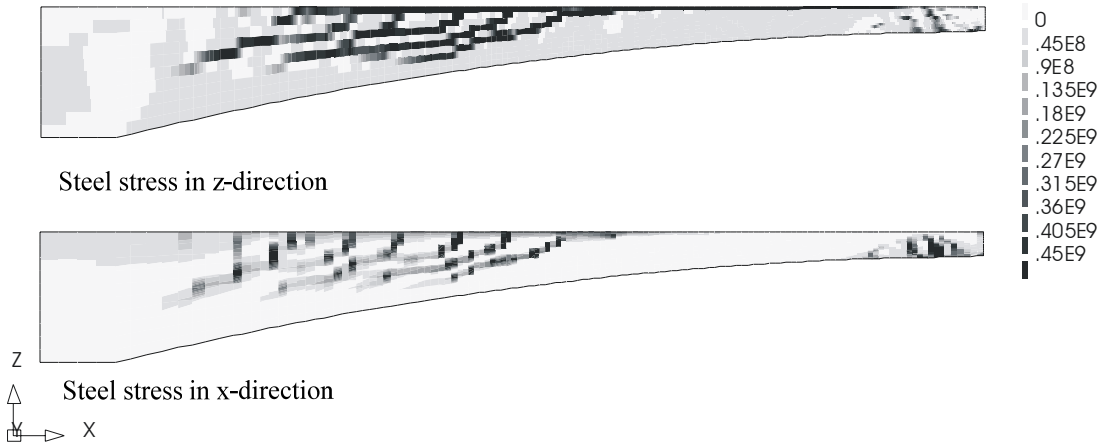

Figure 21 *Steel stress in the outer reinforcement, vertical (z-direction) and longitudinal (x-direction), in the south web. Results from the analysis with mean material properties.*

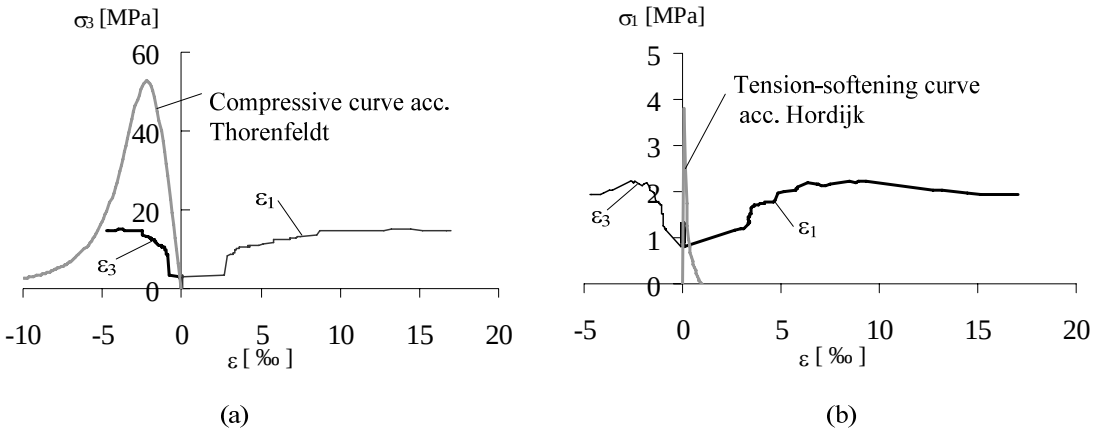

Figure 22 *Results of one concrete element in the top of the south web, from analysis with mean material properties. (a) Principal compressive stress versus principal strains compared with the concrete compressive curve according to Thorenfeldt without reduction due to lateral tensile strains. (b) Principal tensile stress versus principal strains compared with the concrete tension-softening curve according to Hordijk.*

In the analysis with all material properties given their design values, the failure occurred for a bogie load lower than the required design bogie load, B = 190 kN, i.e. for a load level lower than when the displacement-controlled loading started. To obtain a clearly interpretable maximum bogie load for this analysis, the point loads of the vertical traffic load were excluded from the fourth load step including variable loads up to the design value. The point loads were then applied by displacement-controlled loading in the last step. The maximum obtained bogie load was then B_{Rd} = 182 kN; see Figure 23. Also this analysis showed the same failure mode as in all the other analyses, i.e. crushing of concrete due to bending. In this analysis the shear cracks in the south web occurred for a bogie load of B = 95 kN, when the top flange was still uncracked. For a bogie load of B = 134 kN shear cracks occurred also in the north web and bending cracks occurred in the top flange.

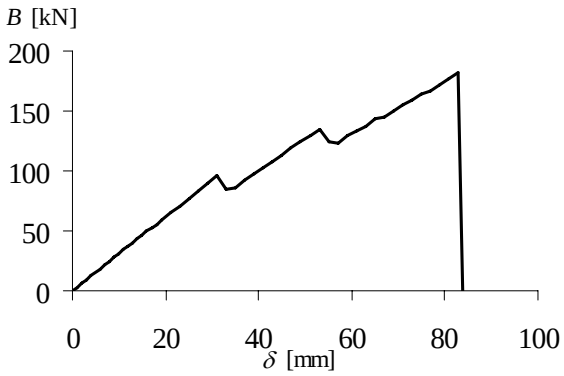

Figure 23 *The vertical traffic point load (Bogie load) versus the applied deformation as result from the analysis with design material properties.*

Figure 24a shows the magnitude of the torsional moment that was transferred through the link between cantilever II and cantilever III. It can be seen that more of the torsional moment was transferred after shear cracking of cantilever II. This can be compared with how much shear force was transferred (see Figure 24b), which shows that the shear cracking had almost no effect on the shear transfer.

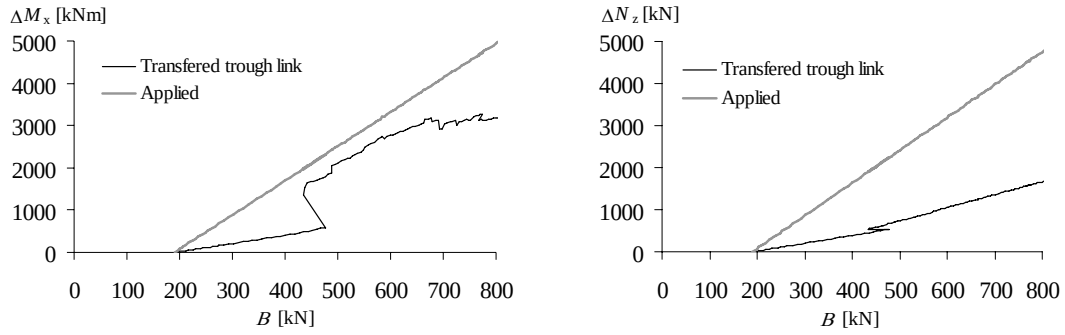

(a) (b)

Figure 24 *Results from analysis with mean material properties. Applied bogie load B versus increase of (a) torsional moment M_x and (b) vertical shear N_z.*

As can be seen in Figure 20, a large part of the south web is cracked in shear. When the load increased, the strain localized in a smaller region, which indicates a main shear crack; see Figure 25. This main shear crack developed between section 17.5 m and section 26.5 m, measured from the centre of the west pier. The inclination of this main shear crack could be estimated as approximately 20°.

Table 3 presents the load-carrying capacity, expressed as bogie load resistance, estimated according to the safety formats presented – i.e. the semi-probabilistic ECOV method (ECOV), the method presented in EN1992-2 (EN), and by using partial safety factors (PSF). The bogie load resistances determined with the safety formats are also related to the maximum bogie load obtained from the analysis with mean material properties. It should be mentioned that in these calculations and analyses, only variations in material properties and not in actions have been accounted for.

Table 3 *Load carrying-capacity for combined shear and torsion, expressed as a bogie load resistance and safety level*

	Previously made assessment		Assessment made in this study		
	Conventional	FEA	PSF	EN	ECOV
B_R [kN]	<210	250	182	497	454
B_{mean}/B_R			4.42	1.62	1.78

Discussion

The non-linear FE analysis made with characteristic material properties showed a maximum bogie load of 626 kN. This is about 50% higher than in the previous analysis made by Plos and Gylltoft[13]. The analyses made in this study were improved, as mentioned, but also performed with other types of elements and other material models. In the analysis made by Plos and Gylltoft[13] the web started to crack in shear for a bogie load of B = 360 kN, and after a small increase of load the solution was not convergent, which resulted in a maximum load of B = 410 kN. In the present analysis, the shear cracks in the web occurred for a bogie load of B = 344 kN and the maximum load was B = 626 kN. The main part of the increased capacity is probably governed by the use of a more stable material model for cracked concrete and by the displacement-controlled loading, which gives a possibility to increase the load after occurrence of shear cracks in the web. Taking into account the hardening of the ordinary reinforcement also increased the load-carrying capacity; this increase was, however, quite small due to the failure mode.

In Figure 22 it can be seen that, even though the principal tensile strain for a cracked element is larger than the ultimate crack strain, tensile stresses are transferred. This may be due to a known drawback with rotating crack models when the orientation of the crack band differs from the orientation of the principal tensile strains; see Jirásek[39]. In the previously analysed shear panel tests, no stresses were transferred after the ultimate crack strain was reached; see Broo *et al.*[18].

The analysis with partial safety factors, using design values of the material properties, gave a very conservative load-carrying capacity, see Table 3. This was due to the fact that effects from both shear and bending interacted in the part of the cantilever where the failure occurred; the reduced concrete compressive strength due to lateral tensile strains affects the bending moment capacity considerably in this part. The south web cracked for a low bogie load due to the low value of the concrete tensile strength, f_{ctd} = 1.43 MPa. When the bending crack close to the end developed later, the lateral tensile strains in the top of the web had increased greatly, and the already low concrete compressive strength, i.e. the design value, decreased even more. Consequently, the moment capacity was influenced both by the concrete tensile strength and by the concrete compressive strength. In a normal bending failure, either the concrete compressive strength or the steel strength will govern the moment capacity. As can be seen in Table 3 the other two safety formats gave approximately the same results, a load-carrying capacity about 80 % higher than in the previously made FE analysis and more than 100 % higher than in the conventionally made assessment. The disadvantage with the ECOV method mentioned by Cervenka *et al.*[20] is the need of making two analyses. However, in the authors' opinion, the effort of creating a model is sufficiently larger than the effort of running two analyses while only changing the material properties. Besides, the analysis made with mean material properties simulates the most probable response and would preferably be made anyhow.

From the non-linear FE analyses presented here, it could be seen, Figure 25, that the main shear crack developed between section 17.5 m and section 26.5 m, which also agrees with the results from the previous analyses made by Plos and Gylltoft[13]. The previous structural assessment using analytical calculation methods was made with

sectional forces for section 29.5 m and cross-sectional values for this section; see Enochsson *et al.*[32]. All these analytical calculations indicate that the section needed to be strengthened to resist a bogie load of B = 210 kN.

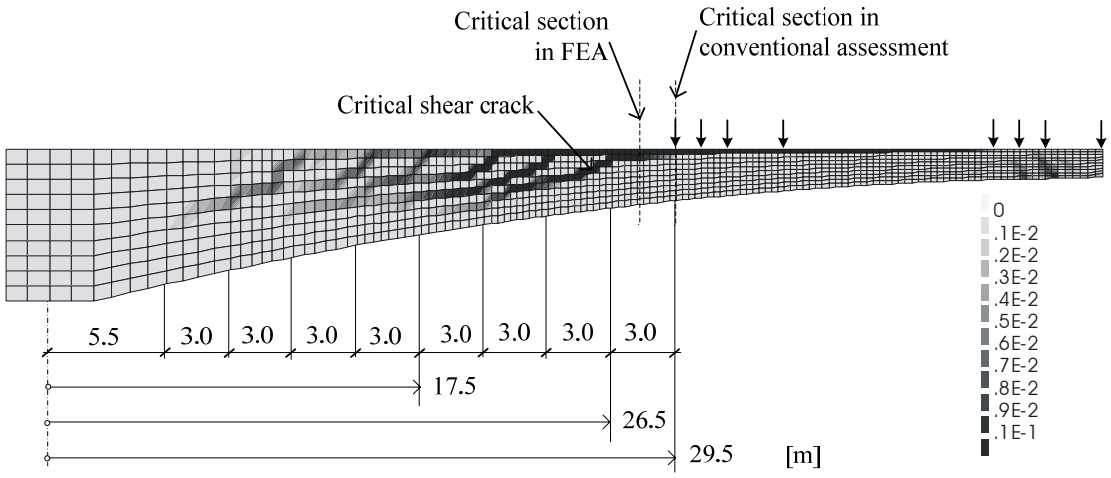

Figure 25 *Principal tensile strains in the south web at maximum load as result from the analysis with mean material properties. Assumed critical section was 29.5 m from centre of the west pier; in the analysis the main shear crack develops between sections 17.5 m and 26.5 m from centre of west pier*

The higher load-carrying capacity achieved, using non-linear FE analysis for the assessment compared to conventional methods, is mainly governed by the location and inclination of the critical shear crack. The web height increases in the shear crack direction. This influences the length of the shear crack and the amount of reinforcement activated in the shear crack. This is not taken into account in the conventional assessment; see Figure 25 and Table 4. Assuming the same critical section as in the conventional assessment, but with the correct length of the shear crack, the reinforcement contribution to the shear capacity for one web increase with 13 % and 39% for a crack inclination correspondent to $\cot\theta$ =1 and $\cot\theta$ =2.5, respectively. For the shear crack in the FE analysis this increase was even higher, 48%. The redistribution of torsional moment due to cracking may also have a positive influence on the capacity. However, the redistribution of the torsional moment shown in Figure 24a could be questioned, because cantilever III is modelled with linear response. If the load effect in cantilever III is high enough to cause cracking, the stiffness of this part would decrease and the redistribution would have become smaller.

Table 4 *Contribution from the shear reinforcement to the shear capacity determined from a truss model. Only the shear crack in the south web is considered for the calculations.*

	V_s [kN]		
	In the conventional assessment	Corrected	FEA
$\cot\theta$ = 1	537	605	
$\cot\theta$ = 2.5	1343	1866	1988

Conclusions

In this study it was shown, with a case study, that the modelling method using shell elements with non-linear material response for the critical part of a bridge, in combination with beam elements and linear response for the rest of the bridge, can simulate the shear response. Although a final shear failure was not achieved in the analyses, it could be concluded that the shear capacity of this part of the bridge, for this load combination, is higher than the load-carrying capacity determined.

The bridge used for the case study presented has previously been evaluated both with conventional methods and with non-linear FE analysis; see Plos and Gylltoft[13]. The evaluation in this study was improved in several respects: the FE modelling method used was verified, the final loading was made in a displacement-controlled process, effects of creep and reinforcement hardening were included, and safety formats suitable for non-linear analysis were adopted. Here, two semi-probabilistic formats; the so-called ECOV method and the method presented in EN1992-2 were used and compared with the deterministic format using partial safety factors.

The FE analysis performed in this study revealed a load-carrying capacity corresponding to about 80 % higher bogie load than in the previously performed FE analysis and over 100% higher than in a conventionally made assessment. The higher load-carrying capacity shown using non-linear FE analysis for the assessment, compared to conventional methods, is chiefly governed by the location and inclination of the main shear crack. Most of the increased capacity compared with the previous FE analyses is probably due to the use of a more stable material model for cracked concrete and to the displacement-controlled loading.

According to the investigated safety formats, for this structure and this particular load combination, the analyses with partial safety factors (material properties with design values) give a very conservative load-carrying capacity, compared to the more correct semi-probabilistic formats for non-linear FE analysis.

In the case study presented, only one critical load combination and one critical region were evaluated. In a complete assessment of a bridge, alternative load cases also need to be evaluated.

Acknowledgments

The research was financed by the Swedish Road Administration (Vägverket) and the Swedish Rail Administration (Banverket).

References

1. MOKHTAR, A.-S. A. and GHAIL, A. Computer Analysis and Design of Concrete Beams and Girds. *Journal of Structural Engineering*, 1988, **114**, No. 12, 2669-2691.

2. SHUSHKEWICH, K. W. Approximate Analysis of Concrete Box Girder Bridge. *Journal of Structural Engineering*, 1988, **114**, No. 7, 1644-1657.

3. PICARD, A. and MASSICOTTE, B. Serviceability Design of Prestressed Concrete Bridges. *Journal of Bridge Engineering*, 1999, **4**, No. 1, 48-55.

4. SHUSHKEWICH, K. W. Transverse analysis of strutted box girder bridges. *Journal of Bridge Engineering*, 2006, **11**, No. 1, 33-47.

5. SUSTAINABLE BRIDGES. D4.2 Guideline for load and resistance assessment of existing European railway bridges. D4_2-WP4-05-070521, 2007.

6. HURIA, V., LEE, K.-L., and AKTAN, A. E. Nonlinear Finite Element analysis of RC Slab Bridge. *Journal of Structural Engineering*, 1993, **119**, No. 1, 88-107.

7. CHOWDHURY, M. R. and RAY, J. C. Further Considerations for Nonlinear Finite-Element Analysis. *Journal of Structural Engineering*, 1995, **121**, No. 9, 1377-1379.

8. SHAHROOZ, B. M., HO, I. K., AKTAN, A. E., BORST, R. D., BLAAUWENDRAAD, J., VEEN, C. V. D., IDING, R. H., and MILLER, R. A. Nonlinear Finite Element Analysis of Deteriorated RC Slab Bridge. *Journal of Structural Engineering*, 1994, **120**, No. 2, 422-440.

9. HO, I.-K. and SHAHROOZ, B. M. Finite element modeling of deteriorated R.C. slab bridge: lessons learned and recommendations. *Structural Engineering and Mechanics*, 1998, **6**, No. 3, 259-274.

10. SONG, H.-W., YOU, D.-W., BYUN, K.-J., and MAEKAWA, K. Finite element failure analysis of reinforced concrete T-girder bridges. *Engineering Structures*, 2002, **24**, No. 2, 151-162.

11. PLOS, M. Improved bridge assessment using non-linear finite element analyses. *First international conference on bridge maintenance, safety and management*, Barcelona, 2002. IABMAS, pp.

12. PLOS, M. and GYLLTOFT, K. Bärighetsutredningar av broar i framtiden. Institutionen för konstruktionsteknik, Chalmers tekniska Högskola, Göteborg Rapport nr. 02:6, April 2002.

13. PLOS, M. and GYLLTOFT, K. Evaluation of shear capacity of a prestressed concrete box girder bridge using non-linear FEM. *Structural Engineering International*, 2006, **16**, No. 3, 213-221.

14. AYOUB, A. and FILIPPOU, F. C. Nonlinear Finite-Element Analysis of RC Shear Panels and Walls. *Journal of Structural Engineering*, 1998, **124**, No. 3, 298-308.

15. YAMAMOTO, T. and VECCHIO, F. J. Analysis of Reinforced Concrete Shells for Transverse Shear and Torsion. *ACI Structural Journal*, 2001, **98**, No. 2, 191-199.

16. VECCHIO, F. J. and SHIM, W. Experimental and Analytical Reexamination of Classical beam Tests. *Journal of Structural Engineering*, 2004, **130**, No. 3, 460-469.

17. KETTIL, P., RÓDENAS, J. J., AGUILERA TORRES, C., and WIBERG, N.-E. Strength and deformation of arbitrary beam sections using adaptive FEM. *Submitted to Computers & Structures*, 2005, No.

18. BROO, H., PLOS, M., LUNDGREN, K., and ENGSTRÖM, B. Simulation of shear-type cracking and failure with non-linear finite element method. *Magazine of Concrete Research*, 2007, **59**, No. 9, 673-687.

19. EN1992-2, C. T. S. *Eurocode 2: Design of concrete structures Part 2: Concrete bridges Design and detailing rules*, vol. EN1992-2. European Committee for Standardization, Brussels, 2005.

20. CERVENKA, V., CERVENKA, J., and PUKL, R. Safety assessment in fracture analysis of concrete structures. *The 6th international conference on fracture mechanics of concrete and concrete stuctures*, Catania, Italy, 2007. Taylor & Francis, pp. 1043-1049.

21. HEGGER, J., SHERIF, A., and GÖRTZ, S. Investigation of Pre- and postcracking Shear Behavior of Prestressed Concrete Beams Using Innovative measuring Techniques. *ACI Structural Journal*, 2004, **101**, No. 2, 183-192.

22. VÄGVERKET. Allmän teknisk beskrivning för klassningsberäkning av vägbroar (Swedish regulations for structural assessment of road bridges, in Swedish). Vägverket, Borlänge, Sweden publikation 1998:78, 1998.

23. VECCHIO, F. J. and COLLINS, M. P. The modified compression-field theory for reinforced concrete elements subjected to shear. *Journal of the American Concrete Institute*, 1986, **83**, No. 2, 219-231.

24. PANG, X.-B. D. and HSU, T. T. C. Behavior of reinforced concrete membrane elements in shear. *ACI Structural Journal*, 1995, **92**, No. 6, 665-679.

25. PANG, X.-B. D. and HSU, T. T. C. Fixed angle softened truss model for reinforced concrete. *ACI Structural Journal*, 1996, **93**, No. 2, 197-207.

26. PLOS, M., GYLLTOFT, K., JEPPSON, J., CARLSSON, F., THELANDERSSON, S., ENOCHSSON, O., and ELFGREN, L. Evaluering av bärförmåga hos broar med hjälp av förfinade analysmetoder Ett samarbetsprojekt mellan LTH, LTU och Chalmers. Institutionen för konstruktion och mekanik, Betongbyggnad, Göteborg Rapport 04:3, 2004.

27. BROO, H., LUNDGREN, K., and ENGSTRÖM, B. Shear and torsion in prestressed hollow core units: Finite element analyses of full-scale tests. *Structural Concrete*, 2007, **8**, No. 2, 87-100.

28. LUNDGREN, K., BROO, H., and ENGSTRÖM, B. Analyses of hollow core floors subjected to shear and torsion. *Structural Concrete*, 2004, **5**, No. 4, 1464-4177.

29. TNO. *DIANA Finite Element Analysis User's Manual release 9*. TNO DIANA BV, Delft, the Netherlands, 2004.

30. COLLINS, M. P. and MITCHELL, D. *Prestressed Concrete Structures*. Prentice Hall, Englewood Cliffs, New Jersey, 1991.

31. PLOS, M. Structural Assessment of the Källösund bridge using Finite Element Analysis - Evaluation of the load carrying capacity for ULS. Concrete Structures, Department of Structural and Mechanical Engineering, Chalmers University of Technology, Göteborg Rapport 04:1, March 2004.

32. ENOCHSSON, O., PUURULA, A., and ELFGREN, L. Beräkning av betongbroars bärförmåga - Interaktion mellan tvärkraft, vridmoment och böjmoment i Källösundsbron. Institutionen för samhällsbyggnad, Luleå tekniska universitet, Luleå, Sweden 2004:15, 2004.

33. BOVERKET. *Boverkets handbok om betongkonstruktioner BBK 94* Karlskrona, 1994.

34. JEPPSON, J., CARLSSON, F., and THELANDERSSON, S. Klassningsberäkning med hjälp av tillförlitlighetsanalys. Avdelningen för konstruktionsteknik, Lunds Tekniska Högskola, Lund, Sweden Rapport TVBK - 3050, 2004.

35. FB_ENGINEERING. Konstruktionsberäkningar O497, Bro över Källösund mellan Stenungsön och Källön å väg 160 (Structural assessment and design of strengthening for the Källösund Bridge, in Swedish). FB Engineering AB, Göteborg 1650494-16-06-BER-001, 2002.

36. FIB. *Structural concrete. Textbook on behaviour, Design and performance updated knowledge of the CEB/FIP model code 1990*, vol. 2. International Federation for Structural Concrete (fib), Lausanne, Switzerland, 1999.

37. BOVERKET. *Boverkets handbok om betongkonstruktioner BBK 04* Karlskrona, 2004.

38. EN1992-1-1, C. T. S. *Eurocode 2: Design of concrete structures - Part 1: General rules and rules for buildings*, vol. EN1992-1-1, prEN 1992-1-1 Draft for Stage 49 ed. European Committee for Standardization, Brussels, 2004.

39. JIRÁSEK, M. *Modeling of localized inelastic deformation - Lecture notes*. Czech Technical University, Prague, 2004.

Paper VI

A parametric study of the shear response in a prestressed concrete bridge using non-linear finite element analysis.

Broo H., Plos M., Lundgren K. and Engström B.

Submitted to *Magazine of Concrete Research*, April, 2008.

A parametric study of the shear response in a prestressed concrete bridge using non-linear finite element analysis

Helén Broo	Mario Plos	Karin Lundgren	Björn Engström
Research Assistant	Assistant Professor	Associate Professor	Professor
helen.broo@chalmers.se	mario.plos@chalmers.se	karin.lundgren@chalmers.se	bjorn.engstrom@chalmers.se

Department of Civil and Environmental Engineering
Structural Engineering, Concrete Structures
Chalmers University of Technology
SE-412 96 Göteborg, Sweden
Telephone: +46 31 772 00 00
Fax: +46 31 772 22 60

Abstract

For prestressed concrete box-girder bridges the risk of failure due to combined shear and torsion can be a major problem. To satisfy performance demands in the service state and to prevent problems related to unsatisfactory durability, it is important to prevent shear cracking or to limit the width of shear cracks. The aim of this study is to show how a previously proposed modelling method, for non-linear finite element analysis, can be used to investigate the influence of various design parameters on the shear response in a prestressed concrete box-girder bridge.

The reference case corresponds to a real bridge, the Källösund Bridge, which was used to verify the applicability of the proposed modelling method. The whole bridge was modelled, but only the part that was most critical to shear and torsion was modelled in detail and then combined with beam elements for the rest of the bridge. Several non-linear finite element analyses were performed and results such as load-displacement relation, cracking load, crack pattern, crack widths, failure mode and load-carrying capacity were compared. Most of the results conformed to expectation; both increased amount of web reinforcement and increased web thickness showed decreased crack widths, decreased stresses in the web reinforcement, and thereby increased load-carrying capacities. Reduced longitudinal prestressing decreased the cracking load and the stiffness but had almost no effect on the load-carrying capacity. Some results did not conform to expectation; inclined web reinforcement did not reveal higher load-carrying capacity or decreased width of shear cracks in comparison with vertical reinforcement. This could however be explained since the top flange was separating from the web in the vertical direction.

Through this study the proposed modelling method was further verified; the analyses with various design parameters revealed expected results in almost all cases. With the information given by the analysis the complicated behaviour during the failure could be explained also when unexpected results were revealed. Thereby, the knowledge and understanding of how various design parameters affect the shear response was improved, and the ability to use non-linear finite element analysis to verify the designs of box-girder bridges was refined.

Introduction

Prestressed concrete box-girder bridges constructed with the free balancing cantilever method are mainly prestressed in the top flange; the webs are proportionally thin and sparsely reinforced. Hence, the risk of cracking or failure due to combined shear and torsion can be a major problem. To satisfy performance demands in the service state and to prevent problems caused by unsatisfying durability, it is important to prevent shear cracking or to limit the width of shear cracks. Common models for estimation of crack width caused by shear are poor and often minimum requirements or simplified approaches are used in design for the serviceability limit state, see Malm[1]. In the Swedish code for bridge design the requirements for minimum reinforcement in the webs have been increased during the years. The latest change was due to shear cracks discovered in the newly constructed prestressed concrete box-girder bridges in Stockholm, the Gröndal Bridge and the Alvik Bridge, see Malm[1].

Design for shear and torsion in the ultimate limit state is made for sectional forces usually determined with a linear beam or frame analysis. The conventional methods used for design are based on the truss model and valid only to determine the ultimate capacity. To predict the shear response of reinforced concrete members, more advanced methods are needed, for example the modified compression field theory (MCFT) of Vecchio and Collins[2], the rotating-angle softened truss model (RA-STM) of Pang and Hsu[3], and the fixed-angle softened truss model (FA-STM) of Pang and Hsu[4]. However, results from these more advanced methods are still compared with sectional forces determined from a separate, usually linear, structural analysis. In reinforced concrete members the occurrence of cracks and yielding of reinforcement cause stress redistribution within the member. The non-linear finite element (FE) method makes it possible to take such non-linear response into account. In a non-linear FE analysis the response and the load-carrying capacity are determined directly in the overall structural analysis. The FE analysis can be used to study the behaviour in the service state as well as in the ultimate limit state.

In Broo *et al.*[5] a verified modelling method for non-linear FE analysis of the shear response was proposed and in Broo *et al.*[6] it was demonstrated on a prestressed concrete box-girder bridge, the Källösund Bridge. The aim of this study is to further verify the proposed modelling method by showing how it can be used to investigate the influence of various design parameters on the shear response in a prestressed concrete box-girder bridge. Thereby, the knowledge and understanding of how various design parameters affect the shear response can be improved and the ability to use non-linear FE analysis to verify designs of cantilevering box-girder bridges will increase.

Several non-linear FE analyses were performed, varying the amount and inclination of web reinforcement, web thickness and longitudinal prestressing level. Results such as: load-displacement relation, cracking load, crack pattern, crack width, failure mode and load-carrying capacity were compared.

The reference case

The bridge model used in the previous case study was used as a reference in this study, Broo *et al.*[6]. The modelling method used was proposed and verified for large concrete members with shear reinforcement in Broo *et al.*[5]. The reference case corresponds to the Källösund Bridge, which has previously been extensively assessed with conventional assessment methods and non-linear FE analyses, see Plos *et al.*[7] and Broo *et al.*[6]. According to the conventional assessment, the most critical part with regard to shear and torsion was found to be in Cantilever II; see Figure 1.

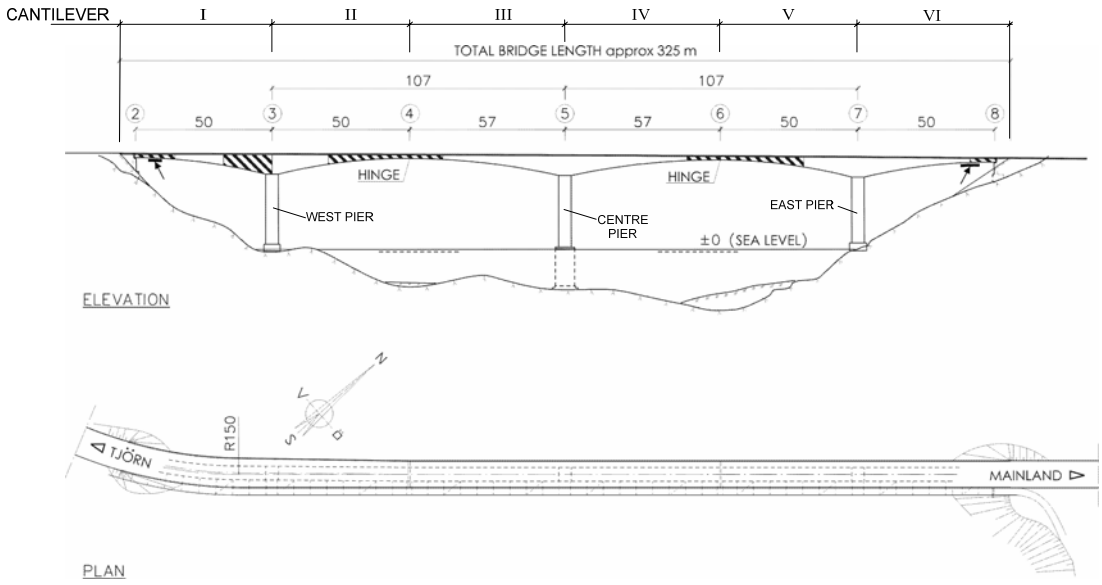

Figure 1 *Elevation and plan of the Källösund Bridge. Modified from Enochsson et al.* [9].

General description of the Källösund Bridge

The Källösund Bridge is a prestressed concrete box-girder bridge, built in 1958-1959 on the Swedish west coast. The bridge was constructed with the free cantilevering method and cast *in-situ*. The total length of the bridge is about 325 m, divided in four spans with theoretical span widths of 50 m, 107 m, 107 m and 50 m. It is supported on three piers and two end abutments. Elevation and plan of the bridge are shown in Figure 1. In 1982 the bridge was complemented with a causeway for pedestrians and bicycles. This causeway was constructed in steel and mounted on the south side of the bridge; see Figure 2, which shows the bridge girder cross-sections over the pier and in the mid-span region. The bridge girders are prestressed with tendons mainly positioned in the top flange. The ends of the longitudinal prestressing tendons are positioned diagonally in the webs in the outer parts of the cantilevers, see Figure 3. The bridge slab is also prestressed in the transversal direction. The level of the prestressing is, after long-term losses, about 530 MPa and 620 MPa for the longitudinal and the transversal prestressing tendons respectively. The bridge girders have a quite low amount of reinforcement, generally $\phi 10\ s\,300$ in orthogonal

directions, see Figure 4. More detailed descriptions of the bridge can be found in Plos *et al.*[7], Plos[8], Enochsson *et al.*[9] and Plos and Gylltoft[10].

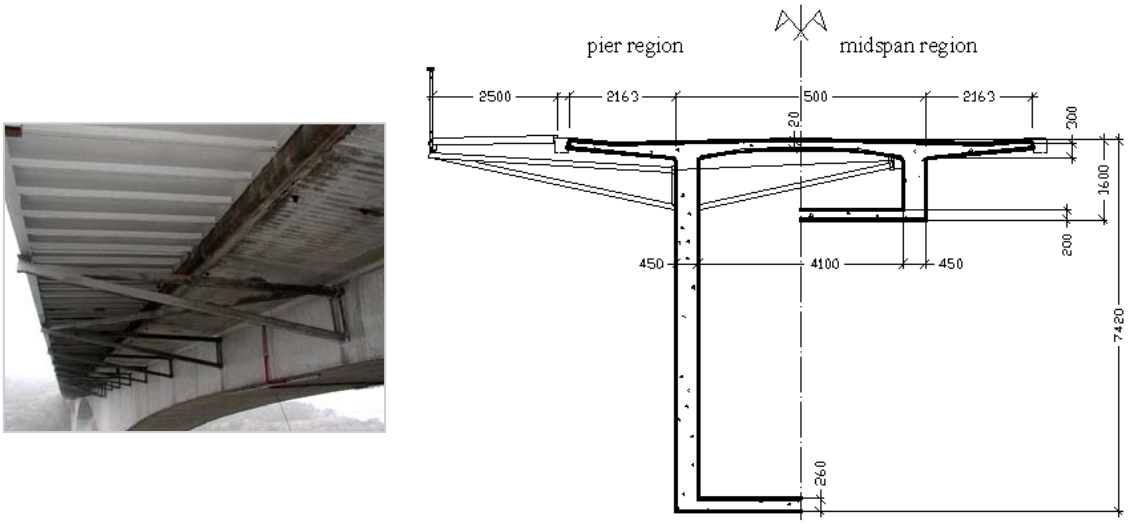

(a) *(b)*

Figure 2 *a) The bicycle and pedestrian cause way on the south side of the bridge. b) Bridge girder cross-section, including the bicycle and pedestrian causeway, in the pier and mid-span region.*

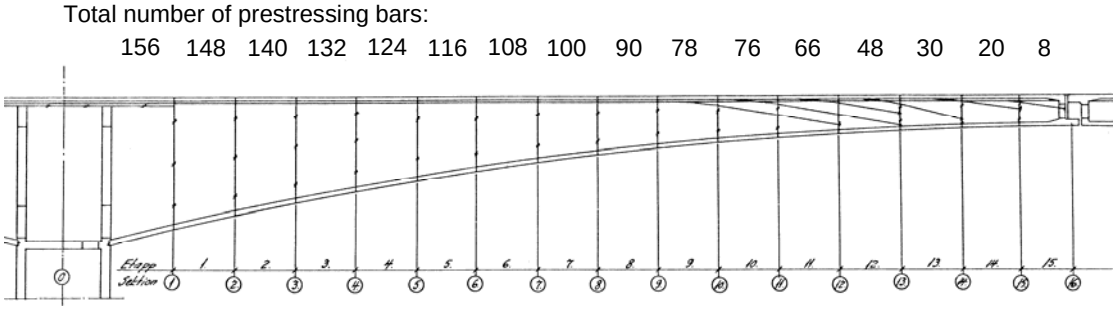

Figure 3 *Longitudinal prestressing tendons in the Cantilever II. From drawing O497ap.*

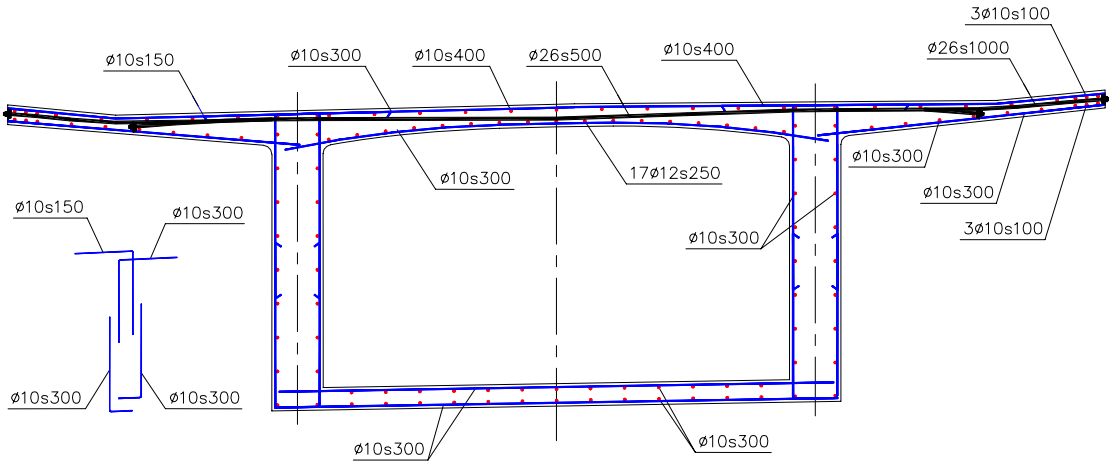

Figure 4 *Cross-section and reinforcement layout in the critical section (29.5 m from the west pier, in the west 50 m cantilever). Modified from Plos et al. [7].*

The finite element model

The FE program Diana, TNO[11], was used for the modelling and the non-linear analyses. The whole bridge was modelled, but only the part that was most critical to shear and torsion failure, Cantilever II, was modelled more in detail according to the previously worked out modelling method Broo *et al.*[5], see Figure 5. In Cantilever II, the concrete was modelled with four-node shell elements, and a constitutive model, based on non-linear fracture mechanics, and a rotating crack model, based on total strain, were used, see TNO[11]. Full interaction was assumed between the reinforcement or prestressing tendons and the concrete, by using embedded reinforcement layers. The rest of the bridge was modelled with two-node beam elements and linear elastic material properties. The piers were assumed to be fixed at the bottom end and the end spans were simply supported at the abutments. At mid-span the cantilevers were connected with pendulum hinges. The modelling of the supports and connections is described in Broo *et al.*[6].

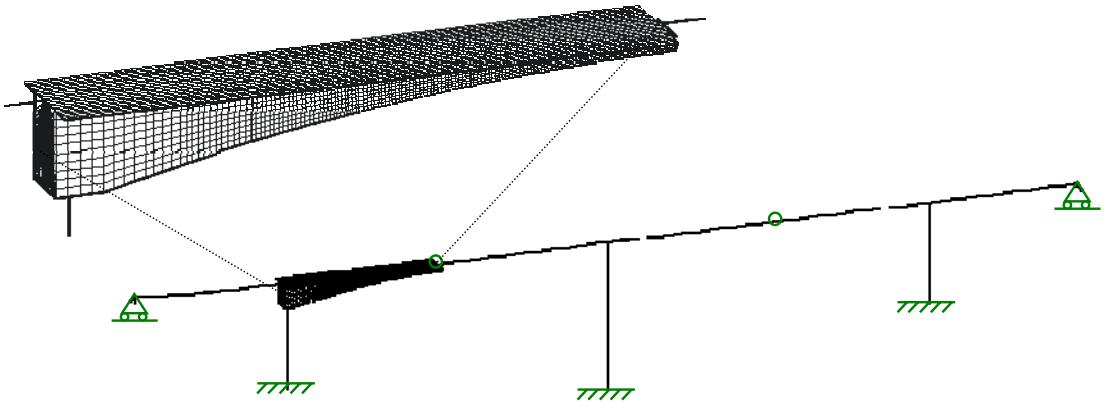

Figure 5 *The FE model of the Källösund Bridge used as a reference case in this study. Only the part of the bridge critical for shear and torsion is modelled in detail with curved shell elements, embedded reinforcement and non-linear material properties. The rest of the bridge is modelled with beam elements and linear elastic material properties.*

The material properties used for the analyses are presented in Tables 1 and 2; these corresponds to mean material properties and are the same as the ones used in Broo *et al.*[6]. The constitutive relations of the reinforcing and prestressing steel were modelled by the von Mises yield criterion with an associated flow rule and isotropic hardening. The hardening of concrete in compression was described by the expression of Thorenfeldt, and the reduction of the compressive strength due to transverse tensile strain was modelled according to Vecchio and Collins, as described in TNO[11]. For the tension softening of cracked concrete, the curve by Hordijk as described in TNO[11] was used. The crack response was smeared over a length, h, the crack band width, which corresponds to the mean crack spacing. The mean crack spacing was calculated for a member with reinforcement in two orthogonal directions, where the angle between the axes of principal stress and the direction of the reinforcement is $\theta > 15°$ according to BBK04[12].

$$s_{\mathrm{rm}} = \frac{1}{\dfrac{\cos\theta}{s_{\mathrm{rm,x}}} + \dfrac{\sin\theta}{s_{\mathrm{rm,y}}}} \qquad (1)$$

where $s_{\mathrm{rm,x}}$ and $s_{\mathrm{rm,y}}$ are the mean crack spacing calculated in the longitudinal and vertical directions respectively. The angle was chosen as $\theta = 21.8°$, which corresponds with the crack inclination obtained in the analysis of the reference case, Broo *et al.*[6]. For the reference model, the crack band width was calculated to be $h = 0.3$ m. The crack band width for the concrete in the webs varied in the parametric study due to the chosen reinforcement diameter and spacing; see Table 3.

Table 1 *Material properties used for the concrete in the analyses*

	E_{cm} [GPa]	f_{ccm} [MPa]	f_{ctm} [MPa]	G_{fm} [Nm/m^2]
Cantilevers	37.4	52.7	3.80	186
Piers	32.6	–	–	–

Table 2 Material properties used for the reinforcement in the analyses

Reinforcing steel	ϕ 10	f_{ym} [MPa]	450
		f_{um} [MPa]	630
		ε_{um} [–]	0.15
		E_{sm} [GPa]	204
Prestressing steel	ϕ 26	f_{pm} [MPa]	860
		f_{um} [MPa]	1110
		ε_{gm} [–]	0.07
		E_{pm} [GPa]	178

Table 3 Parameters for amount and inclination of web reinforcement

Analysis	t [m]	α [degrees]	ϕ [mm]	s [mm]	A_s [mm^2/m]	ρ [%]	$s_{rm,x,y}$ [mm]	h [m]
Ref	0.45	0	10	300	261.8	0.116	376	0.30
		90	10	300	261.8	0.116	376	
2V	0.45	0	10	300	261.8	0.116	376	0.28
		90	10	150	523.6	0.233	355	
2VL	0.45	0	10	150	523.6	0.233	355	0.27
		90	10	150	523.6	0.233	355	
4VL	0.45	0	12	100	1131.0	0.503	220	0.17
		90	12	100	1131.0	0.503	220	
Inc	0.45	0	10	300	261.8	0.116	376	0.30
		45	10	300	261.8	0.116	376	
P80	0.45	0	10	300	261.8	0.058	376	0.30
		90	10	300	261.8	0.116	376	
2TH	0.90	0	10	300	261.8	0.116	376	0.30
		90	10	300	261.8	0.058	376	

It is well known that the shear capacity in a shear sliding mode is often larger than what can be explained by the reinforcement contribution determined from a truss model. This increase, the *concrete contribution*, is influenced by tension-softening, tension-stiffening, dowel action and friction due to aggregate interlock. The *concrete contribution* can be taken into account in an approximate way by modifications of the constitutive relationships describing the materials, e.g. for the concrete in tension. In Broo *et al.*[5] two approaches for the tension softening were compared:

- the curve by Hordijk (see TNO[11]), where only the fracture energy of plain concrete is taken into account; and
- a curve modified according to the expression from the modified compression field theory (MCFT) of Collins and Mitchell[13], which also attempts to take into account the *concrete contribution*,

see Figure 6.

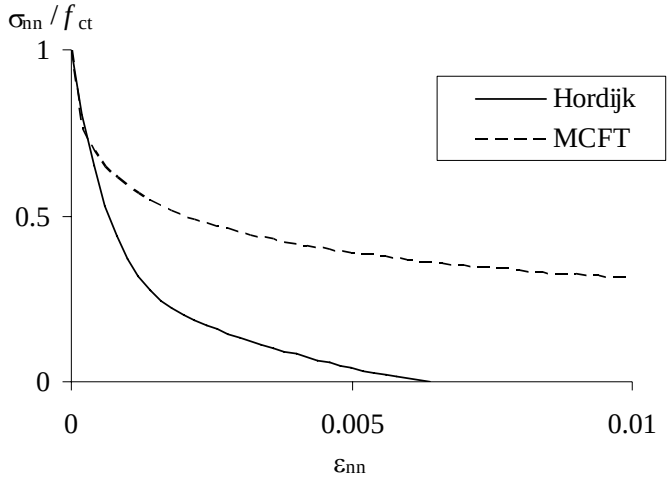

Figure 6 *Comparison of tension-softening relationships according to Hordijk as described in TNO[11], only fracture energy of plain concrete, and according to MCFT ,Collins and Mitchel[13] including the concrete contribution when subjected to shear.*

Results from the analyses in Broo *et al.*[5] showed that with the Hordijk curve, the shear capacity was underestimated and the average strains, i.e. the crack widths, were overestimated. On the other hand, if the *concrete contribution* to the shear capacity was considered with the expression from MCFT, the capacity was in many cases overestimated and the average strains underestimated. It was shown that the expression in MCFT gave a response that was too stiff after cracking and before yielding, for the parts of a member which were subjected to tension or bending but not to shear. Consequently, this way to consider the *concrete contribution* is not general, and was therefore not used in the analyses in this study. This means that the principal tensile strains, and accordingly the widths of cracks, evaluated from the analyses are likely to become overestimated.

The finite element analysis

The analyses were made in steps to consider the influence of the construction sequence and the loading history, see Plos[8] and Broo *et al.*[6]. The gravity loads were gradually increased and the abutments and the mid-span hinges were introduced at certain stages in agreement with the construction process. The bridge was loaded with several variable loads simultaneously up to their design values: crowd load on the causeway, distributed traffic load, horizontal traffic loads, and wind loads. The failure was reached by increasing the vertical point loads of the traffic, a bogie load B defined according to Vägverket[14], to obtain the bogie load resistance, B_R. Several point loads were increased simultaneously, using displacement control. This was made possible by a separately modelled statically determinate system of beams; a prescribed displacement was applied at one point and the reaction forces were transferred, in a controlled way, by the beam system to several points in the model. The loading and analysis procedures were the same in all analyses, and followed the analysis with design material properties in Broo *et al.*[6].

Results

The response of the whole bridge was linear until the vertical traffic point loads were applied. This can be seen in Figure 7 showing the vertical support reaction in the west pier versus the end deflection of Cantilever II. Figure 7 also indicates which part of the loading each part of the response emanates from. In the reference analysis, the cracking of the concrete started at B = 438 kN, with flexural-shear cracks, starting in the top flange and developing down into the webs; see Figure 8. The cracks occurred in the sections where the prestressing tendons are anchored in the top flange. With increased load shear cracks developed in large regions in the webs; thus a shear response was observed. However, the failure obtained in this FE analysis was due to bending, see Figure 9. In the part of the cantilever where the bending mode changed from tension in the top to tension in the bottom, the top row of elements in the webs cracked in shear; see Figure 10. Thereafter, when a bending crack developed in the bottom of the cross-section close to the end of the cantilever, the concrete compressive strength in the top of the web was reduced due to lateral tensile strain. Hence, due to the low remaining compressive strength, the internal lever arm decreased and the concrete in the compressive zone crushed when the tensile reinforcement in this section yielded.

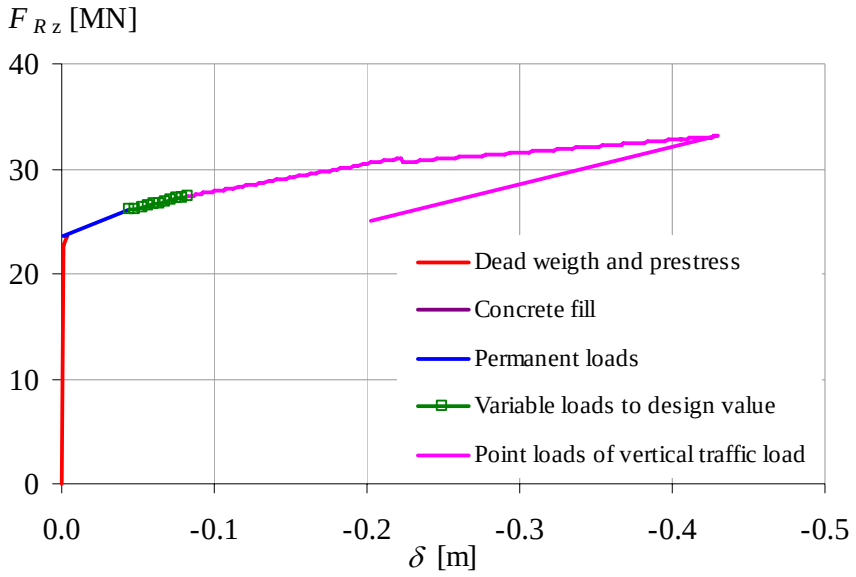

Figure 7 *Vertical support reaction in the west pier versus vertical displacement of the end of Cantilever II. Result from analysis of the reference case.*

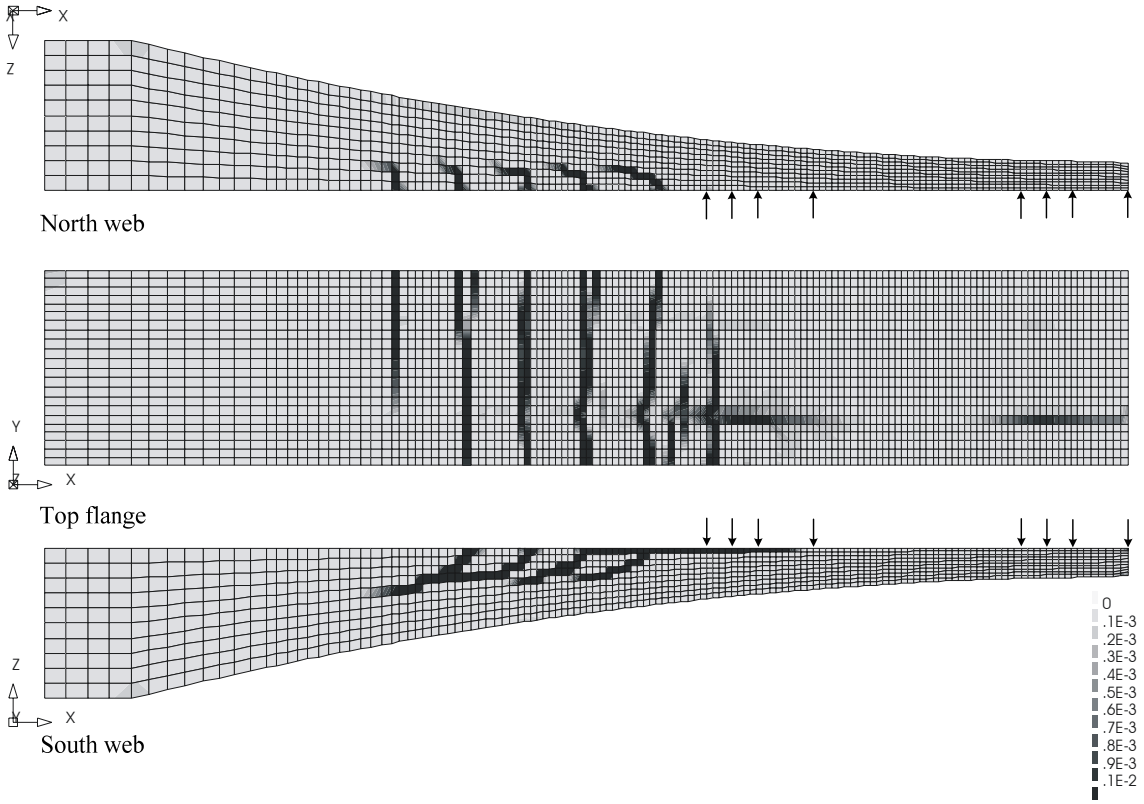

Figure 8 *Results from analysis of the reference case; north web, top flange, and south web, principal tensile strain after crack initiation for a bogie load of B = 438 kN.*

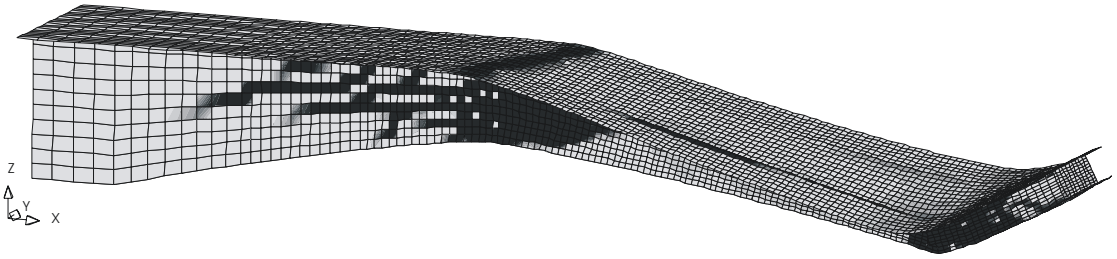

Figure 9 *Deformed shape of and principal tensile strain in Cantilever II just after maximum load. Result from analysis of the reference case.*

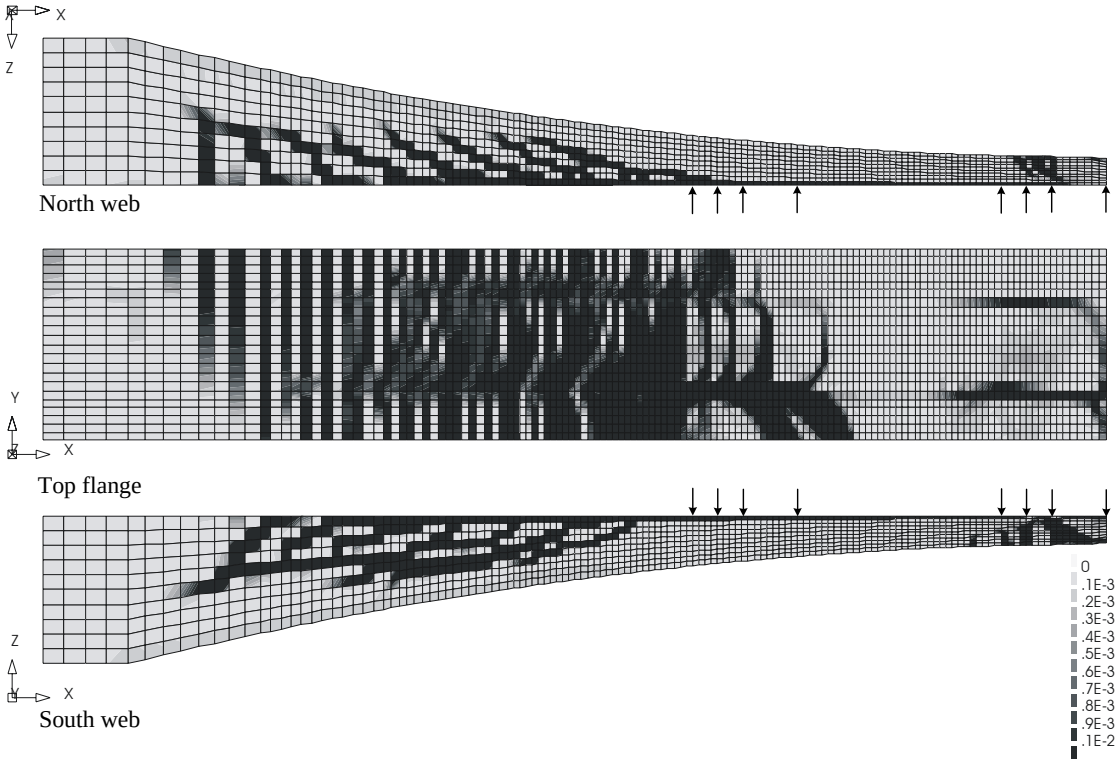

Figure 10 *Results from analysis of the reference case; north web, top flange, and south web, principal tensile strain at maximum load, a bogie load of B = 799 kN.*

The parametric study

The influence on the shear response of various design parameters was investigated. Several non-linear FE analyses were performed and results such as crack pattern, crack widths, failure mode, and load-carrying capacity were compared.

Parameter variation

The following parameters were varied: amount and inclination of web reinforcement, level of longitudinal prestressing, and web thickness, see Table 3. The reason for these choices was considerations concerning the structural behaviour, as explained in the following.

Possible failure modes in shear are (1) sliding along a shear crack and (2) crushing of the concrete between two shear cracks. When there is reinforcement crossing the shear crack, shear sliding cannot take place before this reinforcement yields. Accordingly, the amount of web reinforcement in the vertical and longitudinal directions is expected to have a great influence on the shear response, widths of shear cracks and the shear capacity. This was studied in three analyses with varying amount of web reinforcement. In the current Swedish code for bridge design, BRO 2004[15], the minimum reinforcement area in the webs is 400 mm^2/m, placed with a maximum spacing of 300 mm. Additionally, when the characteristic concrete tensile strength, f_{ctk}, is higher than 2.0 MPa the amount of reinforcement should be increased,

multiplied by a factor of f_{ctk} / 2.0. For the reference bridge the characteristic concrete tensile strength is f_{ctk} = 2.58 MPa, and the minimum reinforcement amount according to the new bridge code is then 516 mm^2/m, which corresponds to $\phi 10\ s\ 150$ or $\phi 12\ s\ 210$. This is considerably more than the actual reinforcement, in the bridge used for the reference case, $\phi\ 10\ s\ 300$, see Figure 4. Therefore, the amount of web reinforcement was increased compared to the reference case, in all variations.

Inclined shear reinforcement should according to conventional design methods based on the truss-model increase the shear capacity, compared to a corresponding case with vertical reinforcement of the same amount. When the reinforcement is perpendicular to the shear cracks the widths of the shear cracks are expected to be smaller. To investigate this one additional analysis was performed where the vertical web reinforcement was replaced by the same amount of inclined web reinforcement.

In a cantilevering box-girder the longitudinal prestressing tendons are mainly positioned in the top flange. Here, it was investigated to what extent the longitudinal prestressing affect the occurrence of shear cracks in the webs and the further development of the shear cracks. One model with decreased longitudinal prestressing level was analysed, see Table 3.

Multiple actions govern the design of the box cross-section. The combined effect of vertical shear and torsional moment is critical for the choice of the thickness of the webs. Therefore, the thickness of the webs was chosen as a parameter to study; and one model with increased web thickness was analysed, see Table 3.

Increased amount of web reinforcement

The influence on the shear response of the amount of web reinforcement was studied with three analyses, see Table 3. In the analysis denoted 2V, the amount of vertical web reinforcement was doubled. In the analysis denoted 2VL, both the amounts of vertical and longitudinal web reinforcement were doubled. This amount of web reinforcement corresponds to the required minimum according to the new Swedish code for bridge design. In the third analysis, 4VL, both the amounts of vertical and longitudinal web reinforcement were approximately four times the original amounts, i.e. approximately twice the required minimum according to the new Swedish code for bridge design.

In Figure 11 the bogie load, *B*, versus applied displacement is shown for the analyses with various amounts of web reinforcement. As can be seen from the results, the stiffness until cracking and the cracking load are rather similar. After cracking the structures with higher reinforcement amounts are stiffer and have higher failure loads, see Table 4, as could be expected. All analyses except 4VL showed the same failure mode as in the reference case, bending failure in the end of Cantilever II. In the analysis with highest amount of web reinforcement, 4VL, a shear failure was obtained instead. In this analysis no shear crack occurred in the top row of elements in the south web. Thus, the compressive strength was not reduced and the moment capacity of the end part of the cantilever was high enough to prevent the kind of bending failure that occurred in the other analyses, see section “Results”. Instead a shear

failure in the central part of the cantilever was revealed. This can be seen by comparing the crack patterns obtained from the analyses, Figures 8, 10, 12 and 13.

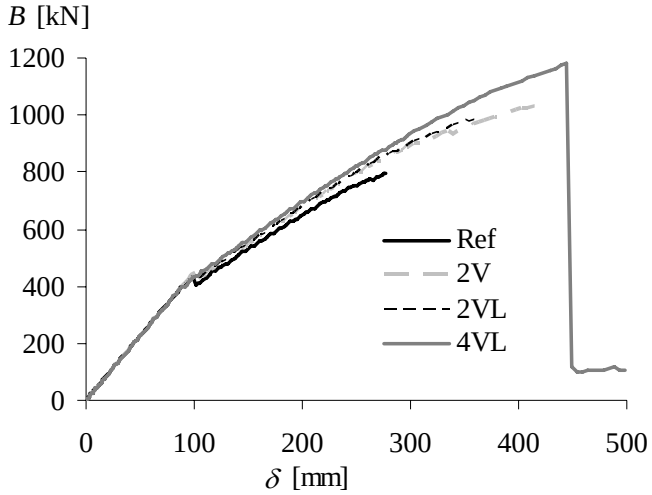

Figure 11 *Bogie load versus applied displacement as result from analyses with increased web reinforcement.*

Table 4 *Cracking load, B_{cr}, and load-carrying capacity, B_R, expressed as a Bogie load.*

	Ref	2V	2VL	4VL	Inc	P80	2TH
Bcr [kN]	438	458	399	399	416	307	392
BR [kN]	799	1033	983	1179	684	765	1006

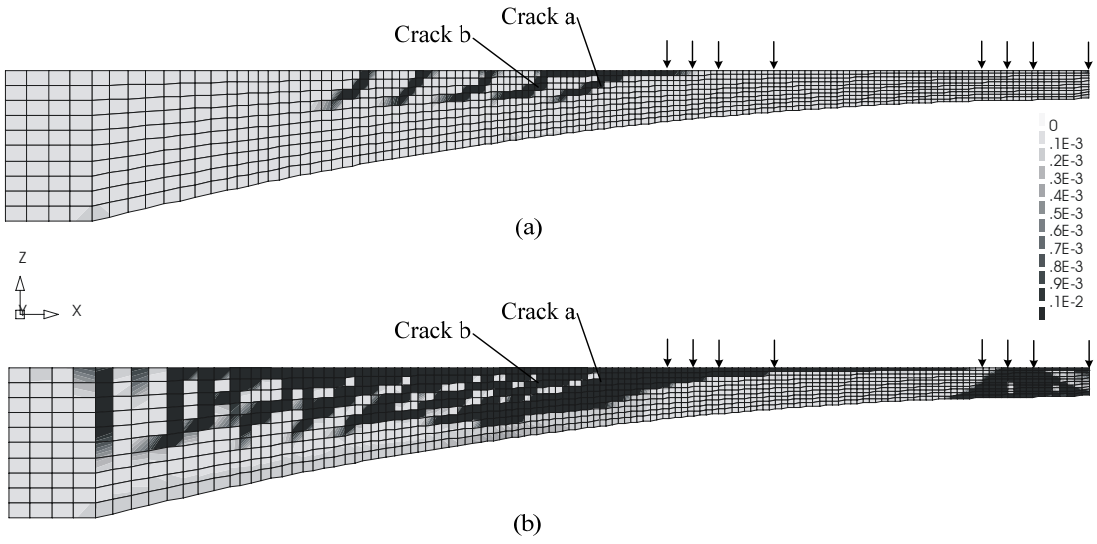

Figure 12 *Crack pattern in south web from analysis with increased vertical web reinforcement, 2V. (a) When cracking in the south web was initiated. (b) At maximum load.*

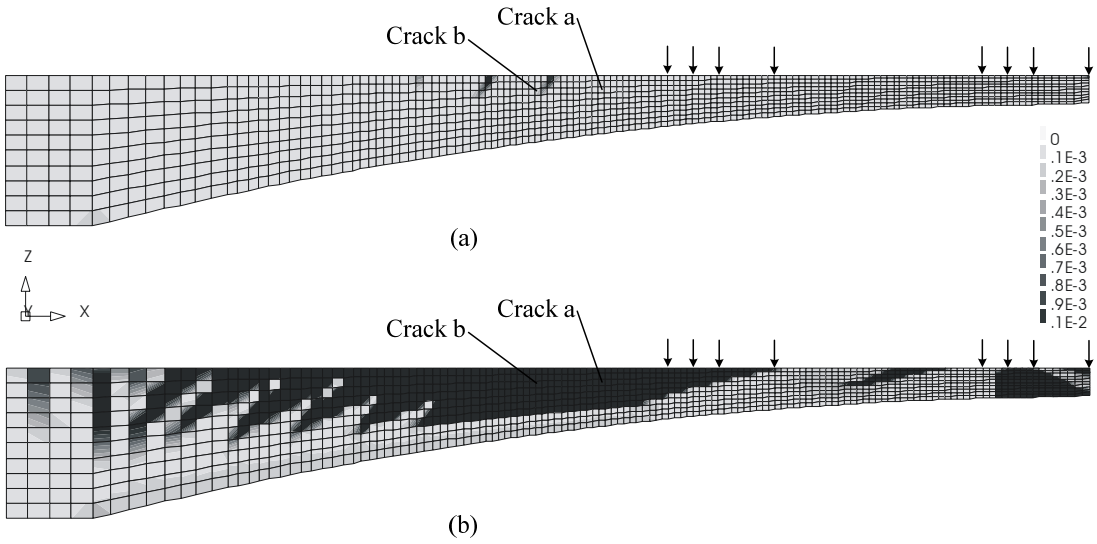

Figure 13 *Crack pattern in south web from analyses with increased web reinforcement, 4VL. (a) When cracking in the south web starts. (b) At maximum load.*

In Figure 14, the development of the crack widths for two of the shear cracks is shown. The crack widths, w, are calculated approximately from the principal tensile strain, ε_1, obtained from the analyses.

$$w = \varepsilon_1 \cdot h \qquad (1)$$

where h is the crack band width, corresponding to the mean crack spacing, see Table 3.

As can be seen the crack widths decreased with increased reinforcement amount. Although the crack widths were substantially reduced, see Figures 15 (a) and (c), they are still quite large; even while forming they exceeded allowable crack widths according to codes which normally are limited to $0.2 – 0.4$ mm depending on exposure class and type of reinforcement.

According to the Swedish code for bridge design a simplified approach can be used to limit the crack widths in the serviceability limit state; namely the design strength of the shear reinforcement is limited to 250 MPa in the ultimate limit state. Figures 15 (c) and (d) show that also the steel stresses in the analysis were higher than 250 MPa for a small load increase after cracking. Using the simple approach in the code in order to limit the shear crack widths would, in this case, lead to an ultimate limit capacity of approximately $B = 430$ kN, see Figures 16 (c) and (d).

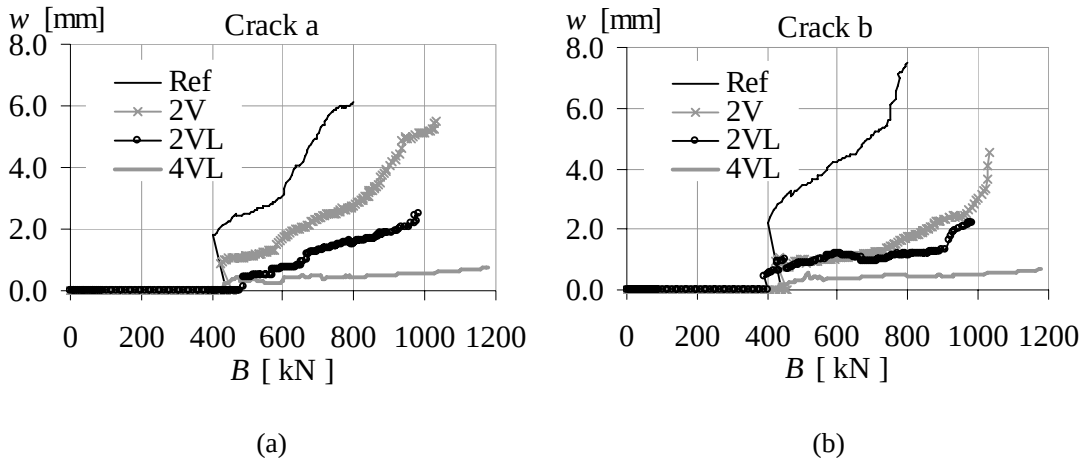

Figure 14 *Results from analyses with reference web reinforcement, Ref, and increased web reinforcement, 2V, 2VL and 4VL, are compared; bogie load versus crack widths. (a) Crack a, (b) Crack b.*

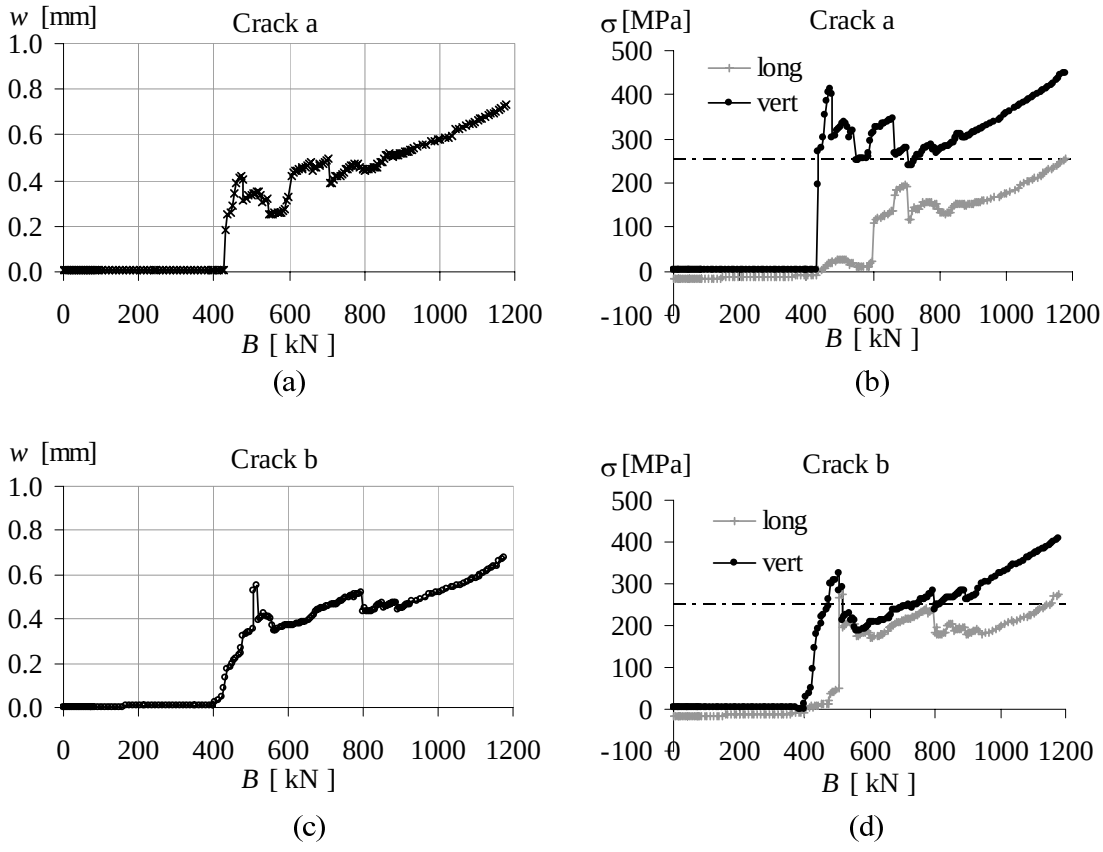

Figure 15 *Bogie load versus crack widths calculated with results from analysis with web reinforcement increased to ϕ12 s100 in both longitudinal and vertical directions, 4VL, (a) Crack a, and (c) Crack b. Bogie load versus stress in longitudinal and vertical web reinforcement. The dash-doted line indicates a steel stress of 250 MPa, which could be used as a limitation according to the Swedish code, BRO 2004[15]; (b) Crack a, and (d) Crack b.*

As mentioned in section “The finite element model”, the *concrete contribution* to the shear capacity was not fully taken into account by the constitutive relationship describing the materials. Therefore, the principal tensile strains evaluated with the analyses are likely to be overestimated, and thus also the crack widths. The modelling method used was verified to be on the safe side for the shear response and the shear capacity. However, the crack spacing or crack widths were not included in the verification; i.e. the global deformations were compared, but not crack spacing or crack widths.

Inclined web reinforcement

The influence on the shear response of inclined web reinforcement was studied with one analysis denoted Inc, see Table 3. The bogie load, *B*, versus applied displacement is shown in Figure 16. As can be seen from the results, the stiffness was similar for the case with inclined reinforcement as for the reference case with the same amount of vertical reinforcement. Moreover, both analyses showed the same failure mode. However, the analysis with inclined web reinforcement revealed a lower load-carrying capacity compared to the analysis with vertical web reinforcement, see Table 4. This is due to the obtained failure mode, bending failure. As mentioned previously, the bending capacity of the end of the Cantilever II was decreased due to the occurrence of shear cracks in the top row of elements in the south web, see Figure 17. In Figure 18, global strains and deformed shape of one of these elements are shown. It can be seen that both the shear strain and the vertical strain are larger in the analysis with inclined reinforcement. This can be interpreted as if the top flange is separating from the web in the vertical direction. When a bending crack developed in the bottom of the cross-section close to the end of the cantilever, the concrete compressive strength in the top of the web was reduced due to lateral tensile strain. Hence, due to the low remaining compressive strength, the internal lever arm decreased and the moment capacity was reduced. With inclined web reinforcement, the forces that could be carried in the vertical direction by the reinforcement were lower, which is why this vertical separation was more significant. Hence, the moment capacity was more reduced.

Comparing the crack patterns obtained in the analyses, Figures 8 and 17, it can be seen that the initial shear cracks in the analysis with inclined web reinforcement are more horizontal than those in the analysis with vertical web reinforcement. However, there were no major differences regarding crack widths, whether the web reinforcement was vertical or inclined, Figure 19. This is due to the low amount of web reinforcement – when the web cracked, yielding was initiated in the vertical web reinforcement as well as in the inclined web reinforcement, Figure 20.

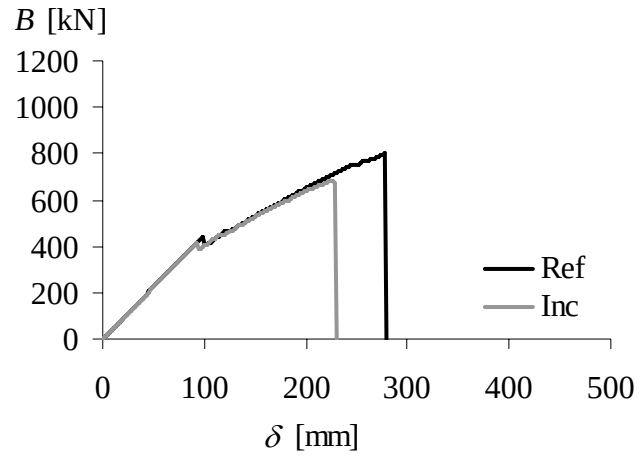

Figure 16 *Bogie load versus applied displacement as result from analyses with vertical web reinforcement and inclined web reinforcement.*

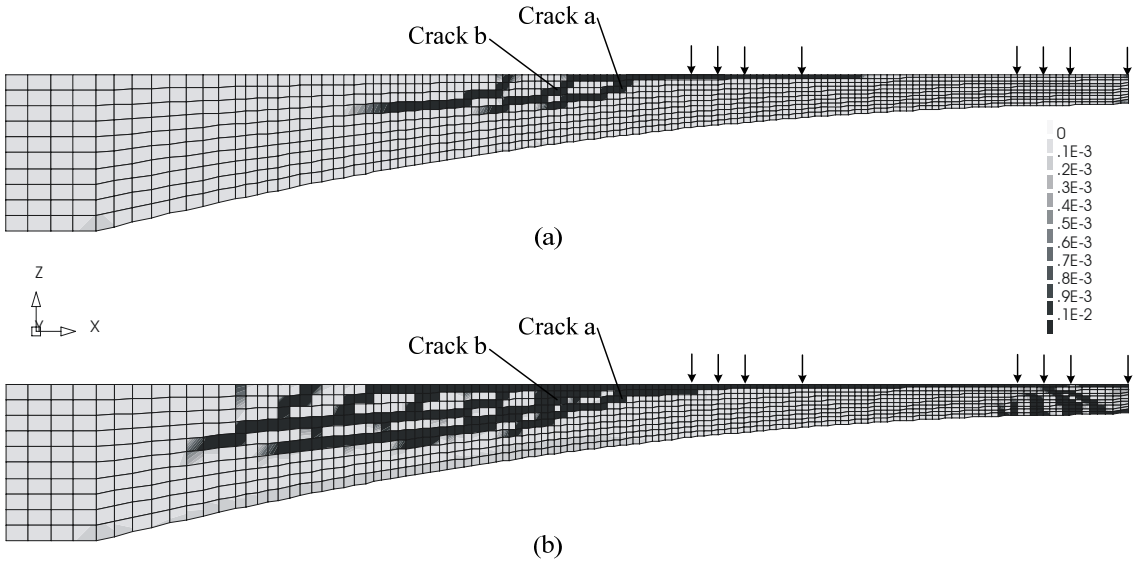

Figure 17 *Crack pattern in the south web from analysis with inclined web reinforcement, Inc. (a) When cracking in the south web was initiated. (b) At maximum load.*

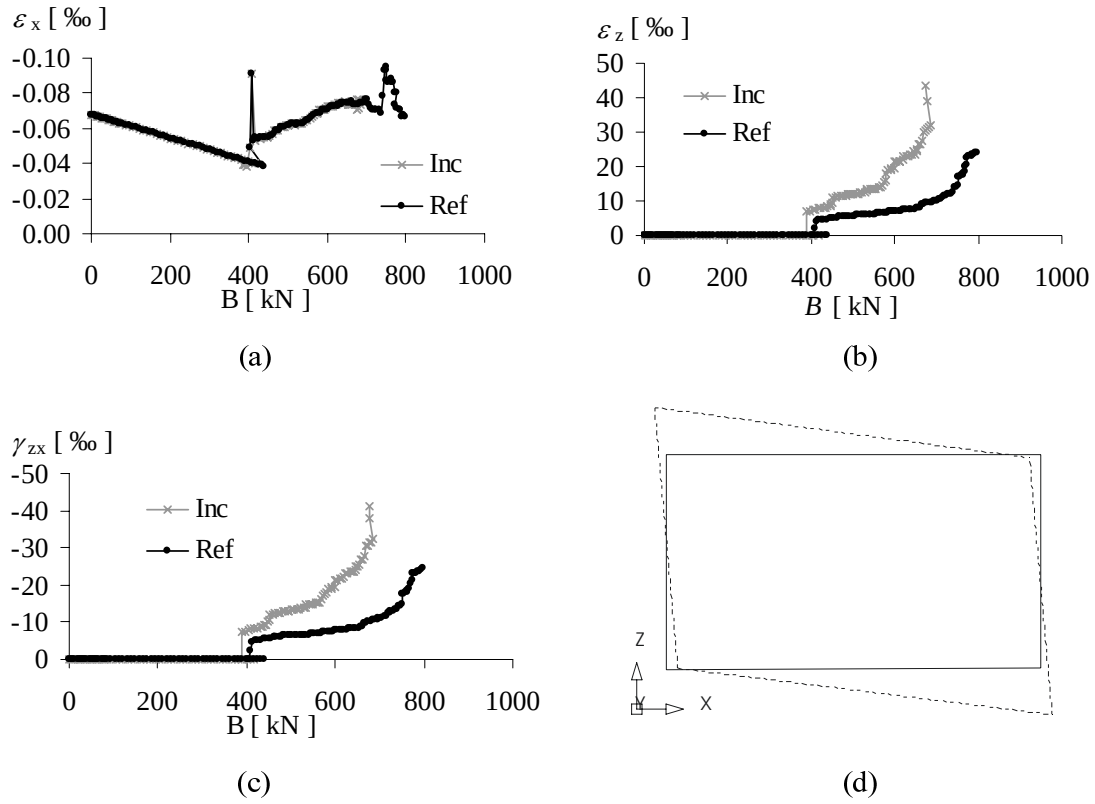

Figure 18 *Results from analyses with original web reinforcement, Ref, and inclined web reinforcement, Inc, are compared. Global concrete strains in one of the top row elements in the south web: (a) longitudinal strains, (b) vertical strains, and (c) shear strains. (d) Original and deformed shape of the element for which the strains are compared.*

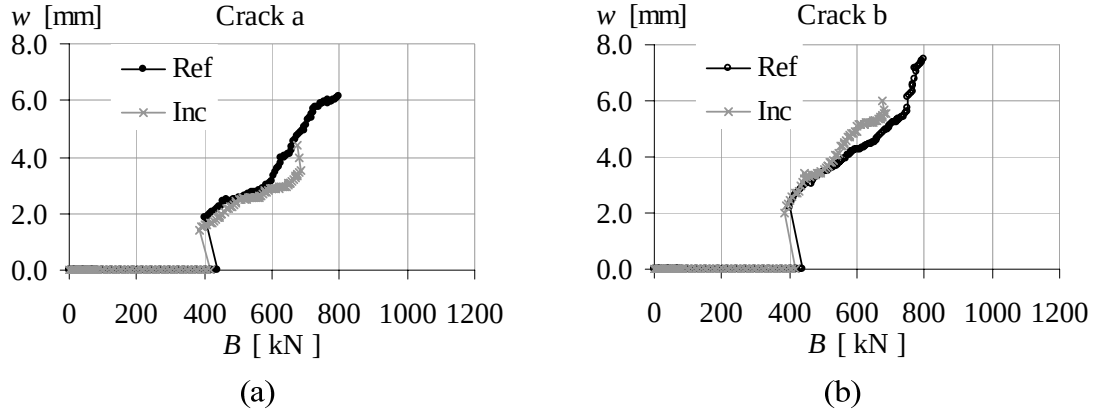

Figure 19 *Results from analyses with original web reinforcement, Ref, and inclined web reinforcement, Inc, are compared; bogie load versus crack widths (a) Crack a, (b) Crack b.*

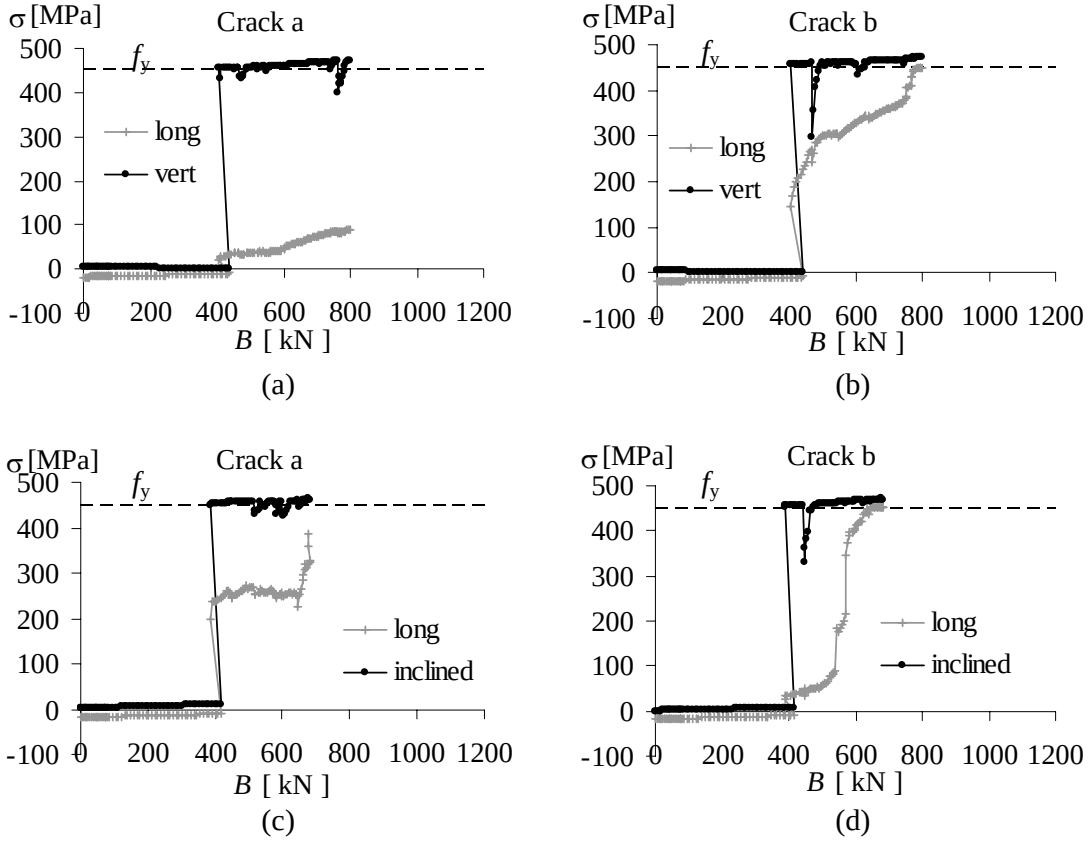

Figure 20 *Bogie load versus stress in longitudinal and vertical or inclined web reinforcement; (a) and (b) from analysis with vertical web reinforcement, Ref; (c) and (d) from analysis with inclined web reinforcement, Inc.*

Decreased longitudinal prestressing level

The influence of decreased longitudinal prestressing on the shear response was studied with one analysis denoted P80. In the analysis, the prestressing level was decreased to 80% of the original, from 527 MPa to 422 MPa. In Figure 21 the bogie load, *B*, versus applied displacement is shown for the reference analysis, Ref, and the analysis with decreased longitudinal prestressing, P80. As can be seen from the results, with decreased prestressing the cracking started at a lower load level and the response of the bridge was softer. However, the load-carrying capacity was just slightly reduced, see Table 4.

In the analysis with decreased longitudinal prestressing the crack, denoted a, did not occur when the cracking started, and when it occurred it did not propagate down into the web, see Figure 22. The development of the crack widths is compared in Figure 23. As could be expected, the longitudinal prestressing is an important parameter to control the occurrence of shear cracks and to control the crack widths in the service state, but it has only a minor influence on the load-carrying capacity. It is interesting, though, that this effect is so clear even when the prestressing is applied in the top flange, not in the webs where the shear cracking takes place.

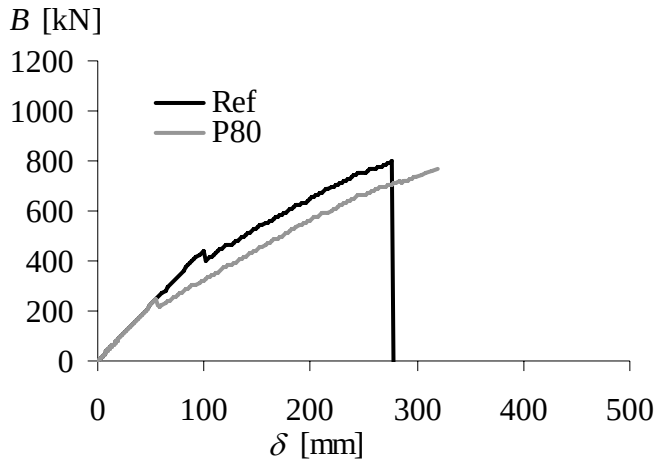

Figure 21 *Bogie load versus applied displacement as a result from analyses with reference longitudinal prestressing, Ref, and reduced longitudinal prestressing, P80.*

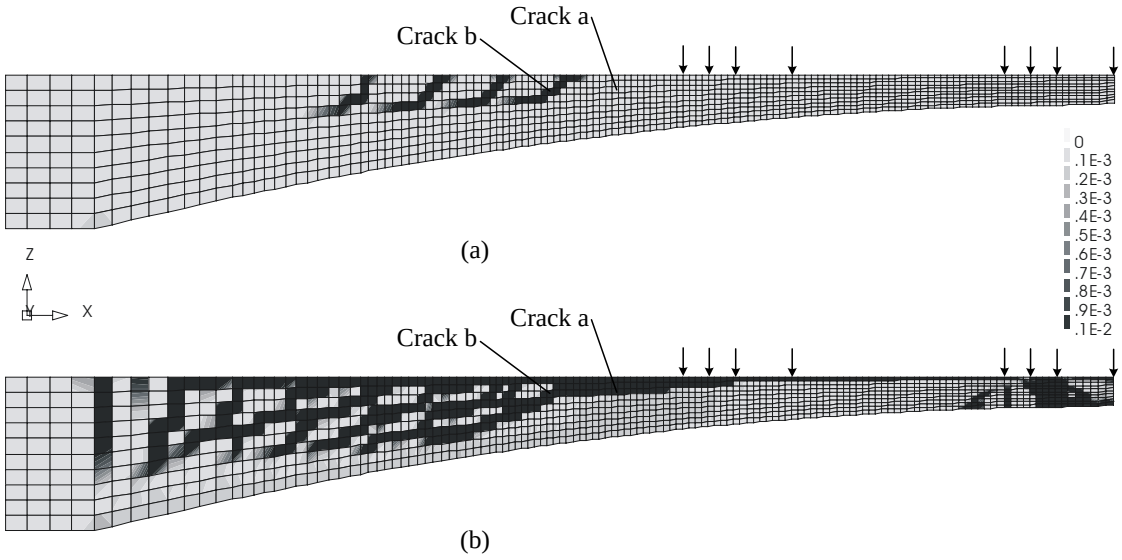

Figure 22 *Crack pattern in south web from analyses with decreased longitudinal prestressing, P80. (a) When cracking in the south web was initiated. (b) At maximum load.*

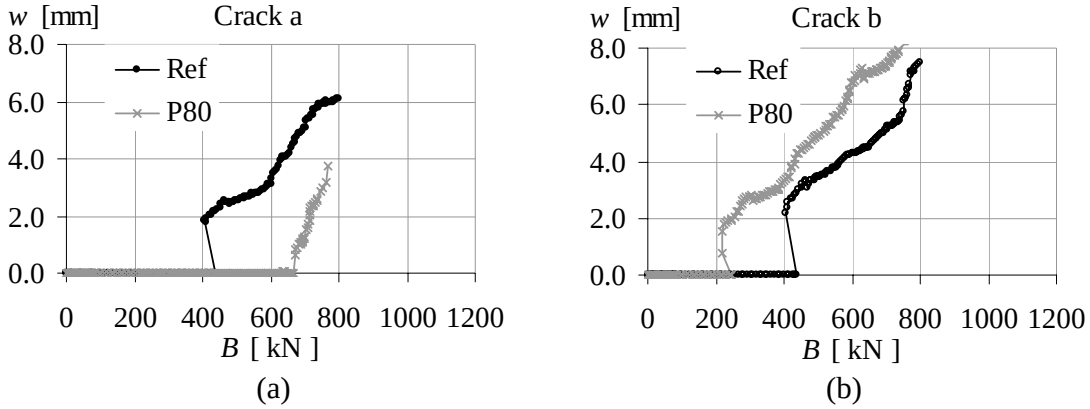

Figure 23 *Results from analyses with reference longitudinal prestressing, Ref, and decreased longitudinal prestressing, P80, are compared; bogie load versus crack widths (a) Crack a, (b) Crack b.*

Increased web thickness

The influence of increased web thickness on the shear response was studied with one analysis denoted 2TH. In the analysis the thickness of the webs was increased from 450 mm to 900 mm. In order not to change the loading, the density of the concrete in the webs was reduced by 50%.

The relations between the bogie loads, B, and the applied displacement are shown in Figure 24. Only the thickness of the webs in the Cantilever II was increased, thus the stiffness of this cantilever became higher than in the other cantilevers in the bridge. Consequently, more loading was attracted to this part of the structure and therefore the cracking load was lower than in the reference analysis, see also Table 4. The analysis with increased thickness of the webs revealed the same failure mode as the reference case, bending failure. In the analysis with increased web thickness the development of the shear crack widths was slower compared with the reference analysis – see Figures 25 and 26 – which was as anticipated. Accordingly, higher loads were needed to obtain the same reduction of the compressive strength due to lateral tensile strain. Thus, higher load-carrying capacity was shown.

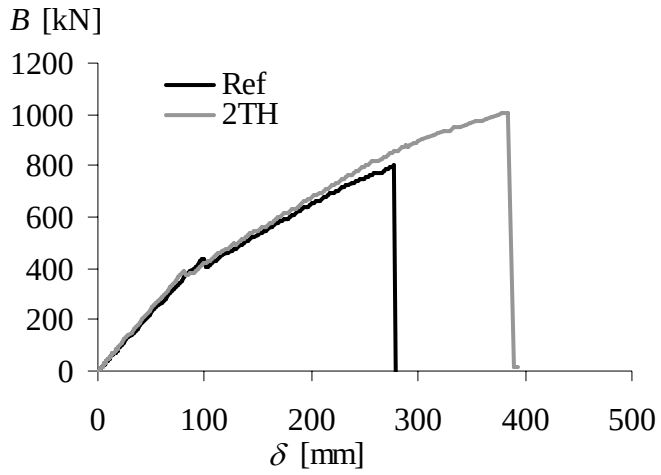

Figure 24 *Bogie load versus applied displacement as a result from analyses with original web thickness and increased web thickness.*

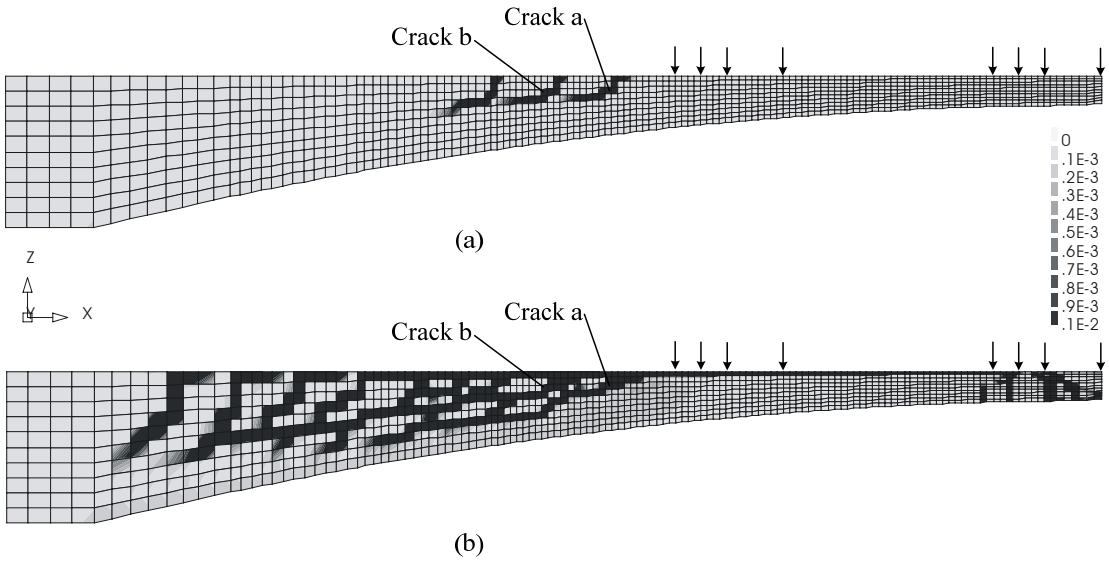

Figure 25 *Crack pattern in south web from analyses with increased web thickness. (a) When cracking in the south web was initiated. (b) At maximum load.*

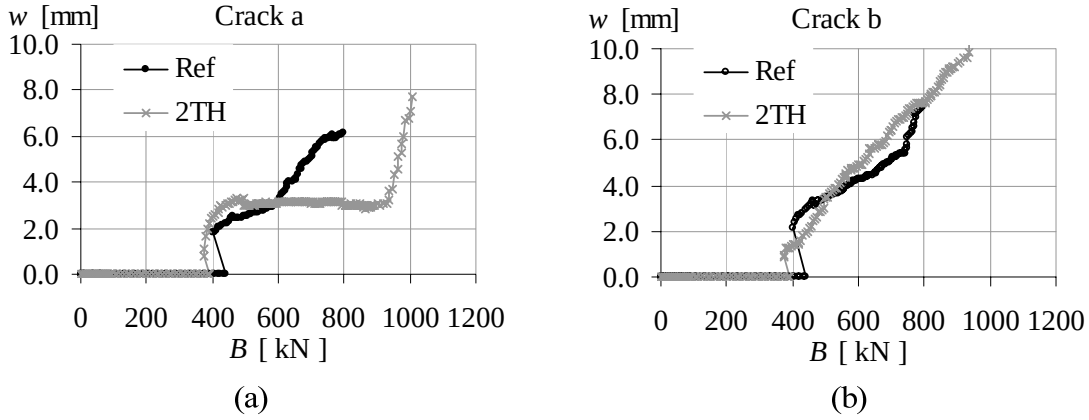

Figure 26 *Results from analyses with original web thickness and increased web thickness are compared; bogie load versus crack widths (a) Crack a, (b) Crack b.*

Conclusions

With this study it was shown how non-linear FE analysis can be used to study the influence of various design parameters on the shear response in prestressed concrete bridges, both in the service state and in the ultimate limit state. The influence on the shear response of a prestressed concrete box-girder bridge was investigated for the following design parameters: amount and inclination of web reinforcement, web thickness, and level of prestressing in the longitudinal direction. Non-linear FE analyses were used.

The results showed that an increase of the amount of web reinforcement, from $\phi 10\ s\ 300$ to $\phi 12\ s\ 100$ in orthogonal directions (i.e. approximately twice the required minimum according to the new Swedish code for bridge design.), led to an increased load-carrying capacity for traffic bogie load of about 50 %. As could be expected, the crack widths decreased with increased reinforcement amount. Although the crack widths were substantially reduced, they were still quite large. Even while forming they exceeded allowable crack widths according to codes. It should be noted, however that the crack widths evaluated from the analyses are probably overestimated. The modelling method used was verified for the shear response and the shear capacity, but not for crack widths; i.e. the global deformations were compared, but not crack spacing or crack widths.

In contrast to expectation, the analysis with inclined web reinforcement did not show reduced widths of shear cracks or higher load-carrying capacity. This could however be explained: results from the analysis revealed that the top flange was separating from the web in the vertical direction. With inclined web reinforcement, the forces that could be carried in the vertical direction by the reinforcement were lower, so this separation was more significant. Hence, the moment capacity was more reduced. Due to the low amount of web reinforcement, yielding was initiated in the vertical web reinforcement as well as in the inclined web reinforcement, when the web cracked.

Consequently, there were no major differences regarding crack widths whether the web reinforcement was vertical or inclined.

Moreover, the analysis of a model with only 80% of the longitudinal prestressing level in the reference case showed that the longitudinal prestressing is an important parameter to control the occurrence of shear cracks and to limit the crack widths in the service state, but it had only a minor influence on the load-carrying capacity. This was as could be expected; it is interesting, though, that this effect is so clear even when the prestressing is applied in the top flange, not in the webs where the shear cracking takes place. As anticipated, the thickness of the web affected the development of the shear cracks, and the load-carrying capacity.

By the parametric study of the bridge, the proposed modelling method was further verified; analyses with various design parameters almost always gave the expected results. With the information given by the analysis the complicated behaviour during the failure could be explained also when unexpected results were revealed. Accordingly, the knowledge and understanding of how various design parameters affect the shear response were improved, and the ability to use non-linear FE analysis to verify the design of box-girder bridges was refined.

Acknowledgments

The research was financed by the Swedish Road Administration (Vägverket) and the Swedish Rail Administration (Banverket).

References

1. MALM, R. *Shear cracks in concrete structures subjected to in-plane stresses*. Licentiate Thesis, Structural Design and Bridges, Architecture and the Built Environment, The Royal Institute of Technology (KTH), Stockholm, Sweden, 2006.
2. VECCHIO, F. J. and COLLINS, M. P. The modified compression-field theory for reinforced concrete elements subjected to shear. *Journal of the American Concrete Institute*, 1986, **83**, No. 2, 219-231.
3. PANG, X.-B. D. and HSU, T. T. C. Behavior of reinforced concrete membrane elements in shear. *ACI Structural Journal*, 1995, **92**, No. 6, 665-679.
4. PANG, X.-B. D. and HSU, T. T. C. Fixed angle softened truss model for reinforced concrete. *ACI Structural Journal*, 1996, **93**, No. 2, 197-207.
5. BROO, H., PLOS, M., LUNDGREN, K., and ENGSTRÖM, B. Simulation of shear-type cracking and failure with non-linear finite element method. *Magazine of Concrete Research*, 2007, **59**, No. 9, 673-687.

6. BROO, H., PLOS, M., LUNDGREN, K., and ENGSTRÖM, B. Non-linear finite element analysis of the shear response in prestressed concrete bridges. *Submitted to Magazine of Concrete Research in February 2008*.

7. PLOS, M., GYLLTOFT, K., JEPPSON, J., CARLSSON, F., THELANDERSSON, S., ENOCHSSON, O., and ELFGREN, L. Evaluering av bärförmåga hos broar med hjälp av förfinade analysmetoder Ett samarbetsprojekt mellan LTH, LTU och Chalmers, (In Swedish). Institutionen för konstruktion och mekanik, Betongbyggnad, Göteborg, Sweden Rapport 04:3, 2004.

8. PLOS, M. Structural Assessment of the Källösund Bridge using Finite Element Analysis - Evaluation of the load carrying capacity for ULS. Concrete Structures, Department of Structural and Mechanical Engineering, Chalmers University of Technology, Göteborg, Sweden Rapport 04:1, March 2004.

9. ENOCHSSON, O., PUURULA, A., and ELFGREN, L. Beräkning av betongbroars bärförmåga - Interaktion mellan tvärkraft, vridmoment och böjmoment i Källösundsbron, (In Swedish). Institutionen för samhällsbyggnad, Luleå tekniska universitet, Luleå, Sweden 2004:15, 2004.

10. PLOS, M. and GYLLTOFT, K. Evaluation of shear capacity of a prestressed concrete box girder bridge using non-linear FEM. *Structural Engineering International*, 2006, **16**, No. 3, 213-221.

11. TNO. *DIANA Finite Element Analysis User's Manual release 9*. TNO DIANA BV, Delft, the Netherlands, 2004.

12. BBK04. *Boverkets handbok om betongkonstruktioner: BBK 04*. Boverket, Karlskrona, 2004.

13. COLLINS, M. P. and MITCHELL, D. *Prestressed Concrete Structures*. Prentice Hall, Englewood Cliffs, New Jersey, 1991.

14. VÄGVERKET. Allmän teknisk beskrivning för klassningsberäkning av vägbroar (Swedish regulations for structural assessment of road bridges, in Swedish). Vägverket, Borlänge, Sweden publikation 1998:78, 1998.

15. BRO 2004. Vägverkets allmänna tekniska beskrivning för nybyggande och förbättring av broar, (In Swedish). Vägverket (Swedish Road Administration), Borlänge, Sweden Publikation 2004:56, 2004.

Licentiate Theses and Doctoral Theses, Concrete Structures,

Chalmers University of Technology, 1990-2008

90:1 Stig Öberg: Post Tensioned Shear Reinforcement in Rectangular RC Beams. Publication 90:1. Göteborg, April 1990. 603 pp. (No. 1021). Doctoral Thesis.

90:2 Johan Hedin: *Långtidsegenskaper hos samverkanskonstruktioner av stål och betong (Long Time Behaviour of Composite Steel Concrete Structures).* Publication 90:2. Göteborg, August 1990. 53 pp. (No. 1079). Licentiate Thesis.

92:1 Björn Engström: *Ductility of Tie Connections in Precast Structures*. Publication 92:1. Göteborg, October 1992. 368 pp. (Nos. 936, 999, 1023, 1052). Doctoral Thesis.

93:1 Mario Plos: *Shear Behaviour in Concrete Bridges - Full Scale Shear Test. Fracture Mechanics Analyses and Evaluation of Code Model*. Publication 93:1. Göteborg, April 1993. 70 pp. (Nos. 1088, 1084). Licentiate Thesis.

93:2 Marianne Grauers: *Composite Columns of Hollow Steel Sections Filled with High Strength Concrete*. Publication 93:2. Göteborg, June 1993. 140 pp. (No. 1077). Doctoral Thesis.

93:4 Li An: *Load Bearing Capacity and Behaviour of Composite Slabs with Profiled Steel Sheet*. Publication 93:4. Göteborg, September 1993. 134 pp. (No. 1075). Doctoral Thesis.

93:5 Magnus Åkesson: *Fracture Mechanics Analysis of the Transmission in Zone in Prestressed Hollow Core Slabs*. Publication 93:5. Göteborg, November, 1993. 64 pp. (No 1112). Licentiate Thesis.

95:1 Christina Claeson: *Behavior of Reinforced High Strength Concrete Columns*. Publication 95:1. Göteborg, June 1995. 54 pp. (No. 1105). Licentiate Thesis.

95:2 Karin Lundgren: *Slender Precast Systems with Load-Bearing Facades*. Publication 95:2. Göteborg, November 1995. 60 pp. (No. 1098). Licentiate Thesis.

95:3 Mario Plos: *Application of Fracture Mechanics to Concrete Bridges. Finite Element Analysis and Experiments*. Publication 95:3. Göteborg, November 1995. 127 pp. (Nos. 1067, 1084, 1088, 1106). Doctoral Thesis.

96:1 Morgan Johansson: *New Reinforcement Detailing in Concrete Frame Corners of Civil Shelters. Non-linear Finite Element Analyses and Experiments*. Publication 96:1. Göteborg, November 1996. 77 pp. (No. 1106). Licentiate Thesis.

96:2 Magnus Åkesson: *Implementation and Application of Fracture Mechanics Models for Concrete Structures*. Publication 96:2. Göteborg, November 1996. 159 pp. (No. 1112). Doctoral Thesis.

97:1 Jonas Magnusson: *Bond and Anchorage of Deformed Bars in High-Strength Concrete*. Publication 97:1. Göteborg, November 1997. 234 pp. (No. 1113). Licentiate Thesis.

98:1 Christina Claeson: *Structural Behavior of Reinforced High-Strength Concrete Columns*. Publication 98:1. Göteborg 1998. 92 pp + I-IV, 75 pp. (No. 1105). Doctoral Thesis.

99:1 Karin Lundgren: *Three-Dimensional Modelling of Bond in Reinforced Concrete. Theoretical Model, Experiments and Applications*. Publication 99:1. Göteborg, November 1999. 129 pp. (No. 37). Doctoral Thesis.

00:1 Jonas Magnusson: *Bond and Anchorage of Ribbed Bars in High-Strength Concrete*. Publication 00:1. Göteborg, February 2000. 300 pp. (No. 1113). Doctoral Thesis.

00:2 Morgan Johansson: *Structural Behaviour in Concrete Frame Corners of Civil Defence Shelters*. Publication 00:2. Göteborg, March 2000. 220 pp. (No. 1106). Doctoral Thesis.

00:3 Rikard Gustavsson: *Static and Dynamic Finite Element Analyses of Concrete Sleepers*. Publication 00:3. Göteborg, March 2000. 58 pp. (No. 41). Licentiate Thesis.

00:4 Mathias Johansson: *Structural Behaviour of Circular Steel-Concrete Columns. Non-linear Finite Element Analyses and Experiments*. Publication 00:4. Göteborg, March 2000. 64 pp. (No. 48). Licentiate Thesis.

01:3 Gunnar Holmberg: *Fatigue of Concrete Piles of High Strength Concrete Exposed to Impact Load*. Publication 01:3. Göteborg, August 2001. 69 pp. (No. 55). Licentiate Thesis.

02:1 Peter Harryson: *Industrial Bridge Construction – merging developments of process, productivity and products with technical solutions*. Publication 02:1. Göteborg, January 2002. 90 pp. (No. 34). Licentiate Thesis.

02:2 Ingemar Löfgren: *In-situ concrete building systems – developments for industrial constructions*. Publication 02:2. Göteborg, March 2002. 125 pp. (No. 35). Licentiate Thesis.

02:4 Joosef Leppänen: *Dynamic Behaviour of Concrete Structures subjected to Blast and Fragment Impacts.* Publication 02:4. Göteborg, April 2002. 78 pp. (No. 31). Licentiate Thesis.

02:5 Peter Grassl: *Constitutive Modelling of Concrete in Compression*. Publication 02:5. Göteborg, May 2002. 95 pp. (No. 37). Licentiate Thesis.

02:6 Rikard Gustavson: *Structural Behaviour of Concrete Railway Sleepers*. Publication 02:6. Göteborg, September 2002. 180 pp. (No. 32). Doctoral Thesis.

02:8 Mathias Johansson: *Composite Action and Confinement Effects in Tubular Steel-Concrete Columns*. Publication 02:8. Göteborg, November 2002. 173 pp. (No. 33). Doctoral Thesis.

03:1 Per-Ola Svahn: *Impact-Loaded Concrete Piles – Theoretical and experimental study of load effects and capacity*. Publication 03:1. Göteborg, May 2002. 99 pp. (No. 38). Licentiate Thesis.

04:3 Peter Grassl: *Plasticity and Damage Mechanics for Modeling Concrete Failure*. Publication 04:3. Göteborg, September 2004. 159 pp. Doctoral Thesis.

04:4 Joosef Leppänen: *Concrete Structures Subjected to Fragment Impacts – Dynamic Behaviour and Material Modelling*. Publication 04:4. Göteborg, October 2004. 125 pp. (No. 31). Doctoral Thesis.

2005 Helen Broo: *Shear and Torsion Interaction in Prestressed Hollow Core Slabs.* Lic 2005:2. Göteborg 2005. 83 pp. Licentiate Thesis.

2005 Per-Ola Svahn: *Dynamic Behaviour of Reinforced Concrete Structures: Analyses with a Strong Discontinuity Approach.* Ny serie nr 2366. Göteborg 2005. 159 pp. Doctoral Thesis.

2005 Ingemar Löfgren: *Fibre-reinforced Concrete for Industrial Construction – a fracture mechanics approach to material testing and structural analysis.* Ny serie nr. 2378. Göteborg 2005. 243 pp. Doctoral Thesis.

2006 Rasmus Rempling: *Constitutive Modelling of Concrete Subjected to Tensile Monotonic and Cyclic Loading*. Lic 2006:4. Göteborg 2006. 59 pp. Licentiate Thesis.

2008 Anette Jansson: *Fibres in Reinforced Concrete Structures – analysis, experiments and design*. Lic 2008:3. Göteborg 2008. 84 pp. Licentiate Thesis.

2008 Ulrika Nyström: *Concrete Structures Subjected to Blast and Fragment Impacts, Numerical Simulations of Reinforced and Fibre-reinforced Concrete*. Lic 2008:4. Göteborg 2008. 117 pp. Licentiate Thesis.

2008 Kamyab Zandi Hanjari: *Load-Carrying Capacity of Damaged Concrete Structures*. Lic 2008:6. Göteborg 2008. 108 pp. Licentiate Thesis.

2008 Peter Harryson: *Industrial Bridge Engineering – Structural developments for more efficient bridge construction*, Ny serie nr. 2810. Göteborg 2008. Doctoral Thesis.